TRANSPORTATION RESEARCH
RECORD

No. 1447

Soils, Geology,
and Foundations

Design and Construction of Auger Cast Piles, and Other Foundation Issues

A peer-reviewed publication of the Transportation Research Board

TRANSPORTATION RESEARCH BOARD
NATIONAL RESEARCH COUNCIL

NATIONAL ACADEMY PRESS
WASHINGTON, D.C. 1994

Transportation Research Record 1447
ISSN 0361-1981
ISBN 0-309-06053-2
Price: $26.00

Subscriber Category
IIIA soils, geology, and foundations

Printed in the United States of America

Sponsorship of Transportation Research Record 1447

GROUP 2—DESIGN AND CONSTRUCTION OF TRANSPORTATION FACILITIES
Chairman: Charles T. Edson, Greenman Pederson, Inc.

Soil Mechanics Section
Chairman: Michael G. Katona, U.S. Air Force, Armstrong Laboratory

Committee on Foundations of Bridges and Other Structures
Chairman: Joseph A. Caliendo, Utah State University
Secretary: Christopher Dumas, Federal Highway Administration
Nariman Abar, Roy H. Borden, Jean-Louis Briaud, Dan A. Brown, Donald A. Bruce, Robert G. Carroll, Jr., Ronald G. Chassie, Albert F. Dimillio, Victor Elias, Roger Alain Frank, Todd L. Harrison, Mohamad Hussein, Edward G. Keane, Donald E. Keenan, James H. Long, Randolph W. Losch, Michael C. McVay, Gary M. Norris, Michael Wayne O'Neill, James M. Sheahan, John L. Walkinshaw, David E. Weatherby, Gdalyah Wiseman, James L. Withiam

Transportation Research Board Staff
Robert E. Spicher, Director, Technical Activities
G. P. Jayaprakash, Engineer of Soils, Geology, and Foundations
Nancy A. Ackerman, Director, Reports and Editorial Services
Luanne Crayton, Editor

The organizational units, officers, and members are as of December 31, 1993.

Transportation Research Record 1447

Contents

Part 2—Other Foundation Issues

Foreword

The 14 papers in this volume are arranged in two groups. The initial eight papers are on design and construction of auger cast piles, and the remaining six papers present information on other foundation-related issues.

O'Neill describes the continuous flight auger and screw pile, two augered pile systems that are used extensively in Europe. He also discusses design guidelines and construction methods for auger cast pile systems.

McVay et al. report on Florida's experience with auger cast-in-place (ACIP) piles, and Lacy et al. describe how ACIP piles have successfully minimized both vibration-induced differential settlement and damage to adjacent structures. Esrig et al. indicate that managing pile installation to minimize ground displacement is critical in urban areas, where nearby structures or buried utilities might be affected. Rausche et al. focus on the principles, applications, and limitations of the "low-strain integrity testing" of auger cast piling.

England reports on a high-quality control process that has been developed in the United Kingdom for monitoring pile installation. De Cock and Imbo, and Whitworth describe their experiences, respectively, with concrete Atlas screw piles in Belgium and Starsol pile construction in France.

The remaining six papers provide information on other issues related to foundations, such as details on Ontario's Load and Resistance Factor Design procedure, general foundation models that are appropriate for modeling soil-structure interaction in seismic bridge analysis, and a general solution for the critical buckling capacity of long, slender friction piles in clay using the minimal potential energy method. Also included are a case history illustrating how blast densification may be used to densify a loose debris flow; a new, nondestructive test method that employs dispersive stress-wave propagation and special signal-processing techniques to find the lengths of installed timber piles; and results of a direct-shear apparatus and rod-shear test on effectiveness of bitumen coating in mitigating downdrag in cohesionless soils.

PART 1

Design and Construction of Auger Cast Piles

Review of Augered Pile Practice Outside the United States

MICHAEL W. O'NEILL

The objective is to document procedures used abroad in order to increase U.S. transportation engineers' confidence in the augered pile system when properly applied to highway construction. Two construction systems for augered piles used extensively in Europe are described: the continuous-flight auger system and the screw-pile system. Real-time acquisition of critical construction data by electronic sensing devices ensures the integrity of such systems; one real-time data-acquisition system is examined. Simple design rules for estimating axial capacity are documented, and some innovative design and construction methods are evaluated.

Augered piles are commonly used for building and transportation construction in Europe and other parts of the world. Augered piles can be distinguished from drilled shafts (bored piles) and from driven piles by the magnitude of effective stress changes they produce in the surrounding soil during construction. To create a drilled shaft, a commonplace in the United States, an auger is repeatedly inserted and withdrawn from the borehole to excavate soil, then the excavated borehole is filled with concrete. In general no attempt is made to maintain the stresses that existed in the ground before construction. With a driven pile, the soil is displaced—even in a so-called nondisplacement pile—and the ground stresses are increased. With an augered pile, ground stresses are maintained near the value that existed before construction by using a continuous flight auger and maintaining high pressure in the concrete as the auger is withdrawn. In principle, the augered pile possesses load-settlement behavior that falls between that of a drilled shaft and a driven pile (Figure 1).

Public transportation facilities in the United States have taken almost no advantage of augered piles. Reasons for not using them include concerns about control of structural integrity and unavailability of design methods (methods for capacity estimation). EBA Engineering Inc. recently reported on U.S. practice; the study discussed equipment, costs, and case histories (*1*). However, few authorities and experts contacted by EBA were willing to discuss design methods for augered piles, which may suggest that no one has developed a standard practice for estimating static capacity. In contrast, quality control and assurance in U.S. practice are covered in detail in a recent manual published by the Deep Foundations Institute (*2*), which describes materials, equipment, tolerances, adjacent piles, installation procedures, and other issues in a guide-specification format for U.S. practice.

Certain aspects of European and international practice for construction and design of augered piles may be of interest to U.S. transportation foundation engineers who are considering whether to use augered piles. Two of the many types of cast-in-place, augered piles commonly used in Europe are the continuous flight auger (CFA) pile, in which excavation is made with a continuous flight auger and the borehole is grouted as the auger is withdrawn (commonly known in the United States as "augercast" piles), and the screw pile (SP), in which a single-turn auger is screwed into the soil and then screwed back out as the concrete is placed. Such piles typically range from 0.3 to 0.8 m in diameter and may be up to 30 m deep.

Department of Civil and Environmental Engineering, University of Houston, Houston, Tex. 77204-4791.

CONSTRUCTION PROCEDURES FOR CFA PILES AND SPs

General methods of construction for CFA piles and SPs are shown in Figure 2 (*3,4*). With the CFA pile, soil is excavated by a double-flight continuous auger (Figure 2*a*). Following the Starsol CFA method, once the maximum depth has been reached, the auger is withdrawn a small distance (0.5 m); however, the discharge end of the grout pump line, which is housed but slides freely within the central stem of the auger, remains on the bottom of the hole, and the space beneath the auger and the base of the shaft is grouted with high-pressure grout or concrete with very fine coarse aggregate, which may or may not be fiber reinforced (Figure 2*b*). This procedure contrasts with past U.S. practice, whereby the auger is lifted about 0.3 m, grout is introduced through the stem, and the auger turned and thrust back to the bottom of the borehole once grout pressure increases sufficiently (*4*). Thereafter the auger and grout tube are lifted together, with the outlet port on the grout tube remaining a short distance below the base of the auger during continuous grouting. A reinforcing cage, if specified, is then in-

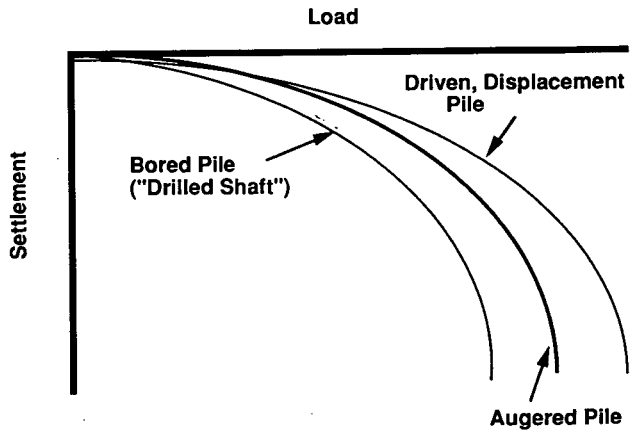

FIGURE 1 Hypothetical difference in behavior among bored, driven, and augered piles.

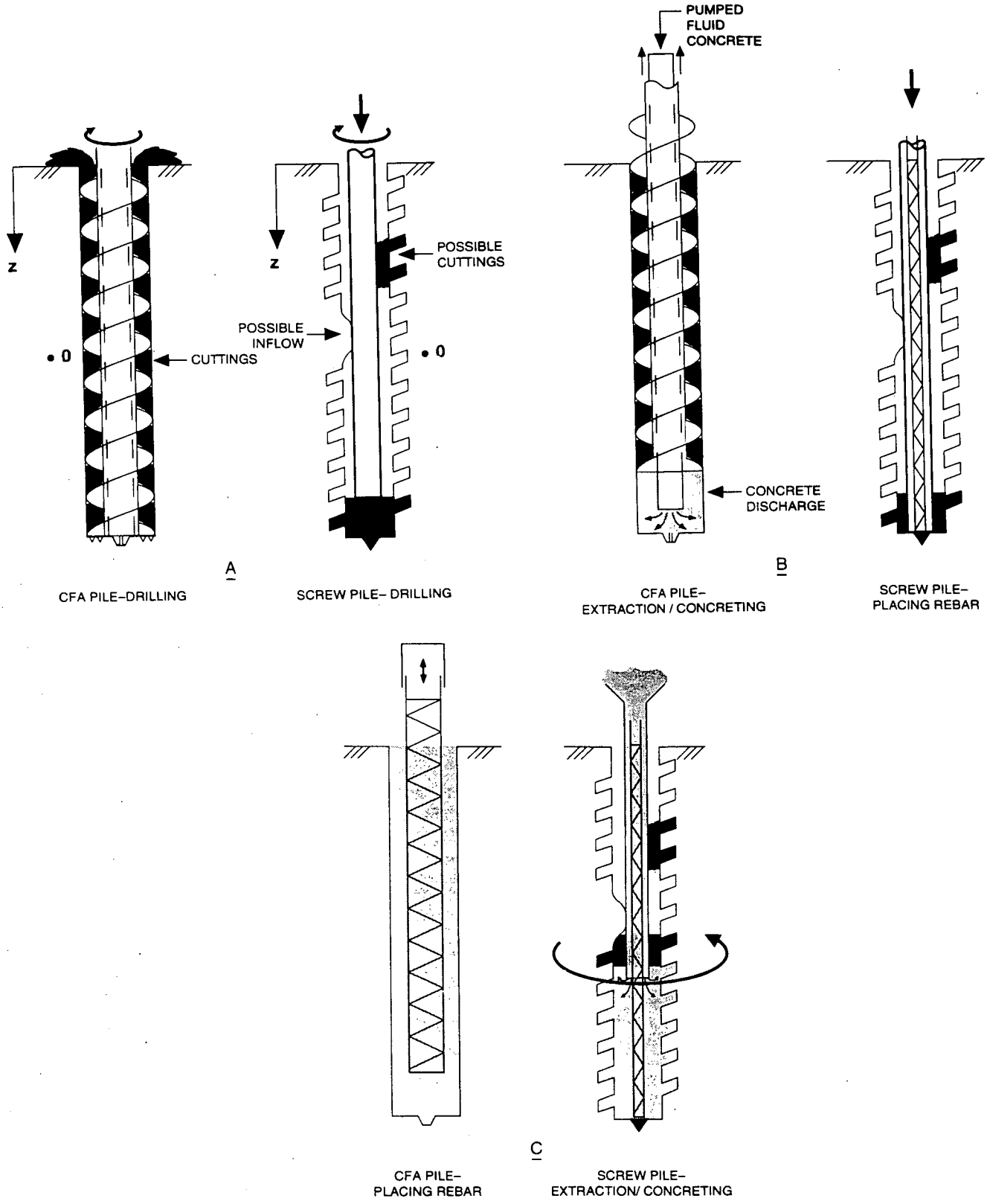

FIGURE 2 Abbreviated construction procedures for continuous flight auger piles and screw piles (*3,4*).

serted into the fresh grout by vibrating it into place after the auger has been completely withdrawn (Figure 2*c*). Obviously the grout or concrete must be designed to resist segregation caused by vibrating the cage.

With the SP, the borehole is formed by rotating a thick-flanged, single-turn auger into the soil without removing the soil (or removing as little as possible) (Figure 2*a*). Instead, the soil is compressed back into the sides of the borehole, especially if the soil possesses some cohesion, forming a screw "tap." When an SP borehole is driven in granular soils, some soil deforms inward ("possible cuttings" and "possible inflow") (Figures 2*a* and 2*b*). Once the maximum depth is reached, the reinforcing cage, if any, is placed through the hollow axle of the auger before any concrete is placed (Figure 2*b*). The axle typically has a larger diameter than the stem of the CFA pile, to accommodate cage placement. Finally, the auger is screwed out, reestablishing the tap pattern in areas where inflow or caving may have occurred. Simultaneously, concrete is added through the hollow core of the axle from a hopper affixed to the top of the axle, providing several meters of excess head for gravity flow of the concrete into the tapped borehole through the bottom of the axle (Figure 2*c*). The point of the auger, which protects the open axle during drilling, is left on the bottom of the borehole as the auger and axle are retracted, which also presumably ensures minimal disturbance of the bearing surface.

The shape of the CFA pile is generally cylindrical, whereas that of the screw pile is generally that of a cylindrical screw. Concrete strength and fluidity are important in the construction of both types of piles, but especially for the SP.

When installing either a CFA pile or SP the strategy is to ensure that effective stresses in the soil are maintained during both excavation and concrete placement. In Figure 2, horizontal effective stresses are measured at a hypothetical Point 0. During construction, effective stresses exist in two ways, as shown conceptually in Figure 3, which depicts the lateral earth pressure coefficient K′ as a function of the depth of the tip of the auger. In one scenario, depicted by the dashed line, the construction process produces a steadily increasing K′, except during the short period of time after the tip of the auger passes Point 0. Note especially that the effective stresses on withdrawal of the auger generally increase as a result of maintenance of high fluid-grout pressure; so, at the end of the process, the change in K′ ($\Delta K'$) is either zero or slightly positive. In the scenario depicted by the solid line, some stress relief occurs after the tip of the auger has passed Point 0, perhaps to inflowing, waterbearing sand. Reductions also occur during extraction of the auger, perhaps because sufficient pressure is not maintained in the grout during extraction or the auger is withdrawn too rapidly.

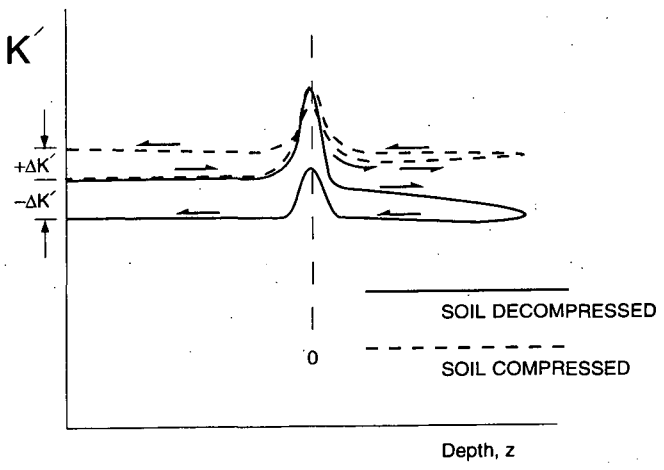

FIGURE 3 Change in lateral earth pressure coefficient during construction.

Quality Control

Maintenance of insufficient lateral stress in the soil may be accompanied by inward movement of the soil and loss of ground, which can be detrimental to adjacent structures. Maintenance of concrete or grout pressures lower than the total soil pressures beneath the extracting auger may cause necking and structurally defective piles. Instrumentation is frequently used in European practice to prevent these two phenomena. For example, the Enbesol instrumentation system, used to monitor augered pile construction by Soletanche, is shown in Figure 4. Four parameters are monitored: (*a*) machine torque as the auger is being inserted, (*b*) drilling rate, that is, penetration velocity, (*c*) concrete or grout pressure at the pump, and (*d*) ratio of actual to theoretical concrete or grout taken by the borehole.

These data are acquired by electronic sensing devices, and a continuous printout is usually provided to the drilling machine operator and kept for construction records. The operator and field engineer can use the data display diagnostically to correct errors in drilling. For example, if the grout pressure drops below the total vertical pressure in the soil at a given level and the actual/theoretical grout concrete take drops below 1, there is probably a necking problem in the pile. In order to correct the problem, the operator can stop auger extraction and concreting, redrill through the fluid concrete to below the level of the probable neck, then reintroduce the grout or concrete at the proper pressure (perhaps after increasing pump pressure), and extract the auger (perhaps more slowly than before). Other CFA systems used in Europe have similar automated data-acquisition systems.

In addition, penetration velocity data can be used to assess quality, and torque data can be used to verify crudely the soil profile and shaft resistance of the constructed pile.

The one difficulty with such real-time systems is that concrete or grout pressure is measured either at the pump or in the pump line at the top of the auger, so that an assumption must be made about head loss in the grout tube that extends through the stem of the auger. A device that measures pressure directly on the bottom of the auger would be better.

Variations

Several variations exist on the construction method described previously. One such promising variation has been applied by European contractors for several years: the use of an expandable body (*5*). The body consists of a folded, thin steel sleeve. With a CFA pile or an SP, the expanding body can be affixed to the bottom of the reinforcing cage. After introduction it fits between the bottom of the cage and the bottom of the borehole, where it then expands against the sides and base of the borehole when filled with grout under high pressure. Massarsch and Wetterling found significant increases in pile capacity (*5*).

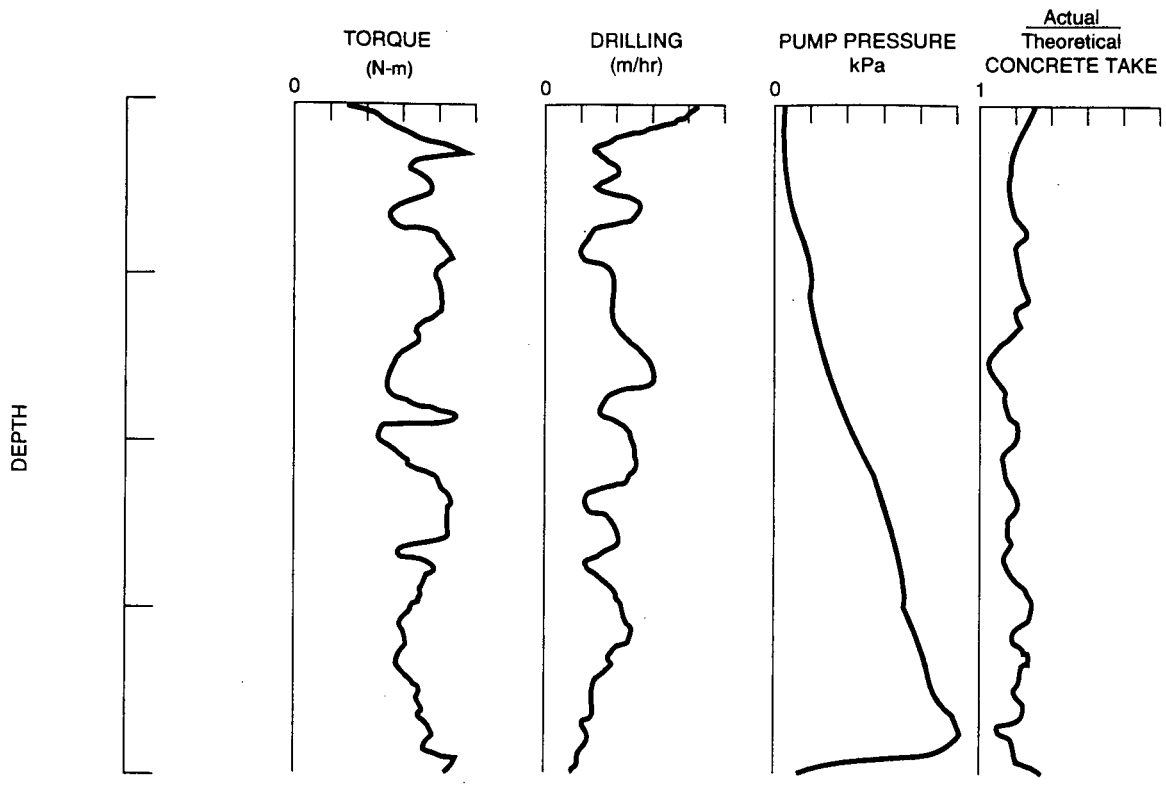

FIGURE 4 Monitored parameters during construction (*4*).

ENSURING NO SOIL DECOMPRESSION WITH CFA PILES

One of the key concerns when using CFA piles is that the soil surrounding the pile not be decompressed during drilling (i.e., effective ground stresses not be reduced through inward flowing of the soil). Viggiani (*6*) presents a simple analysis of the displacement produced by the hollow stem of the CFA auger, compared with the soil removed by the drilling action of the auger. If d_o = diameter of the auger stem (axle), and v = rate of downward penetration of the auger, the volume of soil displaced by the stem V_d in a time increment Δt is given by

$$V_d \doteq \frac{\pi d_o^2}{4} v \, \Delta t \tag{1}$$

The volume of soil removed by the rotating action of the auger V_r is given by

$$V_r = \frac{\pi}{4} (d^2 - d_o^2)(n \, p - v) \, \Delta t \tag{2}$$

where

d = outside diameter of the auger (flange tip to flange tip),
n = number of revolutions of the auger per unit of time, and
p = pitch of the auger in units of length (e.g., m per turn).

For there to be no soil decompression, $V_d \geq V_r$, so that

$$v \geq n \, p \left[1 - \frac{d_o^2}{d^2} \right] \tag{3}$$

If the velocity of penetration is less than the expression on the right in Equation 3, decompression can occur. In fact, decompression can occur even if the above condition is satisfied, if the soil being excavated is waterbearing sand with sufficient groundwater head to force the cuttings up the auger. A contractor must provide a drilling rig with sufficient torque and crowd to obtain the velocity of penetration in Equation 3. Otherwise, the equations for computing bearing capacity may not be conservative. According to Van Impe et al. (*7*), the same relationship can be used for screw piles.

ESTIMATION OF AXIAL CAPACITY OF CFA PILES

European and other engineers use several methods for estimating the static capacity of CFA augered piles.

German Standard

According to Rizkallah (*8*), the German standard for estimating capacity of augered, cast-in-place piles does not distinguish between bored piles (drilled shafts) and CFA piles. DIN 4014 (*9*) specifies computations based on the tip resistance, q_c, in the cone penetration test, as follows:

Sand

$$f_{max} = 0.008 \, q_c \tag{4}$$

$$q_{0.05}\ (\text{MPa}) = 0.12\ q_c + 0.1 \qquad (q_c \leq 25\ \text{MPa}) \tag{5}$$

where f_{max} is the maximum unit side shearing resistance on the pile, which has the nominal diameter of the auger, and $q_{0.05}$ is the unit end-bearing corresponding to a movement of 5 percent of the pile diameter, which, according to Reese and O'Neill (*10*) can be considered the deflection corresponding to end-bearing failure in bored piles. Note that the ultimate axial capacity of the pile is equal to the net unit base capacity $q_{0.05}$ times the base area, plus the unit shaft capacity f_{max} times the shaft area (taken in segments, if appropriate).

Clay

$$f_{max}\ (\text{MPa}) = 0.02 + 0.2\ c_u \quad (0.025 \leq c_u \leq 0.2\ \text{MPa}) \tag{6}$$

$$q_{0.05} = 6\ c_u \qquad (0.025 \leq c_u \leq 0.2\ \text{MPa}) \tag{7}$$

where the undrained shear strength c_u is given by Equation 8.

$$c_u = \frac{q_c - \sigma_{vz}}{16 - 22} \tag{8}$$

and σ_{vz} is the total vertical stress at the elevation of the bottom of the pile. Presumably, c_u could also be determined conservatively from unconfined compression tests, with $c_u = 0.5\ q_u$, where q_u = unconfined compression strength. This method is typical of other methods used currently in Europe.

Rizkallah compared the results of axial loading tests from a large data base and concluded that the above formulae were accurate for prediction of capacity of "nondisplacement" CFA piles and were conservative for predicting capacity of "displacement-type" screw piles.

Other Methods

Viggiani (*6*) suggests simple correlations for CFA piles in cohesionless pyroclastic soils, based on pile-loading tests and corresponding cone penetration tests in the Naples, Italy, area:

$$f_{max} = \alpha\ q_c \tag{9}$$

$$q_b = q_{c\ avg(+4d,-4d)} \tag{10}$$

where

q_b = net ultimate unit-bearing capacity of the pile base,
$q_{c\ avg(+4d,-4d)}$ = average CPT tip reading between 4 pile diameters above the base and 4 diameters below the base, and
α = a correlation factor given by Equation 11.

$$\alpha = \frac{6.6 + 0.32\ q_c\ (\text{MPa})}{300 + 60\ q_c\ (\text{MPa})} \tag{11}$$

Decourt (*11*) proposed a method for estimating the capacity of CFA piles in residual silts from the maximum torque measured when twisting a standard split-spoon sampler—after having been driven into the bottom of the sample borehole—as per a normal standard penetration test (SPT), to remove the influence of the dynamic driving conditions in the normal SPT. Correlations with loading tests indicate that

$$f_{max} = f_{max}(\text{SPT-T test}) \tag{12}$$

$$q_b = 0.5\ K'\ N_{cq} \tag{13}$$

where K' is a soil factor [0.10 MPa for clays, 0.12 MPa for clayey silts, 0.14 MPa for sandy silts, and 0.20 MPa for sands (at the base of the pile)] and N_{cq} is the average equivalent N value from the SPT-T (blows/0.3 m) test near the base of the pile, which can be taken as a dimensionless correlation factor. According to Decourt, in residual silts, $N_{cq} = T/1.2$, where T is the torque (in kgf-m, units reported in Decourt's original publication) measured by twisting the SPT split-spoon sampler. For large bored piles and barrettes, Decourt suggests that the corresponding values from Equations 12 and 13 be halved (for unit shaft resistance, Equation 12) and doubled (for base capacity, Equation 13).

D. O. Wong (personal communication, 1993) studied the load-settlement behavior of two CFA piles in the United States that were constructed in hydraulic fill that behaved as a normally consolidated clay. Wong concluded that $f_{max} = c_u$, where c_u is measured following the usual U.S. practice of recovering and testing cohesive soil samples using undrained compression tests. Reese et al. (*12*) describe tests on CFA piles at a site with a layered profile of normally consolidated and heavily overconsolidated clay. S.-T. Wang (personal communication, 1993) indicated that the parameters recommended by Reese and O'Neill (*10*) for estimating the capacities of bored piles provided accurate estimates of capacities of the augered piles at this test site, that is, on the average $f_{max} = 0.55\ c_u$ and unit bearing capacity = $9\ c_u$ (at pile base).

Neely (*13*), on review of "augercast" pile tests in sand from around the world, found that the unit shaft resistance was essentially independent of the relative density of the sand, which is consistent with Reese and O'Neill's study (*10*), which addresses only bored piles. Neely proposed that Equation 14 be used to evaluate average unit-shaft resistance, based on an analysis of 58 loading tests in sand:

$$f_{max}(avg) = \beta\ \sigma'_v(avg) \tag{14}$$

where β is a correlation factor given in Figure 5 (*13*) and $\sigma'_v(avg)$ is the average vertical effective stress in the soil between the pile head and base. It follows, then, that $f_{max}(avg)$ is the average unit-shaft resistance along the pile.

Neely, through analysis of the same data base, also proposed that the unit end-bearing resistance of CFA piles in sand, q_b, could be related to the uncorrected SPT value (N) in blows/0.3 m at the pile base, as follows:

$$q_b(\text{tsf}) = 1.9\ N \leq 75\ \text{tsf, or} \tag{15a}$$

$$q_b(\text{MPa}) = 0.19\ N \leq 7.5\ \text{MPa} \tag{15b}$$

ESTIMATION OF AXIAL CAPACITY OF SCREW PILES

Bustamante and Gianeselli (*14*) summarize procedures for calculating axial capacities of screw piles from in situ soil tests based on numerous correlations with field tests on such piles.

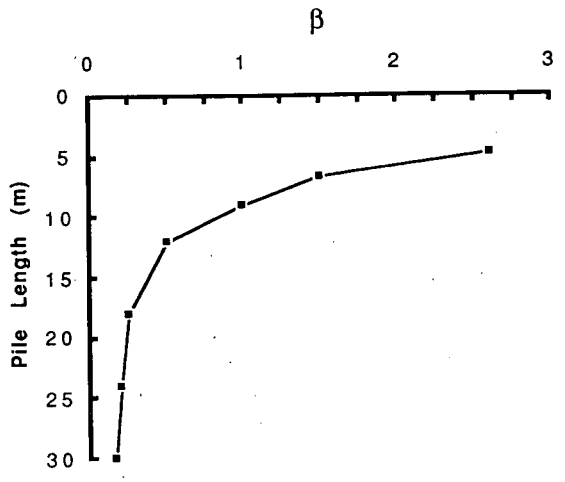

FIGURE 5 Correlation factor β versus pile length (*13*).

Base Capacity

The base capacity Q_b is computed in Equation 16:

$$Q_b(MN) = K A_b \alpha' \tag{16}$$

where

A_b = base area of the pile, conservatively estimated using diameter as 0.9 d, where d is the outside diameter of the flanges (m^2);
α' = adjusted ultimate base pressure factor [limit pressure p_L at pile base (MPa) for Menard-type pressuremeter, q_c at pile base for CPT (MPa), or SPT N value at pile base (blows/0.3 m)], and
K = dimensionless correlation factor from Table 1.

In each case an adjusted value of the in situ test parameter is taken for the computation of α', as follows:

Menard-Type Pressuremeter

$$p_L(\text{adjusted}) = [(p_L + a)(p_L)(p_L - a)]^{0.333} \tag{17}$$

where

$p_L + a$ = ultimate limit pressure at 0.5 m below base of pile,
$p_L - a$ = ultimate limit pressure at 0.5 m above base of pile, and
p_L = ultimate limit pressure at elevation of base of pile.

Cone Penetration Test

The following procedure is used to compute q_c(adjusted):

1. Smooth the q_c versus depth curve to eliminate local irregularities;
2. From the smoothed curve, determine mean q_c ($q_{c\,mean}$) from 1.5 pile diameters above the base of the pile to 1.5 diameters below the base of the pile;

TABLE 1 *K* Values for Various Geomaterials

Type of Geomaterial	Type of *In Situ* Test		
	Menard PMT	CPT	SPT
Clay	1.6 - 1.8	0.55 - 0.65	0.9 - 1.2
Sand	3.6 - 4.2	0.50 - 0.75	1.8 - 2.1
Gravels*	≥ 3.6	≥ 0.5	unknown
Chalk	≥ 2.4	≥ 0.6	≥ 2.6
Marl	≥ 2.4	≥ 0.7	≥ 1.2

* CPT and SPT results are questionable

3. Clip all q_c values < 0.7 $q_{c\,mean}$ and > 1.3 $q_{c\,mean}$; and
4. Compute q_c(adjusted) as the mean q_c value obtained from the clipped, smoothed q_c-depth curves within the depth interval indicated in Step 2.

Note that it is assumed that the M1 mechanical cone based on the International Society of Soil Mechanics and Foundation Engineering (ISSMFE) Standard TC-16 has been used to the obtain q_c values. However, if the electronic cone has been used, the values must be corrected according to Equation 18:

$$q_c(\text{M1}) = \beta\, q_c(\text{electronic}), \tag{18}$$

where β is 1.4 to 1.7 for cohesive soils and 1.3 for saturated sands.

Standard Penetration Test

$$N(\text{adjusted}) = 1000[(N_{+a})(N)(N_{-a})]^{0.333} \tag{19}$$

where

N = N in blows per 0.3 m, uncorrected, at elevation of pile base,
N_{+a} = N in blows per 0.3 m, uncorrected, at 0.5 m below pile base, and
N_{-a} = N in blows per 0.3 m, uncorrected, at 0.5 m above pile base.

Shaft Capacity

The ultimate shaft capacity, Q_s, is computed from Equation 20:

$$Q_{u,s} = \sum_{i=1}^{N} q_{si} S_{li} \tag{20}$$

where

q_{si} = ultimate unit shaft resistance (equivalent to f_{max}) in MPa in Segment i,
i = Segment number,
S_{li} = lateral or perimeter area of Segment i, using shaft diameter = 0.9d, and
N = total number of segments.

The value for q_{si} is chosen from Figure 6 (*14*), based on curve selection indicated in Table 2.

The expressions on the right-hand sides of Equations 16 and 20 can be added to give the ultimate pile capacity. The author

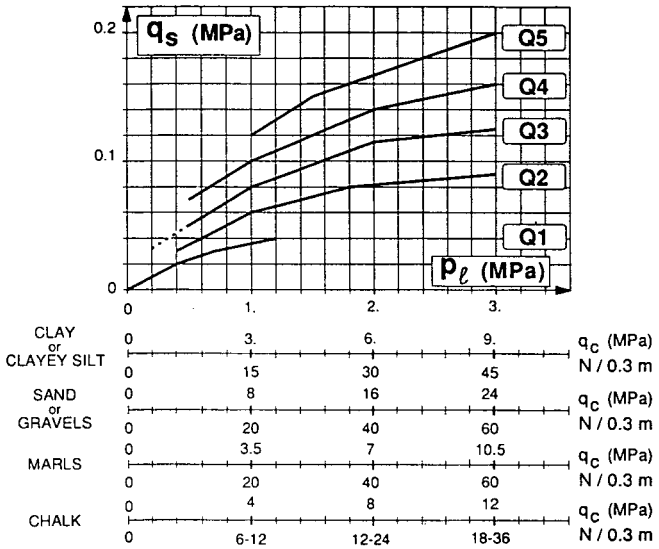

FIGURE 6 q_s (MPa) based on ultimate limit pressure from Menard-type pressuremeter, q_c from cone penetration test, and N (uncorrected) from standard penetration test (*14*).

TABLE 2 Suggested Curves To Be Used from Figure 6

Geomaterial	Range of Values for p_L and q_c		Applicable Curve (Fig. 6)
	p_L (MPa)	q_c (MPa)	
Clay, clayey silt	< 0.3	< 1.0	Q1
or sandy clay	≥ 0.5	≥ 1.5	Q3
	≥ 1.0	≥3.0	Q4
Sand or gravel	< 0.3	< 1.0	Q1
	> 0.5	> 3.5	Q4
	> 1.2	> 8.0	Q5
Chalk	≥ 0.5	≥ 1.5	Q4
	> 1.2	> 4.5	Q5
Marl	< 1.2	< 4.0	Q4
	≥ 1.5	≥ 4.0	Q5

Note that Table 2 refers only to cast-in-place screw piles, and not for piles that are cased.

suggests that a factor of safety of 2 be used on the result to assign allowable pile capacity. Where piles are used under settlement-sensitive structures, settlement at working load should be checked.

PILE SETTLEMENT

Recent studies focus on how to predict the settlement of augered piles and thereby estimate service-limit loads for the structures they support. One such method unique to CFA piles is described by Fleming (*15*), who uses hyperbolic functions to represent load-movement behavior of the shaft and base and considers elastic shortening of the pile. The reader is referred to that reference for further details.

CONCLUSION

Augered piles have been used successfully in Europe and elsewhere for transportation engineering. With the application of modern monitoring devices for concrete pressure, volume, and other parameters, and equations for static capacity, based on numerous correlations between values given by in situ testing tools and observed behavior of test piles, it is possible to use augered piles. A number of methods have been documented in this paper. Applications of foreign CFA practice by the U.S. transportation-engineering community should produce increased confidence in the use of augered piles for the construction of bridge and wall foundations.

ACKNOWLEDGMENTS

This paper was prepared under a contract from Earth Engineering and Sciences, Inc., with the cooperation of the FHWA Office of Research. The author appreciates the assistance of both organizations.

REFERENCES

1. EBA Engineering, Inc. *Final Report: Summary Results Obtained from the Auger Cast Piles Investigation.* Study DTFH 692-Q-00062. FHWA, U.S. Department of Transportation, 1992.
2. *Augered Cast-In-Place Piles Manual.* Deep Foundations Institute, Sparta, N.J., 1990.
3. *Screwed-In Atlas Piles,* Franki Atlas Palen, Koekelare, Belgium, n.d.
4. Frossard, A., A. Beaume, and J. P. Soulie. "Starsol-Enbesol: Bilan de Sept Années d'Existence - Point sur le Procédé Quatre Ans Après le Prix de l'Innovation FNTP, *Fondations Profondes,* Presses de l'École National des Ponts de Chaussées, Paris, France, 1991, pp. 51–58.
5. Massarsch, K. R., and S. Wetterling. Improvement of Augercast Pile Performance by Expander Body System. *Proc., Second International Conference on Deep Foundations on Bored and Auger Piles* (W. Van Impe, ed.), Balkema, Rotterdam, Netherlands, 1993, pp. 417–428.
6. Viggiani, C. Further Experiences with Auger Piles in the Naples Area. *Proc., Second International Conference on Deep Foundations on Bored and Auger Piles* (W. Van Impe, ed.), Balkema, Rotterdam, Netherlands, 1993, pp. 445–455.
7. Van Impe, W. F., H. Peiffer, and W. Haegeman. Considerations on the Effects of Installation on the Displacement Auger Pile Capacity. In *Fondations Profondes,* Presses de l'École National des Ponts et Chaussées, Paris, France, 1991, pp. 319–327.
8. Rizkallah, V. Comparison of Predicted and Measured Bearing Capacity of Auger Piles. *Proc., International Conference on Deep Foundations on Bored and Auger Piles,* Balkema, Rotterdam, Netherlands, 1988, pp. 471–475.
9. DIN 4014, Entwurf, Federal Republic of Germany, Feb. 1987.
10. Reese, L. C., and M. W. O'Neill. *Drilled Shafts: Construction Procedures and Design Methods.* Report FHWA-HI-88-042. U.S. Department of Transportation, 1988.
11. Decourt, L. Predicted and Measured Behavior of Non-Displacement Piles in Residual Soils. *Proc., Second International Conference on Deep Foundations on Bored and Auger Piles,* Balkema, Rotterdam, Netherlands, 1993, pp. 369–376.
12. Reese, L. C., S.-T. Wang, and R. Reuss. Tests of Auger Piles for the Design of Pile-Supported Rafts. *Proc., Second International Conference on Deep Foundations on Bored and Augered Piles,* Balkema, Rotterdam, Netherlands, 1993, pp. 343–346.
13. Neely, W. J. Bearing Capacity of Auger-Cast Piles in Sand. *Journal of Geotechnical Engineering,* ASCE, Vol. 117, No. 2, Feb. 1991, pp. 331–345.
14. Bustamante, M., and L. Gianeselli. Design of Auger Displacement Piles from In Situ Tests. *Proc., Second International Conference on Deep Foundations on Bored and Auger Piles,* Balkema, Rotterdam, Netherlands, 1993, pp. 21–34.
15. Fleming, W. G. K. A New Method for Single Pile Settlement Prediction and Analysis. *Geotechnique,* Vol. 42, No. 3, 1992, pp. 411–425.

Design and Construction of Auger-Cast Piles in Florida

MICHAEL MCVAY, BILIND ARMAGHANI, AND ROBERT CASPER

The use of augered cast-in-place piles has seen a tremendous growth in Florida because of the price and ease of installing them in coastal shell-filled sands. Discussed is the construction of augered cast-in-place piles, including equipment selection, drilling rate, grout fluidity, grout's aggregate size, grout pumping, and auger removal. Also presented is a comparison between a data base of 21 pile load tests (17 compression and 4 tension) from Florida and five design methods. Three of the methods were developed for augered cast-in-place piles, the other two for driven piles and drilled shafts. The predicted capacities of these methods were compared with three types of settlements of the piles' diameters. All of the methods compared most favorably to the 5 percent criterion. The drilled-shaft approach gave the best prediction for the whole data base, with a mean of 1.08 and a standard deviation of 0.28 for the ratios of predicted to measured capacity and, in the case of compression loadings only (17 piles), a mean of 0.98 and a standard deviation of 0.16. The latter finding suggests that augered case-in-place piles behave more like drilled shafts than driven piles because of the installation method.

The use of augered cast-in-place piles under 3- to 6-story structures has grown tremendously in Florida during the past 20 years. Problems with densification (vibration) and heave associated with driven piles in loose to dense sands do not occur with properly installed augered piles. Augered cast-in-place piles have been constructed with diameters of .31 m (12 in.) and lengths up to 6.1 m (20 ft) since the 1950s. However, with the advent of better drilling equipment, diameters varying from .41 m (16 ft) to .51 m (20 in.) and maximum depths ranging from 18.3 m (60 ft) to 24.4 m (80 ft) are achievable. Reinforcement may vary froma single high-strength rebar (Grade 60) at the top of the pile to a continuous steel cage, depending on loading (compression, tension-uplift, and lateral). Typical axial design loads (compression) for a single augered cast-in-place pile range from 445 kN (50 tons) to 890 kN (100 tons).

As with most drilled shafts, the quality of augered cast-in-place piles is strongly affected by their construction: equipment selection, drilling rate, grout fluidity, grout's aggregate size, grout pumping, and auger-removal process all significantly affect the quality of the pile and its load carrying capacity. In Florida it is common practice for an architect or engineer to ask prospective pile contractors for evidence that they have sucessfully installed augered cast-in-place piles under similar job and subsurface conditions. If there are questions regarding the quality or load-test results of installed piles, dynamic testing of pile integrity is usually performed as well.

Design of augered cast-in-place piles varies; the pile is either considered a drilled shaft or a large displacement-driven pile. Both effective- and total-stress methods are often used. Five of the most common design methods are presented and compared to a data base of 21 augered cast-in-place piles in Florida soils.

Department of Civil Engineering, University of Florida, Gainesville 32611.

CONSTRUCTION

An augered pile's capacity is strongly influenced by its construction. Augered cast-in-place piles are constructed using an electrically or hydraulically powered, continuous hollow-stem auger mounted on either a steel lattice or on pipe leads. The power supply and the auger both play a significant role in a successful pile installation. The power supply should be rated at or above 27 kN-m (20,000 ft-lb), and the auger should have pitch equal to one-half its diameter, for drilling in either cohesionless or cohesive soils. In cohesionless soils, the use of lower power torques and greater flight pitches may result in "weak drilling" (*1*). In this practice, which is not evident to the average client (*2*), the vertical speed of the auger, v, is less than the pitch of auger's flight, p, multiplied by the rotational speed of the auger, w (revolutions per minute). Since the auger's vertical flight speed is greater than the rate of auger penetration, soil is transported to the ground surface, loosening the soil adjacent to the auger and possibly resulting in the auger partially filling with soil. The diminished in situ stresses (soil loosenings) will result in a diminished pile capacity; the partially filled auger will cause the grout to flow up and down the auger, possibly contaminating the pile. The practice of "weak drilling" allows the contractor to employ less powerful, less expensive equipment; penetrate deeper depths; and have high production rates at the expense of pile capacity and quality control. Since cohesive soils are more difficult to drill because the soil adheres to the auger, use of higher power torques and lower flight pitch [such as 27 kN-m (20,000 ft-lb) and pitch equal to one-half the auger's diameter] will aid successful installation.

After reaching the required depth, the auger is usually raised approximately .61 m (2 ft) and grout is pumped in. The auger is then lowered to its original depth to establish a positive head of grout. Finally, the auger is raised while continuously pumping group out of the bottom or side of the hollow stem auger. Care must be exercised to maintain the grout head approximately 1.5 m (5 ft) to 3 m (10 ft) above the tip of the auger, to ensure that soil does not mix with the grout and the pile diameter does not neck inward. To maintain the positive grout head, 10 to 15 percent more than the theoretical volume is pumped in for each 1.5 m (5 ft) interval. The grout take of a pile segment is much more important than the average for the whole pile. Typical grout factor ratios of pumped to theoretical volumes are 1.4 to 1.5 for piles .35 m (14 in.) to .41 m (16 in.) in diameter constructed in sand (*1,3*). In the case of South Florida's cemented sands or Miami's oolites, which are vuggy (solution channels), a pressure gauge

mounted near the auger on the grout feed is monitored closely for pressure loss. The gauge indicates the loss of grout head at the auger tip but not the grout pressure in the pile (*2*). If the grout head is lost at any stage of the auger withdrawal, then the auger should be lowered 5 to 10 ft (1.5 to 3 m) into the grout and withdrawal reinitiated. When grouting has been completed as far as the ground surface, a single rebar or cage is placed while the grout is fluid. The reinforcement should be installed so it can move to the final depth of the pile without obstruction. In the event the steel is refused, the pile should be redrilled and re-grouted. The free advancement of the steel to the pile tip is one of the best indicators that inclusions have not occurred. The practice of dipping or scooping grout out of the top of the pile while the grout is still fluid, for example, when these are pile cutoff elevations below the ground surface, is not recommended. The practice has been known to contaminate the top portion of the pile with soil and cause pile failure. Piles should be cast to the drilling grade, allowed to set (harden or hydrate), and then cut off.

The grout used in augered cast-in-place piles must be of low enough viscosity to be pumped and of high enough viscosity to displace fines as the auger tip is extracted. The proportions by weight of cement, water, fine aggregate, and fly ash in a typical grout mix are 1: 0.59: 2.5: 0.15. This mix is very similar to ASTM C-109, which is used for mortar cube testing (but without fly ash). Fly ash is used in the grout mix for two reasons: it increases the fluidity of the grout, and it results in a hydrated grout that is less permeable. One disadvantage is that strength gain with time is slower with this grout mix than with a mix wherein an equivalent amount of cement is used in lieu of fly ash. Whereas the grain-size characteristic of the fine aggregate is considered important to preventing segregation problems by some researchers (*1*) it is not deemed important by others (*3*). Sands with a fineness modulus of about 1.2 are recommended. Plasticizers are added to increase fluidity, other additives to control shrinkage. The optimal grout viscosity for pumping and displacement of fines corresponds to flow rates of approximately 15 to 25 sec through an ASTM C939-81 cone fitted with an outlet 19 mm (¾ in.) in diameter. Typical compressive strengths are 27.6 MPa (4000 psi) after 28 days on 51 mm (2 in.) cubes. Samples usually are tested after 7 and 14 days as well.

DESIGN

During the past 15 years a number of different methods have been proposed to estimate the capacities of augered cast-in-place piles. The methods vary; some consider augered piles driven piles, others view them as drilled shafts. Lately, a number of design methods specific to augered piles have been proposed (*1*). What follows is a comparison of three commonly used methods as well as a drilled-shaft and a driven-pile approach for 21 Florida sites whose load tests were performed. Seventeen of the cases were compression loadings and four were tension loadings. Since all the methods are empirical, the predicted capacities were compared to failure as defined by Davisson (*4*), 2 percent, and 5 percent pile-diameter settlements. A brief discussion of each method is given first, followed by a summary of the data base.

Wright and Reese (1979)

In 1979 Wright and Reese (*5*) published a design method for constructing bored piles and augered cast-in-place piles in sand. The average mobilized skin friction stress on a pile is given by

$$fs = Po' \, Ks \tan \phi \qquad \leq 0.15 \text{ MPa (1.6 tsf)} \tag{1}$$

where

Po' = average effective stress along the pile,
Ks = lateral earth pressure coefficient (taken as 1.1), and
ϕ = angle of internal friction of the sand.

The ultimate tip stress for the pile is given by

$$q_{ip} = 2 \, N/3 \qquad \leq 3.8 \text{ MPa (40 tsf)} \tag{2}$$

where N is the standard penetration test (SPT) value at the pile tip. The skin and tip stresses are limited to 1.6 tsf and 3.8 MPa (40 tsf), respectively.

Neely (1991)

Neely (*1*), using a data base of augered cast-in-place piles founded in sand, established the following relationship for the average skin friction stress along a pile:

$$fs = \beta \, PO' \qquad \leq .13 \text{ MPa (1.4 tsf)} \tag{3}$$

where Po' is the average vertical effective stress along the pile and β is an empirical parameter. The β factor was found to be independent of the soil's relative density but a function of the pile's length, as given in Figure 1. Evident from the figure, β has a maximum value of 2.5 and a minimum value of 0.2, depending on total pile length. Using data from both compression and tension testing, Neely (*1*) estimates the ultimate pile tip stress at:

$$q_p = 1.9 \, N \qquad \leq 7.2 \text{ MPa (75 tsf)} \tag{4}$$

where N is the SPT value at the pile tip. The maximum skin friction and tip resistance are limited to 0.13 MPa (1.4 tsf) and 7.2 MPa (75 tsf), respectively. Both fs and q_p were limited by Neely to the recorded maximum data-base values.

Laboratorie Des Ponts et Chausses (LPC)

Bustamante and Gianeselli (*6*) in France have developed a design procedure for various pile types, including H, driven, and bored

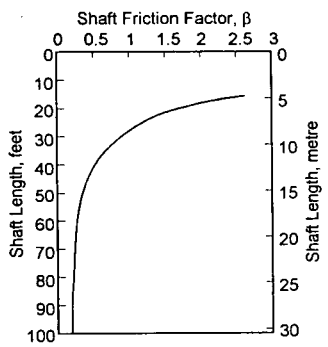

FIGURE 1 Mobilized skin friction coefficient, Neely (1991).

from a data base for use in both cohesive and cohesionless soils. The in situ cone-point resistance, *qc*, is used to calculate both the maximum side friction, *fs*, and the mobilized point resistance, q_p. For an augered cast-in-place pile, Figure 2(a) or 2(b) is used, depending upon soil type, to obtain the average skin friction stress, *fs*, for a particular soil layer. Each figure has two curves (upper and lower bounds), and *fs* is determined by interpolation between the two curves based on the average *qc* for the layer. Since only in situ SPT data were available for the data base evaluated in this paper, the following correlation was used between *qc* and the *N* values for Florida sands (*7*):

$$qc = 3.5 N \tag{5}$$

and, for clay,

$$qc = Su\ Nc + Po \tag{6}$$

where

Su = soil's undrained strength;
Nc = bearing capacity factor, usually taken as 17 (*8*) and
Po = total stress at the layer's center

The ultimate end bearing, q_p, of an augered cast-in-place pile founded in sand by the LPC approach is

$$q_p = 0.15\ qc \tag{7}$$

In the case of clays, LPC recommends an end bearing, q_p, of

$$q_p = 0.375\ qc \tag{8}$$

Reese and O'Neill (1988)

Under the sponsorship of FHWA, Reese and O'Neill (*9*) developed a design procedure for drilled shafts on the basis of an extensive data base for both cohesive and cohesionless soils. In the case of sands, the mobilized skin friction at a given point on the pile is given by

$$fs = K\ Po'\ \tan \phi \tag{9}$$

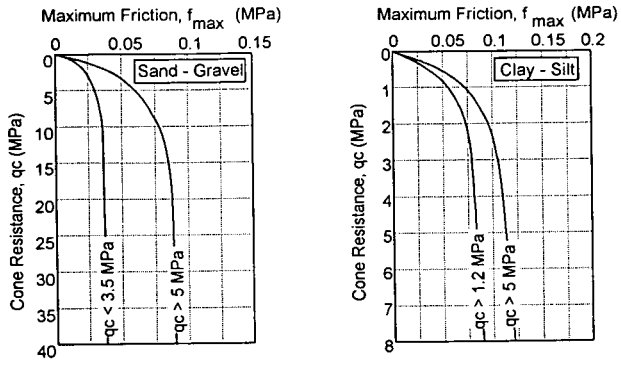

FIGURE 2 LPC's skin friction on pile from cone *qc* data: (*a*) *f* (versus) *qc* for sands; (*b*) *f* versus *qc* for clays.

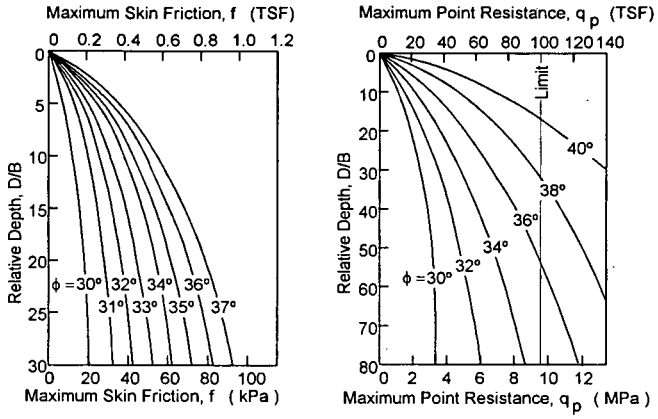

FIGURE 3 Coyle and Castello's pile capacity versus friction angle and embedment: (*a*) skin friction versus embedment; (*b*) end bearing versus embedment.

where, at the depth *z*,

Po' = effective stress,
K = earth pressure coefficient, and
ϕ = angle of internal friction of the soil.

K tan ϕ is replaced by β, given as

$$\beta = K \tan \phi = 1.5 - 0.135(Z)^{0.5} \qquad 0.25 \le \beta \le 1.2 \tag{10}$$

where *Z* is the depth in feet. Equation 10 must be substituted into Equation 9 and integrated over the entire depth of the pile to determine the mobilized skin friction on the pile.

The end bearing, q_p, is based on the SPT *N* value at the drilled shaft's tip, according to the following:

$$q_p = 0.6\ N \qquad 0 \le N \le 75, \text{ or} \tag{11}$$

$$q_p = 4.3 \text{ MPa (45 tsf)} \qquad N > 75 \tag{12}$$

In the case of cohesive soils, the average mobilized skin friction stress, *fs*, on the pile is determined from

$$fs = 0.55\ Su \qquad \le 0.26 \text{ MPa (2.75 tsf)} \tag{13}$$

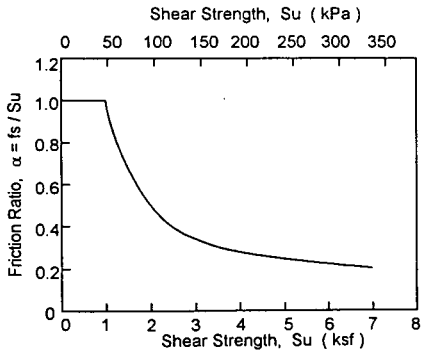

FIGURE 4 α versus undrained strength.

where Su is the average undrained strength along the pile. The end bearing resistance, q_p is determined as

$$q_p = Nc\ Su \qquad \leq 3.8 \text{ MPa (40 tsf)} \qquad (14)$$

where Nc is the bearing capacity factor and Su is the soil's undrained shear strength in the vicinity of the pile tip. A value of 9 is recommended for Nc (*9*).

Coyle and Castello (1981)

The only driven-pile approach to be presented is the one Coyle and Castello (*10*) developed to estimate pile capacities in sand based on a data base. To determine the average skin friction along the pile, Figure 3(a) is used with the angle of internal friction, ϕ, of the sand and the ratio of the pile's embedded depth, D, to its width, B. Coyle and Castello recommend that the angle of friction, ϕ, be obtained by correlation to SPT N on the basis of work by Peck et al. (*11*), if laboratory strength-data are unavailable. In the case of silty sands below the water table, Coyle and Castello recommend that the SPT N values first be corrected with the following expression:

$$N' = 15 + 0.5\ (N - 15) \qquad (15)$$

TABLE 1 Boring Logs

Pile No.	1	2	3	4	5	6	7	8	9	10	11
Location	Plm B.	T. Verd.	Ver. B.	Tr. Isl.	St. Pete.	W. Hav.	Ruskin	St. Pete.	St. Pete.	Tr. Isl.	St. Pete.
Dia. (mm)	.36	.36	.36	.36	.36	.36	.30	.36	.36	.36	.36
Length (m)	9.1	10.7	12.2	9.1	9.1	7.6	9.1	15.2	9.1	13.7	12.2
Depth (m)	SPT-N	SPT-N	SPT-N	SPT-N	SPT-N	SPT-N	SPT-N	SPT-N	SPT-N	SPT-N	SPT-N
1.5	14	18	5	38	16	2	19	30	14	38	30
3.0	5	15	8	22	46	16	15	65	48	22	65
4.6	40	21	10	17	18	20	28	30	45	17	30
6.1	2	30	17	43	2	25	35	14	40	42	14
7.6	40	15	80	21	64	29	25	15	31	21	15
9.1	32	25	33	17	31	25	28	9	29	17	9
10.7		20	15	4	71	34	42	11	32	4	18
12.2			19	3	50	37		23	25	24	23
13.7			45	24				11	2	3	11
15.2			60	3				30	10	11	80
16.8			34	11				60		18	30
18.3			23	18				18			18
19.8								36			36

Pile No.	12	13	14	15	16	17	18	19	20	21
Location	Tampa	Jacks.	Savana	St. Aug.	Palatka	Cocoa	Poinc.	Palm B.	Tallah.	Tallah..
Dia. (mm)	.36	.36	.41	.46	.41	.36	.36	.36	.36	.36
Length (m)	12.2	7.6	13.7	10.7	12.2	9.1	10.7	10.7	21.3	25.9
Depth (m)	SPT-N	SPT-N	SPT-N	SPT-N	SPT-N	SPT-N	SPT-N	SPT-N	SPT-N	SPT-N
1.5	4	7	4	6	11	7	4	31	N.A.[a]	N.A.
3.0	1	9	5	4	12	9	21	39	N.A.	N.A.
4.6	1	8	18	34	17	12	17	40	N.A.	N.A.
6.1	5	35	26	17	14	34	15	28	N.A.	N.A.
7.6	28	26	42	21	49	36	11	17	N.A.	N.A.
9.1	15	19	32	11	62	39	4	2	N.A.	N.A.
10.7	8		36	21	92	37	14	41	N.A.	N.A.
12.2	50		13	14	75	38	41		N.A.	N.A.
13.7	50		16		68		51		N.A.	N.A.
15.2	80		21		82		15		N.A.	N.A.
16.8							5		N.A.	N.A.
18.3							22		N.A.	N.A.
19.8										

NOTE: 0.3048 m = 1 ft 25.4 mm = 1 in 0.1572 kN/m^3 = 1 lb/ft^3
[a] N.A. = Not Available

The mobilized end bearing, q_p, on the pile is found from Figure 3(b), a plot of q_p versus D/B as a function of the friction angle. A maximum end resistance of 100 tsf is stipulated for piles founded in sand.

In the case of clays, Tomlinson's method (*12*) is recommended. The average skin friction stress, *fs*, is given by

$$fs = \alpha\ Su \tag{16}$$

Alpha, which varies between 0.2 and 1.0, is given in Figure 4 as a function of clay layer's undrained shear strength, *Su*. The end-bearing stress, q_p, is given by

$$q_p = 9\ Su \tag{17}$$

where *Su* is the undrained strength of the clay layer.

DATA BASE

The locations and dimensions of the 21 augered cast-in-place piles studied are presented in Table 1. The first 19 sites were located in sands, and the last 2 were found in clays. Cases 1, 4, 8, and 19 were tension (pullout) tests and the rest were compression tests. The uncorrected SPT data are given for each of the sand sites. Table 2 lists the location of the water table and total unit weights. Also provided are the soils' internal angle of friction, based on work by Peck et al. (*11*) for sand sites, and the laboratory-measured, undrained shear strength for clay sites.

Presented in Table 3 are the predicted capacities for the 21 sites for each of the design methods using the soil information provided in Tables 1 and 2. *Qs* is the predicted skin friction, *Qp* is the tip

TABLE 2 Soil Properties

Pile No.	1	2	3	4	5	6	7	8	9	10	11
Location	Plm B.	T. Verd.	Ver. B.	Tr. Isl.	St. Pete.	W. Hav.	Ruskin	St. Pete.	St. Pete.	Tr. Isl.	St. Pete.
UW (kN/m³)	18.1	18.1	18.1	18.1	18.9	18.1	18.1	18.9	18.9	18.1	18.9
GWT (m)	.3	.3	2.7	1.5	2.1	2.1	2.1	.3	.3	1.2	7.6
Depth (m)	Phi	Phi	Phi	Phi	Phi	Phi	Phi	Phi	Phi	Phi	Phi
1.5	31	33	28	38	32	27	33	36	31	38	36
3.0	28	32	29	34	40	32	32	43	40	34	43
4.6	39	34	30	32	33	33	36	36	40	32	36
6.1	27	36	32	39	27	35	37	31	39	39	31
7.6	39	32	45	34	43	36	35	32	36	34	32
9.1	37	35	37	32	36	35	36	30	36	32	30
10.7		33	32	28	44	37	39	30	37	28	33
12.2			33	27	41	38		34	35	34	34
13.7								30	27	27	30
15.2								36	30	30	45
16.8											
18.3											
19.8											

Pile No.	12	13	14	15	16	17	18	19	20	21
Location	Tampa	Jacks.	Savana	St. Aug.	Palatka	Cocoa	Poinc.	Palm B.	Tallah.	Tallah..
UW (kN/m³)	18.1	18.1	18.1	18.1	18.9	18.9	18.1	18.1	17.3	17.3
GWT (m)	3.4	1.5	1.5	1.5	2.1	2.1	2.1	2.1	2.1	2.1
Depth (m)	Phi	Phi	Phi	Phi	Phi	Phi	Phi	Phi	Su (kPa)	Su (kPa)
1.5	28	29	28	29	30	29	28	36		
3.0	27	30	28	28	31	30	34	38		
4.6	27	29	33	37	32	31	32	39	57.4	57.4
6.1	28	37	35	32	31	37	32	36		
7.6	36	35	39	34	40	38	30	32	62.2	62.2
9.1	32	33	37	30	43	38	28	27		
10.7	29		38	34	47	38	31	39	86.2	86.2
12.2	41		31	31	45	38	39	26		
13.7								26		
15.2								36	119.7	119.7
16.8										
18.3									129.3	129.3
19.8										

NOTE: 0.3048 m = 1 ft 47.88 kN/m² = 1 ksf 0.1572 kN/m³ = 1 lb/ft³

TABLE 3 Pile Capacities

Predicted Capacities (kiloNewtons)							Measured Capacities (kiloNewtons)		
Pile No.	Capacity	Wright	Neely	LPC	FHWA	Coyle	2% Dia.	Davisson	5% Dia.
	Qs	338	418	587	391	489	196	205	294
1	Qp	205	578	160	205	516			
Tension	Qt	543	996	747	596	1005			
	Qs	445	436	774	525	498			
2	Qp	125	365	98	125	952			
	Qt	570	801	872	649	1450	436	365	560
	Qs	801	614	1014	898	489			
3	Qp	125	347	98	98	952			
	Qt	925	961	1112	996	1441	1005	970	979
	Qs	489	516	890	569	480			
4	Qp	107	311	89	80	267			
Tension	Qt	596	827	979	649	747			
	Qs	489	569	872	560	454			
5	Qp	196	560	151	169	943			
	Qt	685	1130	1023	729	1397	445	400	667
	Qs	320	578	605	427	302			
6	Qp	187	525	142	151	552			
	Qt	507	1103	747	578	854	649	578	783
	Qs	391	489	658	480	454			
7	Qp	133	374	107	107	658			
	Qt	525	863	765	587	1112	498	454	694
	Qs	881	427	996	898	694	285	249	445
8	Qp	187	543	151	116	952			
Tension	Qt	1068	970	1148	1014	1646			
	Qs	391	418	898	569	614			
9	Qp	187	525	142	169	943			
	Qt	578	943	1041	738	1557	569	623	818
	Qs	810	480	1103	890	676			
10	Qp	18	53	18	18	294			
	Qt	827	534	1121	907	970	783	667	890
	Qs	1112	827	1156	1130	952			
11	Qp	142	418	116	116	890			
	Qt	1254	1245	1272	1245	1841	1050	827	1201
	Qs	845	623	916	952	356			
12	Qp	320	712	249	285	667			
	Qt	1165	1334	1165	1237	1023	934	1139	1156

(continued on next page)

resistance, and *Qt* is their sum. None of the SPT data were corrected for overburden, and the pile-tip capacities were based on *N* values measured at the pile tip. Also given in the table are the measured capacities determined from load-test data by the Davisson method (*4*) as well as the measured loads at the pile top for settlements of 2 percent and 5 percent of the pile diameters. Neither Wright's nor Neely's methods are applicable, since the methods apply only to sands. The *K* value of 1.1 was used in the Wright and Reese approach for all cases. For each design approach, Table 4 presents the ratio of the predicted to measured capacities for each failure criterion and case. Also given at the bottom of Table 4 are the mean and standard deviation for the various failure criteria, considering all piles in the data base and considering compression piles only. It is evident from comparing mean values that the 5 percent failure criterion compares much more favorably than the 2 percent Davisson criteria—for all 5 prediction methods. Also apparent is that all of the methods compare much more favorably if the tension piles are not considered.

Presented in Figure 5 are the predicted versus measured capacities (5 percent settlement) for each design method for all piles in the data base. It is evident from Table 4 and Figure 5 that the methods proposed by Wright and FHWA (a standard deviation less than 29 percent) are the best methods of predicting the failure capacity, whereas Coyle's driven-pile approach is too high. The finding may suggest that augered cast-in-place piles behave more like drilled shafts than like driven piles. Using the 5 percent failure

TABLE 3 *(continued)*

Predicted Capacities (kiloNewtons)							Measured Capacities (kiloNewtons)		
Pile No.	Capacity	Wright	Neely	LPC	FHWA	Coyle	2% Dia.	Davisson	5% Dia.
	Qs	329	516	641	489	258			
13	Qp	142	400	107	125	952			
	Qt	471	916	747	614	1210	712	445	712
	Qs	979	569	1272	925	792			
14	Qp	133	374	107	116	685			
	Qt	1112	943	1379	1041	1477	979	979	979
	Qs	623	641	979	649	418			
15	Qp	222	632	169	196	605			
	Qt	845	1272	1148	845	1023	578	596	890
	Qs	961	614	1406	845	756			
16	Qp	623	934	489	552	1245			
	Qt	1583	1548	1895	1397	2002	1779	1245	1975
	Qs	418	525	774	560	463			
17	Qp	249	703	196	214	952			
	Qt	667	1228	970	774	1414	890	694	979
	Qs	480	525	649	703	489			
18	Qp	89	249	71	80	952			
	Qt	569	774	721	783	1441	391	302	560
	Qs	560	525	907	703	596	445	445	667
19	Qp	258	712	205	231	952			
Tension	Qt	818	1237	1112	934	1548			
	Qs	N.A.[a]	N.A.	1824	1414	1343			
20	Qp	N.A.	N.A.	116	196	169			
	Qt	N.A.	N.A.	1939	1610	1512	1646	1557	1690
	Qs	N.A.	N.A.	2002	1984	1637			
21	Qp	N.A.	N.A.	133	222	196			
	Qt	N.A.	N.A.	2135	2206	1833	1557	1557	2135

NOTE: 8.9 kN = 1 ton

[a] N.A. = Not Available

criterion, the design load (approximately 50 percent of capacity) would generally result in a settlement of less than 9 mm (0.35 in.), which most structures could sustain without damage (that is, no load-settlement approach is needed).

CONCLUSIONS

Augered cast-in-place piles are being used more and more in Florida, especially on the coast. They are used mainly under three- to six-story structures and provide uplift resistance in the event of a hurricane. They are much easier to install in the coastal, shell-filled sands than are driven, prestressed concrete piles, and they are usually less expensive. However, care in the construction of augered cast-in-place piles is important. It was identified that equipment selection, drilling rate, grout fluidity, grout's aggregate size, grout pumping, and auger removal process all significantly affect both the quality and load-carrying capacity of the pile. For instance, to prevent "weak drilling" in cohesionless sands or premature refusal in fat clays, 27 kN-m (20,000 ft-lb) power torques should be used with the auger's flight pitch equal to one-half its diameter. Grout factors between 1.2 and 1.5 should be measured. Loss of pressure on the grout feed is a good indication that there is a problem that can be corrected only by relowering the auger.

Also presented in the paper were a comparison between a data base of 21 augered cast-in-place piles (17 compression and 4 tension) and five design approaches. Three of the methods were developed for augered cast-in-place piles, the other two for driven piles and drilled shafts. The predicted capacities of various designs were compared with three different failure capacities determined from the load-settlement curves. The failure criteria used were Davisson's 2-percent and 5-percent settlements of the piles' diameter. All of the methods compared most favorably with the 5 percent criterion. Those methods proposed by Reese and O'Neill (FHWA) and by Wright and Reese gave the best predictions of capacities at settlements of 5 percent of the pile diameters. Typical ratios of predicted to measured capacity were from 0.95 to 1.04, with an average standard deviation of only 29 percent for compression and tension piles. In the case of compression loading only (17 piles), FHWA gave a mean of 0.98 with a standard deviation

TABLE 4 Ratio of Predicted to Measured Capacities

	Wright			Neely			LPC			FHWA			Coyle		
Pile No.	Davisson	2% Dia.	5% Dia.	Davisson	2% Dia.	5% Dia.	Davisson	2% Dia.	5% Dia.	Davisson	2% Dia.	5% Dia.	Davisson	2% Dia.	5% Dia.
1	1.71	1.64	1.14	2.15	2.06	1.43	3.00	2.87	2.00	2.00	1.91	1.33	2.50	2.39	1.67
2	1.30	1.56	1.01	1.82	2.18	1.42	2.01	2.40	1.56	1.49	1.78	1.16	3.33	3.98	2.59
3	0.92	0.95	0.95	0.95	0.99	0.98	1.11	1.15	1.14	0.99	1.03	1.02	1.43	1.49	1.47
4	0.81	0.87	0.70	0.86	0.92	0.75	1.47	1.58	1.28	0.94	1.02	0.82	0.79	0.86	0.69
5	1.55	1.72	1.03	2.54	2.82	1.69	2.30	2.55	1.53	1.64	1.82	1.09	3.14	3.49	2.09
6	0.77	0.87	0.64	1.69	1.90	1.41	1.15	1.29	0.96	0.89	1.00	0.74	1.32	1.48	1.09
7	1.04	1.14	0.75	1.72	1.89	1.24	1.52	1.67	1.09	1.18	1.29	0.85	2.23	2.45	1.60
8	3.10	3.54	1.98	1.51	1.72	0.96	3.49	3.99	2.24	3.16	3.61	2.02	2.44	2.79	1.56
9	1.01	0.93	0.71	1.66	1.52	1.15	1.83	1.68	1.28	1.30	1.19	0.90	2.73	2.50	1.90
10	1.06	1.25	0.94	0.69	0.81	0.61	1.42	1.67	1.25	1.16	1.36	1.02	1.24	1.45	1.09
11	1.19	1.52	1.04	1.18	1.50	1.03	1.21	1.54	1.06	1.19	1.51	1.04	1.75	2.23	1.53
12	1.24	1.02	1.00	1.43	1.17	1.15	1.25	1.02	1.01	1.32	1.09	1.07	1.10	0.90	0.88
13	0.66	1.05	0.66	1.28	2.05	1.28	1.06	1.69	1.06	0.86	1.38	0.86	1.70	2.72	1.70
14	1.13	1.13	1.13	0.97	0.97	0.97	1.41	1.41	1.41	1.06	1.06	1.06	1.51	1.51	1.51
15	1.46	1.41	0.95	2.19	2.13	1.43	1.99	1.93	1.29	1.46	1.42	0.95	1.77	1.72	1.15
16	0.89	1.27	0.80	0.87	1.24	0.78	1.07	1.52	0.96	0.79	1.12	0.71	1.13	1.61	1.01
17	0.75	0.96	0.68	1.38	1.77	1.25	1.08	1.39	0.99	0.87	1.12	0.79	1.59	2.04	1.45
18	1.46	1.90	1.02	1.99	2.57	1.39	1.84	2.38	1.29	2.00	2.59	1.40	3.68	4.76	2.57
19	1.26	1.26	0.84	1.18	1.18	0.79	2.03	2.03	1.36	1.58	1.58	1.05	1.34	1.34	0.89
20	N.A.	N.A.	N.A.	N.A.	N.A.	N.A.	1.18	1.25	1.15	0.98	1.03	0.95	0.92	0.97	0.89
21	N.A.	N.A.	N.A.	N.A.	N.A.	N.A.	1.40	1.40	1.02	1.42	1.42	1.03	1.18	1.18	0.86
i. Mean	1.23	1.37	0.95	1.48	1.65	1.14	1.66	1.83	1.28	1.35	1.49	1.04	1.85	2.09	1.44
St. Dev.	0.52	0.59	0.29	0.50	0.56	0.28	0.63	0.68	0.32	0.53	0.61	0.28	0.81	1.01	0.52
ii. Mean	1.10	1.24	0.89	1.49	1.70	1.19	1.46	1.64	1.18	1.21	1.36	0.98	1.87	2.14	1.49
St. Dev.	0.26	0.30	0.16	0.50	0.58	0.27	0.38	0.43	0.19	0.31	0.39	0.16	0.93	1.05	0.53

i. includes both compression and tension piles
ii. includes compression piles only
N.A. - not applicable

of 0.16, and Wright gave a mean of 0.89 with a standard deviation of 0.16. Another important conclusion from the case studies is that augered cast-in-place piles behave more as drilled shafts than as driven piles. The use of 5 percent of the pile's diameter for the failure criterion is believed to be acceptable for typical augered cast-in-place piles in the .30 m (12 in.) to .41 m (16 in.) range, since settlements of 7.6 mm (.3 in.) to 10.2 mm (0.4 in.) are considered acceptable for most structures.

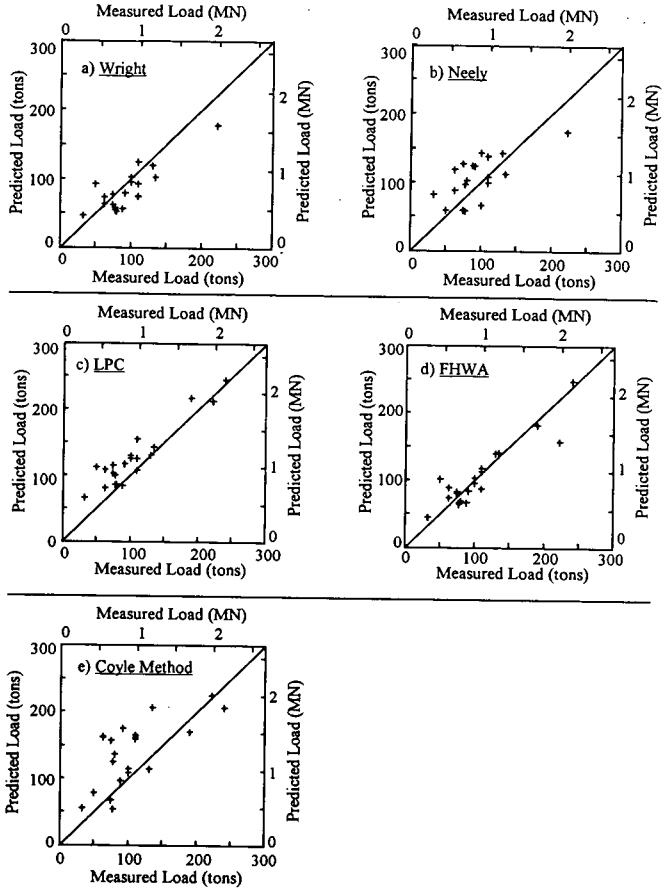

FIGURE 5 Predicted versus measured capacities at 5 percent pile diameter settlement.

ACKNOWLEDGMENTS

The authors would like to acknowledge the following corporations for providing the valuable case histories in the data base: Ardaman & Associates, Inc. of Orlando, Ft. Myers, and Tallahassee; Foundation Services, Inc. of Orlando; Law Engineering, Inc. of Jacksonville and Tampa; West Coast Foundations, Inc. of St. Petersburg; and Williams Earth Sciences, Inc. of Clearwater.

REFERENCES

1. W. J. Neely. Installation, Design and Quality Control of Auger Cast Piles. *Pile Buck*, Jupiter, Fla., Dec. 1991,pp. 2B–24B.
2. Van Weele, A.F. Cast-in-situ Piles—Installation Methods, Soil Disturbance and Resulting Pile Behavior. *Proc., 1st International Geotechnical Seminar on Deep Foundations on Bored and Auger Piles.* Ghent, Belgium. Balkema, Rottersdam, Netherlands, 1988, pp. 219–226.
3. *Augered Cast-In-Place Piles Manual.* Committee on Augered Cast-In-Place Pile Committee, Deep Foundation Institute, Sparta, N.J., 1990.
4. Sharp, M. R., M. C. McVay, F. C. Townsend, and C. R. Barnett. Evaluation of Pile Capacity from In Situ Test. *Geotechnical Special Publication No. 17*, ASCE, 1988, pp. 134–156.
5. Wright, S. J., and L. C. Reese. Design of Large Diameter Bored Piles. *Ground Engineering*, London, United Kingdom, Vol. 12, No. 8, 1979, pp. 47–51.
6. Bustamante, M., and L. Gianeselli. Portance Reele et Portance Calculée des Pieux Isolés, Sollicités Verticalement. *Revue Francaise de Geotechnique*, No. 16, 1981.
7. Schmertmann, J. H. *Guidelines for Use in the Soils Investigation and Design of Foundations for Bridge Structures in the State of Florida.* Research Bulletin 121-A. Florida Department of Transportation, Gainesville, 1967.
8. Lunne, T., and A. Kleven. Role of CPT in North Sea Foundation Engineering. *Symposium on Cone Penetration Testing and Experience.* Geotechnical Engineering Division, ASCE, Oct. 1981, pp. 49–75.
9. Reese, L., and M. O'Neill. *Drilled Shafts, Student Workbook.* Publication FHWA-HI-88-042. FHWA, U.S. Department of Transportation 1988.
10. Coyle, H. M., and R. Castello. New Design Correlations for Piles in Sand. *Journal of the Geotechnical Engineering Division*, ASCE, Vol. 107, No. GT 7, 1981, pp. 965–986.
11. Peck, R., W. E. Hansen, and T. H. Thornburn. *Foundation Engineering.* John Wiley and Sons, Inc., New York, N.Y., 1974.
12. Tomlinson, M. J. The Adhesion of Piles Driven in Clay Soils. *Proc., 4th International Conference on Soil Mechanics and Foundation Engineering*, London, England. Butterworths Scientific Publications, Ltd., London, England, Vol. 2, 1957, pp. 66–71.

Reduced Impact on Adjacent Structures Using Augered Cast-In-Place Piles

HUGH S. LACY, JOEL MOSKOWITZ, AND STANLEY MERJAN

In many cases when deep foundations are necessary to support a new structure, driven piles or other traditional support systems are inappropriate to use because of the need to protect existing structures. Often, vibrations or vibration-induced settlement that result from pile installation are major concerns. A number of projects are reviewed in which augered cast-in-place (ACIP) piles were found to be effective alternatives to other support systems. Case histories also illustrate some of the problems that can arise when using ACIP piles. A checklist is provided to assist those who are preparing to install ACIP piles and want to avoid unnecessary problems.

Pile driving often causes vibrations with peak particle velocities that are too low to structurally damage buildings but sometimes causes densification of already medium dense sands (*1*), resulting in differential settlement and damage to adjacent structures. In many of the case histories cited herein, augered cast-in-place (ACIP) piles were used as an alternative pile type after significant settlement of adjacent structures during pile driving. For example, Table 1 illustrates projects for which ACIP piles were substituted for driven piles. Designers are increasingly specifying low vibration drilled-in piles or piers for projects adjacent to vibration-sensitive structures. ACIP piles are one of the types of piles being used to address this problem.

INSTALLATION OF ACIP PILES

An ACIP pile is installed by drilling a hole with a continuous-flight hollow-stem auger, which is plugged at the toe, to a predetermined depth. To protect adjacent structures, it is desirable to screw the augers into the ground with the least amount of soil being raised to the ground surface on the auger blades in order to avoid significant loss of ground around the pile. Fluid grout is pumped into the auger stem under sufficient pressure to eject the plug and to start forcing grout upward in the auger flights. To prevent collapse of the hole, the auger is slowly withdrawn while grout is continuously pumped. The completed grout column forms a cast-in-place pile. A single reinforcing bar can be installed through the hollow stem in advance of grouting, or 5-m-long reinforcing cages, small H-sections, or pipes can be inserted directly into the grout column while the grout is still fluid. It is necessary to provide 50 mm or more clearance. Installing longer steel members has proven difficult.

DEVELOPMENT OF ACIP PILES

The equipment and techniques to construct ACIP piles have evolved since the pile's inception by Intrusion-Prepakt, Inc. in the 1940s (*2*).

H. S. Lacy and J. Moskowitz, Mueser Rutledge Consulting Engineers, 708 Third Avenue, New York, N.Y. 10017. S. Merjan, Underpinning & Foundation Constructors, Inc., 46–36 54th Road, Maspeth, N.Y. 11378.

In its early form, the pile was constructed by placing grout through a pipe into an open augered hole. Depth was limited to about 6 m for a 305-mm diameter pile by available equipment. One modification to the method was to place coarse aggregate in the open hole after the grout pipe was inserted and allow the grout to intrude into the aggregate. Alternatively, piles were formed by grouting through a separately drilled pipe into the bottom of the augered hole as the auger was withdrawn.

Raymond Patterson was granted a patent in 1956 for these techniques and a method for placing grout through a hollow-stem auger with a removable plug at the toe of the auger, the basic methodology still in use. Augers are commonly powered by hydraulic systems capable of installing piles that are 508 mm or more in diameter to depths of more than 38 m. Equipment varies from low-torque, high-velocity turntables to high-torque, low-velocity equipment capable of virtually screwing the auger into the ground.

The size of the hollow stem increased in the 1960s with the development of pumps that could pump grout containing coarse sand aggregate. Pumps are now available that can pump grout containing pea-gravel aggregate. Hollow stems are now of sufficient size to permit installation of a central reinforcing bar without interfering with grout placement. Other, more innovations in equipment include computerized systems that monitor grout pressure and volume, auger rotation speed, torque, and depth.

ACIP piles are used for conventional foundation support elements, both vertical and battered, as underpinning piles, and as tangent soldier piles to form a continuous earth support system in conjunction with wales and tiebacks. Use of the system demands a thorough subsurface investigation to determine depth to the bearing stratum and the materials to be penetrated. Boulders or other obstructions may cause problems. Pile load-tests, usually to three times the design load, or failure, are recommended because the piles are installed to a predetermined depth without verifying resistance to penetration, as is done with driven piles. An experienced contractor, proper equipment, quality-control measures and detailed inspection of a site are requisites to successful completion of difficult projects.

ACIP piles are used throughout the United States, especially in the Midwest. They are also common in Europe and in parts of Africa. They are often referred to by the proprietary names of individual contractors who install them. The name augered cast-in-place piles is a generic name adopted by the Deep Foundations Institute's Committee on Augered Cast-In-Place Piles (*2*).

WHY INSPECTION AND INSTALLATION METHODS ARE IMPORTANT

Table 1 and several case histories illustrate that the ACIP pile-installation method, especially within certain types of soil or

TABLE 1 Settlement of Structures During Pile Driving and Following Substitution of ACIP Piles

Project		Soil		Initial Pile			ACIP PILE		
No.	Location	Type	Ave N	Type	Distance From Structure	Settlement of Structure	Dia. mm	Distance From Structure	Settlement of Structure
1	Manhattan	m-c sand tr.silt	20	TPT[2]	3m+	6mm	406	1m	0
2	Southern Brooklyn,NY	m-f sand	23	273mm pipe	8m	70mm	356	3m	38mm
3	Manhattan	m sand tr.silt	20	TPT[2]	8m	0	406	1m	0
4	Southern Nassau Co. NY[1]	m-f sand	25	-	-	-	508	1.5m	0
5	Brooklyn,NY	m-f sand	20	wood piles	0.7m+	6mm	305	0.5m	0
6	West Brooklyn	m-f sand	25 45	14HP73	1m	61mm	356	1m	0
7	Tri-beca Manhattan	f-c sand tr.silt	25	203mm O.E.[3]	6m+ most 1.5m few	70mm	406	1.2m	25mm

Notes: (1) ACIP piles were specified due to vibration sensitive equipment in an adjacent building.
(2) TPT - Tapered Pile Tip pile used by Underpinning and Foundation Constructors, Inc., Maspeth, NY.
(3) O.E. - Open-end pipe pile

groundwater conditions, can result in the detrimental settlement of adjacent structures. Methods for reducing detrimental settlement, by minimizing the amount of soil removed during insertion of the auger, for example, are described in two of the case histories.

The continuous integrity of an ACIP pile usually is controlled by monitoring the volume of grout pumped for each 1.5 m of auger withdrawal. It is common to require 110 percent of the neat volume of the augered hole with reduced rates, but continuous pumping for the last 1.5 to 3 m of auger withdrawal below the ground surface—even though grout is usually flowing onto the ground from around the auger flights. Pile installation also appears to be more successful if the auger is withdrawn slowly and continuously instead of removed more quickly in interrupted increments. Grout pressure in the hose close to the auger is monitored to identify quickly any blockage of flow and to ensure continuity from pile to pile.

PILE CAPACITY

A range of pile capacities has been verified through load tests. Load tests performed on ACIP piles of varying diameter (*3*) are illustrated in Figure 1. Only three of these piles were loaded to soil failure. Load tests commonly were carried to three times the planned design load. Design loads generally ranged from 222 to 534 kN (25 to 60 tons) for 305-mm to 406-mm piles. The sites shown in this figure are located in areas underlain by glacial-outwash sands of similar gradation and density, and most of the sites are located near New York City.

The 356-mm-diameter ACIP piles at the Southern Brooklyn site penetrated 15 m into the bearing stratum and were loaded to 1334 kN (150 tons) or three times the design load without failure. At a nearby site, a different contractor test-loaded two piles to failure that extended only 12 m into the bearing stratum at only 801- and 1112-kN (90- and 125-ton) loads. A 15-m pile was then load-tested at the second site to failure at 979 kN (110 tons), a lower load than was sustained at the adjacent first site. The authors concluded from a comparison of results for these two sites (Figure 1) that a contractor's technique for installing this pile type is more

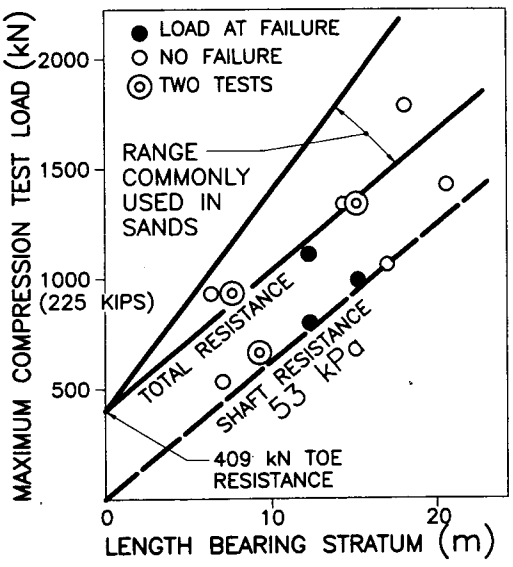

FIGURE 1 ACIP pile load test results.

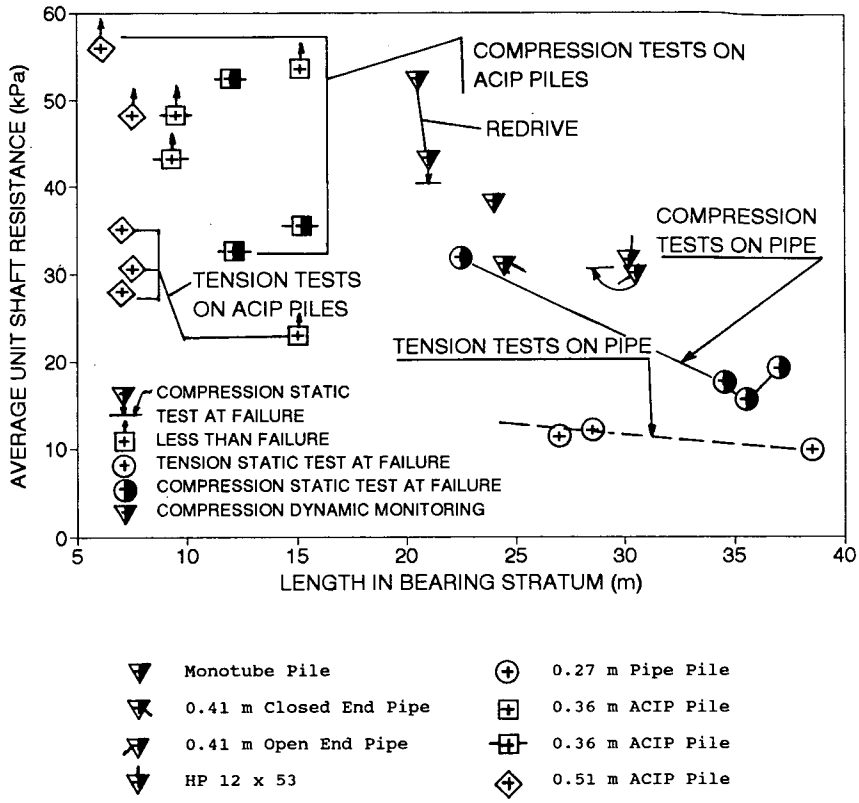

FIGURE 2 Average unit shaft resistance.

important than small variations in soil density and the grain size of the soil in which the pile is installed.

Unit shaft resistance for ACIP piles (*3*) is illustrated in Figure 2, which plots shaft resistance over length of pile in the bearing stratum. Results of both compression and tension tests are plotted. Unit shaft resistance in compression is estimated after subtracting toe bearing, which is determined either from telltales used during the load test or by estimating the static toe-bearing capacity based on soil parameters and the shape of the static load-test curve. Developed unit-shaft resistance varied for ACIP piles between 31 to 54 kPa (0.7 and 1.2 ksf). A number of the developed unit-shaft resistances were for piles that did not reach failure during the load test. Figure 2 also shows unit-shaft resistances for other types of prismatic piles. The pipe piles developed significantly lower unit-shaft resistances than ACIP piles, H-piles, or monotubes at failure, both in tension and compression. There is a definite trend of reduced unit-shaft friction with increasing depth.

Analysis of pile load-tests using telltales to measure the pile-toe movement indicates that nearly all of the pile capacity is in shaft resistance at service loads. As the load is increased to two and three times the design load, most of the increase is initially supported in shaft resistance. The amount of resistance provided by the toe of the pile increases with increasing load and over the duration of the load test.

CASE HISTORIES

The following case histories are presented to illustrate both how ACIP piles can be advantageous to a project and, in some cases, present limitations and dangers with inappropriate use.

Protecting an Old Sewer

A developer proposed to construct an 18-story office building with two basements adjacent to a street containing a 75-year-old, unreinforced concrete interceptor sewer with a 3.5-m inside diameter, as shown in Figure 3. A parking garage was planned for construction directly over the sewer. The sewer had a history of collapses in sections within a few kilometers of the site. A pre-construction walk-through inspection confirmed what our finite-element studies predicted, namely, the presence of tension cracks in the sewer crown and at invert. Piles were considered necessary to transfer building loads to a bearing stratum below the sewer, but driven piles were considered inappropriate because vibration from installation could potentially damage the sewer. Relocating or upgrading the sewer would be too expensive; since the sewer flowed full and was occasionally under surcharge all but about 4 hr per week, the sewer could not be taken out of service or damaged.

The subsurface profile shown in Figure 3 is composed of about 3 m of heterogeneous fill over a deep deposit of interlayered medium-compact to compact-fine sand, varved silt and clay. The fine sands were particularly troublesome because of their tendency to run under unbalanced hydrostatic conditions. Groundwater was about 4 ft below the level of the proposed basement slab.

An instrumentation program that included five slope-inclinometer casings, settlement points, and pore-pressure monitoring devices was instituted at the beginning of construction to provide an early-warning system that would permit time for corrective measures that could safeguard the sewer. Inclinometers were to be read and

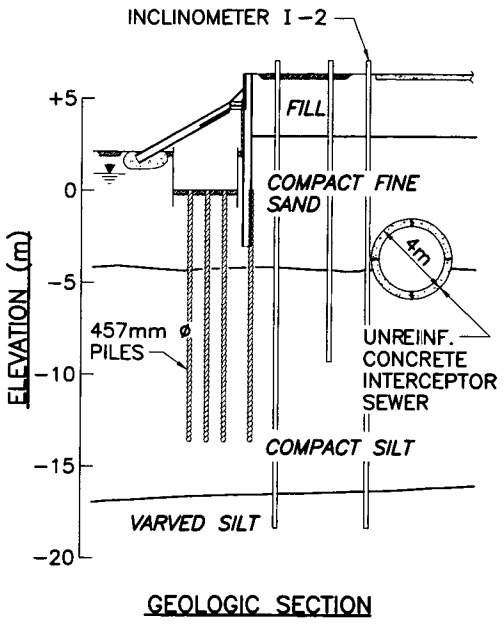

FIGURE 3 Protecting an old sewer.

the data reduced daily. The ACIP pile load-test program led to the selection of a 457-mm diameter, 667-kN (75-ton) design load pile installed to a depth of about 7.6 m below the sewer.

Production ACIP-pile installation began in mid-June of 1987. The contractor used a low-torque, high-rotation-rate gear box to power the augers. We observed that the augers were rotating as many as 20 times per advance of 1 auger pitch. Volumes of spoil during auger insertion were difficult to estimate because of the fluidity of the material as it came off the augers. However, monitoring of grout takes showed volumes averaging about two times the nominal volume of the augered hole, indicating significant loss of soil during auger insertion.

Figure 4 is a plot of horizontal ground movements over time for one of the initial inclinometers. The graph, annotated with construction events, shows that significant, rapid ground move-

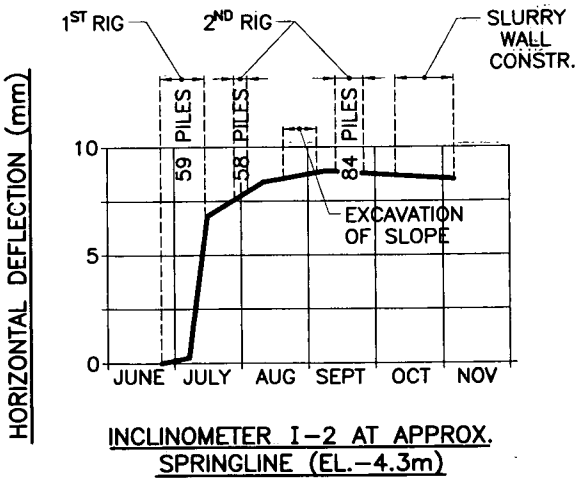

FIGURE 4 Deflection of inclinometer at springline.

ments were observed shortly after production-pile installation began. The piezometers and settlement points showed no response. However, on the basis of field observations of the work and movements indicated by slope inclinometers, the contractor was ordered to stop work.

After reviewing the work, the contractors, owner, and engineers met, and the contractor arranged to provide a turntable with a higher rated torque of 43 kN.m (32,000 foot-pounds) with the ability to throttle down the auger rotation rate. Rotation was limited to two or fewer revolutions of the auger per advance into the ground equal to the length of one pitch of the flight. We observed an immediate reduction in the volume of grout taken in each pile to about 60 percent above the nominal volume of the hole drilled by the auger. Note that these volumes included spoil grout at the surface after removal of the auger from the ground, as well as any volume that may have remained in the hoses after completion of the pile. Typical total grout take on most projects is targeted in the vicinity of 25 to 40 percent over the nominal volume.

During the first work stoppage, additional instrumentation was installed to monitor earth movements. When work resumed, a small amount of additional movement was observed. We judged that no further reduction in the ratio of auger rotation per pitch to penetration could be made and concluded that the unbalanced earth pressure resulting from the retained slope was contributing to the movements. The slope was cut back, creep ceased, and production piling was resumed. Negligible movements were observed thereafter.

Later when a second contract was let for the garage piles, the contract stipulated a minimum torque requirement for the rig, and a maximum rotation rate during advance and withdrawal of the augers. ACIP piles of similar size and capacity were installed on both sides of the sewer, and movements in small fractions of inches were observed. A postconstruction condition survey of the sewer revealed no further cracking or damage. However, in order to permit long-term monitoring of the sewer, provisions were made in the design to install permanent sewer settlement points through accessible boxes in the garage floor. Piles for both structures were designed for full loss of soil support in an influence zone adjacent to the sewer in the event of any future collapse.

Tri-Beca, Manhattan

A 52-story residential tower planned in a congested site (shown in Figure 5) was bordered by two buildings, two and six stories in height, respectively. The site is underlain by more than 30 m of medium compact-fine to medium sand as illustrated in Figure 6. The original foundation consisted of 178-mm outer diameter, open-ended pipe piles, with a design capacity of 445 kN (50 tons), driven to depths of about 30 m. Vibration in medium-dense sand causes soil densification and settlement. A test program was carried out to observe the effects of vibrations on these two buildings. The engineers for this building estimated that the landmark six-story building might settle between 13 and 25 mm and the two-story building might settle 25 to 50 mm when production piles were driven, based on extrapolation from field measurements of ground settlement from driving the test piles. The estimate for the two-story building was higher because more piles were concentrated closer to it.

Pile driving began at the beginning of 1989. Piles farthest from the existing buildings were driven first. As soon as pile driving

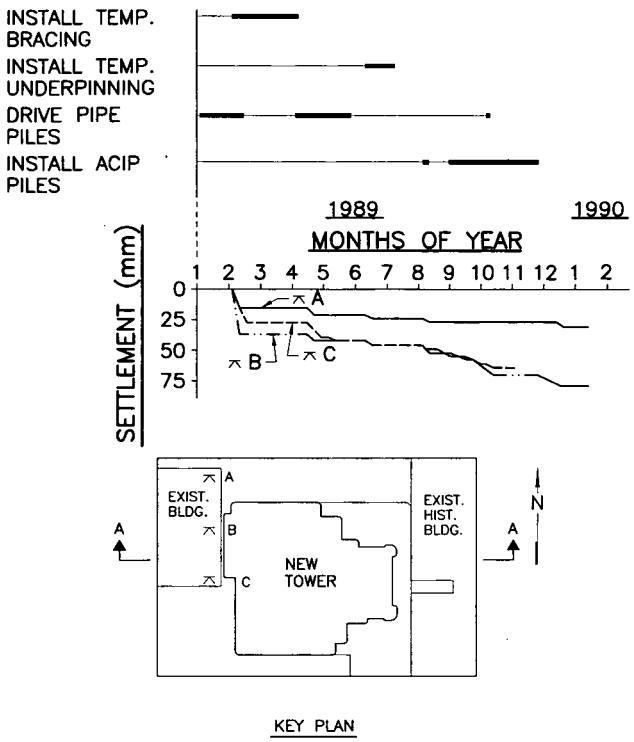

FIGURE 5 Tri-Beca building settlement.

moved to the center of the site between the two buildings, the two-story building started settling rapidly reaching as much as 38 mm, as shown in Figure 5. The contractor attempted to pre-auger the first 15 m and insert the pile to this depth without driving. There appeared to be no benefit to this procedure as most of the driving resistance and the vibrations generated occurred in the bottom 9 m of driving. Although both buildings experienced settlement, the discussions herein will concentrate on the two-story building, being the one the authors were primarily involved in.

All pile driving was stopped, and the contractor installed raker bracing that was not completed until April when the pile driving resumed. However, additional building settlement resulted and

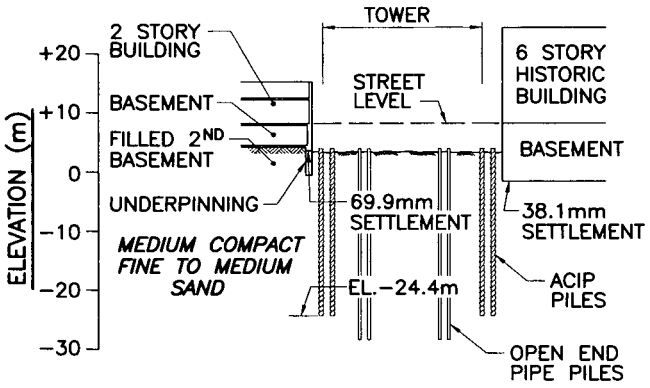

FIGURE 6 Tri-Beca geologic section A-A.

pile driving was stopped in June when the contractor proposed that underpinning be installed. The underpinning consisted of a series of jacks installed both above the existing footings and within the wall, using a continuously reinforced concrete beam to minimize further settlement by lifting the building as the footing settled more. All the settlements shown are net settlements for the building. Settlement of the footings was significantly more than what is shown after installation of the underpinning. It was then the developer's engineers decided to complete the foundations using ACIP piles.

A test-pile program was implemented in August, and production proceeded from September through November. Even though the underpinning jacks reduced settlement, it could be seen that the south end of the building experienced an additional 25 mm of settlement when ACIP piles were being installed. This illustrates that ACIP piles may not, at some sites, eliminate adjacent settlement due to loss of soil into the auger blades. However, we concluded that if the originally planned pipe piles instead of the ACIP piles had been driven in close proximity to this building, much more building settlement would have resulted, probably requiring demolition of the building. The building was occupied during construction, and repairs to the building were made.

Southern Brooklyn

Foundations installed for a sludge-degritter building for a sewage treatment plant consisted of 273-mm outer diameter, closed-end pipe piles. Test piles demonstrated it was necessary to extend these piles 37 m below the excavation level to obtain an allowable capacity of 418 kN (47 tons). As the piles were being installed, monitoring indicated that the adjacent aeration tanks were settling differentially. After approximately two-thirds of the piles had been installed and settlement of the corner of the aeration tank closest to the new construction had reached about 70 mm, it was decided to stop driving the piles and complete the foundations by installing ACIP piles. The relative locations of the structures are shown in Figure 7. Figure 8 is a cross section through the structures and shows typical piles.

Most of the remaining piles to be installed were in close proximity to the aeration tanks, as it had been decided when settlement was first noted to concentrate pile driving as far away from the aeration tanks as possible, to not delay the project. Figure 7 shows the progressive settlement of three locations on adjacent structures during pile driving between March and June 1983. The aeration tanks were emptied during the early part of the pile-driving program, when settlement was first observed. Subsequently, the ACIP test-pile program was carried out. During August, the tanks were refilled, and in October production ACIP-pile installation proceeded.

An additional 38 mm of settlement occurred during the ACIP-pile installation. Figure 9 illustrates the settlement that occurred at varying distances from the expansion joint in the middle of the aeration tank, with the 37-m distance or monitoring point being at the excavation. Curves 1, 2, 3, and 4 show a progressive increase in the aeration tank's settlement during pile driving and 17 days after the piles were driven. Note that significant settlement extended more than 30 m from the edge of excavation during pile driving. Also shown in Figure 9 is additional incremental settlement that occurred during ACIP-pile installation, which at the edge of excavation equaled the maximum settlement that occurred

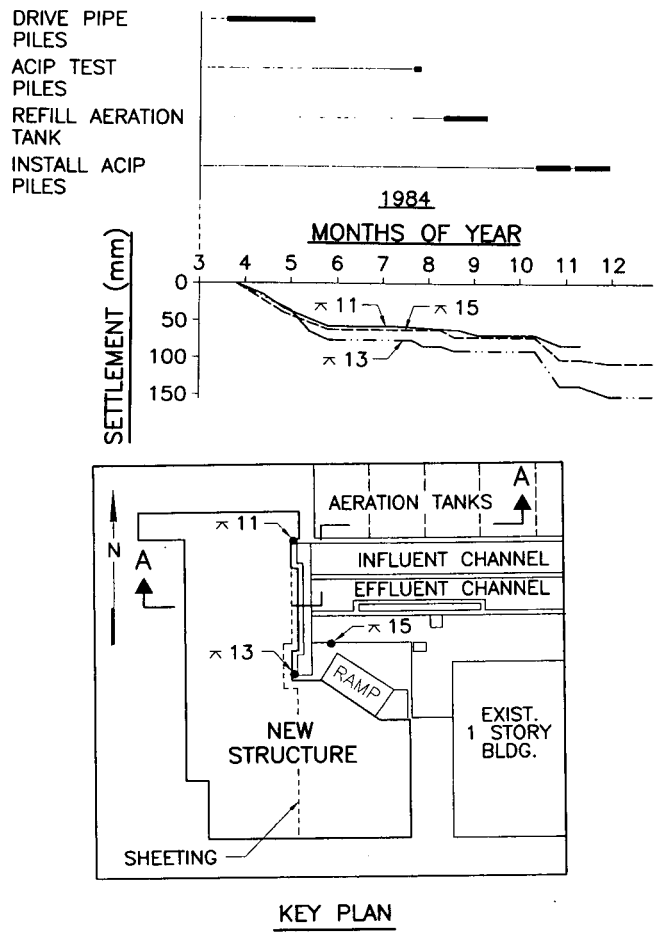

FIGURE 7 South Brooklyn tank settlement.

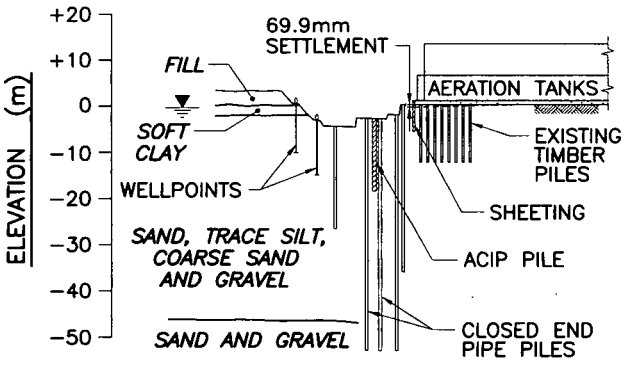

FIGURE 8 South Brooklyn geologic section A-A.

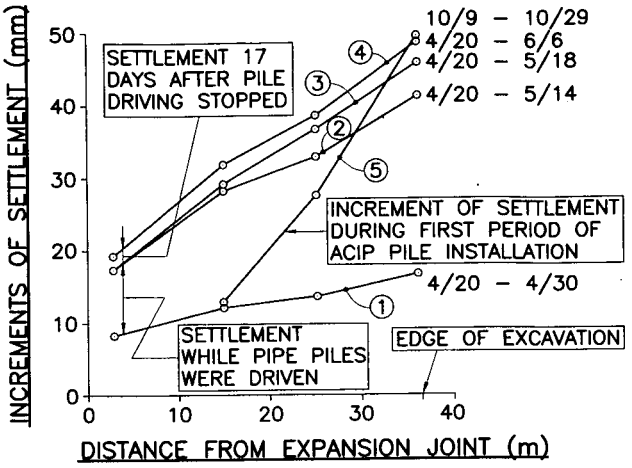

FIGURE 9 South Brooklyn building settlement versus distance.

during pile driving. The magnitude of settlement decreased much more rapidly with increasing distance from the excavation.

Horizontal movement of cantilever steel sheeting installed through and along the edge of the excavation was observed during installation of the ACIP piles. This sheeting also had moved much more during pile driving. As the sheeting had been placed very close to the permanent structure, with the intent of casting the wall against the sheeting, the sheeting's movement became a critical consideration. The top of the sheeting moved as much as 50 mm, while at the level of excavation subgrade it moved about 25 mm during ACIP-pile installation.

In the immediate vicinity of the sheeting, it was noted that the amount of sand that had accumulated around the auger blades at excavation subgrade during auger advance was substantially greater than elsewhere on site. Approximate estimates of the cone of soil indicated the volume of sand being removed from the hole was 50 to 70 percent of the neat volume of the augered hole. Grout pumped was generally in excess of 200 percent of the neat volume, including grout waste. Over the rest of the site, volumes of soil removed during auger insertion and grout pumped during auger extraction were 15 percent and 125 to 140 percent, respectively. The volumes of soil and grout resulted from the high passive-pressure stresses present below subgrade in front of the cantilever sheeting. The stresses caused greater amounts of sand to press into the loose materials riding on the auger blades as the auger penetrated to the design elevation. As a result, the removal of extra materials, as each pile was progressively installed along the wall, resulted in a release of the passive pressure and deflection of the sheeting before the passive resistance was restored. If ACIP piles are to be used next to sheeting, and deflection of the sheeting is important, they should be used cautiously.

West Brooklyn

Figure 10 illustrates another site where H-piles were being driven to depths as much as 46 m immediately adjacent to an existing 2-story structure. The adjacent structure was supported on short timber piles that were supported by a layer of loose, fine sand, underlain by a medium-compact sand. The piles generally penetrated just a short distance into the medium-compact sand. Vibrations from pile driving densified the sand and caused one corner

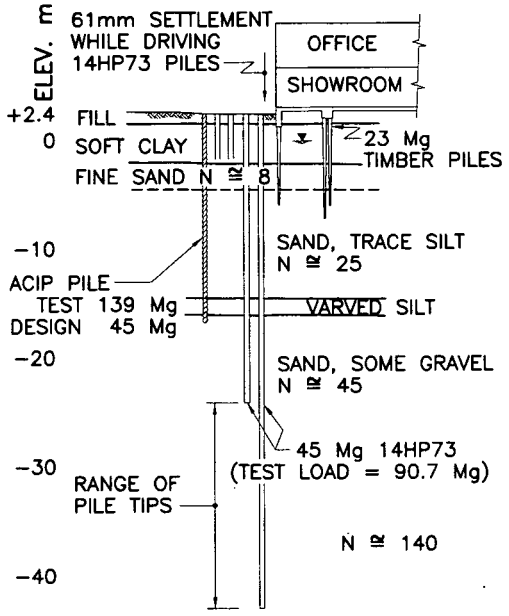

FIGURE 10 West Brooklyn geologic section.

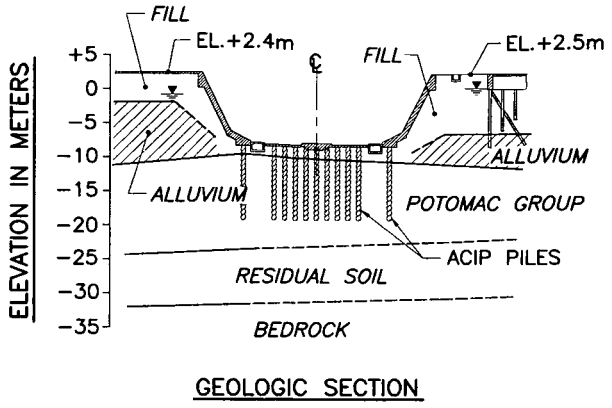

FIGURE 11 Building in a graving dock.

of the 2-story structure to settle as much as 61 mm. Pile driving was stopped, and ACIP piles were substituted for H-piles during the remainder of the project. The ACIP piles extended into the bearing stratum for a design load of 445 kN (50 tons). They were successfully load-tested to a 1.33 MN (150-ton) capacity. On this project the contractor was paid on a unit-price basis for the H-piles. As a result, the much shorter ACIP piles resulted in a net savings to the project, even though additional pile load-testing had to be performed.

Building Inside a Graving Dock

A new residential and recreational waterfront development was proposed on the site of a former shipyard. The centerpiece of the project included two 27-story residences to be constructed inside a graving dock originally built of timber at the turn of the century and rebuilt with concrete during the 1940s and 1950s.

Figure 11 shows a transverse section through the graving dock. In the plan, the graving dock is surrounded by land on the inboard end and along its south side. Its north side is adjacent to a pier, separated from open water by about 9 m of fill and a somewhat deteriorated steel sheetpile wall that was to be repaired. The floor of the graving dock is about 8 m below local Mean Sea Level. Below the floor of the graving dock, the subsurface profile consists of approximately 1.8 to 2.4 m of alluvium and gravel fill, underlain by interbedded, hard red clay and very compact sand of the Potomac Group (Cretaceous Age).

In some locations within the graving dock, standard sampler penetration resistances in the Cretaceous layer were in excess of 100 blows per 0.3 m, whereas at other locations penetration resistances in the upper sand were as low as 22 blows per 0.3 m. During the subsurface exploration program, fine sand layers were encountered in the Cretaceous layer, which ran up in the borehole casing despite the use of weighted drill fluid. Piezometric levels in the upper portion of the Cretaceous layer were observed to be 2 to 4.6 m above the graving dock floor. Water flowed out of borings made through the graving dock floor.

Consideration was given to the use of spread foundations or driven concrete piles to support the new structures. A support scheme was developed to protect the graving dock walls. Spread foundations would have required substantial dewatering effort, and the project appeared to be moving toward the use of high-capacity precast concrete piles. An experienced local contractor proposed ACIP piles as an alternative, at a substantial savings to the owner. Concerns were voiced about their use, particularly because of the presence of running sand and the effective "artesian" condition. The contractor proposed to perform load tests demonstrating the capability of ACIP piles to achieve 150-tons working capacity, at no cost to the owner if the tests failed. Demonstration tests were performed outside the graving dock, where hydrostatic groundwater conditions existed. The contractor elected to install 406-mm-diameter piles only 4.6 to 6.1 m into the Cretaceous layer; the contractor then successfully loaded the piles to twice the required capacity.

Before starting production work, a load-test program was undertaken inside the graving dock to develop installation criteria, including penetration into the bearing stratum, volume of grout, pumping pressures, and allowable capacity. Both tension and compression test piles were installed. Reinforcing typically consisted of a single #18 bar installed with centralizers. A limited number of piles received short cages for additional lateral capacity. The load tests, which included installation of telltales to the pile toe, proved valuable. Not only were the tests helpful in developing acceptability criteria, they gave some indication of problems the contractor would encounter.

The load-test program proved that compression piles with only 130-tons working load could be installed at a penetration of 11.6 m into the Cretaceous layer. Grout volume was established about 60 to 70 percent over nominal pile volume, pumped at a gage pressure of about 517 to 689 kPa (75 to 100 psi). Our analysis of the load-test data suggested that ultimate unit-shaft resistance amounted to as much as 192 kPa (4 ksf) and ultimate end bearing may have been as high as 6.7 MPa (140 ksf), probably due in part to the proximity to the residual soil layer. Tension capacity was estimated to be 356-kN (40-tons) working load.

Two significant problems besides reduction in capacity occurred, both relating to the unbalanced hydrostatic condition. After grouting of the pile was completed and the auger withdrawn, wa-

ter was observed flowing upward around the perimeter of the pile, or through the pile itself around the central reinforcing bar. Often, the condition was not apparent until a couple of hours after installation. Both conditions were considered cause for rejection of the pile. Keeping the reinforcing bar 1 to 2 ft above the toe of the pile and deleting a grout additive tended to reduce the likelihood of seepage but was not always successful. The contractor had much less control in cases where water seeped upward around the pile, and a number of piles had to be redrilled, raising the cost.

The project demonstrated that ACIP piles could be installed to surprisingly high capacities for short penetrations into Cretaceous soil. However, the case history also illustrates that unbalanced groundwater can be a severe hazard. The two structures are now near completion, and the piles are performing as designed.

CONCLUSIONS

Augered cast-in-place piles have proven successful alternatives to driven piles for a number of projects; however, ACIP piles are not without their own limitations and dangers. The case histories we discussed highlight problems that can arise when using ACIP piles, although ACIP-pile projects can be trouble free. We offer these recommendations and cautions:

1. Understand the subsurface conditions. Artesian water, boulders and other obstructions, and running ground can be especially troublesome.
2. Use an experienced contractor with experienced lead field personnel. ACIP piles require specialized equipment, techniques, and quality control measures.
3. Consider whether specifications need to be project specific. The reasons for rejecting unacceptable piles should be clear. Nondestructive integrity-test methods are available for evaluating the pile cross section, but they do not determine capacity. It is least disruptive to the project, and in the long run probably most economical, to redrill piles immediately instead of relying on remote testing or additional load testing of piles.
4. Provide full-time resident inspection of the work. The inspector's responsibility and authority must be clear. Require detailed records of grout pressure and volume of flow for each increment of auger withdrawal.
5. Monitor adjacent structures just as would be done for driven piles or excavation. Unbalanced earth pressures can be troublesome.
6. Conduct a pile load-test program in advance of production work. Production should follow the same installation procedure and use the same equipment and materials that were used for the test.

REFERENCES

1. Lacy, H., and J. Gould. Settlement from Pile Driving in Sands, *Vibration Problems in Geotechnical Engineering*, ASCE Convention, Detroit, Mich., 1985.
2. *Augered Cast-In-Place Piles Manual.* Deep Foundations Institute, Sparta, N.J., 1990.
3. Lacy, H., and J. Moskowitz. Pile Capacity in Medium Dense Sand, *Application of Stress Wave Theory to Piles, Third International Conference*, International Society for Soil Mechanics and Foundation Engineering and Canadian Geotechnical Society, Ottawa, Ontario, May 1988.

Managing the Installation of Augered Cast-In-Place Piles

MELVIN I. ESRIG, JACEK K. LEZNICKI, AND ROBERT G. GAIBROIS

Installation of augered cast-in-place (ACIP) piles, which are uncased as the auger is removed and the pile is grouted, will always be accompanied by ground displacements. Managing the installation to minimize ground displacements can be of special importance in urban areas where nearby structures or buried utilities might be affected adversely. Experience with ACIP installations in New York City and southern Florida has led to the development of recommended procedures to reduce soil loss during installation and the associated ground displacements. Rationales for recommended rates of auger insertion, auger rotation during grouting, grout pressures, and pile spacing are provided. Observations confirm that soil loss during installation is less when ACIP piles are installed in cohesive soils instead of other materials. To help engineers to manage the installation of ACIP piles, information is provided in some detail.

Augered cast-in-place (ACIP) piles, known in Europe as continuous flight auger piles (and by several other names in the United States) are low-vibration, low-displacement, and frequently low-cost deep-foundation elements commonly used to support loads between 40 tons (0.36 MN) and 80 tons (0.71 MN). ACIP piles, which are cast in diameters ranging from 12 in. (300 mm) to 20 in. (500 mm), have been used in southern Florida to support building loads of as much as 110 tons (0.98 MN), and some people reported their reaching higher capacities. ACIP piles are commonly believed to afford a particular advantage in loose-sand environments, where the energy associated with driving conventional displacement piles is likely to cause sand densification and the settlement of nearby structures or facilities.

In this paper ACIP piles are characterized as low-displacement, deep-foundation elements to contrast them with driven piles, which displace their volume as they are installed. We emphasize that the installation of every deep-foundation element has the potential to cause some soil displacement. The displacements may be either positive, flowing outward when driven piles are installed, or negative, flowing inward when an augered or washed hole is created and then filled with grout or concrete to form a pile. Displacements inevitably result from the installation of ACIP piles; managing the displacements is a primary focus of this paper because the displacements from new installations can structurally harm existing structures, buried sewers or pipelines in proximity to the site.

Most building codes explicitly permit the use of ACIP piles. Recently, the limitations on their length included in many codes have been reduced significantly, as long as a professional and knowledgeable geotechnical engineer is involved with the construction (*1*). However, one exception is the New York City Building Code, adopted in 1968; it still does not permit the use of piles that are not fully cased throughout the installation process (except for the compacted concrete foundation or Franki pile), not without petition to and approval by the building department. This restriction reportedly was included in the code because of the failure of certain uncased piles before the code was written.

Today knowledgeable geotechnical engineers agree that the safe installation of ACIP piles requires both an experienced contractor, one who is dedicated to providing a quality product, who will have experienced personnel install the piles, and an engineering-inspection force that understands the potential problems associated with pile installation and how the contractor can best avoid them.

Recommendations for managing the installation of ACIP piles are provided that are the outgrowth of the authors' experiences with installations in New York City and southern Florida.

Woodward-Clyde Consultants, 201 Willowbrook Boulevard, Wayne, N.J. 07470.

ISSUES TO CONSIDER

ACIP piles are formed by rotating into the ground a hollow-stem, continuous-flight auger to a predetermined depth and by continuously injecting grout under pressure through the hollow stem as the auger is withdrawn. Soil is brought to the surface by the auger as it penetrates into the ground. Control of the volume of material excavated by the auger is frequently critical in urban areas where ground displacements can result from excessive excavation and cause damage to nearby facilities.

One issue relates to the volume changes that occur as grout is injected and the auger is withdrawn to form the pile. The relationship between the volume of grout injected, the rate of auger withdrawal, and the additional volume of soil brought to the surface as the auger is slowly rotated during withdrawal must be considered.

Other considerations include what grout pressures to use during installation, how to space piles to avoid damaging members already installed, the quality of grout at the head of the pile, and whether to use reinforcing steel to provide resistance to lateral loads.

Volume Changes During Augering Down

Ninety-foot-long (27.4 m) ACIP piles, 16 in. (400 mm) in diameter, with a 75-ton (0.67 MN) capacity were installed in lower Manhattan (New York City) within 4 ft (1.2 m) of two nineteenth-century buildings founded on rubble-stone foundations. One of these buildings is designated as a public landmark. Details of this case history have been published elsewhere (*2–4*), so only selected information is repeated.

As a consequence of installing the first 19 (of a total of 230 ACIP piles) within 4 ft (1.2 m) to 15 ft (4.6 m) of the landmark

building, settlement of up to 1.5 in. (38 mm) was observed. Most of this settlement was attributed to the loss of soil that resulted from redrilling after equipment failure. The bottom plug of the hollow-stem auger was too small for the bung hole and imploded twice before the problem was diagnosed, filling the auger with sand and requiring auger removal and redrilling. The implosion problem was exacerbated by the need to auger through rubble fill. Consequently, a protective guard was designed and constructed by the contractor and the plug shape and size altered. Redrilling was also required at other times because of premature grout setup and clogs in the grout-injection system as well as a malfunctioning grout pump.

During this initial period of pile installation, a study was made of the volume of soil excavated by the auger and how to reduce the loss of ground. It was observed that at an auger installation rate of between 11 ft/min (3.35 m/min) and 13 ft/min (4 m/min) (fast rotation), between 8 yd^3 (6 m^3) and 12 yd^3 (9 m^3) of soil was brought to the surface by the auger; the "neat" or theoretical volume of the pile is about 5 yd^3 (3.8 m^3). The ratio of actual volume of injected grout to the neat volume of the pile ranged between 1.8 and 2.4.

An experimental testing program was undertaken to reduce the volume of soil removed by the augers. The program was able to

- Slow the rate of auger rotation and increase, to the extent possible, the down-pressure so that the auger penetrated at an average vertical rate between 6 ft/min (1.8 m/min) and 7.5 ft/min (2.3 m/min). Time for auger installation almost doubled to between 12 min and 15 min.
- Lower the volume of soil removed to between 5 yd^3 (3.8 m^3) and 6 yd^3 (4.6 m^3) by modifying the procedure.
- Lower the ratio of the actual volume of injected grout to the pile's neat volume to between 1.4 and 1.8.

The ideal would be to screw the auger into the ground and to excavate only the volume of the auger and stem, if that were possible. For installation procedures to approximate the ideal, however, contractors would need to use equipment capable of delivering high torque and rotating slowly as the auger penetrates the ground. Lacy and Moskowitz (*5*) found, on a project in Newark, New Jersey, about 5 mi (8 km) west of lower Manhattan, that when rotation rates were limited to two or fewer revolutions of the auger per advance into the ground equal to the length of one pitch of the flight, the volume of grout required to form each pile was reduced to about 60 percent above the nominal volume of the hole drilled by the auger. (See also their paper in this Record.) The same average ratio was achieved for ACIP piles in lower Manhattan.

Typical specifications in the United States for ACIP piles require a minimum ratio of actual to neat volume of 1.4 to account for normal oversizing of the pile as the auger wobbles during insertion, and to provide comfort to the engineer that the area of the pile at all cross sections is equal to or greater than the design area. It appears, however, that in the United Kingdom, where ACIP piles are common, most installations are in cohesive materials, and concrete is pumped routinely instead of grout, ratios of actual to neat volume in excess of 1.2 are considered excessive (Greenwood, 1993, unpublished data). Experience in the United States with ACIP piles in cohesive soils also indicates that ratios of about 1.25 are sufficient; such ratios may be all that can be achieved without the auger being lifted by grout-injection pressure.

Managing Volume Changes During Grout Injection

As grout injection begins, the auger is withdrawn about 1 ft (0.3 m) and a high grout pressure is developed at the toe by injecting 10 to 20 pulses of a grout pump, delivering between $^1/_3$ ft^3 (9 L) and $^1/_2$ ft^3 (14 L) per stroke. The pile then is redrilled to the original depth and the auger withdrawn slowly at a rate compatible with the volume of grout injected. Grout injection for each 5-ft-long (1.5-m) section is measured and recorded. No individual 5-ft (1.5-m) section may have less that 115 percent of the neat volume of the pile injected. The final volume of grout injected must equal at least 140 percent of the neat volume of piles cast in other than cohesive materials. The minimum acceptable volume of grout injected depends on the material and amount of lost ground.

Many building codes (*1*) permit no rotation of the auger as it is withdrawn and grout is injected. This "dead pull," which avoids loss of ground during the pile casting, is generally not possible for piles more than 30-ft (9-m) long, because of equipment limitations. It is probably not desirable to execute a dead pull on long piles. Large suction (negative) pressures can develop, potentially collapsing the hole and producing a neck in the pile, if the pull rate were, at any time, to exceed the rate of grout injection. Therefore, a very slow rate of positive (clockwise) rotation accompanies auger withdrawal, increasing the volume of the pile to be filled with grout. Grout pressures and grout injection rates should be sufficiently high to control the negative consequences of this increase in lost ground.

Grout pressures during grout injection are not well understood. Pressures are measured at the grout pump instead of at the point of injection. Grout pump pressures vary; typically they range between 75 psi (500 kPa) and 150 psi (1,000 kPa). In one case, 250 psi (1,700 kPa) of pressure was used in lower Manhattan, when observations during a field-testing program suggested that high pressures at the grout pump reduced ground displacements.

Pressure losses in the grout lines that run from the grout pump to the highest point on the auger are unknown, however. Therefore, the actual pressure at the point of injection is uncertain. However, it is important for several reasons:

- Inadequate pressure can lead to a reduction in the cross-sectional area of the pile (necking).
- Excess pressure can result in grout loss by hydrofracture and the potential to damage recently cast, nearby piles by the upward movement of the ground.
- Sufficient pressure is necessary to cause an upward flow of groundwater around the auger, followed by a flow of grout, when the auger is still 25 ft (7.5 m) to 30 ft (9 m) in the ground.

Once grout flow has appeared at the ground surface, the auger can be removed without rotation. The fact that a satisfactory rate of grout injection is being maintained can be verified by observing a continuous flow of grout at the surface, in addition to continuously measuring the volume of grout pumped. Grout should fill the auger flights as they are withdrawn.

Significant loss of ground can occur when piles are cast if sufficient grout is not available to complete the casting of a pile, and it must be reaugered and regrouted. This is a frequent problem in

congested urban areas where grout delivery can be delayed by traffic. Such a problem occurred in Minneapolis, Minnesota, when a crane operator, inexperienced with the installation of ACIP piles in the loose river sands, decided to auger several holes while waiting for grout delivery. A portion of the adjacent building settled 1 in. (25 mm) because of the loss of ground. As a safeguard, the policy for the lower Manhattan installation was that no pile could be drilled until sufficient grout was on-site to complete the pile.

Spacing of Piles

It is common practice to design piles for center-to-center spacings of 2- to 3-pile diameters. The 16 in. (400 mm) ACIP piles in lower Manhattan were spaced 3 ft (0.9 m) on centers. When injection pressures were increased to 250 psi (1,700 kPa), the original specification that piles installed on any day could not be less than 6 ft (1.8 m) apart was increased to 9 ft (2.7 m) apart. Piles could be installed 6 ft (1.8 m) apart after curing for at least 24 hrs.

These modifications were made in response to the fear that upward ground movement from hydrofracture could heave and pull apart unreinforced, weak piles. Survey measurements of 19 piles during the period of installation indicated no heave or settlement related to the installation process.

Quality of Grout at Pile Head

The slow rotation of the auger as it is withdrawn, its slight wobble as it is raised, and the continuous upward flow of grout to the ground surface combine to produce the broad top of the pile, often weakened by the mixing of grout and soil near the ground surface. It is, therefore, advantageous to install an 18 in. (460 mm) to 36 in. (915 mm) section of metal shell at the top as soon as the casting of the pile is completed and to "clean the grout". Clip-on sections of metal shell and a "pile screen" to clean the grout within the shell are available for this purpose. When a metal shell was not used properly at a site in Brooklyn, New York, and cleaning was not done, the grout strength at the pile head was reduced by the mixing with soil from the specified 4,000 psi (27.6 MPa) to 2,500 psi (17 MPa) or less. The low-strength concrete was removed before casting the pile cap, and the cap deepened to engage grout of adequate strength.

Weakened grout at the pile head has also been reported when excessive "bleeding" of grout occurs at the top and when upward water flow from the ground washes out the cement and segregates the grout components.

Comparative tests of the Brooklyn and lower Manhattan installations show that reasonably reliable indications of the strength of the grout at the pile head can be obtained using a concrete rebound hammer (Schmidt hammer). The use of the Schmidt hammer to provide an initial indication of the adequacy of the grout strength is recommended.

Reinforcing Steel

ACIP piles can be reinforced to resist lateral forces and to increase axial compression or tension capacity. The most common reinforcement is a single steel bar introduced into the pile immediately after casting and penetrates to the bottom of the pile. Centralizers are required to be certain that the bar remains within the pile section. Less common is introducing the bar through the hollow stem as grouting begins. A bar that is at or near the center of the pile has only a modest effect on the bending resistance but can provide significant tension capacity if adequate bond strength is available.

Bending strength can be provided readily by introducing a reinforcing cage or a steel member like a lightweight H section or a pipe into the pile just after grouting has been completed and before the grout has set. These sections also require centralizers to ensure that they remain within the grout section as they are pushed into place. In general, there has been limited success pushing steel sections or cages to depths greater than 20 ft (6 m). Ordinarily this depth is sufficient to reinforce the pile against horizontal forces applied at the ground surface, but a shorter depth limits the usefulness of the ACIP pile for use in cantilever retaining structures that are more than 10 ft (3 m) to 15 ft (4.5 m) high.

CONCLUDING COMMENTS

That surface displacements inevitably result from ACIP pile installations in granular soils is now well documented. Displacements of the landmark structure in lower Manhattan of 2 in. (50 mm) to 3 in. (75 mm) primarily resulted from equipment failure and pile redrilling. It is estimated from the available data that trouble-free pile installation would have produced between 0.5 in. (13 mm) and 0.8 in. (20 mm) of building displacement. It was surprising to observe that about half the estimated trouble-free displacement occurred during a 10-week period after pile installation was completed. The cause of this "secondary compression" of granular soils is unknown. Also well documented is the fact that careful management of the installation process by contractors and engineers can limit the magnitude of displacements.

REFERENCES

1. BOCA Basic Building Code. Building Officials and Code Administrators International, Inc., Chicago, Ill., 1991.
2. Esrig, M. I., J. K. Leznicki, and R. G. Gaibrois. Building Displacements Resulting from Pile Installation in New York City. *Proc., International Conference on Deep Foundations*, l'École Nationale des Ponts et Chaussees, 1991, pp. 559–565.
3. Leznicki, J. K., M. I. Esrig, and R. G. Gaibrois. Loss of Ground During CFA Pile Installation in Inner Urban Areas. *Journal of Geotechnical Engineering*, Vol. 118, No. 6, June 1992, pp. 947–950.
4. Leznicki, J. K., M. I. Esrig, and R. G. Gaibrois. Tribeca Tower Foundation System. *Proc., 3rd International Conference on Case Histories in Geotechnical Engineering*, St. Louis, Mo., Paper 1.14, June 1993, pp. 53–60.
5. Lacy, H. S., and J. Moskowitz. The Use of Augered Cast-in-Place Piles to Limit Damage to Adjacent Structures. Presented to the Construction Group, ASCE Metropolitan Section, New York, Feb. 1993.

Formalized Procedure for Quality Assessment of Cast-In-Place Shafts Using Sonic Pulse Echo Methods

FRANK RAUSCHE, GARLAND LIKINS, AND MOHAMAD HUSSEIN

Cast-in-place concrete piles are produced by drilling holes in the ground and filling them with concrete. The constructed shape and structural integrity of this pile type is dependent on concrete quality, subsurface conditions, and workmanship. Many engineers are willing to consider this type of piling but require adequate inspection and shaft integrity verification. Dynamic low-strain testing and analysis by the Sonic Pulse Echo Method with equipment such as the Pile Integrity Tester provide a quick and inexpensive means to assess the integrity of all types of concrete piles (where modulus is much higher than surrounding soil) by measuring top motion (and force) under the impact of a small hand-held hammer and then applying one-dimensional wave propagation theories. Data interpretation can be either a simple visual inspection of the dynamic pile records, a rigorous numerical analysis, or a technique that generates an "impedance profile" as a function of length. Testing and data evaluation require experience and engineering judgment. The principles, application, and limitations of the low-strain integrity testing method are presented, and a step-by-step record evaluation and interpretation procedure is proposed. Finally, the value of the record for the quality-assurance process of pile foundations is assessed.

The nondestructive low-strain method of concrete pile testing has become a routine quality-assurance test in several countries. For example, the Institution of Civil Engineers in the United Kingdom has issued a specification for this test type (*1*). Similarly, in Germany the test is recognized through a "recommendation for dynamic pile tests" (*2*). Apparently, engineers in Holland, Belgium, and Austria also routinely use this test type in response to generally mandated quality-assurance requirements. In the United States the test primarily has been performed after difficulties occur during execution of a drilled or driven-pile foundation. Goble Rausche Likins and Associates, Inc. (*3*) has written a specification for the testing procedure that has been used as a guide for agencies contracting for this type of work. For specific projects, other specifications have been proposed. However, there still are considerable differences in opinion as to the proper application and interpretation of the test and exactly how the results should be used in the quality assurance and acceptance process of a pile or shaft.

The method has been employed frequently both in Europe and the United States, particularly on auger-cast (continuous-flight-auger or pressure-grouted) pile projects, in which construction control is difficult because a direct inspection of the drilled hole before grouting is not possible. Correlation tests on auger-cast shafts constructed with planned defects have not been performed, primarily because it is difficult to determine shaft diameter by depth. However, integrity testing and analysis are well supported by contractors' experiences with standard cast-in-place shafts and driven concrete piles. The test methods are generally considered applicable to auger-cast shafts also, and they are used to test auger-cast shafts throughout the United Kingdom.

The nondestructive low-strain method is relatively simple to execute; however, interpretation of the data collected is sometimes difficult. As for other nondestructive test (NDT) methods, the records collected may be divided into four categories:

- Category A—Clear indication of a sound pile shaft;
- Category B—Clear indication of a serious defect;
- Category C—Indication of a possibly defective pile shaft; and
- Category D—Inconclusive data.

The authors briefly discuss records falling into these four categories, drawing examples from actual case histories. Furthermore, because it is desirable to derive quantitative results from records when there's some indication of a defective pile shaft (Category C), the so-called "Pile Impedance Profile" interpretation method will be explained. Finally, recommendations for implementation are made.

LOW-STRAIN METHOD

When a long-driven or cast-in-place pile is struck with a small hammer, a stress wave is generated that travels down the shaft to the bottom where it is reflected. When the reflected stress wave returns to the top, a measurable pile-top motion occurs. If this reflection wave occurs at the correct time, and if no other earlier reflection is observed at the pile top, then the pile shaft is probably free of major defects.

When a lightweight hand-held hammer strikes the pile top, a small pile top motion (velocity) is generated and can be measured. The associated pile strains are of such a low magnitude that this test is known as a "low strain test." However, the force applied by the hammer can be easily measured by instrumenting the hammer itself. Primarily, the velocity record (and to a lesser degree the force record) contains information about the location and magnitude of pile nonuniformities (*4*).

STRESS WAVE PROPAGATION IN A PILE

An impact applied to the pile top generates a momentary compression and particle velocity, v, of the pile-top surface. If the pile

F. Rausche, Goble Rausche Likins and Associates, Inc., 4535 Emery Industrial Parkway, Cleveland, Ohio 44128. G. Likins, Pile Dynamics, Inc., 4535 Emery Industrial Parkway, Cleveland, Ohio 44128. M. Hussein, Goble Rausche Likins and Associates, Inc., 8008 South Orange Avenue, Orlando, Fla. 32809.

is made of concrete, the stress-wave travels in the pile at a longitudinal wave speed, c, ranging from 3,000 to 4,500 m/sec, where

$$c = \sqrt{\frac{E}{\rho}} \quad (1)$$

where E is the pile's elastic modulus and ρ is its mass density. Figure 1 shows the path of a stress wave in the pile in the form of a time-depth plot, illustrating that cross-section reductions produce a reflection observable at the pile top. This reflection is of the same sign as the input, and the arrival times of reflection waves at the pile top are related proportionately to the depth of the cross section's change by the wave speed. Soil resistance forces also generate reflection waves, but of opposite sign to the input.

PULSE ECHO METHOD

Figure 2 shows a schematic of low-strain instrumentation using as an example the so-called Pile Integrity Tester (P.I.T.) Collector (*4*). Hardware components also include a hand-held hammer with an integral plastic cushion and an accelerometer. The pile integrity tester or P.I.T. processor provides signal conditioning, digital signal processing and storage, and output on a liquid crystal display screen, graphics printer, or plotter. Various other configurations of this system are possible. For example, the signal conditioning can be combined using a personal computer with analog-to-digital data conversion capability.

The first, and sometimes most important, step for any low-strain test is the preparation of the pile-top surface. In fact, depending on the construction method, it may be necessary to remove the upper section of the concrete if it has been contaminated with soil, bentonite slurry, or other foreign materials during construction. After a clean, hard concrete top surface has been exposed, the accelerometer is attached to a smooth spot prepared on the pile-top surface with a thin layer of a soft, paste-like material, such as vaseline or petro wax. After the accelerometer is attached a hand-held hammer is used to strike the pile top to generate accelerations in the 10- to 100-g range, pile strains less than 10^{-5}, velocities less than 30 mm/sec (0.1 ft/sec), and displacements less than 0.03 mm (0.001 in.). Accelerations produced by several hammer blows are integrated to velocities (usually easier to interpret than accelerations) and displayed on the processor's screen. Consistent records are then averaged, reinforcing the repetitive information from pile or soil effects while reducing effects of random noise.

DATA PROCESSING AND INITIAL INTERPRETATION

Observed time can be converted to a length scale by multiplication with the longitudinal wave speed, c. Since wave speeds of piles installed at the same site normally fluctuate ±5 percent, similar differences in predicted length (or depth to cross-section change) must be tolerated. If there are no reference shafts, and wave speeds are only estimated, then the differences between estimated and actual wave speeds may be as much as ±15 percent. On the other hand, assuming that the accurate pile shaft length is known, the wave speed can be back calculated from the time between impact and pile-toe reflection (when observed).

The test engineer inspects the average velocity signal. The first check concerns the "toe signal". If the reflection from the pile toe is not readily apparent, then the velocity usually is multiplied with an amplification function whose magnitude is unity at impact, which increases exponentially with time until it reaches its

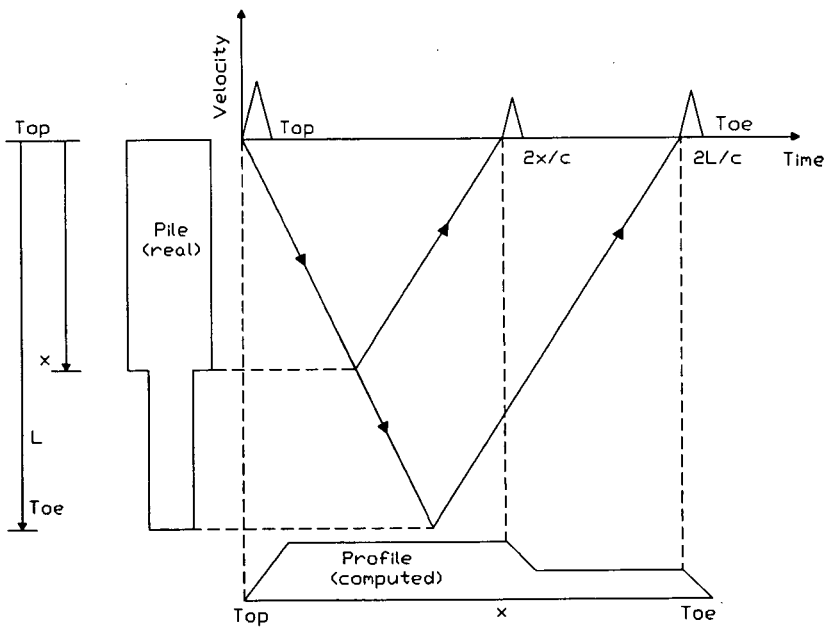

FIGURE 1 Traveling stress waves and the principle of the Pile Profile estimate. Measured velocity at pile top showing input and reflections from cross-section change, and pile-toe and computed-impedance profile.

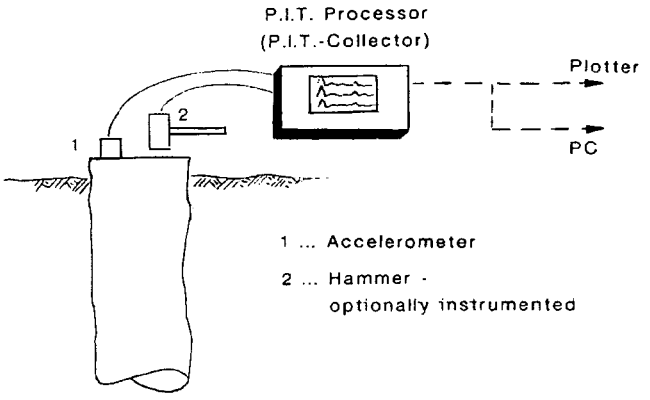

FIGURE 2 Schematic of P.I.T. devices (collector).

maximum intensity at time 2 L/c after impact (Note 2 L/c is the time that the stress wave requires to travel the pile length, L, and return). The amplification may be started at a time after impact that corresponds to the depth at which significant soil resistance in the pile is expected.

Next, the velocity amplitude variations over the first 2 L/c time period are investigated and may be the result of changes in a pile's cross section, the concrete quality, or the degree of soil resistance. For example, increases in relative velocity may result from either a cross-sectional decrease or a soft soil layer. In the absence of soil resistance changes, pile-top variations are caused by pile impedance changes, where impedance is defined as

$$Z = EA/c = A\sqrt{E\rho} = Ac\rho \quad (2)$$

where A is the pile's cross-sectional area. Thus, an impedance reduction can be caused by a decrease either in area, in the concrete's elastic modulus, or in the concrete's density. Since both modulus and density are related to concrete strength, it is fair to say impedance depends on cross-sectional area and concrete quality.

PILE PROFILE INTERPRETATION METHOD

Based on work done by Paquet (*5*), an estimated Pile Profile may be calculated using the measured pile-top velocity. The basic concept of the Pile Profile calculation is that a step-wise change in impedance causes a pulse-like velocity wave effect at the pile top (Figure 1). The profile can be constructed from the time integral of the velocity wave effects at the pile top. First, the input pulse is integrated (to define maximum profile at "top") and forms the reference for later reflections. Next, the subsequent velocity is integrated (now with opposite sign), such that velocity increases (or cross-section reductions) cause proportionate reductions in the profile, with the final reflection from the pile toe causing the profile to "close" (bringing net integral equal to zero) at the toe. In practice, other procedures must also be considered (*4,5*) to account for the effects of soil resistances along the shaft. The calculated Pile Profile result includes the following:

- Calculated pile impedance plotted versus length. The impedance is normally plotted symmetrically to the pile axis even though actual variations may occur on one pile side.
- Relative volume calculated from the apparent Pile Profile. (This value may be compared with actual construction records.) A relative volume of 1.0 corresponds to the pile-top cross-sectional area times the pile length. (Note that the actual pile top cross-sectional area may be greater than the nominal area; this must be considered when comparing volume records from the construction site.)
- Minimum and maximum impedance values along pile shaft (relative to the pile top).
- Measured velocity (solid line) enhanced by the averaging of several blows, by exponential amplification, and by high-pass and low-pass filtering.
- Calculated velocity (dash) considering a set of assumed soil resistance effects. The difference between the measured and calculated velocity curves is interpreted as reflections from pile impedance variations.

The Pile Profile calculation relies to a very high degree on the judgment of the engineer in the generation of a calculated velocity. The judgment could be removed if the record was strongly filtered to remove all low-frequency effects, implying that only quickly changing (high frequency) pile impedance variations can be detected and that soil resistance effects produce slowly varying wave reflections. Both the engineering judgment and the automated filtering method leave some questions as to the actual soil resistance effects on the pile-top velocity record. For this reason, it is always helpful to establish a typical or reference pile on a site.

The difficulty in interpretation lies primarily in separating soil-resistance from pile-impedance effects. Unfortunately, soil resistance influences the velocity records not only in a uniform manner (as it is tacitly assumed when the exponential amplification is performed) but also with differing intensities at different soil layers. If soil-resistance effects were not properly considered, the calculated Pile Profile would show impedance increases or decreases along the pile where soil resistance increases or decreases.

EXAMPLES OF NDT RECORDS

Category A—Clear Indication of a Sound Pile Shaft

Figure 3 presents velocity and acceleration records of a relatively long auger cast pile (the pile is drawn horizontally between the records with the exponential amplification function superimposed). According to plan, the shaft had a length of 24 m and a diameter of 600 mm. It was installed in loose sands that became more competent with depth. After significant exponential amplification (75 times, at time 2 L/c) a clear toe signal (relative velocity increase begins at 24 m) was apparent. Without exponential amplification, the toe signal was practically invisible. A relatively flat record up to 20 m indicates a uniform shaft; a gradual increase from negative (just after impact) to positive velocity values (in the middle of the record) is interpreted as a slight reduction in soil resistance between the top and the middle of the pile. The soil resistance apparently increased quickly when the shaft entered the bearing layer, a few meters above the pile toe. (The record portion after the 2 L/c time is not of interest in assessing pile integrity.) Without further analysis, this shaft can be considered free of any significant defect.

Category B—Clear Indication of a Serious Defect

Several kinds of defects can be detected by the low-strain test method. However, a number of others cannot be detected with the low-strain method, the following for example:

- Local impedance variations that occur over very short distances such as partial cracks are not detected by long impact pulses. As mentioned earlier, soil-resistance effects often mask reflections from gradual impedance variations, or the two may be indistinguishable from each other.
- More than two strong impedance variations (50 percent or greater) create complex records that are difficult to interpret. Major defects below such impedance variations may not be detectable.
- Any defect below a full crack or mechanical splice cannot be detected. A major crack completely separates upper from lower pile sections that the low-energy stress wave cannot traverse.
- Very gradual deterioration in concrete quality or a cross-sectional area change, occurring over a distance of several impact pulse widths (e.g., 5 m), may not be detected.
- Exact length (compared to the planned length) usually cannot be determined because the wave speed, c, of the material, used to convert time (2 L/c) to length, L, is at best known within 5 percent.
- A minor defect, for example, one causing less than 20 percent of the pile impedance, may not be detected.
- A major defect at a pile length that is beyond the reach of the stress wave, typically at a depth below grade (dependent upon soil strength) that is greater than about 30 shaft diameters may not be detected. (Figure 3, however, shows a clear toe signal for a depth to diameter ratio of 40).
- A defect within a short distance of the pile toe may not be detected, unless the toe reflection of a typical or reference pile is known.

The soil not only has a resistance effect but inevitably causes unplanned impedance variations. For example, in weak soils the constructed shaft is often enlarged. Alternatively, where the soil changes from weak to firm, the diameter of the shaft decreases back to the nominal diameter. For this reason it often is necessary to establish the "signature" of a reference pile at a site to show both the soil resistance effects and the unavoidable impedance variations.

Serious defects that can be detected by the low-strain method include the following:

- Shafts that are constructed more than 5 percent shorter than planned (if records from reference piles are available) and those constructed more than 10 percent shorter than specified (if no reference piles are tested).
- A complete crack that separates the full cross section of the shaft. For example, an opened crack caused by shrinkage in an unreinforced shaft or from the inadvertent impact of construction equipment during excavation would produce a complete wave reflection; however, defects below such a crack cannot be detected.
- An impedance reduction greater than 20 percent, as long as sufficient wave energy is available to produce a toe signal in reference piles. When reference piles are not available or do not indicate a toe signal, a less accurate rule of thumb may be used: that is, that defects to a depth of 30 diameters are detectable.

Figure 4 shows the velocity record and impedance log of a shaft drilled to a depth of 29 m. The apparent length is, however, only about 21 m to 23 m at most; the dashed portion of the profile, equal to the input pulse width, is a zone of uncertainty of impedance. The P.I.T. test clearly indicates the point to which the 1.5-m diameter shaft has been cased (reduction begins at end of casing 8 m below top), a subsequent increase in impedance in the shaft between 9 and 14 m, and then a strong relative positive velocity

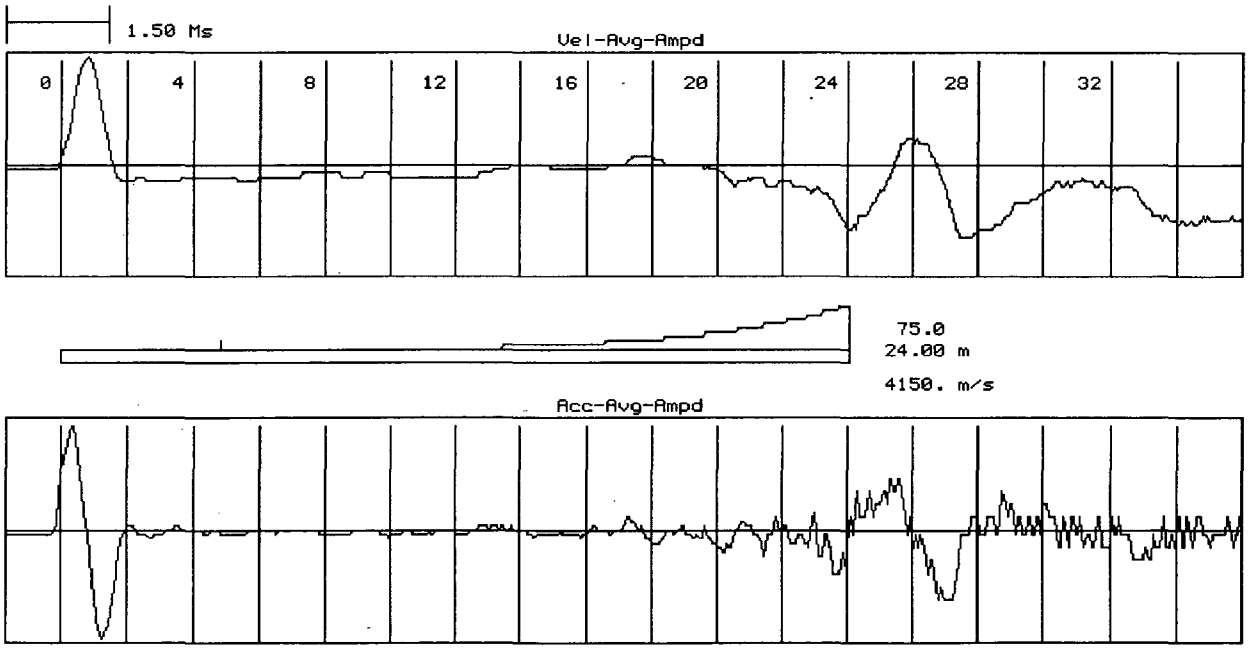

FIGURE 3 Pile-top velocity (*top*) and acceleration (*bottom*) of a 24-m shaft (both with 75 × exponential amplification), with pile model and amplification function (*center*) and a clear toe signal (relative velocity increase) beginning at 24 m.

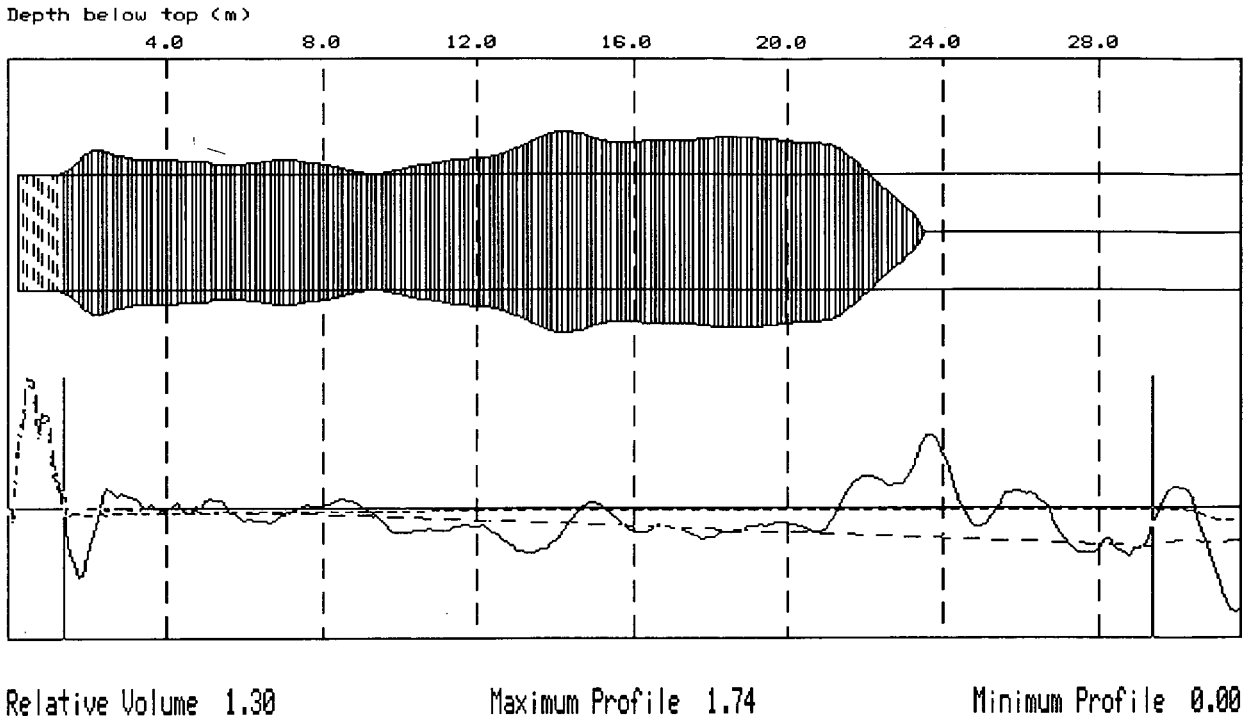

FIGURE 4 Shaft 1.5 m in diameter, and planned length of 29 m, with a casing to 8 m depth, which is oversized below casing and has major defect beginning at 21 m. Impedance profile (*top*) and exponentially amplified velocity (*bottom*).

increase beginning at 21 m. Although it might be argued that a toe reflection (relative velocity increase) is apparent in the velocity record, the earlier reflection is so strong that it must be attributed to a major defect (impedance reduction) that gives the shaft an apparent or effective length of only about 21 m, instead of the design length of 29 m.

Category C—Indication of a Possibly Defective Pile Shaft

Figure 5 shows a record with a positive reflection at a location approximately 3 to 4 m (uncertainty due to input pulse width zone) below the shaft top (*6*). The impedance log shows an increased shaft size shortly below the top, and that cross section may alternatively be used as a reference impedance. Relative to this 12 percent-higher impedance value (maximum profile 1.12), the reduction (minimum profile 0.73, or a 27 percent decrease) appears to be 12 + 27 = 39 percent. Actually, the shaft had been constructed with a planned length of 10.4 m and a planned built-in defect of 50 percent at a depth of about 3 m. A shaft-toe reflection is apparent, and it can be concluded that otherwise the shaft is continuous to its toe.

Quantitative evaluations of impedance (or cross-sectional area reductions) are probably limited to an accuracy of 20 percent of the nominal shaft impedance. Statistically meaningful data currently does not exist to support a stronger statement. This means that a defect of less than 20 percent probably cannot be detected with certainty.

Category D—Inconclusive Data

When the pile top quality is poor, low-strain test results are often inconclusive. For example, Figures 6 and 7 show records from the same shaft, both before and after the pile top had been cleaned off and loose or contaminated concrete removed. A mortar layer for shaft-top smoothing may distort the signal in a similar manner. Another reason the data is inconclusive: heavy reinforcement was protruding above the pile top for more than 3 pile diameters. Even driven precast piles occasionally show inconclusive records shortly after they are driven when microscopic cracks diffuse the impact energy.

Figure 6 would not allow for a clear statement about shaft integrity because of the sine-wave shape of the record; however, neither would it allow the conclusion of a defective shaft. Therefore, it is a Category D record. After the shaft top was cleaned off, the records in Figure 7 were conclusive: the shaft was intact, with a small relative impedance reduction (relative velocity increase) beginning at 18 ft (5.5 m) just before strong soil resistance. The small impedance reduction was probably caused by a return of the shaft to its nominal diameter once it entered more competent soil. Above that location, however, the shaft was probably oversized. The record of Figure 7 also contains an observable toe reflection (relative velocity increase) and therefore falls into either Category C or A.

IMPLEMENTATION OF LOW-STRAIN TEST

Before testing a pile shaft, project managers should consider what actions should be taken if test records indicate a lack of quality.

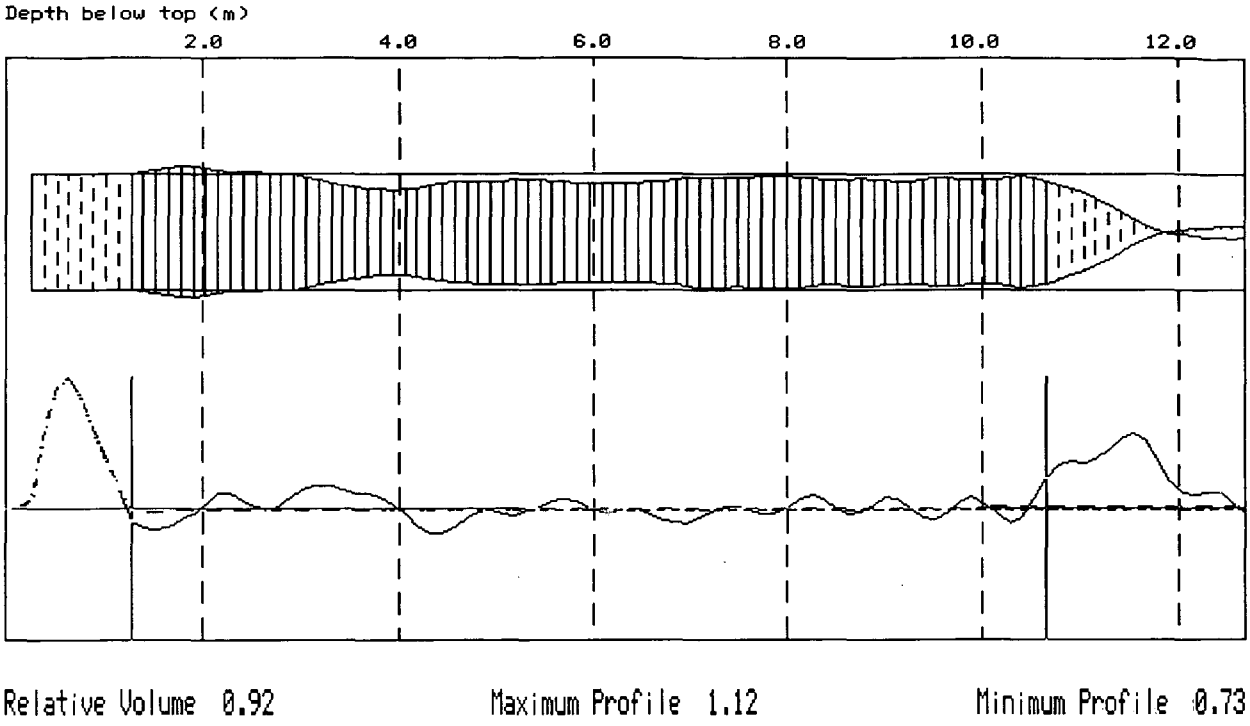

FIGURE 5 Shaft with defect (minimum profile value of 0.73), approximately 3 m to 4 m below top.

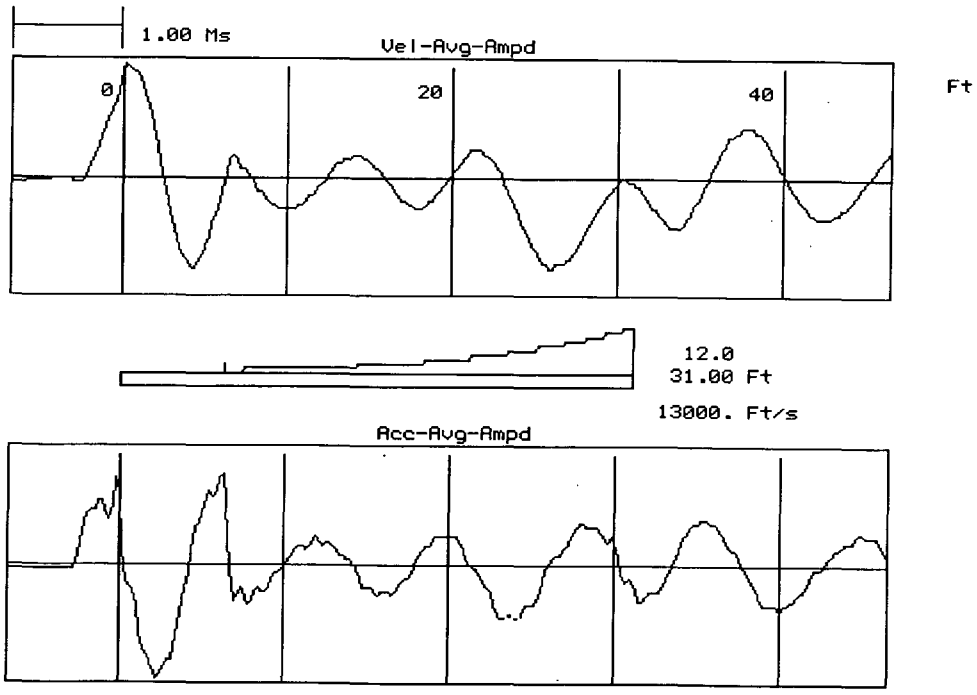

FIGURE 6 Velocity (*top*) and acceleration (*bottom*) records of a shaft before removing contaminated concrete (1 ft = 0.305 m) with pile and amplification function (*center*).

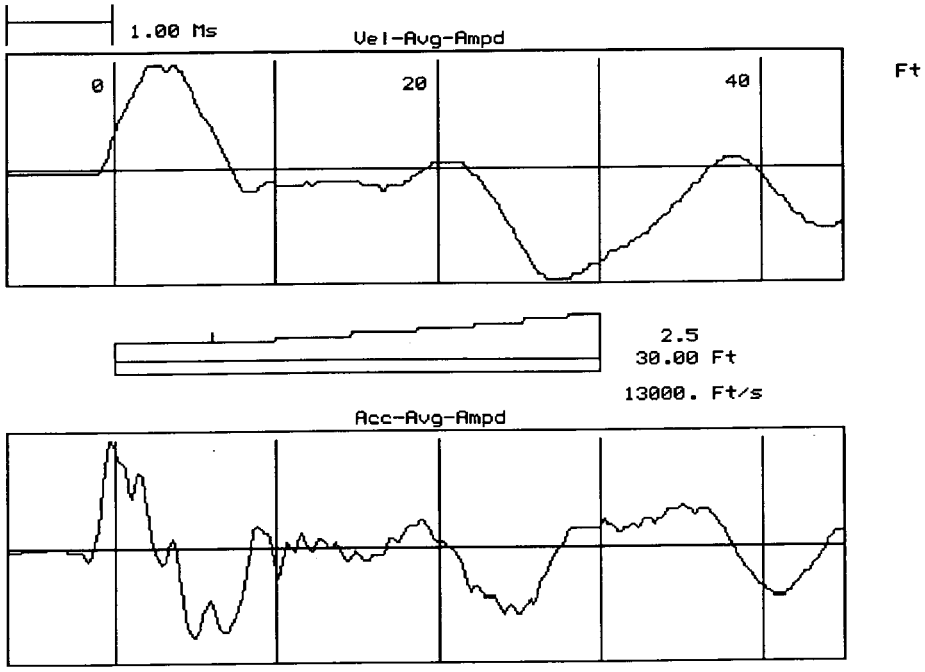

FIGURE 7 Records after removing 1 ft of contaminated concrete from the top of the shaft shown in Figure 6 (1 ft = 0.305 m).

Unless an appropriate "decision tree" is in place for drilled shafts whose P.I.T. records fall under Categories B, C, or D, serious construction delays may result, causing unnecessary work stress for the general and piling contractors, engineers and the testing company. We recommend the following set of actions, according to each record category.

If the test shows a sound pile shaft (Category A) the pile shaft can be immediately accepted whenever its shaft continuity is the only question. If the test reveals a serious defect (Category B), the contractor must assess the foundation's strength either without the defective element or with a reduced element strength. Similarly, if the test indicates the possibility of a defect (Category C), a reduced capacity may be assigned to the defective shaft. In the case of inconclusive records, (Category D) one or more of the following measures may be required:

- Deem a certain percentage of inconclusive records acceptable. Some percentage of records can be accepted as uncertain, particularly, if a very large percentage of piles at a site has been tested. There must be the assurance, however, that Category-B or C piles will not be put into Category D simply to avoid acknowledging defective or possibly defective piles. The acceptable percentage of piles with inconclusive records should be based on the type of structure and the piles' intended use, the redundancies in the foundation (and test results of adjacent piles), the soil type, and the type of pile resistance (for example friction/end bearing).
- Perform the following additional tests or investigations:
  - —Excavation or extraction and subsequent inspection of the affected shaft portion; this is useful when the problem appears to occur only a short distance from the pile top.
  - —Retesting by the low-strain method after cut-off and cleaning the pile top. This is the most common remedy.
  - —Make core borings and make repairs by high pressure grout injection. Unfortunately, this remedy is very expensive, and the boring may or may not move outside the shaft.
  - —High-strain dynamic tests using a Pile Driving Analyzer. This test will yield additional information about the shaft's uniformity (*7*) and about its load-bearing capacity.
  - —Static load-testing. A shaft may pass the static load test, however, if the shaft's deficiency is due to contaminated concrete, honey combing, or other concrete deficiencies that leave sufficient structural strength for the static capacity.

STEP-BY-STEP INTERPRETATION

Compile Information

Complete construction records always should be gathered including:

- Size of drilling equipment (diameter and depth);
- Nominal shaft diameter;
- Observed actual diameter at top of shaft;
- Construction procedure;
- Anticipated oversize;
- Planned cross-sectional variations (diameter changes, bulbs), if any;
- Unplanned but expected cross-sectional variations;
- Casing geometry, wall thickness, if any;
- Length as drilled;
- Theoretical volume based on length drilled and anticipated shaft diameter;
- Actual grout volume versus depth;

- Grout pressure variations versus depth;
- Observations of unusual situations or construction interruptions;
- Time of grouting and concreting;
- Anticipated concrete strength at time of testing;
- Reinforcement details (calculate shaft-impedance variations related to reinforcement);
- Soil borings, including details on water table;
- Static test results, if any; and
- Any other test results.

Establish an expected shaft geometry from these records. For example, when going from soft to firm soil, a reduction in cross-sectional area from an oversized to a nominal diameter may be expected; the actual to theoretical grout-volume ratio can be compared with the relative volume computed by the impedance-profile method. Where high resistance soils start, a compressive wave may be expected.

If one or more static tests were conducted successfully, test these shafts to serve as a reference.

Collect Data

Measure force and velocity whenever possible, but at least velocity, from several hammer blows. Only consistent data should be averaged; readings that differ greatly should be excluded from the average. For shafts with diameters in excess of 1 m, several impact and sensing locations should be chosen. Do not average these records; instead present results for all test locations independently. For shafts with large diameters, records should be obtained with both lighter and heavier hammer weights. Where records appear difficult to interpret, attempt to improve the data by

- Removing contaminated pile-top concrete or loose mortar layers.
- Delaying testing until grout/concrete strength has improved.
- Bending away reinforcement that might produce undesirable shaft top vibrations. If bending of reinforcement is impossible, measure force or velocity at points distant from hammer impact and the reinforcement.
- Testing or sensing at several locations. This is particularly important for large-diameter shafts.

Establish Longitudinal Wave Speed

Test Series with No Reference Shafts

If less than 5 comparable shafts are tested at one site, then it is best to assume a wave speed (typically 4,000 m/sec) for the concrete. Experience values from tests in the same general area, with the same concrete specifications and suppliers, may be used if they can reasonably be expected to have relevance to the test project. Shaft-length calculations are then based on the assumed wave speed and, of course, an observable toe signal. Such shaft-length results might be considered accurate within 10 percent.

Test Series with Reference Shafts

If the tests are conducted on at least five comparable shafts, then it may be possible to establish a reference pile or reference record. With clearly apparent toe reflections, a wave speed should be calculated based on the shaft-length values provided by quality construction records. The length of individual shafts can then be back calculated. Again, wave speeds from shafts that indicate greatly differing values should be excluded from the average.

Process Records

Exponentially amplify records to check for a toe signal. Start amplification at grade or where substantial soil effects are expected to begin (often indicated by a clear velocity decrease), but exclude no more than 20 percent of the full shaft-depth of penetration from exponential amplification. Amplification magnitude should be chosen such that the impact signal equals in magnitude the largest reflection amplitude; both the start of amplification and its magnitude should be similar for all records of like shafts at one site; otherwise establishing typical records is virtually impossible. This requirement may necessitate reprocessing records after all records have been collected.

Establish Reference Record

If more than four shafts are tested, attempt to establish a typical record, identifying consistent effects of soil resistance, or planned or unavoidable cross-sectional variations. Load test piles, whenever available, should be chosen for this purpose. Where less than five shafts have been tested, the reference record may be deduced from soil borings and the construction method.

Classify Records

Descriptions of records for Classes I through VIII follow:

- Class I: Clear toe signal indicating a wave speed within 10 percent of average; amplitude variations less than 20 percent of impact signal, or site-typical variations between top and toe. This is a Category-A shaft.
- Class II: Toe signal apparent; unusual records indicating bulbs or other gains in shaft strength. Strength-gain indications are velocity decreases without a prior increase. This is a Category-A shaft.
- Class III: Toe signal indicates wave speed greater than 110 percent of average. This must be interpreted as a potentially short pile (although it could be caused by a particularly high-quality concrete or grout). If a large number of shafts are tested, a statistical method may be used to identify potentially short shafts. Depending on the seriousness of the shortfall, the shaft may be Category B or C. Decision of rejection should be based on geotechnical considerations.
- Class IV: Toe signal indicates wave speed less than 90 percent of average. Conservatively, this must be interpreted as a potentially poor quality shaft (although the late toe signal could be caused by a long pile). It will be either a Category-B or C shaft, depending on the required concrete strength. For this purpose it may be satisfactory to assume that the concrete strength increases by 14 MPa (2,000 psi) for every 300 m/sec (1,000 ft/sec) of wave-speed increase. This approximate and relative strength-wave speed relationship was based on the ultrasonic pulse velocity method

(*8*), which deals with grout and concrete-strength determination based on ultrasonic wave-speed measurements. Differences between ultrasonic and sonic wave speeds were considered small considering the inherent errors in the proposed relationship.

- Class V: Toe signal apparent; major velocity increases greater than 20 percent of input signal indicate impedance loss not balanced by prior velocity decreases. A Category-B or C shaft, depending on the required strength of the shaft.
- Class VI: No toe signal apparent; minor velocity variations, of 20 percent of input signal or less, or site typical variations between top and where toe signal would be expected or velocity decreases indicating impedance gain not following a velocity increase. A Category-C shaft, it may be accepted if depth of apparent stress wave penetration is considered sufficient.
- Class VII: No toe signal apparent; major velocity increases greater than 20 percent of input signal indicate impedance loss that is not balanced by prior velocity decreases. This would be a Category-B shaft and be rejected as defective unless variations could be considered for the typical site, in which case, it would be classified as Category C.
- Class VIII: Unclear records resulting from major reflections near the pile's top or from high frequency components (for example, poor pile-top quality or reinforcement that sticks out at shaft top) or more than two major (greater than 20 percent of impact signal) reflections (impedance increases or decreases). This constitutes a Category-D shaft; additional tests need to be performed.

Analyze If Needed

Using the Pile Profile method or a simulation of the test process, (for example, signal matching, such as in the pile integrity wave analysis program (*9*), records from various categories should be analyzed to prove that the chosen classification is reasonable. These methods are not helpful if soil effects produce stronger reflections than impedance variations, or if cracks cause the reflections.

Prepare Report

The test report may be short. However, it should include soil boring(s), a summary of the construction records, the dates of construction and testing, design diameter and length, pile layout on the site, and records for each tested pile by category.

SUMMARY

The authors have attempted to remove some of the uncertainty "P.I.T." measurement engineers and their clients face in applying and interpreting the Pulse Echo test—and establish circumstances under which a shaft may be accepted or rejected.

The authors are aware that standardization of this test method is very difficult because of the great variety of site conditions, shaft types, construction methods, and even individuals involved in the construction process. Therefore, there may be many circumstances that would prevent a literal application of the guidelines given here. More importantly, these guidelines should not prevent future improvement in testing methods. On the other hand, the guidelines we afford should be expanded or modified to suit new findings or particular site requirements. With time and sufficient input from other experienced users, the guidelines may become a standard.

REFERENCES

1. Institution of Civil Engineers. Specification for Piling. Thomas Telford Ltd., Telford House, London, United Kingdom, 1988.
2. Franke, E., and J. M. Seitz. Recommendations for Dynamic Pile Tests of the Technical Committee 5 of the German Geotechnical Society. Deutsche Gesellschaft für Erd und Grundbau, Essen, Germany, n.d.
3. Specifications for Pile Integrity Testing. GRL and Associates, Inc., Cleveland, Ohio, 1992.
4. Rausche, F., G. Likins, and Shen Ren Kung. Pile Integrity Testing and Analysis. *Proc., 4th International Conference on the Application of Stress-Wave Theory to Piles*, The Hague, Netherlands, 1992.
5. Paquet, J. A New Method for Testing Integrity of Piles by Dynamic Impulse: The Impedance Log. *Colloque International Fondations Profondes*, Prèsse de l'École Nationale des Ponts et Chaussées, Paris, France, 1991.
6. Baker, C., et al. Drilled Shafts for Bridge Foundations. DTFH-61-88Z-00040. FHWA, U.S. Department of Transportation, 1993.
7. Rausche, F., and G. Goble. Determination of Pile Damage by Top Measurements. *Behavior of Deep Foundations* (Raymond Lundgren, ed.). Special Technical Publication 670. ASTM, Philadelphia, Pa., 1976, pp. 500–506.
8. Naik, Tarun R., and V. M. Malhotra. The Ultrasonic Pulse Velocity Method. *CRC Handbook on Nondestructive Testing of Concrete*, (V. M. Malhotra and N. J. Carino, eds.) CRC Press, Inc., 1991, pp. 169–188.
9. P.I.T.WAP Manual, Version 1.993-1. Goble Rausche Likins and Associates, Inc., Cleveland, Ohio, 1993.

New Techniques for Reliable Pile Installation and Pile Behavior Design and Analysis

MELVIN ENGLAND

Recent advances in rig-mounted computer-controlled monitoring and recording of pile-installation processes have allowed reliable and high-quality control to be developed. An automatic method for assessing the quality of continuous-flight-auger (CFA) pile-installation data, recorded during construction, is now well proven and most successful as both a management tool and as part of internal quality control of Cementation Piling & Foundations Limited in the United Kingdom. The data contain all the pertinent control parameters that when analyzed can identify important imperfections in the pile construction. The impact of these anomalies on the foundation behavior may then be assessed and any additional pile testing or corrective action prescribed if appropriate. Computers have also found their way into the practice of static load-testing for which they may be employed to monitor the pile-head displacement and the load applied by using electronic sensors. In addition, they can be made to control directly the load applied with regularity and accuracy that are unsurpassed. The quality of data returned from such test equipment has promoted the development of pile-behavioral models that have demonstrated remarkable accuracy in characterizing the measured pile behavior. The advances in this field are significant to soil mechanics generally, not just to pile behavior. The technique for modeling pile behavior under load has been developed into an important foundation-design tool that also allows the introduction of a sensible partial-factoring system that can be applied according to specific design conditions.

Since the development of the microprocessor, information technology has expanded to become a major growth industry. The collection, transmission, and analysis of data have become an everyday activity for almost all enterprises, and the piling and ground-engineering industry is no exception. Cementation Piling & Foundations Limited developed its own computer systems specifically for installation on piling rigs to monitor the processes of pile construction and to automate the labor-intensive task of performing static pile load-tests.

The on-board rig computers provide immediate display of information from various sensors on the rig as an aid to the operator. The data for each pile are stored and can be reproduced in graphical form and inspected from an in-cab printer or office-based computer, in many different formats.

Specific analysis software was developed to check automatically every pile installation and reduce the voluminous data produced by the fleet of rigs. This summarized data can be used as the basis for comprehensive statistical reports. Such analysis supplies a very important method for increasing the control of many aspects of a piling operation and can be very rewarding both technically and financially.

Cementation Piling & Foundations Limited, Maple Cross House, Denham Way, Rickmansworth, Hertfordshire, United Kingdom, WD3 2SW.

The introduction of microprocessors to static load testing provides a cost-effective, safer testing method, with a minimum of on-site staff. In addition, the automation of the load application has revealed significant aspects of soil behavior that hitherto have not been identified clearly. Specific pile behavioral models have been developed to study soil interaction with the pile and have greatly enhanced our understanding of pile behavior and provided the industry with new tools for the interpretation and design of foundation performance.

Time, load, and deformation may be regarded as the three dimensions of soil behavior. These components are interdependent, and if their interaction is not addressed the deformation/time and load/settlement diagrams may suffer distortion. On the other hand, if the load is held truly constant, the displacement/time function becomes hyperbolic for each particular element of the behavior, shaft friction and end bearing, and may be modeled mathematically and extrapolated to infinite time. This modeling in turn allows the long-term (fully drained) deformations to be calculated. These are also accurately represented by hyperbolic functions in terms of load.

PILE INSTALLATION MONITORING

Overview

Rapid development of computers over the last decade has enabled small, powerful systems to be used in the cabs of construction equipment. This, together with the advent of the personal computer, has created opportunity to gather and process large amounts of data.

By 1986, continuous-flight-auger (CFA) piling was becoming well established in the United Kingdom, and it was soon realized that, due to the nature of the process, monitoring CFA production was essential. Consequently, a system was developed to incorporate the measurement of concrete flow and concrete pressure as well as auger depth and revolutions. An in-cab printer provided the first major step forward, as the rig operators were required to produce these data for every pile, as unequivocal evidence and assurance of each pile's correct installation. A removable storage module incorporated in the system allows the data to be displayed and reviewed by computer at a head office.

Data retrieval and analysis enabled us to identify some specific innovations that would assist the operators and improve their performance and ability to follow the instrument display.

This commitment to monitor, process, and control site operations led to the Cemcomputer, a completely programmable, robust

instrument. It incorporates up-to-date hardware and requires only minor software adaption to suit various applications.

The first operation to benefit from this rig-mounted system was the CFA operation. The instrumentation of the rigs has optimized the technique and minimized its cost without adversely affecting the piles themselves.

Operators' reluctance to be the "spy in the cab" soon disappeared as the value of the instruments became recognized and the benefits, even for the drivers or operators, became apparent.

A similar system is now installed on many pile-driving rigs for precast concrete and wet-shaft piles, to monitor depth, number of blows, and actual set per blow—providing complete driving records for every pile installed automatically.

CFA Instrumentation

As illustrated in Figure 1, a concrete flow meter and pressure transducer, plus auger-depth and rotation sensors, send their respective measurements to the host display system for processing and storage. The rig operator uses the display for immediate control of the pile installation.

All the displayed information, together with other pertinent data, are stored in a nonvolatile storage module. It is then returned to the head office regularly for analysis by a specifically written software program that polices the data, to ensure that all piles have been constructed correctly. If any anomalous pile installations are detected when the many checks are performed, these are highlighted for inspection by the relevant site engineer or project manager.

The most important aspects of CFA production are to control the auger penetration rate, to make optimum use of the soil/pile friction that can be developed, and to fully and consistently fill the shaft with concrete throughout its length as the auger is withdrawn. Specific attention to the technique employed to initiate the concrete phase of the operation is also needed so that maximum end-bearing results. The data collected are specifically important when installing piles in loose sands or in alternating strata of cohesive and non-cohesive soil.

The amount of data that may accrue from the continuous operation of several instrumented rigs is considerable, and the task of checking every pile record individually prohibitively time consuming and expensive if performed manually.

Policing requirements were developed in consultation with internal piling specialists. The standards contain several different checking levels for the data and produce a printed summary automatically, indicating whether a particular pile has passed or failed each of these criteria—at a rate of approximately 100 piles per min. Should a particular pile fail, the engineering staff can be informed and an assessment is made as to whether any further action is necessary, such as a nondestructive test. The numerous, unexceptional results are documented and filed.

Comprehensive statistical assessments of all the significant aspects of the piling process can be compiled and analyzed, from the number of piles installed by each driver to actual production rates. This additional information provides a satisfactory assessment of the overall operation; it allows areas of poor performance to be identified and highlights options for reducing operating costs.

For instance, statistical analysis may be carried out for specific contracts to reveal actual production rates. Alternatively, analyses can be performed to provide a global picture for all rigs, all contracts, or all drivers and to display actual concrete consumption.

To date, the data base of the CFA operation monitored in this way contains more than 100,000 instrumented pile installations. Histograms are produced automatically for each rig at regular intervals for 36 different parameters. Histograms are employed so that the picture conveyed is not distorted by any atypical data. Therefore, the plots illustrate the general trends instead of the mean values.

Numerous combinations of statistics can be produced. Figure 2 shows the amount of concrete consumed. The dotted line (100 percent) represents the nominal bore of the hole, that is, the calculated volume from the auger diameter. The 125 percent marker indicates the selected target overconsumption that should be achieved.

Figure 3 shows maximum auger travel where the volume of concrete supplied fails to meet the volume of the bore removed by the auger, plus an inset limit. Rig number CM48/2 shows a poor performance for the period, which would warrant investigation.

The habits of a particular crew can be analyzed by examining the start times for each pile. The example shown in Figure 4 illustrates that a crew may have set break times irrespective of other site influences.

Management Tool

The preceding examples illustrate some of the information that can be presented to a management team to help control overall operation, as the system illustrates clearly the performance, technique, equipment and concrete usage, and efficiency of the overall operation.

Concrete-consumption and boring-rate statistics for each rig allow particular operators to be made aware of any poor results and how they may have incurred additional costs or taken risks that could be avoided. Operators who need further training can be identified.

Poor auger-lifting control together with auger boring rates are major concerns. Potentially these problems have very expensive repercussions; now they are specifically identified. Again, more training can be required and a close watch kept on policing results and data analyses to ensure that appropriate corrective action is taken.

Pile-depth and auger-size analyses also provide a picture of trends in the market. Such information is an important aid when purchasing new equipment, as the type and size of rig most able to meet production demand can be selected.

The automated system's benefits are also seen when estimating for new jobs. Actual production rates are available for particular rigs and crews for different requirements and site conditions. The information can be used to schedule jobs and assign particular rigs or crews in order to achieve specific production rates.

Both CFA and driven-pile instrumentation continue to develop. Additional features are regularly incorporated, for example, mast inclinometers, which can be installed readily on the basic system, reducing set-up time.

Conclusions

CFA piles nearly always are constructed in the United Kingdom with the benefit of computerized instrumentation and the require-

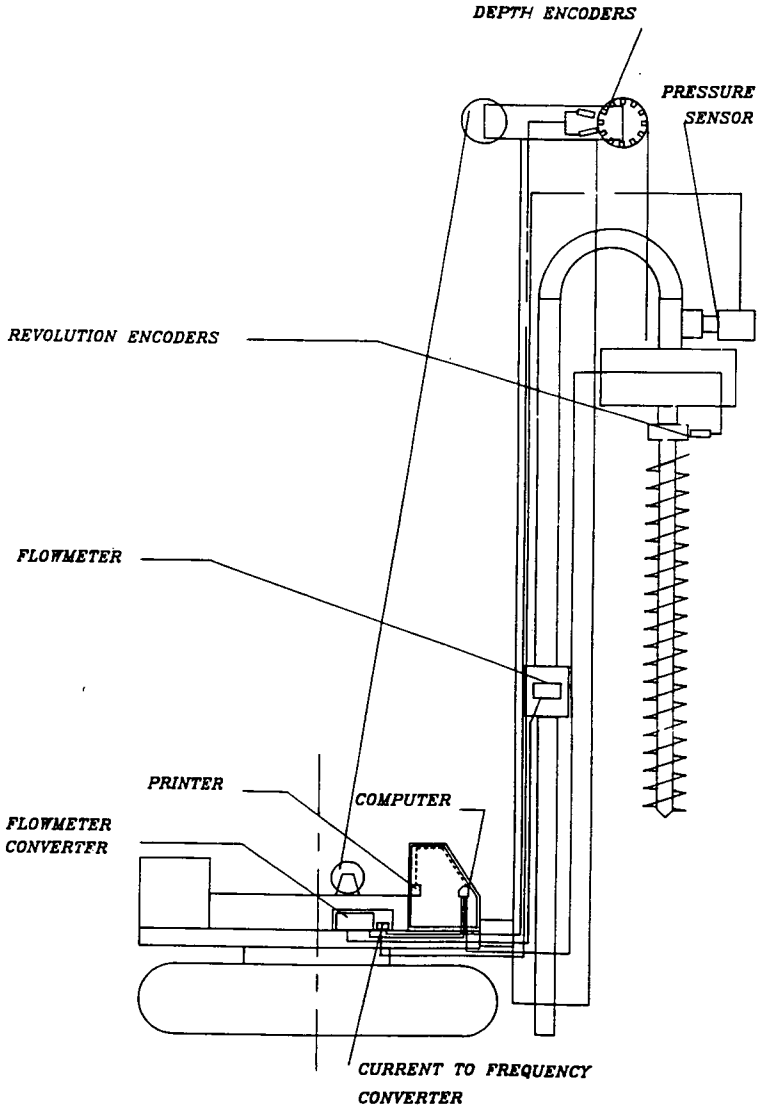

FIGURE 1 CFA instrumentation system diagram.

ment of on-site cab printouts for each pile. If an operator's performance cannot be relied on, client representatives on site may be the first to identify operator deficiencies and demand costly interruptions and remedial works during the piling program.

The policing system provides not only a comprehensive quality-control tool but ensures a high level of operator reliability and a standard of excellence for pile installation. The best reason to use such a system is the opportunity it affords to control the operation.

Analysis of the results of concrete consumption and auger lifting reveals some performance deficiencies. Of course, unless such problems can be identified and corrective action taken, potentially defective piles will continue to be installed.

To control the auger-lifting rate on the basis of concrete delivery can be a demanding task for rig operators, yet the ability to withdraw the auger at a steady rate based on concrete flow is critical. Withdrawal of the auger under computer control may soon be a standard requirement unless quality control methods, such as the self-policing system we describe, are used.

INNOVATIONS IN STATIC LOAD TESTING AND ANALYSIS

Overview

Although the recorded test results from a static load test may be a factual record of the pile displacement during the test, it is not the pile's definitive, long-term behavior that has been measured. Testing a partially drained pile does not allow for the total creep that may ltaer result.

Every pile, at the time of testing, has a single and unique behavior that can be determined by carefully controlled load-application and pile-displacement monitoring. The method we will describe is based on Terzaghi's definition of ultimate bearing capacity (*1*). Definition of the term is unequivocal and may be expressed mathematically as the asymptote of the load/settlement curve.

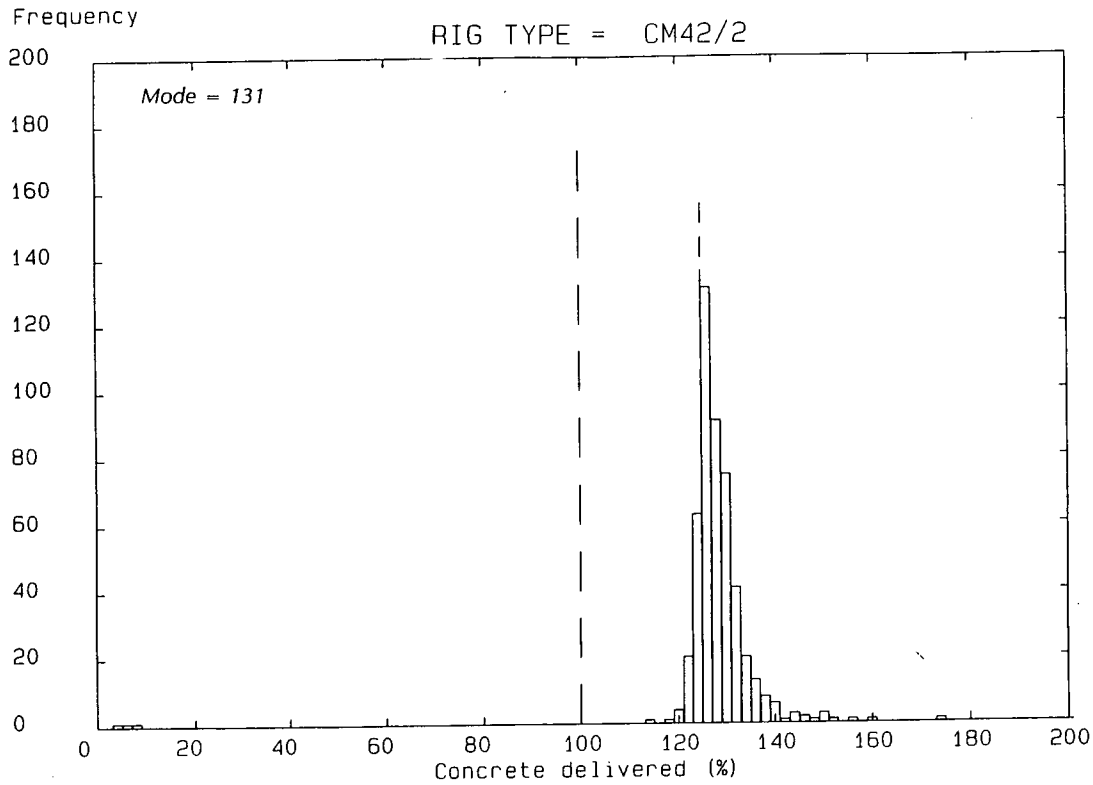

FIGURE 2 Concrete consumption during installation.

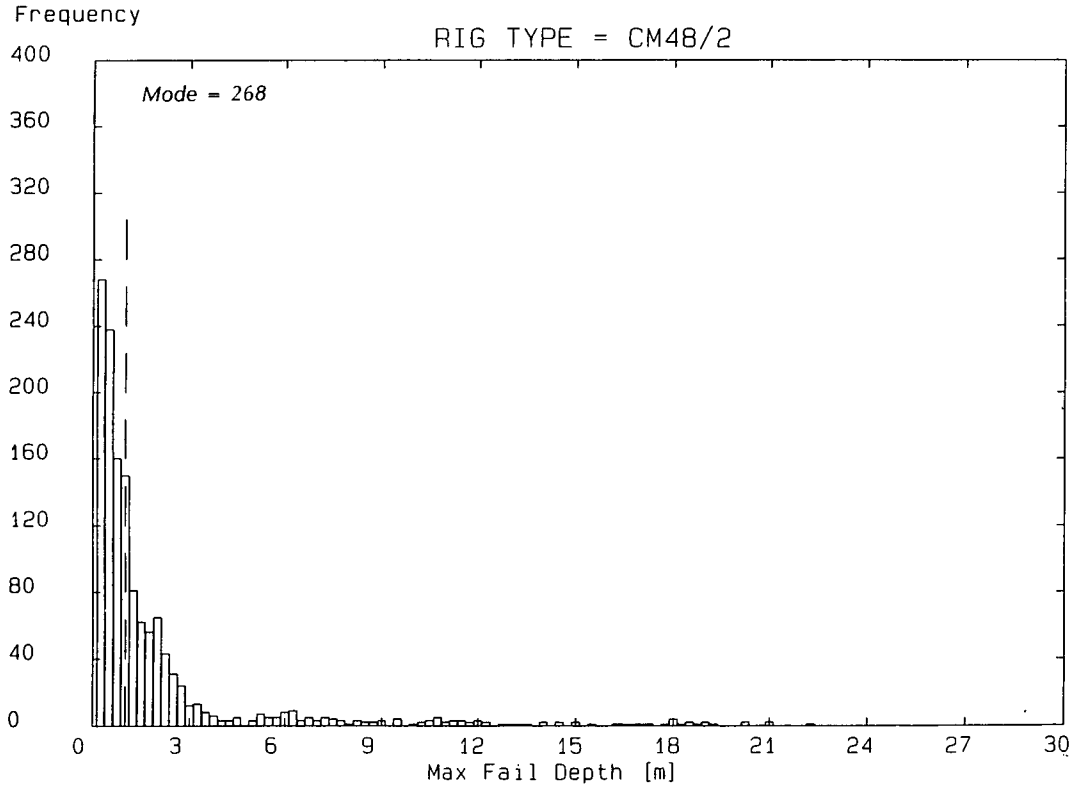

FIGURE 3 Fail depth.

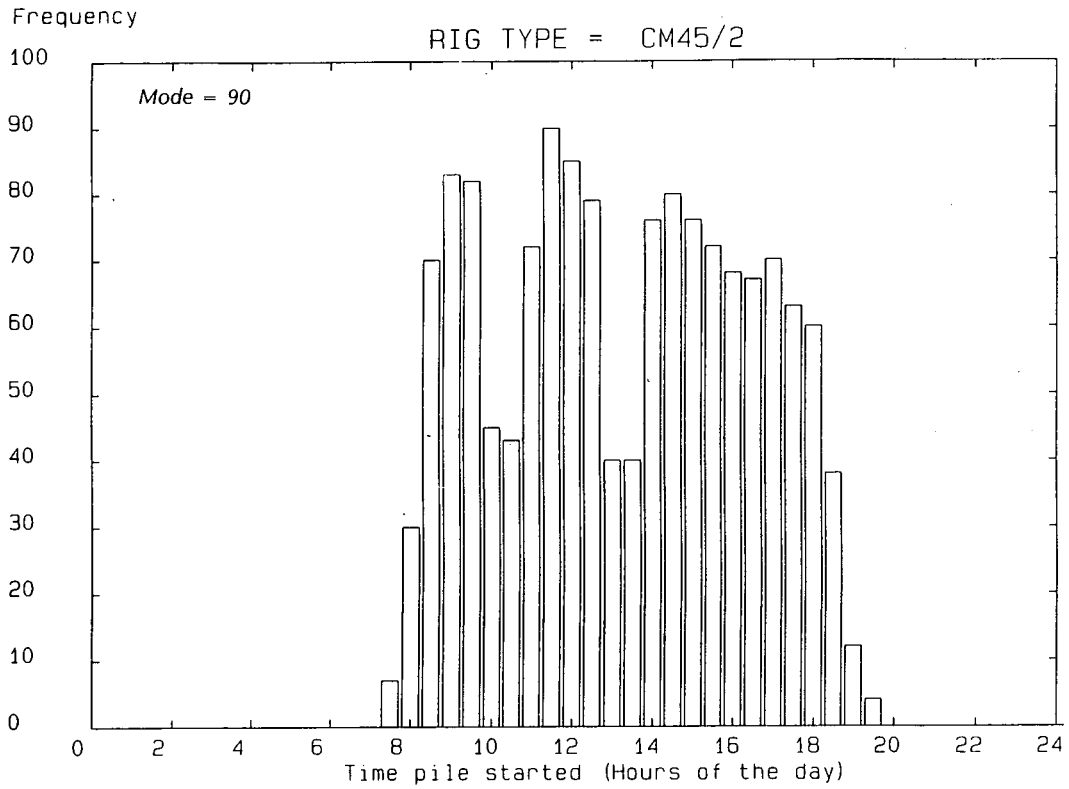

FIGURE 4 Pile start time.

Because the behavioral characteristic of a pile under load is unique, interpretation of results becomes necessary to remove the effects of the test method, the sequence in which and the time and the data are taken. Sometimes accurate evaluation of the pile behavior may be impossible.

Although a considerable amount of test data has been recorded in the past, complete analysis of these data has been difficult because, in general, the conditions under which the data were recorded impede analysis.

The test equipment we describe is basically a computer-controlled loading and pile-head displacement measuring system. Analysis involves a time-displacement model that accurately characterizes the development of both end bearing and shaft friction to derive the final settlements under each load. These settlements can then be used to determine the unique load/settlement behavior and the distribution of load between the shaft and base.

The method employs the major elements that control pile behavior. Soil stiffness and strength, together with changes to them in time, are vital to understanding pile performance. The techniques appear to be applicable to most foundation types for which deformation assessment is significant.

Type of Test

Foundations generally are required to carry axial static loads for a long period of time. During most construction, civil engineers find that the loads applied to the foundation system are gradually increased as work progresses to some final value. The best foundation test that could be employed would be one that replicates the interim and final conditions as closely as possible. However, for practical reasons it is desirable to carry out these tests expeditiously to minimize any external influences and allow construction to progress without interruption.

If a pile test were carried out by long-term application of load, over a range of loads, during which the force applied is constant and the displacement ceases completely at each load stage, then the unique load behavior of the pile would be discovered.

All pile-test methods have to compare with this standard. On the other hand, if the duration of the test is reduced, its effect should be taken into account separately to ensure correct interpretation. For example, the continuous rate of penetration test, which involves pushing the pile into the ground at a constant rate, was not designed to produce the unique pile characteristic. Despite its declared aim, determining the ultimate capacity, a number of authors (*2*) confirm that it generally overestimates pile capacity.

Quick maintained load tests and all impulse or dynamic load-testing systems, present the same problem; they do not reveal unique long-term pile behavior or a pile's ultimate capacity.

The behavior of a correctly constructed pile is controlled by its interaction with surrounding soils. It is fundamental that soil properties are taken into consideration, especially the primary ones governing pile: behavior strength, stiffness, and time.

The time-dependent effects of soil surrounding a pile are generally not addressed in short duration tests, and consequently pile performance is usually overestimated. However, once these effects are correctly assessed, the load/settlement behavior of any pile is unique and independent of the test duration.

Most British engineers use conventional maintained-load testing and it is the basis of the developments we describe here.

Computer-Controlled Load-Test Equipment

Basic computer-controlled load-test equipment consists of several displacement transducers to monitor the pile head movement with respect to a datum, and electronic load-measuring equipment; all are linked to a data logging system. These are the basic components required for any pile-load test. The microprocessor, which regulates all the functions, also checks the load applied to the pile at intervals of a few seconds and effects any changes required by controlling the hydraulic pressure feeding the loading jack, as illustrated in Figure 5. The equipment has been refined to minimize any external influences that might affect the measured pile behavior.

Some of the immediate advantages of employing this equipment are as follows:

- Simultaneous readings of all transducers are made selectively at intervals of between 2 sec and 10 min.
- Printing and plotting of all data are possible directly from the computer, minimizing clerical effort for producing reports.
- Current readings can be displayed remotely, enhancing the safety aspects of the test. Automatic system control allows for unattended operation if required. This feature is particularly suitable for overnight tests, although a security person may need to be in attendance.
- Data are already compatible with a suite of programs for back analysis, allowing accurate and reliable interpretation of the results and characterisation of the dominant materials that surround the pile.

Whereas the measurement of actual elastic properties of the pile and separate base-load sensors are desirable, these are unnecessary when using the analysis techniques developed; therefore, deployment of costly sensors within the pile can be avoided.

Models that Characterize Pile Behavior

Any pile/soil modeling technique or mathematical model must:

1. Characterize accurately the pile behavior both in time and under load.
2. Be able to model the displacement/time behavior accurately so that, with sensible load-holding periods, the final settlement at infinite time under a given load can be determined precisely.
3. Follow load/settlement behavior at each and every load stage up to the ultimate load-bearing capacity, determining the maximum settlement at any load.
4. Encompass the nonlinear behavior of the soil, including parameters relating to strength and stiffness along the pile shaft and beneath the pile base as well as related time constants.
5. Be suited for both pile design and back-analysis of test data.
6. Employ typical pile-head displacement data so that they can be used to back analyze commonly available information from well carried out tests, enabling the evidence and validity of the models to be determined.

Mathematical models now exist that are based on hyperbolic functions and fully satisfy the preceding requirements. One component of a model deals with shaft friction development, and a second component with the behavior of the pile base. Analysis has been performed on many hundreds of test results with out-

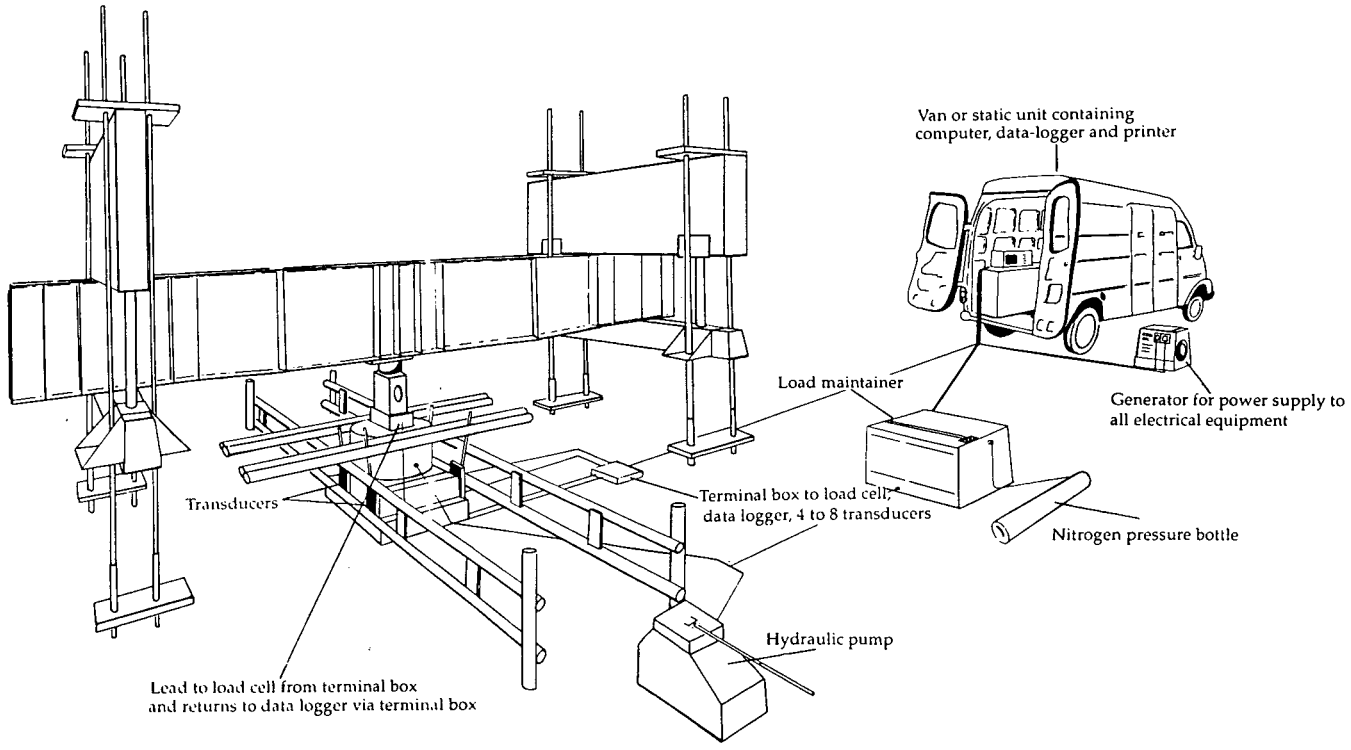

FIGURE 5 Computer controlled static load test equipment.

standing success. One of the features of the technique is its simplicity, as it requires only two parameters to fully characterize the displacement of each element under load. Following is the total parameter set required for the complete model of pile behavior.

Ds = equivalent diameter of the pile shaft,
Db = equivalent diameter of the pile base,
Us = ultimate shaft friction load,
Ub = ultimate pile base load,
Ws = asymptote of shaft development at given load,
Wb = asymptote of base development at given load,
Lo = upper length of pile carrying little or no load by friction,
Lf = length of pile transferring load to the soil by friction,
Ms = flexibility factor representing movement of the pile relative to the soil through friction,
Eb = deformation secant modulus for soil beneath the pile base at 25 percent of ultimate stress,
Ts = shaft material time constant to reach 50 percent of final settlement for a given load,
Tb = base material time constant to reach 50 percent of final settlement for a given load,
Ec = Young's modulus of elasticity of the pile material, and
Ke = factor positioning the effective centroid of the friction transfer diagram.

Assessment of Pile Behavior Against Time

The final pile settlement at a given load is clearly that which would occur at infinite time, when the settlement rate is zero—the asymptote of the displacement/time characteristic. This value is representative of the working condition of the pile.

Until recently, the preferred assessment methods were based on plotting the slope of pile settlement against time on either a semilogarithmic or time-displacement scale. The second of these techniques, proposed by Chin (*3*), has been the most popular, but it allows only the shaft and base settlements to be accurately distinguished when one or the other is insignificant—a rare occurrence unless each load application were held for durations greater than 6 hrs. In effect, accurate assessments of final pile behavior under a given load were seldom achieved.

Now, an algorithm that accurately characterizes both the base- and shaft-time elements has been developed and is contained within a new computer program, (TIMESET), which can track field results with remarkable accuracy provided sufficient data have been recorded. This algorithm, based on hyperbolic functions, allows the displacement behavior of the element to be calculated for points outside the test data; indeed, it can determine the asymptotic value for any load stage. A feature of this form of time analysis is that normalized time constants can be obtained. This allows the total duration of the test specification to be minimized as the normalized time constant for the base behavior remains unchanged by the different loads applied.

An example of a pile-test result, obtained using high-grade monitoring and control equipment, is illustrated in Figure 6. The application of each load was held constant for durations between 30 min and 6 hr, and the measured load/displacement is plotted as a continuous line. The final settlements calculated for each load are indicated as separate points.

This method of analysis allows unambiguous interpretation and is particularly suited to cases in which the load applied effectively has been maintained constant within each load step.

The development of this method of analysis of displacement/time data only has been possible since the advent of fully computer-controlled static load tests, in which the data recorded are more accurate and considerably more frequent than before, and the load applied can be maintained at a constant rate.

The extrapolation of the displacement/time behavior represents a fully drained condition and is unaffected by any previous loads applied to the pile before the one under consideration. However, if the previously applied load were higher, factors such as plastic deformation and the history of the soil may preclude accurately predicting a compatible load-settlement characteristic.

The displacement/time model illustrates why pile-testing methods of short duration reveal pile behavior in an undrained or partially drained state and offers an explanation for the widely recognized over-prediction of pile performance; it also explains why base performance is so often underestimated.

Figure 7 shows displacement/time data recorded with a computer-controlled testing system for one specific load hold period, together with the results from the analysis. The separate components of the time relationships for the shaft and base are obtained by mathematical optimization and are illustrated as broken lines on the figure. The pile displacement/time model is the sum of the two components *Ws* and *Wb*.

The data points, which are plotted continuously, are virtually indistinguishable from the results obtained from the mathematical model. The quality of modeling has been consistently good for all soils we have analyzed to date. Note that this displacement behavior is apparent in cohesive and non-cohesive materials and is therefore not solely due to excess pore-water pressure dissipation.

Assessment of Pile Behavior Under Load

The interpretation of pile settlement/load relationships has been a matter of some controversy. Many empirical rules have been developed in this field, perhaps as a result of differing ground conditions in various parts of the world and favored pile types.

One of the best interpretative methods employs a technique developed by Chin (*4*) in which, when settlement is plotted against settlement divided by load, the slope of the latter part of the data is taken as a good indicator of a pile shaft's ultimate capacity.

Two things have militated against Chin's proposed method. First, because its means of plotting implies a single hyperbolic function, the method fails to give a good result in cases where there are really two strong hyperbolic functions present, one for the shaft and one for the base. Second, the method's definition of "ultimate" pile capacity (*5*) does not suit everyone's structural requirements.

Under these conditions, "serviceability" states should be defined. True "ultimate" states cannot be defined arbitrarily or be based on mechanical dimensions of the pile alone. From a mathematical point of view, the correct definition for foundations has to be the asymptote of the settlement/load relationship. From this asymptotic definition most other definitions of "pile failure" can be derived.

The CEMSET method of prediction (*6*) and the program CEMSOLVE, specifically developed for back-analysis of single-pile behavior under load, overcome the limitations encountered with Chin's method by identifying the fundamental hyperbolic functions that characterize the shaft friction and end bearing

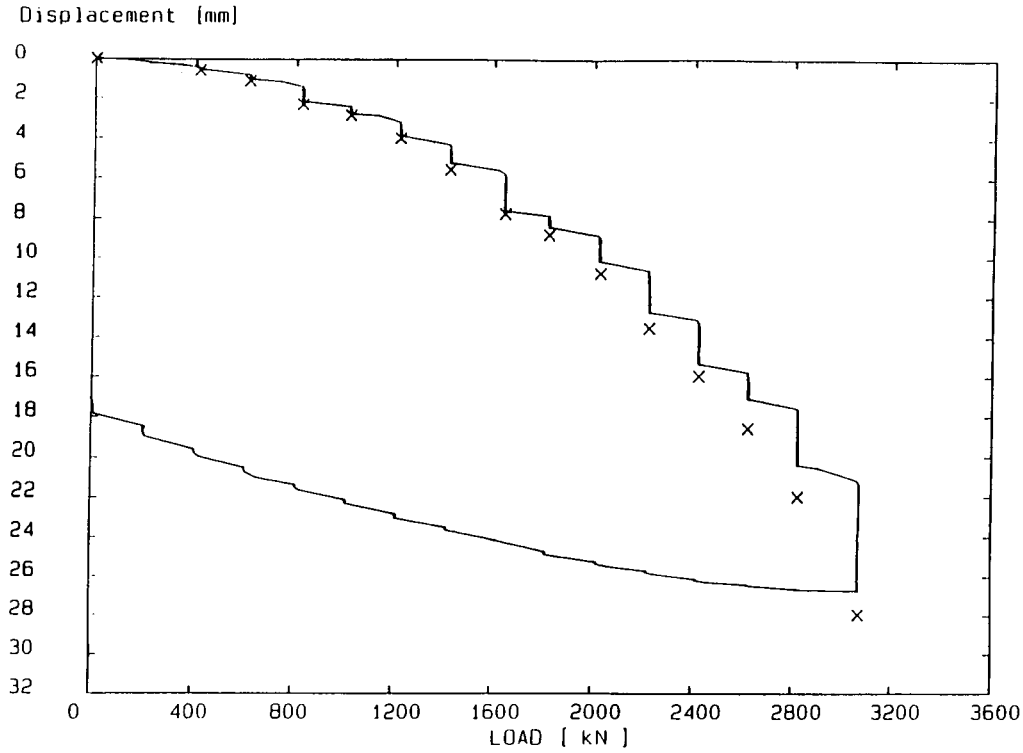

FIGURE 6 Load/displacement diagram.

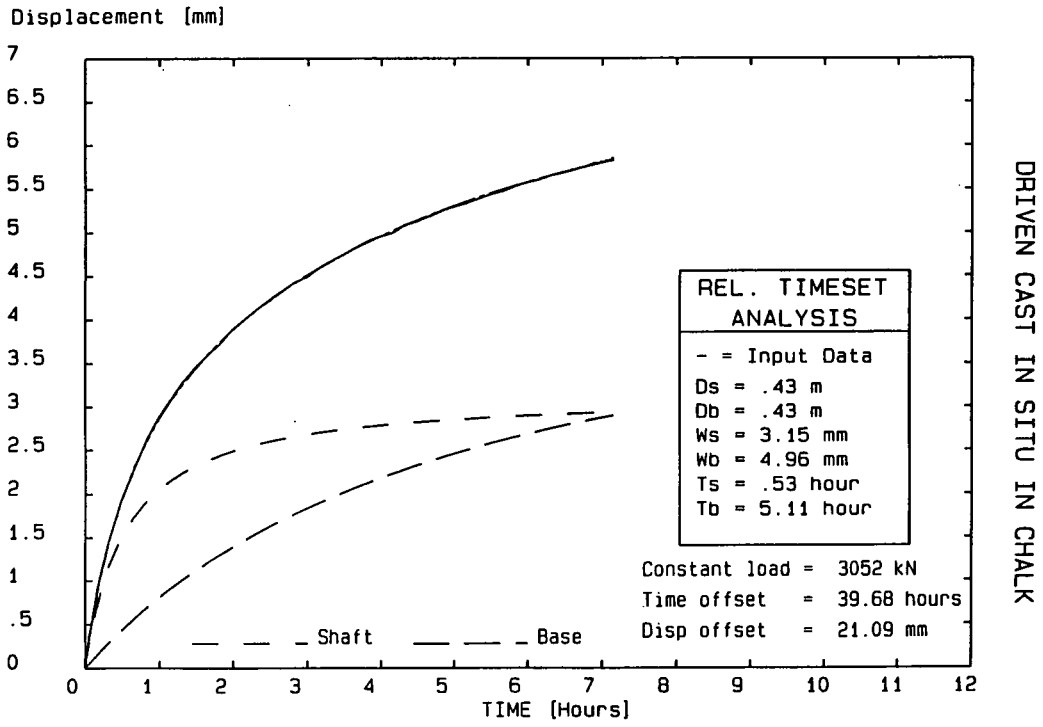

FIGURE 7 Displacement/time diagram.

separately. CEMSET and CEMSOLVE define asymptotes for the ultimate capacities and then include a basic, but sensible, elastic shortening model of the pile material.

Illustrated in Figure 8 is the back-analysis of the data shown in Figure 6. The correlation between total settlement at each load and the line generated from the numerical model is excellent and typical of the results that can be obtained from a computer-controlled load test.

The models return a high level of accuracy in the wide range of ground conditions encountered, provided the settlement and applied load have been well recorded and sufficient data are available. Results from static Maintained Load tests are compared with the model solutions in the program CEMSOLVE and show correlation coefficients that are superior to those obtained by earlier forms of analysis. More than 800 pile-load tests have been analyzed in this way with outstanding success. No case has yet been found in which the mathematical models do not represent with high accuracy the measured pile behavior.

Piles in the same ground conditions but of differing diameters have also been studied. The behavior of soils around piles of differing diameters can be readily characterized. For load/settlement analysis, the potential for installing smaller-diameter test piles to confirm the pile design and obtain all the relevant soil parameters is now a reality.

So accurate are the modeling techniques that they have been extended to characterize the behavior of surface foundations as well as piles. Similarly, unloading and reloading can be tracked and modeled.

Limitations

If a test pile is not moved sufficiently, few of its pertinent characteristics can be accurately defined. But provided the piles mobilize a significant part of their base capacity and overcome skin friction, back analysis using these models can reveal significant characteristics of pile/soil behavior and the distribution between skin friction and end-bearing capacity, although not their location on the pile. This analysis allows contractors to either confirm that the design is good or diagnose how the design is deficient or over conservative with respect to the pile geometry, type, and installation technique.

Back analysis is not intended to provide an accurate measure of the elastic shortening of a test-pile result. It does however, allow for a first approximation by employing one of several models that allow for differing soil-strength distributions along the pile length. There are better and more suitable methods of determining this parameter, such as extensometers within the pile body.

Any results obtained from a static load test are pertinent to the conditions prevailing when the pile was tested, and any subsequent soil (structural) changes cannot readily be identified. For example, a single isolated pile may be tested, but the installation of additional adjacent piles can significantly affect the original pile's performance. Also, if the mechanical properties of the materials or time characteristics of the pile or soils change—either with time or because of moisture content or general consolidation—these may not be assessed.

Note that the TIMESET model is most suitable for use if the pile test load has been maintained constant and sufficient data

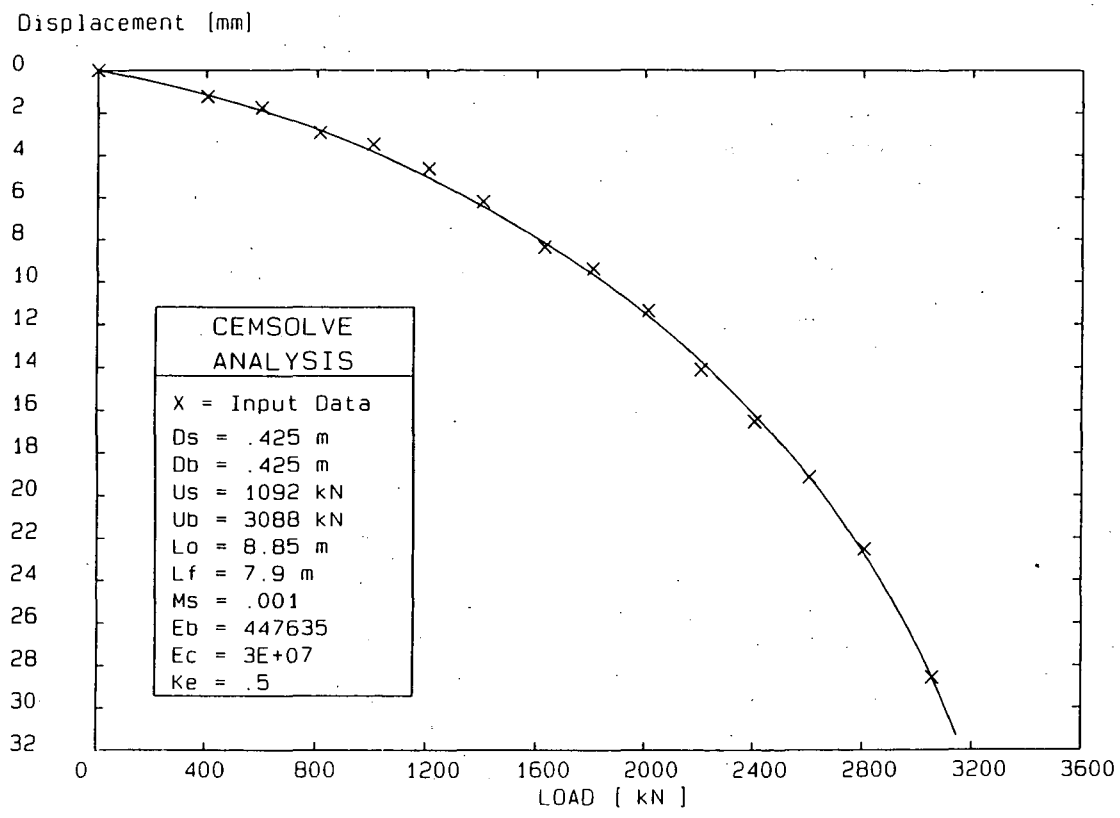

FIGURE 8 Load/settlement diagram.

points have been recorded in order to allow the model to determine the best fit to the data mathematically and calculate uniquely the separation of the components. Similarly, the shaft and base characteristics under load must be sufficiently different for their separation to be possible. Fortuitously this is generally the case.

PILE SETTLEMENT PREDICTION

Overview

To model the displacement over time, hyperbolic relationships are introduced first, then the functions for characterizing the settlement/load. The origin of this approach was the development of a new design technique based on hyperbolic functions linked to soil parameters, which model the behavior of the end bearing and skin friction individually to allow pile-settlement prediction (*6*).

Proving this design method could be applied in many other scenarios required the development of a behavior-analysis technique and appropriate test equipment. The pile behavioral model employed for design is the one we previously described for the analysis of load-settlement.

Some engineers are keen to link this technique to Chin's method and to recognize that it is just an extension of the single hyperbolic function; others are more interested in noting that the stiffness of soils is now recognized as a significant element-controlling pile-settlement behavior, or that it can be considered an extension of the *p-y* technique for characterizing soil behavior.

In this work it is evident that soil stiffness is defined in relation to its in situ value and linked directly to its ultimate capacity. This strength and stiffness relationship thus provides the framework for characterizing the behavior that may result after preloading or reloading.

Currently most information from soil investigations do not indicate the stiffness values directly; therefore, these need to be established by direct experience. The CEMSOLVE analysis method allows for assessment of the resulting soil parameters after pile installation, thereby allowing the designer to take into account the merits of different pile-installation methods. Certain types of soils exhibit marked boundaries and the limiting values, strength and stiffness, are generally well recognized.

The ability to arrive at pile-reaction parameters on a much broader basis than before means that, for example, bearing-capacity coefficients and frictional factors may be derived from real rather than theoretical considerations and that the use of this system as a design tool is not necessarily limited to a specific range of data, soil conditions, or foundation types.

Partial Factors

The parameters used in the CEMSET model for pile behavior allow each of the governing components to be assessed individually. The method also takes into account the likely variation of parameters that could occur, depending upon the method of design or interpretation of soil data. The method suitably applies a sensible, partial factoring system (*7*). The parameters can be assessed independently to determine the degree of confidence in the expected results, so it is no longer necessary to address the problem of how to combine factors on parameters that are interdependent, as it is necessary for some design methods.

The factoring method can also be used during back analysis to review the likely worst-case pile behavior at a particular site. The factors used reduce as the system gathers more detailed and more accurate installation records. In some instances, the installation records can be used directly to determine the worst pile or worst soil conditions on a site.

CONCLUSIONS

The diagnostic value of a single-pile test depends on whether the selected pile is representative of those installed at a particular site. The instrumentation method we have described does provide documented evidence of the quality and reliability of each pile installation.

The pile-behavior analysis system is suitable for use with practically any test specification; it also allows the most effective test specification to be selected. Many engineers now recognize the hyperbolic relationship and realize that there will be one such characteristic for each element of the system being studied.

Test equipment has been developed that maximizes, in a cost-effective way, the information that can be retrieved from a load test and allows the minimum test specification duration to be determined. The new techniques require measurement of only the pile-head displacement under load for complete analysis. No sensors are required within the pile.

The time- and load-settlement modeling performed using the TIMESET and CEMSET/CEMSOLVE algorithms indicates that this method of pile behavior analysis is reliable and superior to any existing method.

Although it is often implicit that specified test methods or testing practices reveal "useful information," it is apparent that the methods described herein extend well beyond normal expectations in this respect, as soil parameters can be deduced from the results.

From a designer's viewpoint, the methods allow the most cost-effective piling system to be identified, to comply with specific settlement requirements, for example. From preliminary test-pile results, the pile parameters can be optimized for both minimum cost and maximum performance. Therefore, its use potentially extends into the field of piling equipment design.

Because unique pile behavior under load can be determined using the method, it is an invaluable tool for design, analysis, and diagnosis. The method is simple to use and greatly improves understanding of pile and soil behavior.

REFERENCES

1. von Terzaghi, K. *Theoretical Soil Mechanics*, 2nd ed., John Wiley and Sons, Inc., New York, May 1944, p. 118.
2. Twine, D., and W. Grose. *Proc., International Chalk Symposium*, Brighton, Thomas Telford, London, England, Sept. 1989, p. 417.
3. Chin, F. K. The Seepage Theory of Primary and Secondary Consolidation, *Proc., of the 4th Southeast Asian Conference on Soil Engineering*, April 1975, pp. 3/54–3/61.
4. Chin, F. K. The Inverse Slope as a Prediction of Ultimate Bearing Capacity of Piles, *Proc., 3rd Southeast Asian Conference on Soil Engineering*, Hong Kong, 1972, pp. 83–91.
5. Fellinius, B. The Analysis of Results from Routine Pile Tests, *Ground Engineering*, Vol. 6, Sept. 1980, pp. 19–31.
6. Fleming, W. G. K. A New Method of Single Pile Settlement Prediction and Analysis, *Geotechnique*, Vol. 42, No. 3, Sept. 1992, pp. 411–425.
7. Fleming, W. G. K. Limit States and Partial Factors in Foundation Design, *Proc., Institution of Civil Engineers*, London, England, Nov. 1992, pp. 185–191.

Atlas Screw Pile: A Vibration-Free, Full Displacement, Cast-In-Place Pile

F. DE COCK AND R. IMBO

Developed in Belgium about 35 years ago, the Atlas screw pile has been used widely during the last decade in Europe and elsewhere. The Atlas screw pile can be defined as a vibration-free, cast-in-place concrete pile with double lateral ground displacement (during penetration as well as during extraction of the casing). The pile's high level of acceptance is related to the reliability of its equipment, the low level of noise pollution and lack of vibration during its construction, and availability of a computerized data-acquisition system to monitor its execution parameters, as well as its excellent bearing performance. Hydraulic rigs allow for production rates in the range of 100 to 150 m per day with a 2-person crew. Standard screw pile diameters range from 45 to 70 cm. Allowable bearing capacity typically is between 1,000 and 2,000 kN in compression and up to 1,000 kN in tension. The pile's method of construction characteristics, range of application, design, performance, and its quality control are described. Piles can be constructed in nearly all soil types in which traditional rammed cast-in-place piles are used. The lateral soil displacement effect, with the virtual absence of any significant spoil, as well as the particular helical screw shape of the concreted pile contribute to its high bearing resistance and stiff settlement behavior.

Since its development in Belgium about 35 years ago, the concrete Atlas screw pile has been introduced successfully in many European countries and in Australia. The pile is fabricated by screwing into the ground a temporary, closed casing with an auger-shaped displacement head at its bottom and by filling the created void with concrete during the extraction of the casing. In effect, the pile is a cast-in-place pile with double lateral soil displacement—occurring once during the penetration and once during the extraction of the casing. The pile is characterized by a particular helical shape over its full shaft length, as shown in Figure 1.

Although the Atlas screw pile sometimes is classified as an auger pile, a clear distinction should be made between two classes of auger piles (Figure 2). First, auger piles of the drilled type, such as continuous flight auger piles, are constructed using an auger with continuous flight on a central stem. An example, with relevant soil extraction, is shown in Figure 2(*a*). Second, (single) auger piles of the screwed type, such as the Atlas screw pile, essentially displace the soil laterally and produce virtually no spoil, as shown in Figure 2(*b*).

It is obvious that the load behavior of auger piles may be quite different depending on whether they are installed by drilling or screwing with drilled piles. There is the detrimental effect of soil decompression because of excessive upward soil displacement during drilling or extraction of the continuous auger. With screwed piles, on the other hand, there is the beneficial effect of soil compaction and an increase in lateral stresses around the pile shaft caused by substantial lateral soil displacement during pile installation.

Franki Foundations S.A., Nieuwbrugstraat 85, B-1830 Machelen, Belgium.

PILING EQUIPMENT

Atlas screw piles are installed by a hydraulic rig built for that purpose. Most rigs allow for vertical piles only. However, with a BTS-50 rig, it is feasible to make batter piles up to an inclination of one third (approximately 20 degrees).

The general configuration of the actual rigs in the BT-40 series is shown in Figure 3. The heart of the rig consists of a drilling table and two hydraulic rams to penetrate and extract the casing. The 2-speed drilling table transmits a rotational movement of the casing at high speed (12 to 16 rpm) or low speed (6 to 8 rpm). The pressure rams can function either separately or in combination. In the former case, one ram exerts a crowd force on the casing, while the inactive ram returns to its initial position to take over when the first ram ends its course. In this way, a continuous rotational and translational movement of the casing is obtained. Both rams also can work together to double the total thrust force. In that case the rotating movement is not continuous. The combined power operation is applied, for example, when hard soil layers have to be penetrated, or at the onset of reversed screwing in order to obtain an enlarged base or a more characteristic helical shape. For the actual machine generation, the torque of the drilling table is a maximum 450 kNm; the maximum crowd force of both rams together is of 240 kN, whereas the maximum extraction force is of 800 kN.

The rig further comprises the following:

- Main framework, which houses the central engine, the pumps, the steering equipment, and the four outriggers for stabilization and leveling of the rig;
- Crane jib with a lifting capacity of 10 kN and a maximum reach of 16 m, used to place the reinforcing cage and to lift the skips to introduce the concrete into the casing;
- Underframe, provided with caterpillar tracks, can spin around.

Another substantial feature of the screw-piling equipment is the casing, which is composed of the following (see Figures 3 and 4):

- Hopper on which the concrete skips are placed.
- Mandrel, consisting of several thick-walled, steel tube segments, joined together by concealed joints. Only one type of casing, all with an external diameter of 324 mm, is used for the various standard pile diameters. On the outside of the mandrel, steel driving laths are welded to transmit the rotational and translational movement from the drilling table and the pressure rams to the casing.

FIGURE 1 Exposed Atlas screw pile.

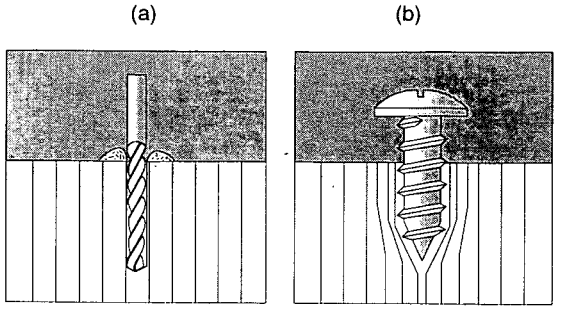

FIGURE 2 Drilling (*a*) and screwing (*b*).

- Hollow dismountable head, consisting of a cast-iron helical body with a minimum diameter D_c, which ensures the lateral displacement of the soil, and a helical flange with an outer diameter D_f, which is welded on this body at the point where the diameter is greatest.
- Sacrificial tip equipped with two one-way carriers; the joint between the tip and the displacement head is sealed to make the casing watertight.

PILE INSTALLATION PROCEDURE

The pile installation sequence is shown in Figure 5. On the site where a screw pile is to be constructed, a rig is placed in the correct operational position by means of four leveling supports, whereby the axis of the casing is placed along the theoretical line of the pile axis. The sacrificial tip is placed under the displacement head and the joint between them sealed with a waterproof-plastic kit.

The combined action of the rotating drilling table and both pressure rams takes the casing down in a continuous clockwise, helical, penetrating movement, causing the first lateral displacement of the surrounding soil. The operation is vibration free and also relatively noise free. Simultaneously the drilling parameters

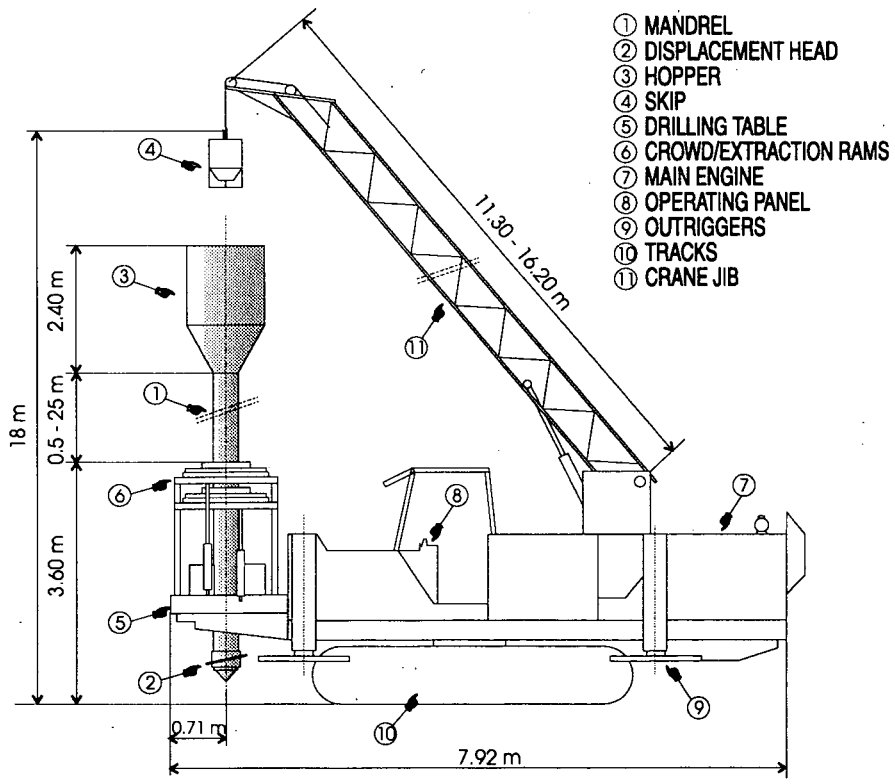

FIGURE 3 The Atlas BT-40 screw pile rig.

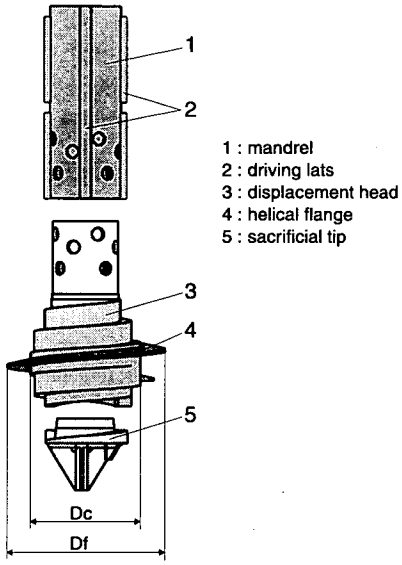

FIGURE 4 Detail of the displacement head and sacrificial tip.

are measured and recorded by a computerized data-acquisition system.

When the required founding depth is reached, a full-length reinforcing cage is placed into the hollow mandrel, and concrete is skipped into the hopper in sufficient quantity to completely fill the pile. To form the pile, the casing is then rotated in the reverse direction and extracted. The initial backward rotation forces off the sacrificial tip, which remains in position in the soil. As the enlarged displacement head is recovered, lateral soil displacement occurs a second time, during the extraction. The concrete immediately fills the void created by the displacement head. Care is taken that the hydrostatic concrete pressure at the bottom of the casing at all times is kept considerably higher than the combined soil and water pressure acting at that point. In this way the danger of shaft constriction is avoided.

After concreting, and when important bending moments have to be take up (for pile walls, for example), a second reinforcing cage can be installed in the fresh concrete by static pushing or by using a small vibratory device. Guidance by the first cage guarantees the centering of the additional cage.

CHARACTERISTICS OF THE ATLAS PILE

Concrete

Van Impe's research on the behavior of auger piles (*1*) shows that the method of casting and the quality of the concrete—water/cement (W/C) ratio and workability—influence the arching effect of the fresh concrete in the casing in an important way and thus affect the real concrete pressure at the outlet. The concrete used should be as plastic as possible without having an excessively high water content, as that would reduce the concrete's strength, and increase the risk of leaching out of the cement. Concrete with a good grain-size distribution—made of low-sized, rounded

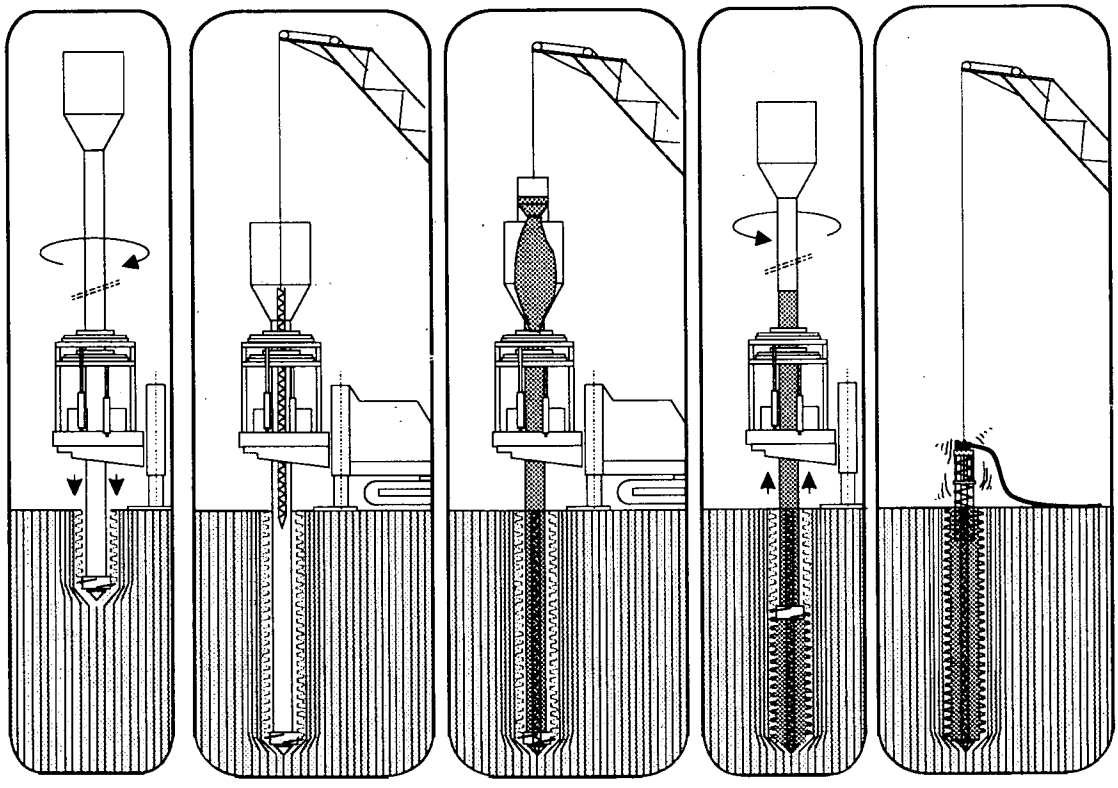

FIGURE 5 Installation sequence for Atlas pile; (from left to right) screwing in, introduction of central reinforcing cage, filling of casing hopper with concrete, screwing out and concreting, and introduction of additional reinforcing cage.

gravel, not too fine sand, a suitable cement type, and eventually an appropriate plasticizer—is of utmost importance to successful construction of a pile.

The following mixture is often used:

- 350 kg cement HK40;
- 1250 kg (approx. 800 l) rounded gravel $^{4}/_{14}$ mm;
- 625 kg (approx. 400 l) sand $^{2}/_{5}$ mm;
- Water/cement (W/C) ratio: 0.5 to 0.8;
- Consistency: slump > 175 mm.

If only a top reinforcing cage has to be installed, somewhat coarser crushed gravel $^{4}/_{28}$ mm can be used.

As an illustration, the average compressive strength of cubes of 200 mm, $f_{cm,cub200}$, is estimated for two W/C ratios on the basis of the empirical relation derived by Lambotte-Van Nieuwenburg (*1*):

$$f_{cm,cub200} = (0.47 \times f_{ccm})/(W/C)$$

where f_{ccm} is the standardized compressive strength of the cement mortar, defined at a W/C ratio of 0.45 (± 45 N/mm^2).

For concrete with a relatively high W/C ratio of 0.7 to be very workable, its estimated mean compressive strength attains

$$f_{cm,cub200} = (0.47 \times 45)/0.7 = 30 \text{ N/mm}^2$$

When using super-plasticizers, similar workability can be obtained, however, with a much lower W/C ratio, 0.45, for example, in which case the mean compressive strength can be increased to a value of the order of

$$f_{cm,cub200} = (0.47 \times 45)/0.45 = 47 \text{ N/mm}^2$$

In terms of its compressive strength, the concrete used for Atlas piles belongs to one of the European standardized strength classes C20/25, C25/30, or C30/37, where the first number equals the characteristic strength $f_{ck,cil}$ (N/mm^2), determined on cylinders ϕ 150 mm and H 300 mm after 28 days, and the second number equals the characteristic strength $f_{ck,cub150}$ (N/mm^2), determined on cubes 150 mm after 28 days.

Characteristic values are summarized in Table 1 using the following relations:

$$f_{ck} = f_{cm} - 1.64\, s$$

where s = standard deviation $\cong$ 15 percent of f_{cm}

$$f_{c,cub200} = f_{c,cub150}/1.05$$

In Europe, concrete with the required mix, workability, and strength in most cases is available through companies certified to sell ready-mixed concrete. In this way, detailed quality-control procedures and supervision by the authorities guarantee the product's conformity and quality.

TABLE 1 Compressive Strength Values

Strength class		C20/25	C25/30	C30/37
$f_{ck,cil}$	N/mm^2	20	25	30
$f_{ck,cub150}$	N/mm^2	25	30	37
$f_{ck,cub200}$	N/mm^2	23.8	28.6	35.2
$f_{cm,cub200}$	N/mm^2	31.6	37.9	46.7

Reinforcement

As standard reinforcement 4 or 5 longitudinal bars ϕ 14 to 16 mm are used. The quality of the steel is generally BE50 (yield stress of 500 N/mm^2 at 0.2 percent elongation). The longitudinal bars are connected to each other by a helical wire ϕ 5 or 6 mm with a pitch of 20 cm. This forms a reinforcing cage with a diameter of 15 to 20 cm that is centered in the mandrel before concreting. If only a top cage is required, installation is done after concreting. In order to take up important bending moments from lateral loads, a second cage of larger diameter can be positioned in the top section of the pile after concreting.

Pile Geometry

Vertical piles may be installed to depths of 22 m by most rigs; exceptionally, piles can extend as much as 25 m. With the most powerful rig (BTS-50), vertical piles up to 28 m and piles inclined over one third (approximately 20 degrees) up to 25 m in depth are feasible.

The typical helical pile shape and shaft cross sections are defined by the displacement head dimensions D_c and D_f as well as by the relationship between rotation and translation speed during extraction. The value D_c is normally considered the minimum diameter for a pile shaft, considering the structural design of a pile. The nominal base and shaft diameter to be introduced in the design for bearing capacity are related to the diameter D_f of the steel flange on the displacement head (see section on Design). A survey of characteristic displacement-head dimensions is summarized in Table 2. The table also provides the maximum allowable structural pile load Q_n, assuming an allowable concrete stress $\sigma' b$ of 7.5 MPa and a full-length standard reinforcement of 5 ϕ 16 mm (steel quality BE50).

APPLICABILITY

Soil Types

It is possible to construct Atlas screw piles in nearly all soil types (sands, clays, silts, chalk, and marls) in which traditionally rammed piles embedded in the soil are feasible (*2*). Penetration of 2 to 3 m in very dense sand or gravel usually poses few problems. In clay soils, it is possible to construct deeper piles with this system than is possible with traditional driving methods. Clay is more easily displaced by static penetration than by dynamic impact. Finally, screwing out the displacement head and the mandrel's continuous movement pose fewer problems than does pull-

TABLE 2 Characteristic Values for Atlas Piles

Head N°	D_C	D_f	Q_n(*)
(-)	(cm)	(cm)	(kN)
1	31	45	671
2	36	50	869
3	41	55	1,095
4	46	60	1,352
5	51	65	1,637
6	56	70	1,953

(*) on basis of an allowable concrete stress of 7.5 Mpa.

ing out a casing for a cast-in-place rammed pile. Occasionally, preboring using a continuous flight auger is done to facilitate penetration through resistant soil layers or backfill on top.

As is true for all cast-in-place piles without permanent casing, care and workmanship are needed in penetrating the very low-resistance layers, for example, sands close to critical density, soft clays, and peats. In these cases an appropriate concrete mix (one with a lower volume weight) can be used to avoid excessive concrete consumption and post-setting by the lateral yielding of fresh concrete in weak ground layers. The presence of large boulders, on the other hand, may impede penetration.

Site and Environmental Aspects

The Atlas pile is appropriate if vibration-free, quiet installation is required (as in urban areas, when operating adjacent to schools, laboratories, or historical buildings). In contaminated soils, the screwed displacement pile has the advantage of producing virtually no spoil, which is a safety risk to people and requires expensive disposal.

Piles can be installed 0.8 m from existing surface structures. Special precautions have to be taken however when working close to fragile structures, in order to avoid possible damage from the soil-displacement effect. Preboring through the top layers and filling the bore with loose sand is often an effective safeguard.

Particular Applications

On several job sites in Belgium, the Atlas pile has been used successfully for the construction of soil-retaining walls. Details on this application have been reported by De Cock and Lhoest (*3*). Piles may have either a temporary or a permanent lateral soil-retaining function combined with a vertical bearing function in such cases. Generally, a discontinuous pile wall is constructed, with the spacing of the piles, axis to axis, 2 to 3 times the pile diameter. Retaining heights of 6 to 8 m are common. In many cases one or two rows of ground anchors are provided. Outlines of the usual construction phases of a discontinuous pile wall are given in Figure 6.

Atlas piles have been used several times for slope stabilization as well. The increase in mean shear characteristics of the pile-soil system along the potential sliding surface, in combination with passive soil resistance on the piles, improves stability, protecting against deep sliding or allowing an increase in the average slope angle, thereby reducing the volume of earth works and area of expropriated land.

Due to the high shaft resistance that can develop with its use, the Atlas pile is also appropriate as a tension pile.

BEHAVIOR OF ATLAS SCREW PILE

Unlike the less powerful pile-screw machines and other auger-pile techniques, Atlas machines are able to displace soil laterally. They use a recoverable displacement head, and soil displacement not only occurs during penetration but also during extraction. Double soil displacement is characteristic of the Atlas technique and is critically important in view of the screw pile's shape and behavior. By displacing soil laterally, and in a volume equal to the pile's volume, soil density and lateral stresses surrounding the pile will increase, depending upon soil type, its initial density, and stress state.

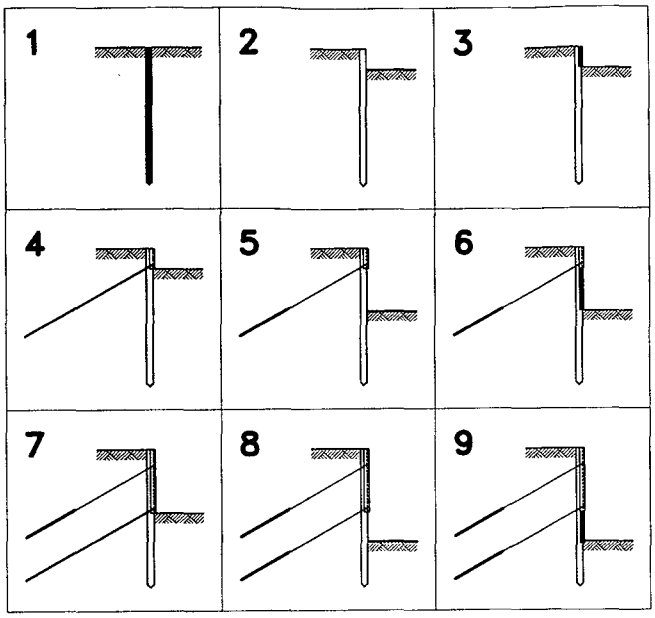

FIGURE 6 Installation phases for anchored discontinuous pile wall.

A selection of representative static load tests on Atlas piles in both granular and cohesive soils is given in Figure 7. See work by Van Impe for a detailed analysis of these tests (*1*). Double soil displacement, which typically occurs with the Atlas screw pile, varies somewhat, depending on soil characteristics.

Displacement in Granular Soils

In granular, loose to medium-dense soils, an important increase in density and thus in shear characteristics may result from the displacement effect. Comparative model tests on different steel-screwed auger piles (having a shape and relative geometry comparable to the Atlas pile) and rammed or jacked tubular piles have been performed in sand by G. Petrasovits of the Technical University of Budapest, Hungary. From these tests it was concluded that for the screwed pile

- No relevant change in soil density was found in the layers underneath the pile base, in contrast to the additional compaction experienced with rammed piles or the eventual decompaction experienced with bored piles;
- Soil essentially moved horizontally along the whole pile;
- Soil between the threads was compacted, the initial dry-bulk density γ_d of 16 kN/m^3 being increased to 17.5 kN/m^3, corresponding to a reduction in void ratio e from 0.67 to 0.51;
- The extent of the compacted zone near the pile was higher for greater initial soil densities.

Densification of sands near the pile shaft also has been revealed in situ. Figure 8, for example, shows the results of a static cone

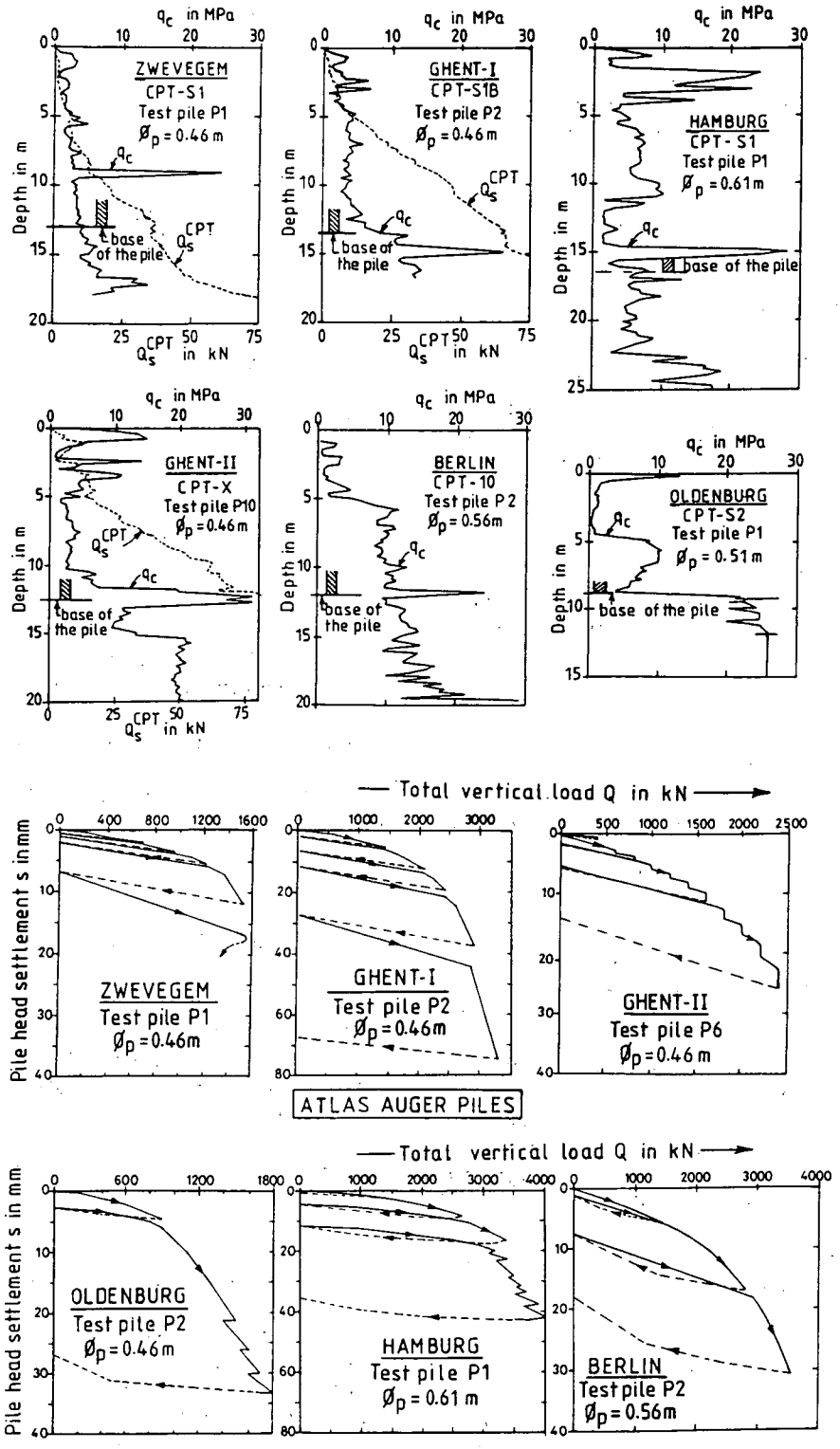

FIGURE 7 Examples of CPT and pile load settlement results in Atlas pile research.

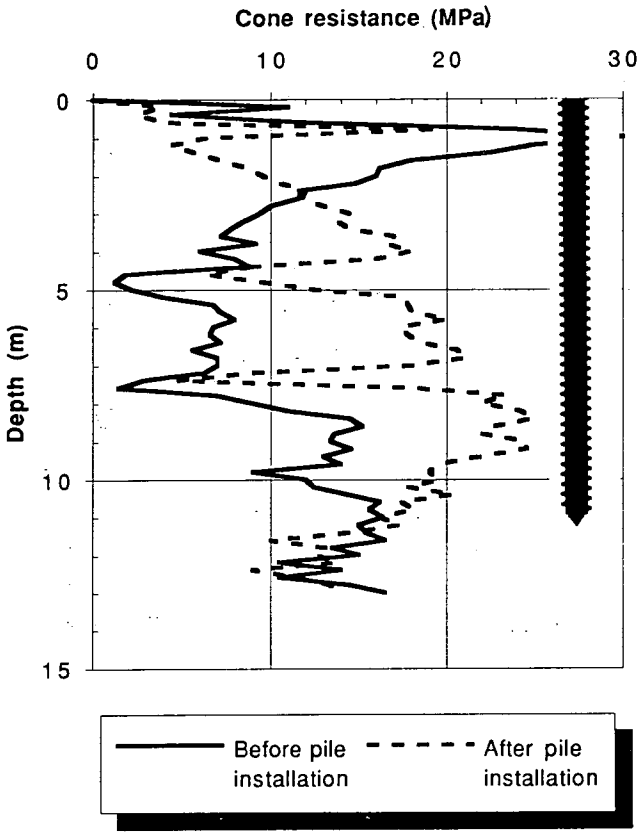

FIGURE 8 CPTs on axis of screw pile before installation and 0.5 m from edge of pile after installation, (Southport Lancs, United Kingdom).

penetration test executed before and after piling works on a job at Southport Lancs, in the United Kingdom (*4*).

In sum, the above-mentioned phenomena will affect pile performance in granular soils in such a way that the ultimate shaft resistance and base resistance of Atlas piles at least are comparable to those of rammed concrete piles. Furthermore, the settlement of end-bearing Atlas piles may be somewhat greater than the settlement of equivalent rammed piles but much less than it would be for comparable drilled piles.

Displacement in Fine-Grained Soils

Soils with a pronounced silt or clay character are less compactible by short-duration forces. In fine-grained soils, the lateral soil displacement by pile installation will essentially result in an increase of locked stresses around the pile shaft.

The stress state during and after installation of Atlas piles has been analyzed in situ at a test site in Koekelare, Belgium (*5*)(*6*). The research program, conducted in 1992, involved the collaboration of Franki Foundations, Belgium, and the University of Ghent. Underneath the silty and clayey top layers (5 to 6 m below), the subsoil consists of stiff, tertiary, overconsolidated clay [Figure 9(*a*)]. Soil stress analysis was performed with a Dilatometer Test (DMT) with the Marchetti dilatometer blade before and after pile execution at a distance of 1.5 times the pile diameter to the pile axis. Comparison of the data for the Atlas piles (diameter 51/65 cm) indicated an average increase in horizontal stress index K_d of about 29 percent and an increase in undrained shear strength, c_u, of 24 percent [Figures 9(*a*) and 9(*b*)]. Note that the measurements were made at a distance of about 65 cm from the outer surface of the shaft. Moreover, the clay layer geologically is already highly overconsolidated.

At a test site in Zwevegem, Belgium, one with the same type of tertiary clay, the soil entrapped in between the concrete flanges of the piles was closely investigated (*1*). The investigation indicated significant remolding and compaction of the clay located between the flanges. On inspection, this enclosed soil was found to consist of very thin, successive lenses of soil squeezed together in thin, vertical spiral seams. The shear parameters of the soil between the flanges ($\phi' = 25$ degrees; $c' = 24.3$ kPa) as defined by triaxial tests were remarkably higher than those of the surrounding natural soil.

In conclusion, all measurements and observations demonstrated the lack of any relevant loss of stress nearby the pile shaft with the installation of an Atlas screw pile and showed improved shear characteristics in the surrounding soil. Again, in the case of silty and clayey soils, the result is a very high shaft resistance on Atlas piles comparable to the shaft resistance on a Franki pile with rammed dry concrete, and even higher resistance than that on rammed cast-in-place piles with vibrated shafts, rammed precast piles, or jacked piles. Second, the end-bearing behavior of Atlas screw piles is quite similar to that of rammed piles.

Again, in the case of silty and clayey soils, the result is a very high shaft resistance on Atlas piles comparable to the shaft resistance on a Franki pile with rammed dry concrete, and even higher resistance than that on rammed cast-in-place piles with vibrated shafts, rammed precast piles, or jacked piles. Second, the end-bearing behavior of Atlas screw piles is quite similar to that of rammed piles.

DESIGN

In Germany, pile design often is based on preliminary load tests at a particular job site, in accordance with the DIN codes. In other countries, such as Belgium, France, the Netherlands, and United Kingdom, the design of pile-bearing capacity is based on calculation, using semi-empirical methods of deduction from currently used in situ soil tests. Before detailing these methods, for completeness, the pile design method based on the theory of plasticity and often used in the United States is mentioned briefly.

Method Based on the Theory of Plasticity

The bearing capacity of single piles subjected to vertical loads may be calculated from the effective shear parameters (angle of friction, ϕ'; cohesion, c'; or adhesion, a) and the effective stresses. The equations for the ultimate unit-base resistance q_{bu} and the ultimate unit shaft resistance q_{su} usually are presented thus:

$$q_{bu} \text{ (for all soil types)} = c' N_c \zeta_c + q_0 N_q \zeta_q$$

$$q_{bu} \text{ (for cohesive soils, } \phi' = 0) = c_u N_c'$$

where

c and ϕ' = effective shear parameters;
q_0 = effective vertical stress at the pile base level;

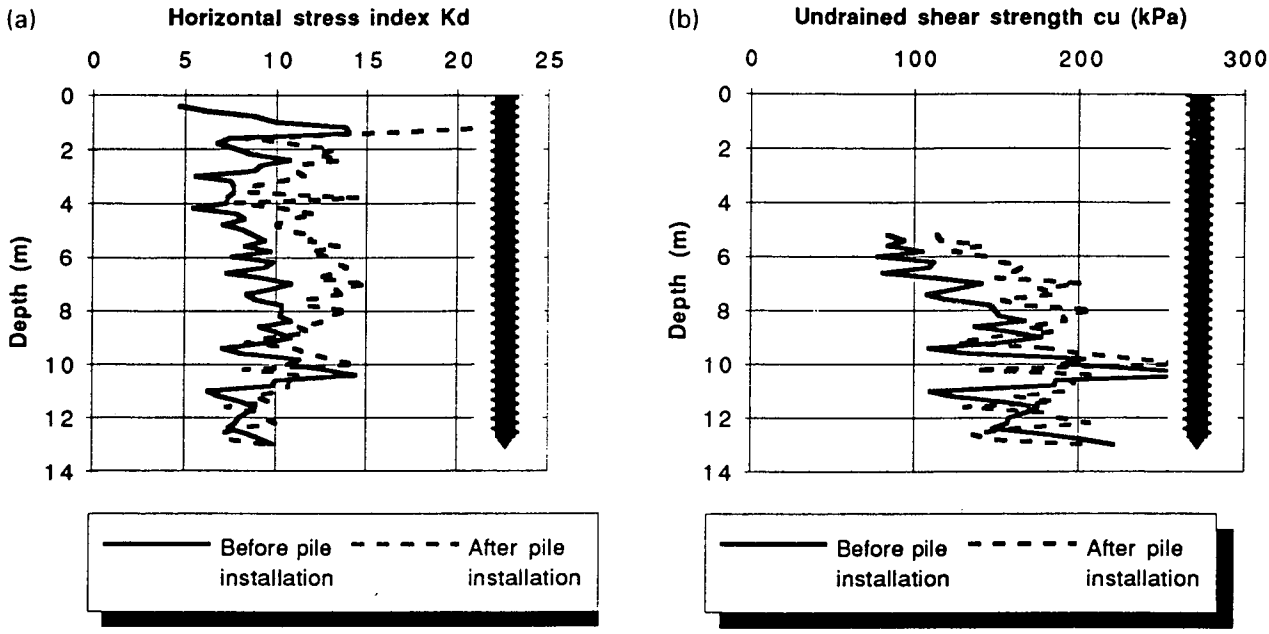

FIGURE 9 DMTs on axis of screw pile before installation and 0.6 m from edge of pile after installation (Koekelare).

N_c and N_q = dimensionless bearing-capacity factors and a function of ϕ', defined by Meyerhoff (7);
ζ_c and ζ_q = shape factors and a function of ϕ';
c_u = undrained shear strength at the pile-base level; and
N_c' = dimensionless bearing-capacity factor, varying between 9 (for pile diameter < 0.5 m) and 6 (for pile diameter > 1.0 m).

$q_{s,z}$ (for noncohesive soils) = $K_s \tan\delta' \sigma_z'$

$q_{s,z}$ (for cohesive soils, $\phi' = 0$) = αc_u

where K_s equals $\sigma_{zh}'/\sigma_{zv}'$, a function of ϕ' and the pile-installation method, and $\tan\delta'$ is the coefficient of friction pile-soil (= 0,7 to 1,0 × $\tan\phi'$).

For the Atlas pile, the parameters and empirical coefficients used for concrete-displacement piles may be applied. Therefore, the following values are proposed for the coefficients mentioned above:

N_c and N_q = as for rammed piles,
$K_s = 1.5\ K_0$ for normally consolidated (NC) soils,
$K_s = 1.0\ K_0$ for over-consolidated (OC) soils,
$\tan\delta' = \tan\phi'$, and
$\alpha = 1.0$.

Deduction Methods for In Situ Soil Tests

The bearing capacity of single piles in both cohesive and noncohesive soils can be derived from the results of in situ soil tests, such as static cone penetration tests (CPT), pressuremeter tests (PMT), or standard penetration tests (SPT), using semi-empirical relations. In general, the empirical coefficients to be introduced for end bearing and skin friction on different pile types in different soil conditions are based on the results of large numbers of representative static load tests. The accuracy and validity of extrapolation from these coefficients depend on the relevance of the test conditions, the number of data available, and the scatter of results.

Bustamante and Gianeselli's analysis of 23 loading tests on concrete Atlas piles was reported in a paper (*8*) that provides practical guidelines and methods given for designing Atlas piles on the basis of the three types of in situ soil tests, the CPT, PMT and SPT mentioned above. In summarizing the proposed design method the authors used somewhat different symbols from the ones used in Bustamante's papers in order to conform with European rules.

Note that in the example that follows the empirical coefficients related to the CPT are valid when using a mechanical Dutch mantle cone (cone type M1). For electrical cones, these approximative relations can be taken into account:

q_c mechanical = $\beta \times q_c$ electrical,

where β is 1.3 to 1.5 for cohesive soils and 1.0 to 1.2 for saturated sands.

Nominal Pile Dimensions

The nominal diameter of the pile base D_b and of the pile shaft D_s to be introduced in the calculation of the cross section of the pile tip A_b and the surface area of the pile shaft A_s depend on the

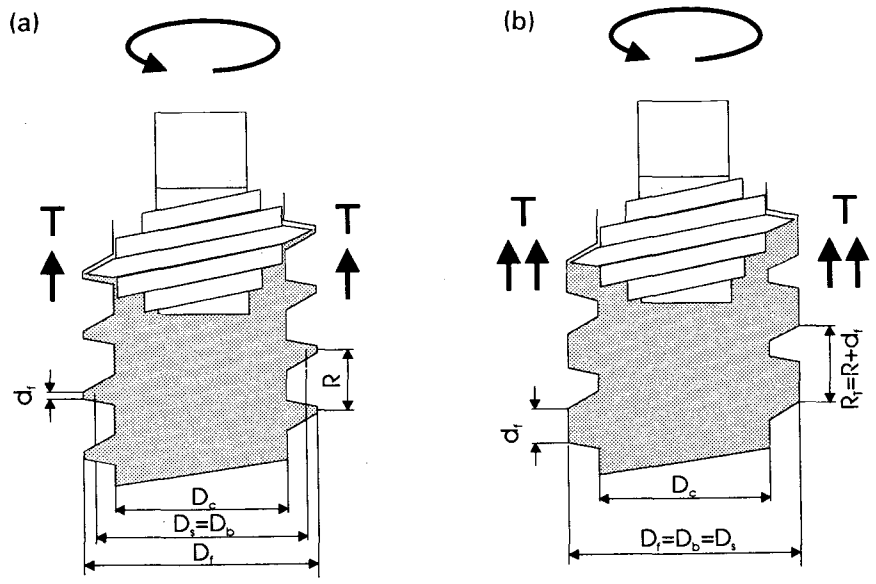

FIGURE 10 Cross section and nominal diameters of Atlas pile (*a*) with thin flanges, (*b*) with thick flanges.

maximum diameter of the displacement head, D_f, that is used. Bustamante proposed these rules:

- When the extraction procedure allows the realization of sufficiently thick flanges, as in Figure 10(*b*), it is generally the case with the powerful BT-40 and BT-50 rigs that

$$D_b = D_s = 1.0 \times D_f$$

- When the thickness of the flanges is small, as in Figure 10(*a*)

$$D_b = D_s = 0.9 \times D_f$$

Base Resistance

The ultimate total base resistance Q_{bu} is expressed as:

$$Q_{bu} = A_b K \alpha$$

where

A_b = the nominal area of the pile base;
K = the bearing factor depending on pile type, soil type, and soil test; and
α = the equivalent unit-base resistance factor, based on soil test data

In practice

$$A_b = (\pi \times D_b^2)/4$$

The bearing factors K_P (for PMTs), K_C (for CPTs), or K_N (for SPTs)—tests for the concrete Atlas pile in various soil types—are given in Table 3. Whereas K_P and K_C are dimensionless, the factor K_N is expressed in terms of stress.

The equivalent unit-base resistance factor α, which characterizes the relevant soil density and shear strength in the vicinity of the pile tip, is derived from the soil-test results; and α corresponds to p_{le}, q_{ce}, or N_e, which are defined as representative average values of the limit pressures p_l, the cone resistances q_c, or the N values over a height a above and below the pile tip. In general a is equal to min {1.0 m; 1.5 × pile diameter}.

Shaft Resistance

The ultimate shaft resistance Q_{su} is obtained from the summation of the shaft resistance over the i shaft-bearing layers:

$$Q_{su} = \sum A_{s,i} \times q_{su,i}$$

where $A_{s,i}$ is lateral pile area in layer i ($H_i \times \pi \times D_s$) and $q_{su,i}$ is ultimate unit skin friction in layer i.

For the unit skin friction q_{su}, both the chart in Figure 11 and Table 4 are used. First the curve to be considered is deduced from Table 4, depending on soil type and soil resistance. Figure 11 then allows us to define q_{su} as a function of the p_l, q_c, or N values.

TABLE 3 End Bearing Factors for Concrete Atlas Piles (*7*)

Type of soil	K_P	K_C	K_N
(-)	(-)	(-)	(MN/m²)
Clay	1.6 - 1.8	0.55 - 0.65	0.9 - 1.2
Sands	3.6 - 4.2	0.5 - 0.75	1.8 - 2.1
Gravels (1)	≥ 3.6	≥ 0.5	undetermined
Chalk	≥ 2.4	≥ 0.6	≥ 2.6
Marls	≥ 2.4	≥ 0.7	≥ 1.2

(1) CPT and SPT results remaining always questionable for gravels.

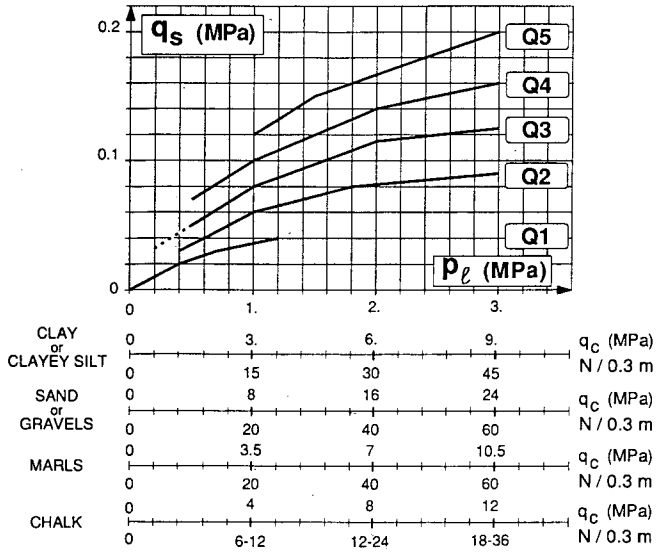

FIGURE 11 Design curves for the choice of unit skin friction q_{su} (7).

Specific Design Method on Basis of CPT: Belgian Practice

The design of displacement-type auger piles, such as the Atlas pile, is described in detail by Van Impe (*1*).

In the authors' considerations of ultimate pile capacity, the ultimate values refer to the conventional rupture load corresponding to the load that causes a relative pile base settlement s_r of 10 percent D_b, where D_b is pile-base diameter. In addition, the empirical factors used are related to the CPT with electrical cone.

Base Resistance

The ultimate unit-base resistance q_{bu} in Belgium is usually obtained from CPT results as

$$q_{bu} = \alpha_b \times \epsilon_b \times q^*_{bu}$$

where

q^*_{bu} = the ultimate unit-base resistance derived directly from the CPT in the natural soil conditions (before piling works);
α_b = an installation factor for the related type of pile and soil;
ϵ_b = a scale factor for soil discontinuities, such as fissuring.

Methods for q^*_{bu} derivation are discussed by De Beer (*8*) and Van Impe et al. (*9*). These methods take into account the resistance of the influencing soil layers beyond and below the pile base over a height depending on a piles diameter.

For cast-in-place auger piles of the displacement type, an α_b factor = 1.0, as is used for rammed piles, has been found to be realistic for both sands and clays.

In the Belgian Boom clay, which is a tertiary, overconsolidated clay, at ϵ_b factor related to the fissuring of hte clay has been found to be approximately equal to

$$\epsilon_b = 1 - 0.01\ (D/d - 1)$$

where D is diameter of the pile and d diameter of the sounding rod = 0.036 m.

For non-fissured soils, ϵ_b can equal 1.0.

Shaft Resistance

Shaft resistance on basis of q_c values can be calculated. More or less similarly to Bustamante, Van Impe (*1,9*) relates the unit-shaft resistance q_{su} to the cone resistance q_c by a coefficient η_p:

$$q_{su} = \eta_p \times q_c$$

Some proposed values of η_p for the displacement auger pile are summarized in Table 5. Again, these values correspond fairly well with the values found for rammed piles, as relevant soil decompressions are avoided by the pile installation method.

Shaft resistance on basis of total CPT skin friction can be determined also. The easiest way for evaluating the total shaft resistance Q_{su} on a pile remains related to the value of the total skin friction F_s measured by the CPT:

$$Q_{su} = \xi_f \times F_s \times \frac{D_s}{d}, \text{ where, for the Atlas pile, } \xi_f \geq 1.25.$$

TABLE 4 Curves To Be Considered for q_s in Function of Soil Type and Soil Resistance (7)

Soil type (-)	pl (MPa)	qc (MPa)	Curve to be taken (-)
Clay or clayey silt or sandy clay	< 0.3	< 1.0	Q1
	> 0.5	> 1.5	Q3
	≥ 1.0	≥ 3.0	Q4
sand or gravel	< 0.3	< 1,0	Q1
	> 0.5	> 3.5	Q4
	> 1.2	> 8.0	Q5
chalk	> 0.5	> 1.5	Q4
	> 1.2	> 4.5	Q5
marls	< 1.2	< 4.0	Q4
	≥ 1.5	≥ 5.0	Q5

TABLE 5 Proposed Values on the Coefficient η_p for Displacement Auger Piles

Soil type (-)	qc value (MPa)	Coefficient ηp (-)	Max. qsu (kPa)
Clay			
Soft to medium	< 1.0	1/20	100
Medium to stiff	1.0 - 4.0	1/40	
Stiff to hard	> 4.0	1/80	
Silt			
Loose	≤ 5.0	1/50	120
Dense	> 5.0	1/100	
Sand			
Loose	≤ 15.0	1/100	140
Dense	> 15.0	1/200	

Calculated and Measured Bearing Capacities Compared

Applying the design method described by Van Impe to the cases given in Figure 7, the calculated, ultimate bearing capacity is compared in Table 6 to the in situ conventional rupture load values (*1*). A fairly good, and somewhat conservative, correlation is found.

QUALITY CONTROL: ATKWAP MONITORING SYSTEM

Computerization has made its way to the job site and piling rigs are beginning to be equipped with data-acquisition systems that record relevant execution parameters. A specific data-acquisition system, ATKWAP, has been developed for the Atlas rigs.

Description of the AKTWAP System

The ATKWAP system is composed of a central computer and data-logging system, and a separate operating box installed near the machine operator. The operating box mainly consists of a small printer unit and touch screen, which can be used by the operator to input the required pile data and displays real-time information during pile installation. Hydraulic pressures, penetration depth, and the number of rotations are continuously measured during the screwing in and extraction of the casing. The data are stored in the central computer and displayed in real-time on the computer screen. In the meantime, a graph of the actual torque as a function of depth and a table of the number of revolutions per meter-depth interval are issued.

The flow chart on Figure 12 gives an overview of the main-screen menus to be handled by the operator. Additional help screens to guide the operator's introduction of the required information are represented by short darts to the right or left of the main-screen displays.

The following parameters are measured and stored during the entire piling process:

- Rotational torque M transmitted to the casing by the drilling table (kNm);
- Vertical thrust N exerted on the casing by the two pressure rams (kN);
- Depth of penetration (m); and
- Number of revolutions from the drilling head and the casing (R).

With these parameters and a time factor, variable parameters can be deduced as a function of depth:

- Torque M (kNm);
- Total vertical thrust N (kN);
- Rotational speed of penetration (rev/min); and
- Vertical speed of penetration (cm/sec).

Sample ATKWAP data are given in Figure 13(a) and (b). The soil stratigraphy successively consists of sandy hydraulic fill, soft alluvial clay, medium-dense to dense quaternary sand, sandy clay, and dense to very dense tertiary sand.

Practical Uses for the ATKWAP System

The ATKWAP system is a practical tool for an operator, giving real-time information on the installation process, guiding the correct operation and manipulation of the machine, and indicating the soil conditions at each pile location. Development of the system would increase its value for the operator (for example, if it were to display the pre-installed pile layout on the screen).

The ATKWAP system may be linked with a reporting system and automatically transfer collected data to generate daily or weekly job reports, reducing time-consuming administrative work for the superintendent. Data from the site can be incorporated in financial reports as well. If statistically analyzed, the data provide the management team useful information on the overall operation team within a short time.

Detailed and automated registration of most relevant execution parameters enables thorough supervision of work performed and provides documentation for a client, supervisor, and contractor's project engineer.

Finally, a data-acquisition system constitutes an important and powerful tool for pile design. To the extent that pile parameters

TABLE 6 Comparison Between CPT Predicted and Measured Conventional Ultimate Bearing Capacity for Auger Piles in Various Soil Conditions (*1*)

		Predicted values			Measured value	
Test site	Pile	Q_{su}	Q_{bu}	Q_{tu}	Q_{ru}	Q_{ru}/Q_{tu}
(-)	(-)	(kN)	(kN)	(kN)	(kN)	(-)
Zwevegem	P1	424.7	949.4	1374.1	1560	1.14
	P2	479.0	1098.9	1577.9	1765	1.12
Ghent-I	P1	834.9	1662.4	2497.3	2763	1.11
	P2	879.7	1690.1	2569.8	3000	1.16
Ghent-II	P6	1617.0	1280.0	2900.0	2800.0	0.97
Oldenburg	P1	1269.2	542.3	1811.5	>(1710)	>(0.94)
Hamburg	P1	965.1	2562.0	3527.1	3710	1.05
Berlin	P1	2290.0	1350.0	3640.0	3700	1.02
	P2	2560.0	1740.0	4300.0	4400	1.02

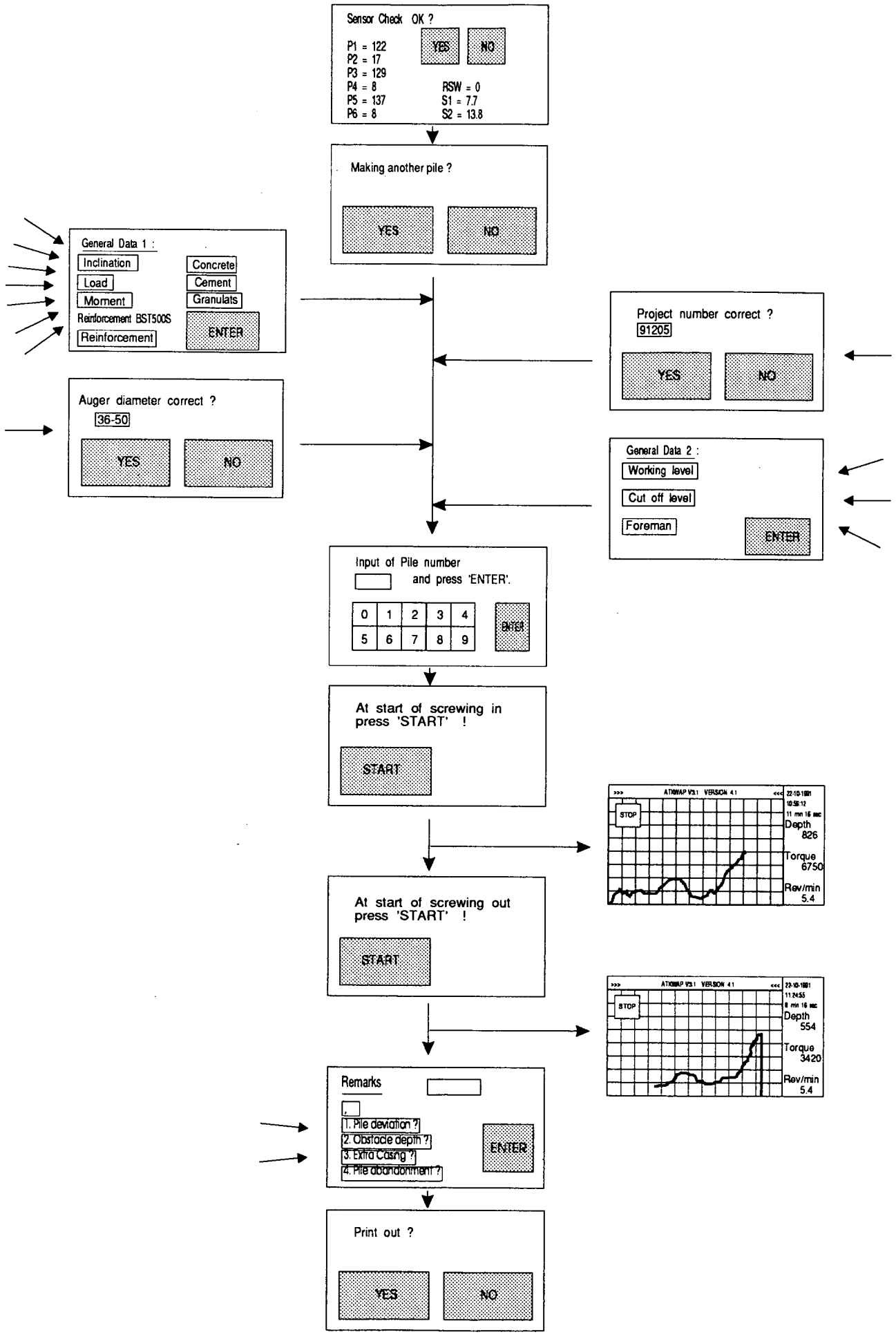

FIGURE 12 Mean operator instruction menus for data acquisition of installation parameters with ATKWAP system.

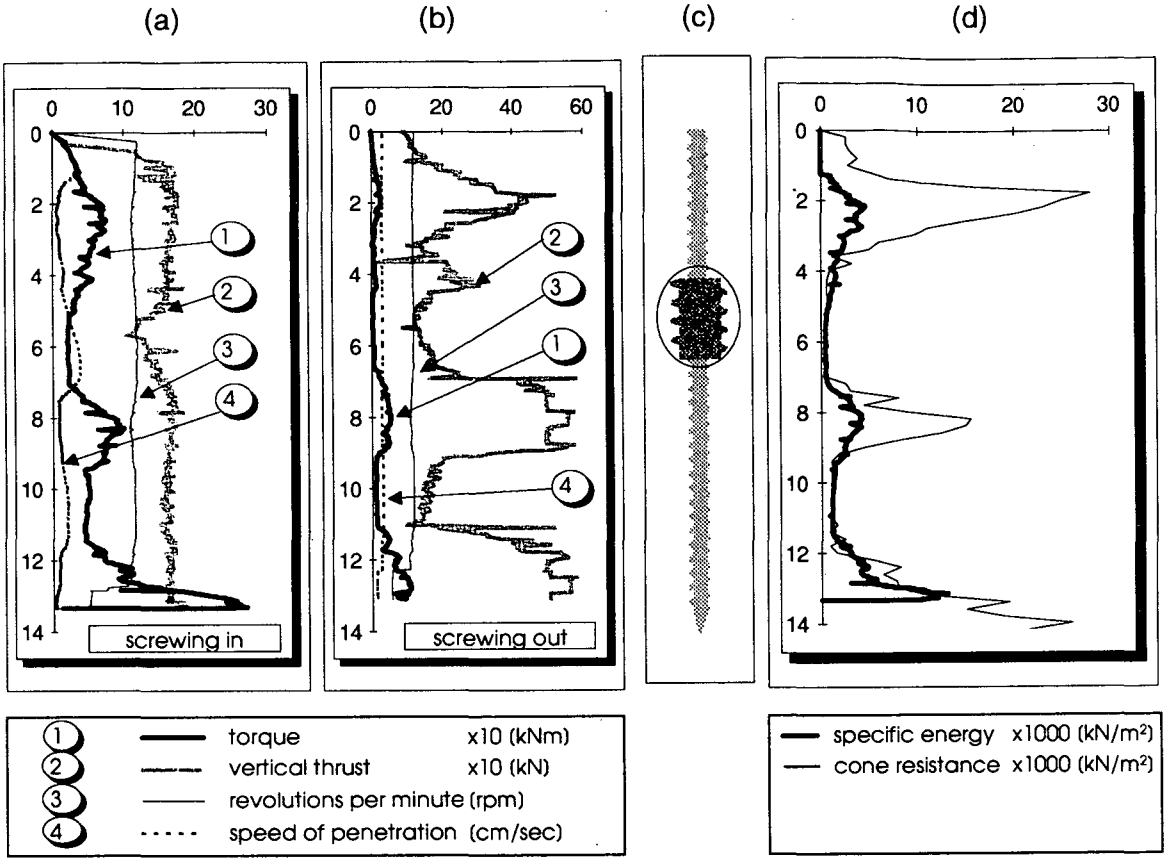

FIGURE 13 Example of ATKWAP installation parameters and deduced values; (*a*) ATKWAP parameters for screwing in, (*b*) ATKWAP parameters for screwing out, (*c*) deduced theoretical pile shape; (*d*) comparison of deduced specific installation energy and q_c values before pile installation.

reveal information on actual piles' geometry and the soil conditions affecting a particular pile, before and after installation, an engineer has a more or less complete answer to a pile's quality and expected performance.

For example, on the basis of the measured vertical and rotational speed of a pile casing during extraction, the pile's theoretical shape or geometry, its depth and the thickness of its flanges, can be delineated [Figure 13(*c*)]. If the concrete flow as a function of depth is known, an even more precise image of the pile shape can be obtained. (In the future, the data-acquisition system will no longer require manual registration.)

Analysis of Specific Installation Energy

One expects the energy required to penetrate a casing to be directly related to soil characteristics (nature and resistance). When the Atlas pile was first developed, rotational torque, which was read out on a manometer, depended to a large extent on the resistance of the soil at the level of the displacement head. It also was found that, when correcting the registered torque by a factor τ equal to the real penetration per revolution over the pitch of the auger, an even closer correlation between this so-called corrected torque and the soil conditions was obtained.

A more fundamental analysis of the installation process takes into account not only torque, but also vertical thrust, penetration speeds, and displacement-head geometry. Van Impe et al. proposed to define an overall installation parameter that has a physical sense, that is, the specific installation energy (*10*) defined as

$$E_s = \frac{A \times N \times v + B \times n \times M}{\Omega \times v}$$

where

E_s = specific installation energy (kJ/m^3 or kNm/m^3);
A and B = machine-installation parameters, depending on displacement-head geometry and soil parameters;
N = vertical thrust (kN);
M = rotational torque (kNm);
v = vertical penetration speed (m/min);
n = rotational speed (revolutions/min); and
Ω = area of the outer projection of the displacement head

The ATKWAP system automatically calculates the specific energy for given values for the parameters A and B. The E_s graph is given in Figure 13(*d*) together with the q_c diagram of a relevant CPT in the vicinity of the considered pile. One can observe remarkable and useful similarities between the specific energy diagram and the cone resistances. The correlation, proven to be valid in all cases, confirms the practical use of the data-acquisition system for active design. In practice, piles are executed at the begin-

ning of the job near the locations of the relevant soil tests that have been the base for the theoretical pile design. This allows for calibration of pile-installation parameters and for definition of the minimum values that have to be achieved for these parameters for other piles at the site. When discordance is revealed (for example, due to changes in local soil conditions), one is able to make appropriate adjustments.

In the future, it should be possible to deduce the degree of ground improvement during the pile installation from the ATKWAP parameters and to make quantitative predictions regarding pile-bearing capacity.

CONCLUSIONS

With the advent of the powerful BT-40 and BT-50 rigs, the Atlas screw pile has been developed into a high-quality foundation system that not only offers solutions to technical problems relating to deep foundation but also meets ever more stringent environmental demands. Soil tests before and after screw-pile installation demonstrate the beneficial effect of these piles' installation on shear parameters or stress state of surrounding soil. This effect results in high base and shaft resistances that are comparable to those of common rammed piles. Additionally, practical design rules for the bearing capacity on basis of CPT, PMT, or SPT tests enable sound prediction of pile performance in various types of loose soils. Supervising pile installation and controlling for soil conditions surrounding a pile are aided by the continuous recording of relevant execution parameters. Further research on interpreting specific installation energy should reveal additional quantitative information on pile quality and expected performance.

REFERENCES

1. Van Impe, W. F. Considerations in the Auger Pile Design. *Proc., 1st Geotechnical Seminar on Deep Foundations on Bored and Auger Piles*, Ghent, Belgium, 1991. A. A. Balkema, Rotterdam, Netherlands, and Brookfield, Vt. 1988, pp. 193–218.
2. Imbo, R. P. The Atlas Screw Pile: an Improved Foundation Technique for the Vibration Free Execution of Piles with Larger Capacity. *Proc., 6th Budapest Conference on Soil Mechanics and Foundation Engineering*, Budapest, Hungary, 1984, pp. 363–372.
3. De Cock, F., and Ch. Lhoest. The Vibration Free Realisation of Soil Retaining Walls, Using Screwed Atlas Piles. *Proc., 2nd International Geotechnical Seminar on Deep Foundations on Bored and Auger Piles*, Ghent, Belgium, 1993. A. A. Balkema, Rotterdam, Netherlands and Brookfield, Vt., 1993, pp. 405–412.
4. Hollingsworth, J. R., and R. P. Imbo. The Atlas Screw Pile: Construction, Design and Performance. *Proc., Piling Europe*. Institution of Civil Engineers, London, England, 1992, pp. 139–145.
5. Peiffer, H., and W. F. Van Impe. Evaluation of Pile Performance Based on Soil Stress Measurements; Field Test Program. *Proc., 2nd International Geotechnical Seminar on Deep Foundations on Bored and Auger Piles*, Ghent, Belgium, 1993. A. A. Balkema, Rotterdam, Netherlands and Brookfield, Vt., 1993, pp. 385–389.
6. De Cock, F., W. F. Van Impe, and H. Peiffer. Atlas Screw Piles and Tube Screw Piles in Stiff Tertiary Clays. Assessment of Pile Performance and Pile Capacity on Basis of Instrumented Loading Tests. *Proc., 2nd International Geotechnical Seminar on Deep Foundations on Bored and Auger Piles*, Ghent, Belgium, 1993. A. A. Balkema, Rotterdam, Netherlands and Brookfield, Vt., 1993, pp. 359–367.
7. Meyerhoff, G. G. The Ultimate Bearing Capacity of Foundations. *Geotechnique*, Vol. 2., 1951, p. 301.
8. Bustamante, M. and L. Gianescelli. Design of Auger Displacement Piles from In Situ Tests. *Proc., 2nd International Geotechnical Seminar on Deep Foundations on Bored and Auger Piles*, Ghent, Belgium, 1993. A. A. Balkema, Rotterdam, Netherlands and Brookfield, Vt., 1993, pp. 21–34.
9. De Beer, E. E. Méthodes de Déduction de la Capacité Portante d'un Pieu à Partir des Résultats des Essais de Pénétration. *Annales des Travaux Publics de Belgique*. No. 4, 5, and 6, 1971.
10. Van Impe, W. F., E. E. De Beer, and E. Lousberg. Prediction of the Single Bearing Capacity in Granular Soils Out of CPT-Results. *Proc., International Symposium on Penetration Testing I*, Specialty Session, Orlando, Fla., March 24, 1988, pp. 1–34.
11. Van Impe, W. F., H. Peiffer, and W. Haegeman. Considerations on the Effects of Installation on the Displacement Auger Pile Capacity. *Proc., Deep Foundations Seminar*, Paris, France, 1992, pp. 319–327.

Design and Construction of Starsol Piles

L. J. WHITWORTH

Use of auger-cast piles has increased dramatically since the late 1970s, when concrete pumping technology enabled piles to be constructed with concrete instead of a sand-cement grout mix. The Starsol rig, introduced into the auger-cast market in the early 1980s, was designed to overcome some of the problems associated with auger-cast piling. The Starsol rig's essential feature is its internal tremie, which constructs a concrete pile shaft of high quality that, in turn, allows for higher concrete working stresses. The Enbesol quality-control system provides real-time pile-construction parameters, enabling rig operators to identify potential problems and rectify them during pile construction. Hard copy print-outs provide clients with a permanent record of a completed pile. Following an independent research project conducted on the load-bearing capacity of the Starsol pile, it was determined the piles could be designed as concrete piles and injected under low pressure.

Auger-cast piles were developed in the United States in the late 1940s. For some 30 years after their introduction, they were constructed using a sand-cement grout mix; but work in Belgium, France, and Holland in the 1960s and 1970s showed that auger-cast piles could be constructed using pumpable concrete mixes. Development of the Starsol piling system was begun in 1980 in an attempt to remedy some of the perceived weaknesses of auger-cast pile construction. This paper describes the Starsol piling rig and pile construction as well as the Enbesol real-time data quality-control logger, and its record-keeping instrumentation. An investigation into the load-bearing capacity of the piles and pile-shaft concrete quality is also detailed.

WHY THE STARSOL SYSTEM WAS DEVELOPED

The conventional auger-cast or continuous-flight-auger (CFA) pile was developed in the United States in the late 1940s. In the early years of the CFA system, engineers found that placing concrete with conventional-size aggregate was more costly than using sand-cement grout, and so for the next 30 years or so, grout piles were the norm (*1*). However, in the 1960s and 1970s, work carried out in Belgium, France, and Holland showed that it was possible to construct augercast piles economically using conventional, pumpable concrete mixes. This discovery spurred the development of a large auger-cast market in Europe. Although considerable problems were encountered in the early stages of the CFA pile's development (*2*), problems rarely were documented. A notable exception was a project at a site in Glasgow in which an engineer and piling contractor worked together to solve several problems (*3*).

Some early problems related to the fact that most of the machines used to drill auger-cast piles had fairly low drilling power, with torques in the 20- to 80-KNm range. Consequently, hard layers frequently could defeat the piling rig. Also, the traditional method of concreting the pile, whereby an auger is raised a few centimeters just before concreting, could disturb the pile base and cause the concrete and soil to mix. The result was often poor pile-base load-settlement characteristics, which are often a feature of auger-cast piles. Finally, if the auger were extracted too rapidly, the soil could collapse and cause necking within the pile shaft. To minimize the problems associated with conventional auger-cast piling, in 1980 a new piling rig was developed: the Starsol system.

DESCRIPTION OF THE STARSOL RIG

At first glance, the Starsol rig looks similar to conventional auger-cast piling rigs (Figure 1). An important difference between them is the Starsol rig's internal tremie pipe, which effectively prevents

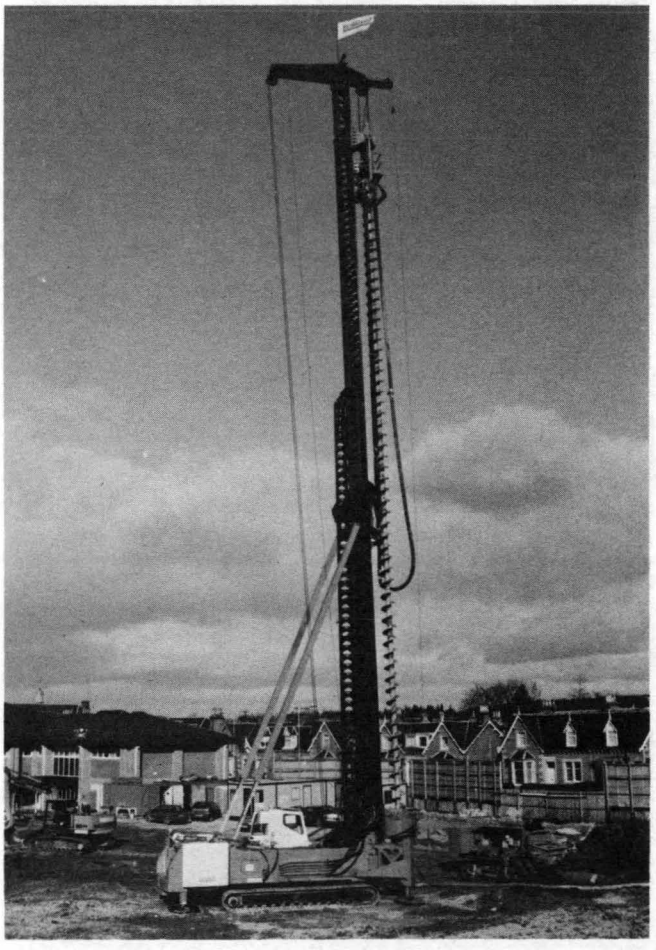

FIGURE 1 Starsol piling rig.

Solétanche Entreprise, 6, rue de Watford, 92000 Nanterre B.P. 511, France.

many of the concreting problems associated with auger-cast piles (Figure 2).

Main features of the Starsol rig (*4*) are shown in Figure 3. Here are the key elements that distinguish it: a hydraulic motor; a continuous-flight-auger around an external tube; a second, central tube sliding inside the first one; a system of hydraulic jacks that allows the central tube to be slid vertically over a length of some 1.5 m; and a spoil-cleaning system. The central tube has two important functions. At its base is a pilot bit or stinger, which can break up tough ground in advance of the main auger. Second, it acts as the concreting tube or tremie.

Depending upon their size, Starsol rigs have torques ranging from 80 to 140 KNm and can produce piles with diameters ranging from 420 to 1420 mm and typical depths of up to 30 m.

STARSOL PILE CONSTRUCTION

Except for the concreting technique Starsol pile construction is similar to that of traditional auger-cast piles.

Drilling

Before drilling commences, a data-logger system is set to "drilling mode" and the hydraulic rams on the drilling head assembly

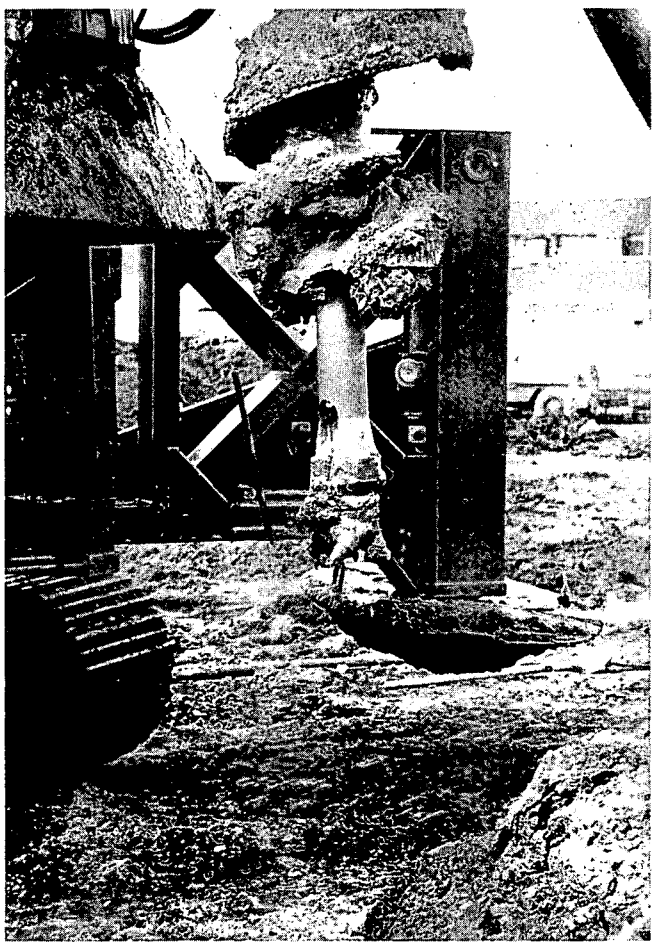

FIGURE 2 Internal tremie pipe.

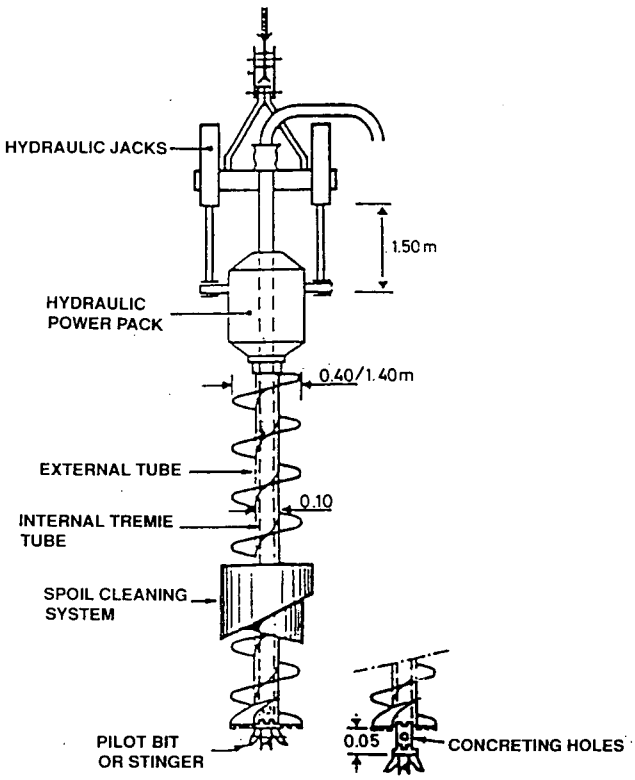

FIGURE 3 Main Starsol features.

are completely opened. At this point, the pilot bit is locked in position immediately below the drilling head of the auger. Drilling begins and the auger and internal tremie turn together, drilling into the ground.

The full drilling torque of the rig is mobilized because of the way the auger blade is designed, with the pilot bit and auger teeth combining over the full surface of attack to cut into the soil. This feature enables the machine to penetrate strata with uniaxial compressive strengths of up to 35 to 50 MPa.

During the drilling phase, the data logger records the torque, advancing speed, and depth. The data are plotted, in real time, on a computer screen in the rig cabin, and the operator can monitor the graphs at any time.

Concreting Phase

During this phase, the main difference between the Starsol method of concreting piles and that of conventional auger-cast piles is observed (Figure 4).

The system is primed by pumping concrete into the internal tremie tube. The rig operator monitors the concrete pressure, and when it is satisfactory the auger assembly, including the rotation table, is raised by two hydraulic rams on the drilling head assembly. During this operation the internal tremie tube and the pilot bit remain at the base of the pile.

As the auger assembly is lifted, two side vents on the tremie pipe are exposed and concrete is injected under pressure at the base of the pile. The auger is lifted in the same manner, until the internal tremie tube is fully extended and the hydraulic rams on

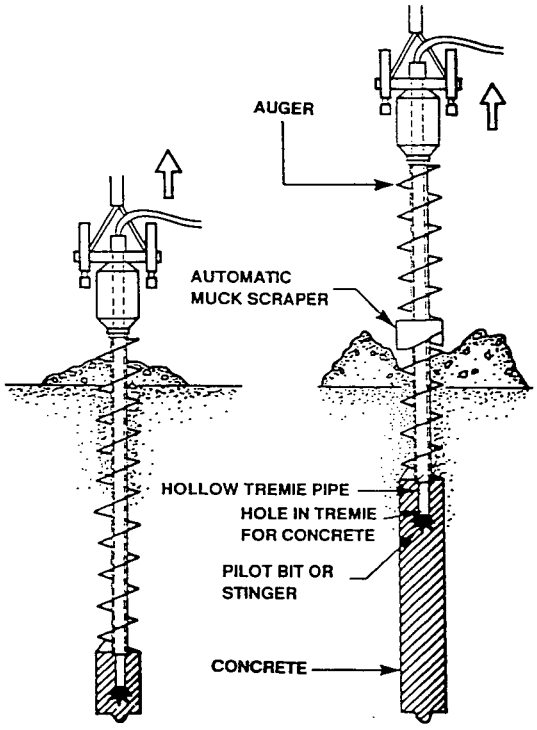

FIGURE 4 Concreting of a Starsol pile.

the drill head assembly are completely closed. When the internal tremie tube is fully exposed, there is approximately 1.5 m between the vents of the tremie and the base of the auger. At this point the internal tremie is locked in position and the whole assembly is raised.

Concreting continues using the tremie. A real-time data logger enables an operator continue to control the concrete pressure (at a minimum, 10 kPa), which ensures the integrity of the pile concrete. The injection of concrete under pressure gives a sound contact between the ground and the concrete over the whole pile shaft.

Auger Cleaning

As the auger is extracted, spoil remains attached to the flights. An auger-cleaner clears the flights and deposits the soil on the ground to the side of the excavation.

After completing the concreting, when the auger and tremie are fully extracted, the rig moves back from the pile position in order to allow access to the pile head.

An excavator quickly removes the spoil that accumulated around the cast pile. The rig is cleaned and prepared to construct the next pile.

As with any tremie technique, contaminated concrete is brought to the surface and must be removed before a reinforcement cage can be inserted. The concrete is removed with an excavator. Then a funnel, with approximately the same diameter as the pile, is inserted in the top of the pile shaft as preparation for the next phase of construction.

Insertion of the Reinforcement Cage

It is possible to position either individual bars or reinforcement cages in the pile. A simple system has been developed that can be used to assist cage placement. With this method it is possible to place long reinforcement cages; the longest inserted to date is 24 m. The reinforcement cage can be inserted either with the aid of the rig or a service crane.

QUALITY CONTROL DURING CONSTRUCTION: ENBESOL DATA-LOGGING SYSTEM

The data-logging system is used to supply a real-time record and ongoing quality-control mechanism during pile construction.

Quality control starts when drilling begins. As the auger penetrates the ground, the rate of advance and the torque mobilized are measured and recorded. In the concreting phase, the pressure and volume of concrete are measured and recorded. This real-time monitoring constitutes a preventive model for quality control: if anomalies occur, the pile can be immediately redrilled.

During the drilling phase, measurement of the penetration rate helps indicate the stiffness of the strata encountered. When these data are examined in conjunction with the torque measurements recorded by the drilling head, an operator gains a pretty good idea of the ground qualities.

In the concreting stage, concrete pressure and volume are measured by the data logger. Pressure is clearly indicated, both in positive and negative values. The software translates this data into a graph representing the ratio of real to theorical volume. The ratio should be over 1.0; in practice it is generally between 1.15 and 1.2. Furthermore, sharp variations on the concrete curve can be observed and avoided; the rig operator is able to control them by varying the lifting speed of the auger and tremie tube.

The concrete-pressure sensor is located at the swan neck at the top of the tremie tube. Although it would be preferable to measure concrete pressure at the discharge point, the base at the auger during drilling and concreting is too harsh an environment for the concrete-pressure sensors.

The concrete pressure at the point of discharge is given by

$$P_c = P_b \cdot h + P_m - P_f - p_b \cdot h_b - p_w \cdot h_w$$

where

P_c = concrete pressure,
p_b = unit weight of the fresh concrete,
h = height or the auger,
P_m = concrete pressure measured at the swan neck,
P_f = friction loss in the tremie pipe,
h_b = depth of discharge below the surface of the concrete,
p_w = unit weight of water, and
h_w = height of water above the discharge point.

The two final terms of the equation are of relatively minor significance compared with the first three. The only unknown value is the friction loss in the tremie tube. This can either be calculated using fluid mechanics or estimated for a specific concrete and particular machine by pumping concrete through the system before screwing the auger into the ground and measuring the concrete pressure at the discharge point. In this manner, the friction-loss value can be found, and hence the formula can be

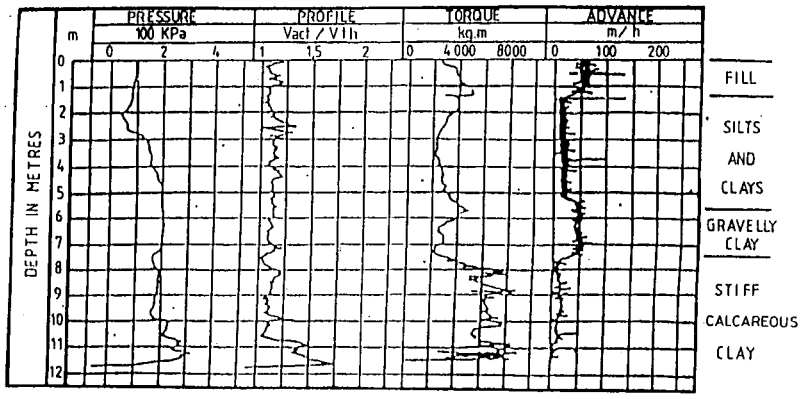

FIGURE 5 Typical Enbesol log.

used to estimate concrete pressure at the discharge point, at any stage of the concreting cycle.

Before lifting the auger to expose the vents at the base of the tremie, concrete is pumped at high pressure to build up a satisfactory head of concrete. The pressures during the whole concreting phase will remain positive, indicating that the tremie pipe is full of concrete. Any anomaly noted can be acted on immediately, and if the situation merits it, the pile can be rebored and the concreting repeated. By monitoring the concrete pressure and the ratio of actual- to theoretical-pile volume, it is possible to reduce concrete consumption without risking the integrity of the pile shaft (*5*).

The Enbesol data-logger system is designed to give a real-time record of pile construction. A print-out provides four graphs—rate of advance, torque, concrete pressure, and volume—all in relation to depth. This information constitutes a substantial part of the pile's record. A typical record is shown in Figure 5.

ULTIMATE PILE CAPACITY OF STARSOL PILES

The ultimate bearing capacity of this type of pile was the subject of an investigation by the Laboratoire Central des Ponts et Chaussées (*6*). Five sites were investigated, as shown in Table 1. At each site, the piles were instrumented using Laboratoire Central des Ponts et Chausées extensometers to determine the load transferred from the pile to the soil at various depths down the pile. A typical set of results, those for the 10.35-m-long pile at Clermont-Ferrand are shown in Figures 6–8.

Ultimate capacity of the piles was determined from these calculations:

1. The load on the pile when the pile settlement was equal to 10 percent of the pile diameter;
2. If the pile settled less than 10 percent of the pile diameter during the test, but the settlement exceeded the Davisson limit (*7*) (defined as the elastic compression of the pile plus 4 mm plus the pile diameter divided by 120), then the ultimate capacity of the pile was estimated using two methods: Chin's (*8*) and Fleming's (*9*) methods. In each case, the pile load corresponding to a predicted settlement of 10 percent of the pile diameter was taken as the ultimate pile capacity.

On the other hand, if the pile did not settle more than the Davisson limit, no attempt was made to analyze the ultimate capacity

TABLE 1 Details of Piles Tested

Site	Soil Type	Net Limit Pressure - Pl* (MPa)	Pile Dimensions Diameter and Length (m)	Estimated Ultimate Capacity (KN)	Curve
COLOMBES	Sand and gravel	2.0-2.6	1.0 x 7.5	3,660	A
STRASBOURG	Gravel	1.6-2.2	0.75 x 4.5	1,950	B
	Gravel	2.2-2.7	0.82 x 5.1	5,400	C
CLERMONT - FERRAND	Sand and clayey silt	0.5	0.82 x 10.35	1,950	D
	Clayey silts	0.5	0.82 x 7.2	-	-
	Cemented sand	2.0-13.0			
PARIS	Sand and gravel	2.0-6.0	0.5 x 15.5	-	-
	Weathered chalk	1.3-1.9			
TOULOUSE	Soft clay	0.45	0.5 x 11.5	4,300	E
	Calcareous clay	4.50			

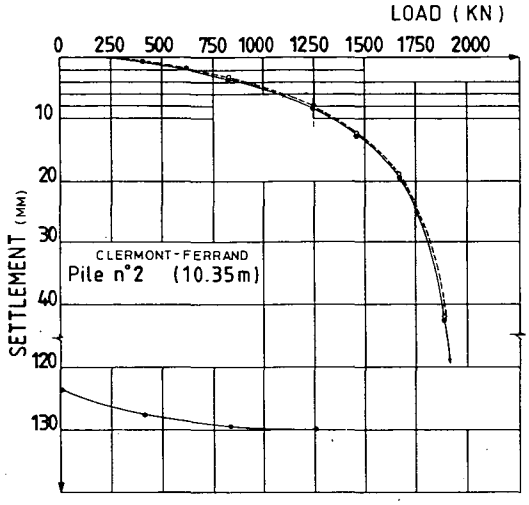

FIGURE 6 Load settlement curve.

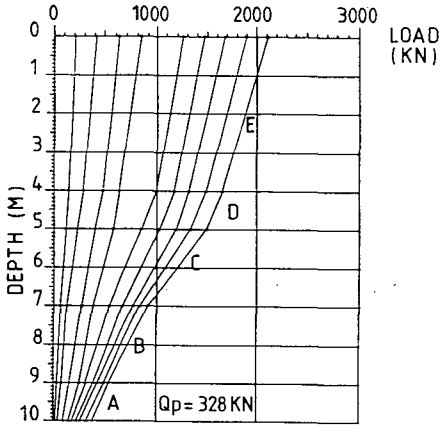

FIGURE 7 Distribution of load along pile length.

of the pile. Figure 9 shows the normalized plots of the five pile tests for which it was possible to determine the ultimate capacity of the piles concerned.

One problem with existing research on the ultimate capacity of the Starsol pile is that it is based mainly on French design practice and the use of a pressuremeter. To enable other engineers to design this type of pile, a review of test data is currently under way with the aim of producing effective stress design methods.

Concrete quality in the piles was monitored by taking concrete cores and testing them some time after pile construction. The results are shown in Table 2.

Results of the load-testing program indicated the following:

- Load-settlement characteristics for this type of pile are similar to those of other piles constructed with different methods; so normal design methods can be applied to piles constructed in this manner.
- Observed ultimate capacities indicated higher ultimate end bearing and ultimate skin friction in Starsol piles than in traditional bored piles. It was believed that these characteristics were the result of good concrete placing via the internal tremie, and minimal disturbance to the surrounding soil because of the boring method that was used.
- High quality, in situ, concrete can be achieved in auger-cast type piles by using the internal tremie system. The system gave the French technical authorities sufficient confidence for them to allow an extra 20 percent compressive stress on the concrete in the pile shaft, an increase from 6 to 7.2 MPa.

On the basis of the load tests, the following design guidelines were proposed.

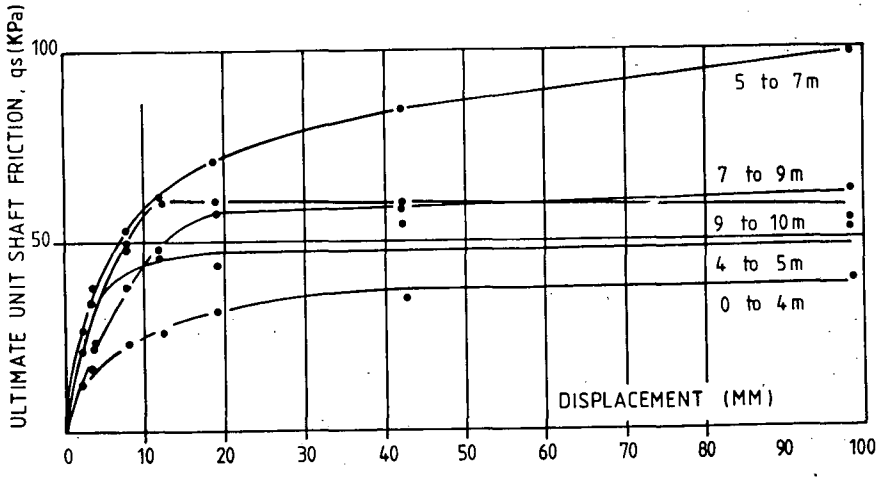

FIGURE 8 Mobilization of shaft friction along the pile length.

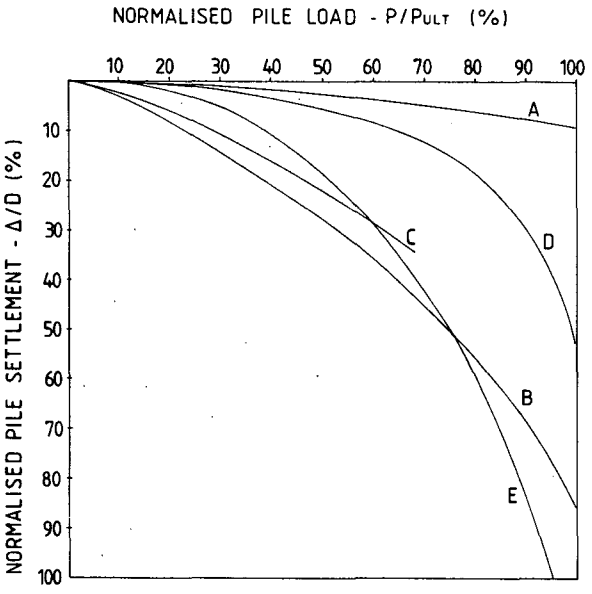

FIGURE 9 Normalized pile load settlement curves.

Ultimate Unit End Bearing

The ultimate unit end bearing is given by

$$a_b = K_p \cdot pl^*$$

where

K_p is the end bearing factor and pl^* is the net limit pressure.

Design values for various soil types are shown in Table 3.

Ultimate Unit Skin Friction

The ultimate unit skin friction for various soil types is shown in Table 4. These skin-friction values should be applied to the "real" pile diameter, which is the nominal pile diameter increased by a small factor as indicated below. Note that the range of skin-friction values found during the testing program was very similar to the values obtained using the current French design code (*10*) and the curve for piles concreted under low pressure.

TABLE 2 Concrete Core Test Results

Site	Age at Testing (days)	Compressive Strength (MPa)	Young's Modulus (GPa)
Colombes	62	31.40-55.20	19.80-26.30
Elsau	435	31.13-37.39	30.68-39.19
Clermont-Ferrand	350	30.90-50.10	24.48-26.43
Toulouse	128	42.40-51.20	27.00-31.50

TABLE 3 Design Values for K_p

Soil Type	Net Limit Pressure pl* (MPa)	K_p
Clayey sand, calcareous clay, clayey silt	0.5 - 4.5	1.2 - 1.4
Weathered chalk	1.3 - 1.9	> 1.8
Sand and gravel	1.6 - 2.7	> 1.8

TABLE 4 Design Ultimate Unit Skin Friction Values

Soil Type	Net Limit Pressure pl* (MPa)	Ultimate Unit Skin Friction q_s (KPa)	Increase in Nominal Diameter
Soft clay, clayey silt and loose sand	0.2 - 0.5	35 - 55	1.1
Sand and gravely sand	1.0 - 2.5	95 - 150	1.15
Sandy gravel and gravel	1.0 - 5.0	100 - 200	1.2
Weathered chalk	1.3 -1.9	> 100	1.1
Very stiff calcareous clay	4.5	200 - 400	1.1

TABLE 5 Correlations Between the Net Limit Pressure and U.S. Soil Tests

Soil Type	Pl* (MPa)	Cu (KPa)	N (blows/300mm)
Sand			15 to 20 pl*
Silt			30 pl*
Chalk			10 to 20 pl*
Clay	< 0.3	182 pl*	
	0.3 to 1.0	83 pl* + 30 or 100 pl* + 25	
	1 to 2.5	29 pl* + 85	
			15 to 20 pl*

Correlation Factors

The approximate correlation factors between the net-limit pressure and more common U.S. soil tests (*11*) are given in Table 5. In each case, the net limit pressure *pl** is in MPa.

CONCLUSION

This Starsol piling technique has proven successful in France. Since 1985, 2 to 3 percent of the 100,000 piles constructed to date have been used for highway or railway bridges.

The Starsol rig's internal tremie system in combination with the Enbesol data-logger, quality-control instrumentation has given the French technical authorities sufficient confidence in this piling method to allow an extra 20 percent compressive stress on the concrete in this type of pile as compared with the requirement for conventional auger-cast piles.

Analysis of load tests carried out on the piles indicated that current French standards for piles concreted under low pressure were broadly applicable to Starsol piles, which provide somewhat better pile-loading capacity than do conventional bored piles. A review of available test data is under way to enable the Starsol piles to be designed using effective stress-pile design methods.

ACKNOWLEDGMENTS

The author would like to thank his colleagues at Solétanche for their assistance in preparing this paper. In particular, he would like to thank Patricia Pierre for typing the paper and the draftsmen in the design office for preparing the figures.

REFERENCES

1. Neate, J. J. Augered Cast in Place Piles *Proc., 13th Annual Meeting*, Deep Foundations Institute, Atlanta, Ga., 1988, pp. 167–175.
2. CFA Pile Problems Need Thorough Study. *New Civil Engineer*, Nov. 19, 1987, p. 69.
3. Couldery, P. A. J., and W. G. K. Fleming. Continuous Flight Auger Piling at St. Enoch Square, Glasgow. *Ground Engineering*, Sept. 1987, pp. 17–28.
4. Fenoux, G., and G. Buysere. Starsol Enbesol Procedure. *Deep Foundations on Bored and Auger Piles*, (Van Impe, ed.), Balkema, Rotterdam, Netherlands, 1988, pp. 325–331.
5. Automation Augers Well. *New Civil Engineer*, Nov. 5, 1992, p. 26.
6. Bustamante, M. Etude Expérimentale du Procédé de Fondations Profondes Starsol. *Bulletin de Liaison des Laboratoires Ponts et Chaussées*, No. 149, May/June 1987.
7. Davisson, M. T. High Capacity Piles. *Proc., Lecture Series: Innovations in Foundation Construction*, Illinois Section, ASCE, 1972, 52 pp.
8. Chin, F. K. Estimation of the Ultimate Load of Piles Not Carried to Failure. *Proc., 2nd Southeast Asian Conference on Soil Engineering*, 1970, pp. 81–90.
9. Fleming, W. G. K. A new Method for Single Pile Settlement Prediction and Analysis. *Géotechnique*, Vol. XLII, No. 3, 1992, pp. 411–426.
10. Règles techniques de conception et de calcul des fondations des ouvrages de Génie Civil. Projet de fascicule 62-titre V. France, 1991.
11. Cassan, M. Les Essais In Situ en Mécanique des sols. Vol. 1, *Réalisation et Interprétation*, 2nd ed., Eyrolles, Paris, France, 1988.

PART 2

Other Foundation Issues

LRFD Code for Ontario Bridge Substructures

R. GREEN

A design procedure for bridge substructure foundations and retaining walls, Load and Resistance Factor Design (LRFD), is documented in the Ontario Highway Bridge Design Code. Details of the procedure are given. Structural and geotechnical design procedures are similar and compatible. LRFD procedures help to clarify the calculation procedures used when soil and structure meet and interact. Few new technical problems result for the geotechnical engineer using LRFD; however, communication between geotechnical and structural engineers is essential to ensure that the serviceability limit and the ultimate limit are identified for structures designed using LRFD. The design process is described and evaluated. Issues relating to earth pressures, shallow and deep foundations, and code writing are discussed.

Load and Resistance Factor Design (LRFD) procedures for bridge superstructures and substructures make up part of the first edition of the Ontario Highway Bridge Design Code (OHBDC), as published in 1979 (*1*). The LRFD code came about because changes in legal truck loads during the 1970s created a need to verify that designs for structures considered these changes in design loads and superstructure analysis.

The 1979 Code addressed design of substructures and retaining walls, interaction between structure and soil, and communication and coordination between geotechnical and structural engineers. Initially, geotechnical engineers did not like or accept the new procedures because of a new terminology, an incomplete understanding of LRFD, and an attempt to codify geotechnical design procedures. Some members of the geotechnical profession believed, incorrectly, that LRFD and associated factors were based solely on statistical concepts. Their negative reaction to a new design procedure was unexpected. LRFD is really a rearrangement of factor of safety design (FSD) provisions, and it has been applied successfully in Denmark for many years (*2*).

DESIGN PROCESS

Structural design and geotechnical design, or other design connecting a structure and soil or rock, have a common objective, namely to provide an acceptable level of reliability, including a minimization of loss of function. Uncertainty exists in the design process because load (force) effects vary. In addition, there is uncertainty related to construction, material characteristics, and resistance predictions. Finally, imperfections in analysis or lack of knowledge about the structure being designed come into play.

Structural design is described as an exact science, and geotechnical design is thought to be experience based. However, in practice there is little to distinguish geotechnical design or evaluation from structural design or evaluation. Both design processes involve the recognition of uncertainty, require sound judgment, and apply historical experience.

Department of Civil Engineering, University of Waterloo, Waterloo, Ontario, Canada, N2L 3G1.

The majority of design procedures used for foundations or structures address one or more limit states. These limit states may be defined in a design specification or as part of an office procedure. The two important limit states are

- Ultimate limit state (ULS): when a failure mechanism forms in the soil or rock, or in a structure, and
- Serviceability limit state (SLS): when loss of serviceability occurs in a structure because of deformation of the soil or rock.

A structure's or soil's reaching an ultimate limit state implies a major loss of lives or capital and damage that is not easily reparable. The collapse of a bridge, for example, may result in considerable economic loss or necessitate complete replacement.

The probability of an ULS condition occurring is about 10^{-3} to 10^{-5} (*3*). SLS occurs with a larger probability than ULS, and the damage or loss of service at SLS is reparable. For example, in a bridge foundation there may be one chance in 20 or 30 that settlement diminishes ride quality. The loss of ride quality either will be accepted, or surface repairs can be made at little or no cost.

SAFETY CONSIDERATIONS

A bridge superstructure or a pile foundation with resistance, R, subject to specified load effects, U, is considered. In design, different R values appropriate to the serviceability limit state, R_s, and the ultimate limit state, R_u, are used with a series of load effects, U, based on various combinations of specified vertical and horizontal loads. Reliability concepts are illustrated for both LRFD and Factor of Safety Design (FSD).

Load and Resistance Factor Design

Using LRFD, specified loads are modified by multiplying the specified load by a load factor that is appropriate to the level of uncertainty associated with a given load and limit state. Values of load factor selected for OHBDC3 (*4*) are given in Table 1. Barker et al. have documented load factor values proposed for U.S. use (*5*). Several combinations of load are usually employed to determine the maximum destabilizing effect of load and thus maximize the probable resistance demands of both the soil and the structure. The design equations, for serviceability (SLS) and strength (ULS), are

$$\text{SLS: } R_s > U \tag{1}$$

$$\text{ULS: } I(\phi R_u) > \alpha u \tag{2}$$

where

ϕ = resistance factor of either the soil or a structural component;
α = average load factor associated with combinations of specified loads U;
R_s = resistance based on a prescribed deformation, typically 25 mm or 50 mm;
R_u = predicted ultimate resistance of soil or rock due to vertical load, including the effects of ground inclination, embedment, layering, and the like;
R_u = ultimate resistance of a structural component; and
I = factor applied to the factored geotechnical resistance, ϕR_u, for load inclination, always less than 1.0.

Equations 1 and 2 apply to both structural design and geotechnical design. Different combinations of load are frequently used as part of the two design processes for the same limit state. Equation 1 is nearly identical to that used in factor of safety design, except that R is equal to R_s, a resistance based on a prescribed deformation. Design for ultimate strength is covered by Equation 2. For geotechnical design at ULS, the value of ultimate resistance is a function of the angle of inclination of the particular load combination forming U. The uncertainties covered by the design equations, Equations 2 and 3, include the following:

1. Selection of specified loads, both structural and geotechnical;
2. Method of analysis, both structural and geotechnical;
3. Choice of geotechnical parameters and resistance for a given stratigraphy; and
4. Variability in material properties and member structural resistances.

With LRFD, the geotechnical engineer normally will supply the values of R_s and R_u of the soil or rock for the design. These values must be consistent and apply to the site. Consider a medium sand supporting a footing 4.0 m in width, where R_s may be specified as 220 kPa for a vertical settlement of 25 mm and R_u as 2,000 kPa for vertical loads. The value of R_u of 2,000 kPa for a 4-m-wide footing may appear to be excessive. However, it is representative of a dry granular soil in which the angle of internal friction is about 33 to 35 degrees.

TABLE 1 Load and Resistance Factors from the Ontario Highway Bridge Design Code (Third Edition) (*4*)

Load	Load Factor	Resistance	Resistance Factor
Dead Load	1.10 to 1.50	Bearing	0.5
Live Load	0.80 to 1.25	Shear, on granular surface	0.8
Earth fill	0.80 to 1.25	Horizontal passive	0.5
Earth pressure	0.80 to 1.24	Static test, pile	0.6
Earth fill plus pressure	1.00 to 1.25	Static analysis, pile	0.4

Factor of Safety Design

A single equation applies for FSD:

$$R > U \tag{3}$$

where R is the lesser of R_s or $(I \cdot R_u)/F$, and F is the factor of safety.

For narrow footings founded on a granular soil, strength expressed by the function, $(I \cdot R_u/F)$, will control the choice of resistance, R, while serviceability, R_s, will generally control the design of wide footings. In Equation 3, all uncertainty is assigned to one function, namely, the factor of safety, F, unlike the separation expressed by Equations 1 and 2. There is little room for improvement in design when a single value covers all uncertainties associated with both load and resistance.

Factors of safety quoted for geotechnical work vary according to the function of the system. For example, factors range from as little as 1.3 for earthworks, for which the problem is almost completely geotechnical, to 3.0 for foundations. Both geotechnical and structural considerations apply in the case of foundation design, and loss of life may be a consideration in design (*6*). The calculated factor of safety for 14 embankments, all of which failed, varied from 1.0 to 1.8. This suggests that uncertainty in both analysis and the choice of the best value for a geotechnical parameter exists (*7*).

RELIABILITY CONSIDERATIONS

OHBDC includes specified permanent loads based on as-built observations of Ontario bridges as well as specified live loads that are mean maximum loads based on existing truck traffic projected over a 50-year design life (*1,4,8*). The observed loads and associated statistical distributions, uncertainty of analysis methods, professional factors, and growth are used to calculate reliability indices and load factors for design.

Various methods can all be used to predict the ultimate resistance of soil under vertical load, ϕR_u:

- Empirical values,
- Assessed values,
- Geotechnical equations,
- Partial coefficients of soil-strength factors, and
- Reliability-based resistance.

Experience is the contributing feature in the selection of any resistance value based on empirical or assessed values. Geotechnical parameters such as unit weight, cohesion, and angle of internal friction are needed for the calculation of the resistance value based on geotechnical equations or reliability considerations. Many geotechnical design resistance values are based on empirical evidence suitably adjusted for historical experience. For example, allowable values for FSD are either limiting deformation or ultimate (capacity) values (factored down for safety with F equal to about 3).

A choice must be made between a global resistance, where the contribution of several parameters are lumped together, or a re-

sistance based on individually factored geotechnical parameters. Both the Danish standard, DS 415 (*2*), and OHBDC2 (*8*) provide procedures for calculating lateral earth pressures using factored parameters. OHBDC3 publishes only resistance values based on global considerations and a system performance factor, which is less than unity (*4*). This factor includes the effects of uncertainty and can be back calculated from existing designs. Detailed knowledge of the contribution made by the friction of the cohesive components of resistance need not be known if global factors are used.

Empirical Values

ULS and SLS resistance values can be developed from empirical relationships between resistance and some indirect measure of the geotechnical parameters, such as the standard penetration test (SPT), cone penetration test (CPT), or pressuremeter data. OHBDC3 (*4*) encourages the use of empirical methods, as they are well proven. A resistance factor of 0.5 is recommended for empirical bearing resistance values in OHBDC3 (*4*) (Table 1), although the procedures used to develop the value may be method driven. The geotechnical engineer selects the empirical method according to particular site conditions; the Code does not recommend a method.

Empirical values are not identical to the presumed values published in many design handbooks. Presumed values appear to apply only to SLS and FSD design, and they cannot be modified easily to apply to an ULS situation.

Assessed Values

Data from completed investigations for one site may be of value when investigating another site, if the sites have similar stratigraphy. Thus, it may be possible to use the ultimate-resistance values from a completed investigation and an appropriate resistance factor for the new site—taken as 0.5 or 0.6 for bearing or axial resistance of piles, respectively (*4*).

Geotechnical Equations

For each design situation, there will be a suite of applicable design equations. A geotechnical engineer usually will favor one or two for resistance prediction of shallow or deep foundation design that are based on historical experience. Each equation provides a different value for the mean of the ratio of observed to calculated resistance, E, based on the geotechnical parameters chosen for the test site. Normally, the value of E should be unity in the absence of other data. The following is used for design purposes:

$$\text{Calculated factored resistance} = \phi \cdot E \cdot R_u \quad (4)$$

where R_u is a calculated resistance that is a function of the geotechnical parameters, drainage conditions, and geometry of the footing and piles.

Partial Coefficients or Soil-Strength Factors

Partial coefficients for geotechnical design appear to have been developed by Hansen (*9*). These coefficients are not based on a reliability assessment of typical soil or rock but were based on a rearrangement of FSD values. This rearrangement permits a two-part separation: namely, uncertainty due to geotechnical resistance (partial coefficients), and uncertainty due to load effects (load factors in LRFD). DS 415 provides values of partial coefficients for various safety classes (*2*). In OHBDC2, partial coefficients are specified and are referred to as soil-strength factors.

The factored soil strength parameters, c_f and tan ϕ_f, (*2*) are

$$\text{Cohesion: } c_f = cF_c \quad (5)$$

$$\text{Internal friction: } \tan \phi_f = F_\phi \tan \phi' \quad (6)$$

where F_c and F_ϕ are soil-strength factors for cohesion, c, and friction, tan ϕ, respectively. The specified values of F_c are 0.65 for stability and earth pressure and 0.50 for footings and piles. F_ϕ has a single value of 0.80 that applies to earth pressure and resistance calculations. Factored soil strength parameters should be used directly in Equation 4, using a resistance factor ϕ of 1.0. If the site investigation provides either SPT or CPT data, these data can be used to develop geotechnical parameters. Many Ontario engineers using OHBDC2 found that this was a very indirect treatment of geotechnical parameter data (*8*). They preferred to obtain empirical values of SLS and ULS bearing resistance directly from SPT, CPT, and pressuremeter test values, without "guessing" geotechnical parameters.

Reliability Based Resistance

For a major structure that involves a high degree of risk, a comprehensive site investigation using continuous monitoring, for example, may be carried out. The results would yield the geotechnical parameters for soils at various locations and strata in terms of a mean and standard deviation. Such a site investigation would reduce uncertainty compred with a more limited, traditional one. Calculation details are available for factored resistance from statistical data (*3*).

Discussion of Selected Resistance

The selection of factored resistance will be a function of the quality of a site investigation and the complexity of the soil conditions at the site. More refined methods may be inappropriate for a site where the subsurface conditions are extremely variable and uncertain. OHBDC2 recommends that soil strength factors be used for ULS values for shallow and deep foundations (*4*). When test data are available for piles, a global resistance can be applied for OHBDC2 assessments. Many users found it difficult to apply soil strength factors to friction piles, as the mathematical results tended to contradict experience. In the latest version of the Ontario Code (*4*), soil strength factors were replaced by performance factors.

SHALLOW FOUNDATIONS

Ultimate bearing resistance may be based on SPT data, CPT data, or on bearing resistance (capacity) theories, if the geotechnical parameters are known. The ratio of observed to calculated ultimate bearing resistance for shallow foundations is 1.20, ac-

cording to Terzaghi's theory (*10*), or 0.86 according to Meyerhof's recommendations (*11*), based on data compiled by Bowles (*12*). Even with accepted resistance-calculation procedures, questions still arise as to the adequacy and conservatism of the calculation. In addition, the final method of selecting the "best" geotechnical parameters to be used in a calculation is not always clear. The author understands that a conservatively chosen, representative mean value is often used.

In an LRFD format, a range of ultimate bearing resistance values should be provided for a shallow foundation, for both footing width and embedment. Figure 1 shows calculated bearing resistance for various widths for an ideal footing founded on the surface. The soil has an average N value of about 20 to 25, and the water table is low. Factored ultimate resistance values increase with footing width. The SLS resistance, based on a deflection of 25 mm, is approximately constant with increasing footing width. The points where a transition occurs from ULS to SLS are indicated by a and b (Figure 1). Ultimate resistances shown in Figure 1 are, in a clockwise direction, a calculated ultimate resistance, R_u, a factored resistance proposed in OHBDC3, ϕR_u, an FSD resistance, $R_u/3.0$, and a factored resistance, $I\phi R_u$, for an inclination factor for an angle equal to 21.4 degrees. In Figure 1, the factored resistance for a footing width of 4 m is nearly five times the SLS resistance.

Foundation reports made available to the author frequently quote a factored resistance that is only one-and-one-half times the SLS value for granular material. The value of 1.5 is assumed to be a back calculation from an SLS value, an F value of 3.0, and applying a resistance factor of 0.5. The FSD values shown in Figure 1 are for an SLS condition and do not include the inclination of load.

With the inclusion of the inclination factor in ULS design (Equation 2), marked changes in bearing resistance resulted for designs based on OHBDC2 (*8*). When calculations for an abutment wall footing without embedment that has a ratio of vertical to horizontal force of 0.15 are made, the calculated (vertical) ultimate resistance for granular material is reduced to approximately 60 percent of the vertical resistance. For a retaining wall that has a smaller mass than an abutment, this ratio of vertical to horizontal force increases to about 0.40 or 21.4 degrees. The ultimate resistance is only 20 percent of that for vertical load. The reduction factors quoted are for footings founded on the surface. An increase in bearing resistance occurs with footing embedment. An additional resistance of about 700 kPa may be added to the values shown in Figure 1 if an embedment of 1.2 m is present. The embedment of 1.2 m is the design frost cover depth in much of Southern Ontario. This additional resistance due to embedment is well known and should be considered by the geotechnical engineer. The geotechnical report should be flexible enough to permit the structural engineer to make a choice between changing the footing width or increasing the embedment during design, and the choice should be made with the geotechnical engineer's knowledge.

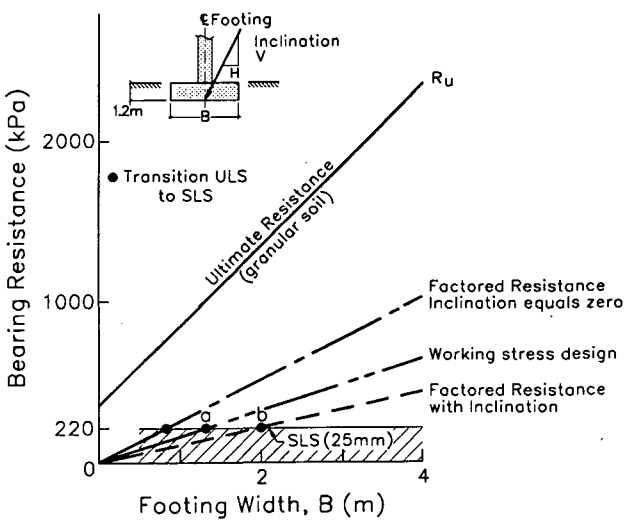

FIGURE 1 Various bearing resistances and footing width.

Few tests of footings with inclined load are available. The data provided by Muhs and Weiss (*13*) for relatively large, 1-m by 3-m footings were compared with the various design proposals of Meyerhof (*11*), Vesić (*14*), and Hansen (*15*). All three theories propose conservative estimates of reduction factors for granular materials with an angle of internal friction equal to about 38 degrees. The ratio of observed to calculated reduction value was 1.4 with a standard deviation of about 0.05. The reduction factor equations of Meyerhof (*11*), assuming 1.2 m embedment, are used in OHBDC3 (*4*). If bearing-resistance values are calculated directly from geotechnical parameters and a resistance equation, reduction factor expressions should be used appropriate to the specific resistance equation that is used (*4*).

EARTH PRESSURE

The use of an equivalent fluid pressure representation for earth pressure of a free-draining, engineered backfill applying the method of Coulomb or Rankine is common in cantilever walls and abutment design (*12,16*). An active pressure condition, *Ka*, is assumed when the shear resistance of the retained material is mobilized at assumed lateral displacements of 0.001 of the wall height, a base rotation of 0.002, or a combination of these. For a retained soil with an angle of internal friction of 30 degrees, the horizontal pressure coefficient K_a is taken as 0.33.

When both the stem and base of the wall do not yield during the installation or compaction of the retained soil, lateral pressures in excess of at-rest pressures (K_o = 0.5, ϕ = 30 degrees) may develop [Figures 2(*a*) and 2(*b*)]. Lateral pressures from compaction will develop on the upper part of a stiff wall (*17*). The stems of most abutment walls and retaining walls are more flexible than gravity walls or culvert walls. These retaining walls translate or rotate during the installation of each layer of compacted soil. Horizontal movements will reduce locked-in compaction stresses and lead to the lateral pressure distribution given in Figure 2(*c*). The additional compaction pressures are not large for light hand-compaction equipment, and they can be calculated (*2,17*). Force effects due to the pressures from light compaction [Figure 2(*c*)] can be approximated using an equivalent fluid pressure for the total pressure due to backfill, K_b. This pressure has a value that is midway between active and at-rest pressure for a typical case.

Ministry of Transportation Ontario data (M. Devata, unpublished data, Ministry of Transportation, Ontario) indicate that the angle of internal friction, ϕ, is between 35 and 46 degrees for rock backfill and between 32 and 42 degrees for a granular backfill suitable for free-draining fill. Many design engineers use a ϕ value

of 30 degrees for calculation purposes. This is conservative; lateral earth forces are overestimated.

A number of pressure distributions (Figures 2 and 3) may exist following installation of the backfill. Figure 3(*a*) shows surcharge and active pressures acting on a wall. Such a pressure distribution may exist following movement of the base, even though the destabilizing effects of the earth forces are resisted by the soil beneath the footing base. This soil is assumed to mobilize its factored resistance and to deform sufficiently to cause an active pressure condition, K_a, to develop in the retained soil. The situation when the soil is beneath the footing has not reached limiting equilibrium (a factored resistance) is illustrated in Figure 2(*c*) and Figure 3(*b*). The earth pressures acting on the wall are not an active pressure, as movement of the base is small. A backfill pressure, K_b, which includes compaction pressures and associated surcharge, is present. This backfill condition occurs when the bearing is competent and non-yielding during compaction of the fill.

The wall shown in Figure 3 should be designed to resist the forces from both pressure conditions [Figure 3(*a*) and Figure 3(*b*)], that is, both K_a and K_b plus any surcharge. Two separate designs are necessary, one in which the base width is selected (active conditions control) and a second in which the structural size of the wall is calculated (backfill pressure conditions control). The design philosophy is to identify the worst case for the design of the stem, toe, and heel, and the worse case for the footing width.

The provisions of DS 415 include a load factor of 1.0 for all vertical and horizontal earth forces (*2*). The procedure was not followed in the Ontario design documents (*1,8*) wherein a load factor of 1.25 was applied to earth pressures that already included an allowance for uncertainty through the use of soil-strength factors. Double counting of the safety provisions in the first two editions, coupled with reduction factors for inclined load, resulted in some footing widths being 50 percent larger than might be obtained using FSD. These proportions were questioned by design engineers. OHBDC3 attempts to rectify the double counting by using one load factor to handle uncertainty in the calculation of active or backfill pressure effects based on unfactored values (*4*). The load factor chosen is 1.25. The uncertainty associated with the horizontal forces and moments due to lateral earth pressure for geotechnical design (Figures 2 and 3) can be managed using either soil strength factors or load factors but not both.

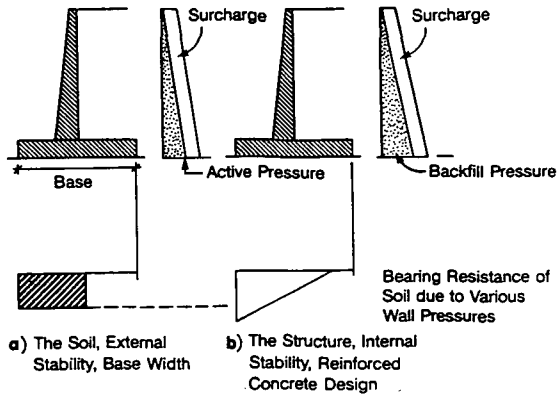

FIGURE 3 Earth pressures and bearing resistances.

DEEP FOUNDATIONS

The design of deep foundations requires a knowledge of the axial and lateral resistances of a pile or group of piles. A calculation procedure whereby the forces acting on a pile due to external actions can be calculated is also required. The geotechnical engineer normally will supply values of ultimate resistance for axial load and may provide lateral resistance values at the ultimate state. The structural engineer will determine the number and the arrangement of the piles, based on the calculation of forces.

Figure 4 shows typical load-deflection data for vertical and horizontal load tests completed in Ontario. The steel piles were driven into fine sand (top 3 m) and then silty clay. ULS and SLS values for vertical load are easily identified [Figure 4(*a*)]. The

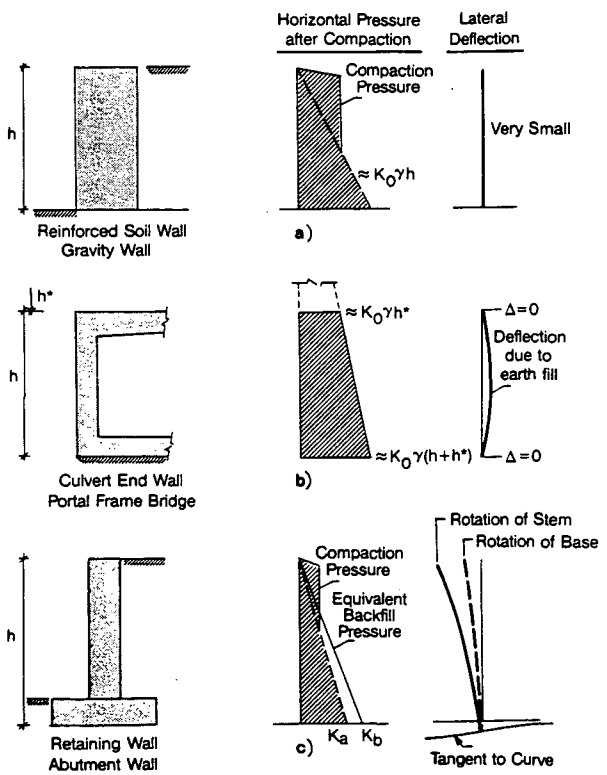

FIGURE 2 Various earth pressure conditions

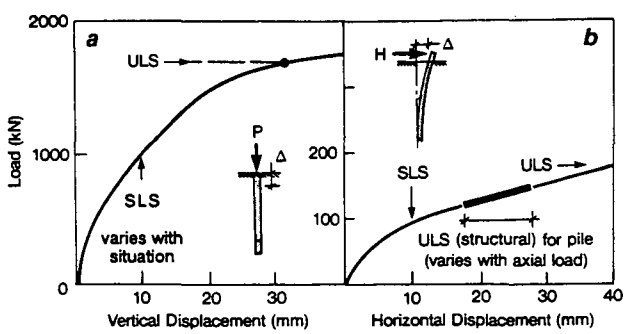

FIGURE 4 Load and deflection test data for both vertical and horizontal loading.

ULS value for the pile is associated with a limiting vertical deflection. The SLS value may be based on a limiting stress or a limiting deflection for a single pile or a group of piles, shown as 10 mm in Figure 4(*a*). Not shown in Figure 4 is an SLS value based on down-drag effects and structural resistance of the pile as well as soil properties.

Figure 4(*b*) illustrates three main design features for horizontal effects. The first is an assumed SLS value based on a lateral movement of the pile of 10 mm (arbitrarily chosen). The other two are ULS resistance values, one based on the soil's passive resistance and the second controlled by the structural resistance of the pile, including lateral load and axial stresses. From simulations made using the procedures of Reese (*18*), the ULS resistance of a pile subjected to horizontal load was found to be controlled by structural rather than geotechnical considerations, except for short piles.

A number of expressions for the axial prediction of pile resistance exist. Many are empirical relationships. Briaud and Tucker (*19*) developed ratios of observed to calculated values for 98 pile tests using 13 methods of calculation and including piles driven in sand or clay as well as in layered soil. Of the 13 methods, only 3 yielded a ratio of observed to calculated greater than unity. This is not a safety problem if an appropriate value of E and the resistance factor ϕ are used for each analytical method in Equation 4, or if conservative values of the geotechnical parameters are used.

The structural engineer requires both simple and detailed methods for the preliminary and final analysis of pile foundations. Soil-structure interaction solutions are available whereby the final designs can be verified (*18*). There does not appear to be a universally accepted method of analysis for the forces in piles. Calculation methods that permit the analysis of pile footings with the very simple geometry given in Figure 5 and consider the interaction between vertical and horizontal forces and associated resistance are required. OHBDC2 provided a limit equilibrium solution for the analysis of vertical load on a pile group (*4*). The code was silent as to how the analysis for vertical load should include horizontal effects, however. The force in individual piles within a pile group is a function of the applied axial load, moment, and the horizontal load applied to the footing of a pile group. Any method of analysis should consider all three load effects concurrently, especially if deformations of the footings and hence superstructure are of import. Analyses that combine the interaction equation for forces due to eccentric load on a footing with a simple, graphic static solution, and include the interaction of vertical and horizontal load, are available (*20*). Even though compatibility of deformation between the structure, piles, and the soil is not considered, this procedure is perhaps the simplest of any for preliminary design. An example of the method is shown in Figure 5.

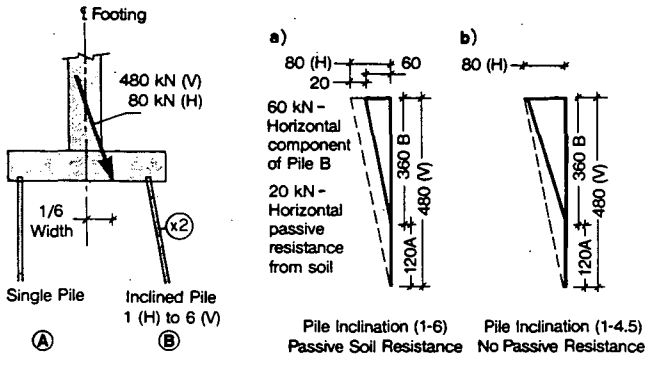

FIGURE 5 Pile force analysis.

In Figure 5 the point of application of the vertical load is chosen to induce equal vertical loads in the single rear pile and each of the two inclined piles. For the loading cases and geometry shown in Figure 5, the two inclined (1 to 6) piles only resist 75 percent of the applied horizontal load of 80 kN. A horizontal passive resistance of 20 kN should be provided by the soil to maintain equilibrium. If all the horizontal resistance is assigned to the inclined piles with none provided by the soil, a design inclination of 1 to 4.5 would be required for the front piles. This design inclination will only be effective for a single-load case. As the ratio of horizontal to vertical load changes, passive resistance would be required from the soil. Conservatively chosen, factored horizontal passive-resistance values are required for design, even if simple manual methods of analysis are used in the absence of the *p-y* compatibility conditions outlined by Reese (*18*).

The example of Figure 5 combined with Huntington's analyses (*20*) suggests a simple method for designing the preliminary proportioning of pile footings that minimizes both rotation and horizontal displacement. The method, which is given elsewhere (*4*), is

1. Select the most common SLS loading condition for the footing; typically this would be the dead load plus any permanent horizontal load.
2. Choose a pile arrangement that results in equal axial load in all piles.
3. Check this pile arrangement to ensure that all other SLS and ULS load combinations are satisfied.
4. If number 3 above is not satisfied, the number of piles (per m run) chosen in step 1 should be increased without changing the centroid of the piles.

Final checks might include 10 to 15 load combinations and would consider the passive horizontal resistance at the pile-soil interface specified by the geotechnical engineer.

DISCUSSION OF RESULTS

LRFD requires the use of little or no new technology for either the structural or the geotechnical engineer. However, LRFD does require cooperation between structural and the geotechnical engineers; a complex project may demand several discussions. Site investigation procedures can remain unchanged. New technology will be used in the future and will reduce uncertainty regarding the identification of the stratigraphy and the soil parameters. Complex structures still demand a high level of investigation. Results from detailed investigations may provide geotechnical data of the quality and quantity necessary for reliability-based predictions of resistance.

A repackaging of the design information developed for FSD design is required for LRFD, as it addresses SLS and ULS as two separate, specific design states (*4,5,21*). The geotechnical engineer should no longer provide a single bearing value for shallow or deep foundations based on the more conservative of either SLS or ULS resistance. Both resistance values are required for struc-

tural design. For structures with components that interact with soil, the serviceability limit may control design aspects involving the soil, whereas the ultimate strength limit may control structural design. Different combinations of load may apply in the proportioning of a footing width (geotechnical) or in selecting a footing depth and the reinforcing steel for that footing. The concept is not new; the process permits design for extreme values and combinations of load. Although some additional computational effort may be required, it is not a problem if design spreadsheets are used.

LRFD procedures demand full understanding of the interaction of soils and structures, and the design process for using these components. The LRFD method leads to complete designs and permits the use of new data in both design and evaluation.

CONCLUSION

LRFD is an appropriate procedure for resolving design problems where interaction between soils and structures is present. Designs evolve where either serviceability or ultimate limits control the final design, thus providing a linkage between FSD and ultimate-strength design. No new technology is required for LRFD. However, a reassessment of current design processes is required.

ACKNOWLEDGMENT

The author wishes to thank the Ministry of Transportation Ontario for an opportunity to work on various OHBDC Committees.

REFERENCES

1. Ontario Highway Bridge Design Code and Commentary, 1st ed. Ministry of Transportation and Communication, Downsview, Ontario, Canada, 1979.
2. DS 415, Dansk Ingenirforening, *Code of Practice for Foundation Engineering, Danish Standard*, Bulletin No. 36, (English translation). Danish Geotechnical Institute, Copenhagen, Denmark, 1985, 53 pp.
3. MacGregor, J. G. Safety and Limits States Design for Reinforced Concrete, *Canadian Journal of Civil Engineering*, Vol. 3, No. 4, 1976, pp. 484–513.
4. Ontario Highway Bridge Design Code, 3rd ed. Ministry of Transportation Ontario, Downsview, Ontario, Canada, 1992.
5. Barker, R. M., et al. *NCHRP Report 343: Manuals for the Design of Bridge Foundations*. TRB, National Research Council, Washington, D.C., 1991, 308 pp.
6. Meyerhof, G. G. Limit States Design in Geotechnical Engineering. *Structural Safety*, Vol. 1, No. 1, 1984, pp. 67–71.
7. Been, K. The Complexity of Soils and Its Influence on Working Stress and Limit States Design. *Symposium on Limits States Design in Foundation Engineering*, Canadian Geotechnical Society, Mississauga, Ontario, Canada, May 1989.
8. Ontario Highway Bridge Design Code and Commentary, 2nd ed. Ministry of Transportation and Communication, Downsview, Ontario, Canada, 1983.
9. Brinch Hansen, J. Limit Design and Partial Safety Factors in Soil Mechanics. Bulletin No. 1. Danish Geotechnical Institute, Copenhagen, Denmark, 1956, 4 pp.
10. Terzaghi, K. *Theoretical Soil Mechanics*. John Wiley and Sons, Inc., New York, N.Y., 1943.
11. Meyerhof, G. G. The Ultimate Bearing Capacity of Foundations. *Geotechnique*, Vol. 2, No. 4, 1951.
12. Bowles, J. E. *Foundation Analysis and Design*. McGraw Hill, Inc., New York, N.Y., 1982.
13. Muhs, H., and K. Weiss. Die Grenztragfähigkeit von Flach Gegründeten Streinfenfundamenten unter Geneigter Belastung nach Theorie und Versuch, *Berichte aus der Bauforschung*, Heft 101, *Mitteilungen der Degebo*, Heft 31, Berlin, Germany, 1975.
14. Vesić, A. S. Bearing Capacity of Shallow Foundations. In *Foundations of Engineering Handbook*, Van Nostrand/Reinhold Book Co., New York, 1975, 751 pp.
15. Brinch Hansen, J. A Revised and Extended Formula for Bearing Capacity, Bulletin No. 28. Danish Geotechnical Institute, Copenhagen, Denmark, 1970, 21 pp.
16. Bolton, M. D. Limit States Design in Geotechnical Engineering. *Ground Engineering*, Vol. 14, No. 6, 1981.
17. Ingold, T. S. The Effects of Compaction on Retaining Walls. *Geotechnique*, Vol. 29, 1979, pp. 265–284.
18. Reese, L. C. Behavior of Piles and Pile Groups Under Lateral Load. Report FHWA/RD-85/106, FHWA, U.S. Department of Transportation, March 1986.
19. Briaud, J. L. and L. M. Tucker. Measured and Predicted Axial Response of 98 Piles, *J. Geo. Div.* Vol. 114, No. 9, Sept 1988, pp. 984–1001.
20. Huntington, W. E. *Earth Pressure and Retaining Walls*. John Wiley and Sons, New York, N.Y., 1957.
21. Duncan, M. et al. Load and Resistance Factor Design for Bridge Foundations. Presented at Symposium on Limits States Design in Foundation Engineering, Canadian Geotechnical Society, Mississauga, Ontario, Canada, May 1989.

The views expressed in this paper are those of the author and not of any sponsor.

Analytical Modeling of Spread Footing Foundations for Seismic Analysis of Bridges

JEFFREY W. MCGUIRE, WILLIAM F. COFER, M. LEE MARSH, AND DAVID I. MCLEAN

The way bridges respond to seismic excitation may be significantly influenced by the dynamic properties of their foundations. Within current design practice, foundation elements typically are considered as elastic springs, without consideration to material and radiation damping. General foundation models are identified that are suitable for (a) modeling soil-structure interaction for the seismic analysis of bridges, (b) modifying an existing, nonlinear, seismic-bridge-analysis computer program to include a new element capable of representing such models, and (c) conducting a parametric study to assess the effect of the increased energy dissipation mechanisms on the seismic response of bridge substructures. Three different models for spread-footing foundations are identified, applied to a typical two-column bridge bent, and compared with conventional elastic and fixed-base models. Three soil-stiffness values are considered, and two earthquake records, each with two different intensities, were applied to the bent. Maximum values of displacement, plastic-hinge rotation, and cumulative plastic hinge rotations were noted and compared. It was concluded that the use of the spread-footing foundation models can produce an important change in the bridge response to seismic activity when compared with that of the fixed-base model—depending on the frequency content of the earthquake and the stiffness of the soil. The effects of radiation damping were observed to be insignificant for foundations on stiff soil but important for those on soft soil. In addition, the performance of the simpler, damped foundation models was found to be quite similar to that of the more complex models. The models' accuracy was not verified, but the structural response of incorporating them was explored.

The way bridges respond to seismic excitation may be significantly influenced by the dynamic characteristics of the foundation (*1–3*). For example, interaction of the bridge superstructure with the abutments has been the cause of significant damage in past earthquakes (*3,4*). Although damage to other foundation elements, such as spread footings and piles, has been shown to be minimal, their performance during seismic excitation can have an important effect on the structural behavior (*5*), especially when the founding soil is soft (*6*).

Although research has shown that a significant amount of seismic energy is dissipated through the material and radiation damping associated with bridge supports and surrounding soil (*7*), these soil-structure interaction effects are not considered in detail in current design practice (*8*), and little emphasis has been placed on studying the role of foundations in the seismic analysis of bridges (*3,9*). Current design guidance is simplistic in that it considers the foundation elements as linear springs (*3,10*). The effects of gaps and the material nonlinearity of soil at abutments are approximated by manually varying the spring constants, such that the soil strength is not exceeded. However, important additional nonlinearities at abutments result from the force developed in the abutment key (*2*) and the energy loss due to impact during expansion-joint gap closure (*11*). Barenberg and Foutch (*12*) have reported that the elastic method is unconservative for abutments.

The role of foundations in seismic analysis is typically recognized through the use of translational and rotational springs. However, nonlinearities can arise from several sources, such as inelastic soil behavior and connection details at pile caps (*5*). Other important considerations include soil stiffness degradation that occurs during cyclic loading (*13*), loss of strength in the soil due to liquefaction, the influence of pile group behavior, and radiation damping. In addition, hysteretic damping may be included intentionally through the use of base-isolation techniques (*14–16*).

In order to properly represent hysteretic material damping and viscous radiation damping, Spyrakos (*8*) has recommended that a general, nonlinear, spring-damper model be used to represent the translational and rotational properties of piles, footings, and abutments. However, most computer software that is available for the dynamic analysis of bridges has only the capability to perform elastic analyses. Energy dissipation analysis is done through proportional damping, whereby a damping coefficient is associated with certain modes of vibration. Concentrated dampers and hysteretic springs, such as those that would be required to accurately model foundations, are not available for this type of analysis.

Nonlinear Earthquake Analysis of Bridge Systems (NEABS) (*17*) is a public-domain dynamic bridge analysis program that is capable of modeling nonlinearities. An algorithm for plastic-hinge formation and a gap-contact element are included in the program. However, there is no concentrated translational or rotational viscous damping element available for foundation modeling, nor is there a provision for stiffness degradation or strain hardening.

In this paper, the modification of the computer program, NEABS, to include discrete dampers and hysteretic springs for foundation modeling is described. The modified version of NEABS is then used to evaluate the effect of various foundation models and soil stiffnesses on the seismic response of a typical bridge bent founded on spread footings.

BACKGROUND

Soil-structure interaction refers to the effect that the founding soil has on the dynamic response of a structure and, conversely, the

J. W. McGuire, Dames and Moore, Inc., 2025 First Avenue, Suite 500, Seattle, Wash. 98121; W. F. Cofer, M. L. Marsh, and D. L. McLean, Department of Civil and Environmental Engineering, Washington State University, Pullman, Wash. 99164-2910.

effect the structure has on soil motion. The structural response often includes an amplification of the translational motion, the introduction of a rocking component for an embedded foundation, an increase in the flexibility of the system, and the addition of damping from hysteretic action of the soil (hysteretic damping) and radiation of energy away from the structure in the form of outward-propagating soil waves (radiation damping).

Two general approaches are available for rationally incorporating soil-structure interaction effects into structural analysis (*18*). In the "direct method," the structure and a portion of the founding soil are both incorporated into a finite element mesh. This is the simplest approach conceptually, but a number of drawbacks, including the need for a large model, energy-absorbing boundaries, and detailed soil properties, make its use prohibitive for all but the most extreme cases.

A simpler, more efficient approach is the substructure method. Here, the structure and the soil are analyzed separately. A simplified model is constructed that can approximate the behavior of the soil at the foundation. This simplified model is then coupled with the structure at the supports, and the structure is analyzed.

The foundation model typically is composed of one or more springs or spring/damper combinations arranged in series or kept parallel for each degree of freedom. The combinations are chosen on the basis of the assumed foundation behavior, which is obtained either experimentally or analytically.

The most common analytical model is one in which the soil domain is considered to be a homogeneous, elastic half-space. The frequency domain solution for the dynamic response of a rigid disk on an elastic half-space has been derived and extended for footings of various other shapes and depths of embedment. One should note that the disk/half-space solution is frequency dependent. For nonlinear dynamic analysis, which must be conducted in the time domain, various foundation models have been proposed that reproduce the analytical foundation response for certain ranges of loading frequencies. Four such models, consisting of combinations of linear springs, masses, and dampers, are shown in Figure 1. For a comprehensive review, one may refer to works by Wolf (*19*) and Richart et al. (*20*).

MODIFICATION OF NEABS

The computer program NEABS was chosen as the means to implement the methods that have been proposed to include the effects of soil-structure interaction in bridge analysis. The source coding for NEABS is in the public domain and it was obtained and modified. In order to apply the models mentioned above to represent the dynamic properties of bridge foundations, a new, discrete foundation element was added—a parallel combination of a spring and viscous damper.

Description of NEABS

NEABS originally was developed by Tseng and Penzien in 1973 to study the seismic performance of long, multiple-span bridges

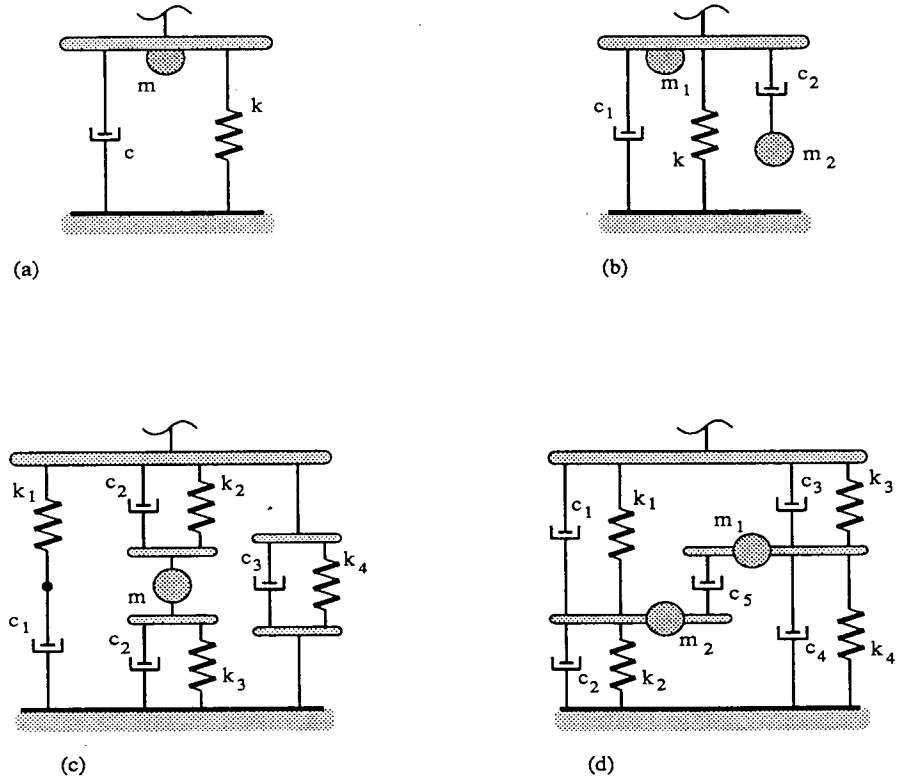

FIGURE 1 Discrete models of elastic half-space system: (*a*) 3 parameters, (*b*) 5 parameters, (*c*) 9 parameters, and (*d*) 11 parameters.

(*21*). Using the finite element method, NEABS idealizes a structure as a discrete system subject to nodal dynamic loadings or prescribed support motions.

Four element types are available to model the structural members of a bridge. Deck sections and columns are modeled with a beam element that may be either elastic or elasto-plastic. In the case of the elasto-plastic beam, the ends are allowed to develop perfectly plastic hinges. An elastic curved beam element is also available. Supports may be given elastic stiffnesses with a boundary spring element. A nonlinear expansion-joint element is included that can model the opening and closing of the joint gap, the impact at gap closure, and elasto-plastic joint tie bars.

Lumped masses and mass moments of inertia may be assigned to structure nodes directly or may be specified through mass densities for both the straight and curved beam elements. Energy dissipation not included as yielding in the elasto-plastic elements is accomplished globally by using two-parameter Rayleigh viscous damping. With Rayleigh damping, the global damping matrix is assumed to be a linear combination of the global mass and stiffness matrices. For an elastic structure, this has the effect of assigning a unique damping ratio to each of the structure's modes of vibration.

Both static and dynamic nodal loadings may be prescribed, as can support motion. Dynamic nodal loads and support motions are specified by supplying load and acceleration-time histories, respectively.

The equations of motion are solved in the time domain to allow nonlinear response, using the Newmark method of direct time integration. Either constant or linear acceleration between time steps may be assumed. At each time step, the out-of-balance force vector from the previous time step is added to the current applied equivalent force to minimize the accumulation of integration errors. In addition, the program will iterate and subdivide the time step used in the integration to ensure that the Euclidean norm of the out-of-balance force vector is within prescribed tolerances. Output consists of both the forces and displacements of the initial static response and time histories of the dynamic response. These time histories may consist of nodal displacements, nodal accelerations, member forces, and, for nonlinear elements, member-nonlinear (plastic) displacements.

Discrete Foundation Element

As previously discussed, the foundation models for soil-structure interaction may range in complexity from simple, linear spring supports to those employing a number of internal nodes, masses, dampers, and nonlinear springs. Accordingly, the Discrete Foundation (DF) element was formulated as a general purpose element to enhance the capabilities of NEABS. The element connects two nodes, which may actually occupy the same location, as in a simple foundation model.

The DF element is a parallel combination of a spring and viscous damper. Thus, to model the more complex systems shown in Figure 1, several DF elements and internal foundation nodes are required. For example, model (*d*) in Figure 1 would require five DF elements and two internal nodes. Note that the DF element used to model *c5* would include damping and zero stiffness.

The model built with DF elements connects the base of the structure element, for example, a column, and a fixed support. Separate properties are used for each of six local degrees of freedom, and there is no stiffness or damping coupling. Mass and mass moments of inertia may be lumped at each end node, including internal foundation nodes, and each degree of freedom, independently.

The DF element spring stiffness is bilinear to allow elasto-plastic behavior and hysteretic material damping. Kinematic strain hardening is incorporated as the default, but isotropic hardening or a combination of the two may be specified. A gap and stiffness degradation, as a function of deformation, may also be included.

The damping coefficients for each DF element may be specified separately for all degrees of freedom, allowing discrete dampers to be included in a foundation model. This damping is independent of the Rayleigh viscous damping in that the contribution of the DF element to the global mass and stiffness matrix is not considered when determining the Rayleigh contribution to the global damping matrix. Thus, the Rayleigh damping concept may be used for the bridge structure without affecting the concentrated dampers present in the foundation models. A complete description of the DF element may be found elsewhere (*22*).

PARAMETRIC STUDY

A parametric study was undertaken to investigate the effects of incorporating foundation models of varying complexity into bridge seismic analysis. The purpose was to compare various foundation models with each other and with a fixed support to evaluate their effect on the structural response of a bridge bent. One should note that, since the study results were not correlated with experimental response data, the study does not constitute a verification test of these models' accuracy. Rather, it is an exploration of the structural response effects of incorporating these models in seismic bridge analysis. The foundation models are consistent with elastic half-space assumptions, as previously discussed. Establishing consistency between these assumptions and actual behavior is beyond the scope of this paper.

Description of the Model

An existing highway bridge was chosen to provide guidance for the development of the structural analysis model. A solitary bridge bent was modeled so that only the effects of the spread footing foundation, and not that of abutments, would be included.

The bent consisted of two 7.6 m long, 91 cm diameter reinforced concrete columns on spread footings, supporting a cross beam, which supported the bridge superstructure. The 107-cm wide, 91-cm deep cross beam was cast monolithically with the diaphragm and deck and, because the resulting composite assembly was quite stiff in comparison with the columns, the cross beam was assumed to be rigid. The bent was assumed to support a dead load of approximately 1050 KN. The centerlines of the two columns were 7.3 m apart. Longitudinal reinforcing bars were spaced evenly around the cross-section perimeter, and they extended into the crossbeam with no splice. The spread footing dimensions were 2.9 m square in plan and 61 cm deep. A schematic of the model analyzed is shown in Figure 2. Specific details of the bent are given elsewhere (*22,23*).

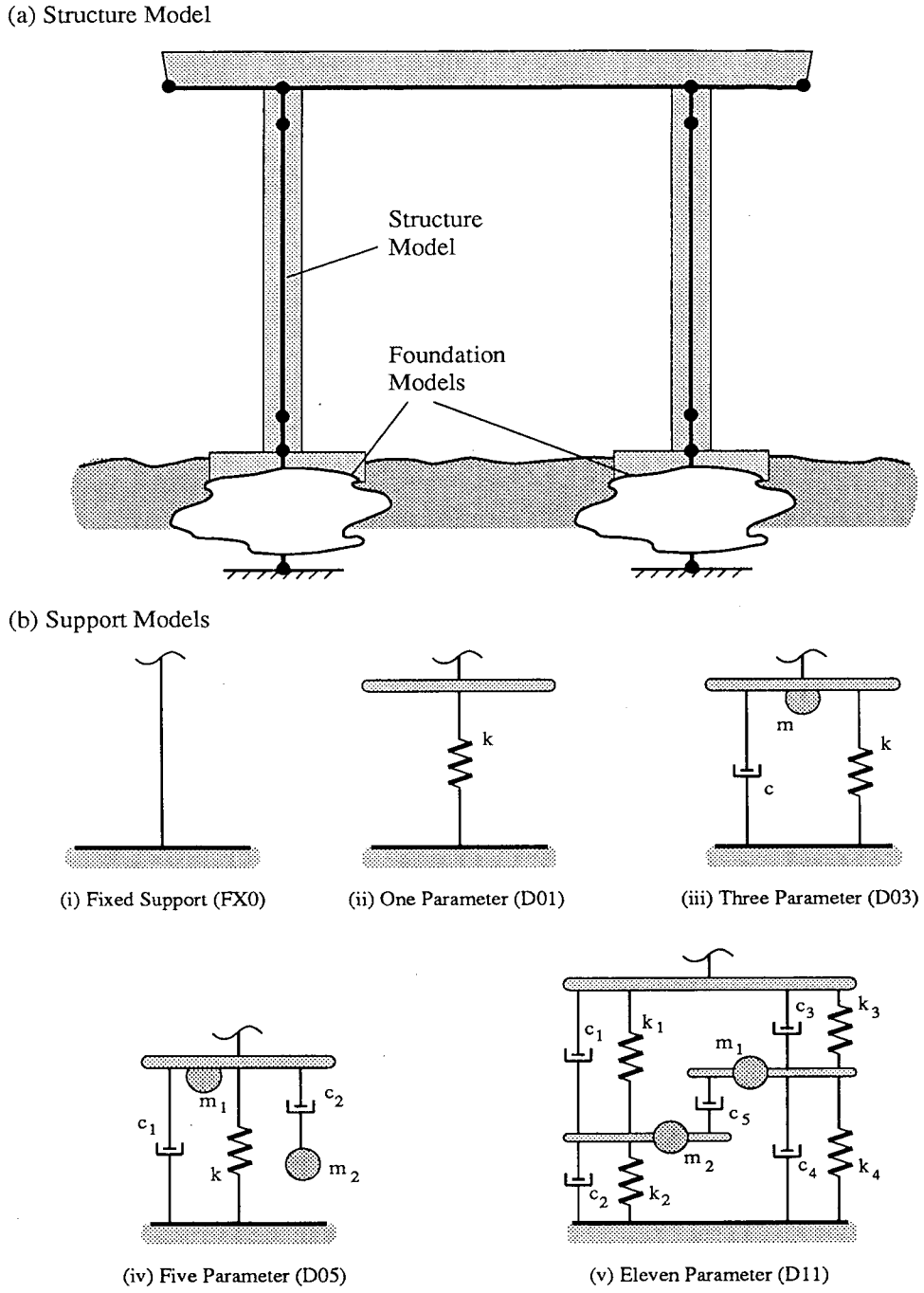

FIGURE 2 Schematic of NEABS models for the spread footing foundation study; (*a*) bent structure, and (*b*) foundation models.

The bent was modeled with nine beam elements and it was supported on the various foundation models, composed of DF elements. The foundation properties were assigned independently to the three planar degrees of freedom: horizontal translation, vertical translation, and rocking. All other degrees of freedom were constrained. The modulus of elasticity that was used for the columns was E = 31.7 GPa. The moment of inertia that was used was half that of the gross transformed column cross section, to account for the effect of initial concrete cracking. The yield surface for the elasto-plastic beam elements was based on the axial force-bending moment strength interaction curve. Rayleigh damping, corresponding to 5 percent of critical for the fundamental period of the fixed-base bent, was added to the structure.

Five foundation models were considered, as shown in Figure 2. One model consisted of fixed supports, one consisted of elastic supports, and three had damped elastic supports that required 3,

5, and 11 parameters per degree of freedom, respectively. All but the fixed support are discrete approximations of the elastic half-space continuum model, but with increasing levels of complexity. The footings were not assumed to be embedded. Because the half-space is elastic, the damping that is present in the foundation models corresponds to radiation damping only. Energy dissipation from material damping has not been quantified and, therefore, it is not included.

Three soil stiffness values were used in testing each model. The stiffnesses were selected to span a range of values commonly encountered. The unit weight of the soil was taken to be 10.8 kN/m^3. Three shear wave velocities, of 91.5, 213.5, and 396.5 m/sec, were chosen to produce the three soil stiffnesses. For the given soil density and the assumption of small strain, these corresponded to soil shear moduli, G, of 14.7, 80.3, and 277 MPa, respectively. Poisson's ratio for the soil was taken to be $\nu = 0.33$. The stiffness, mass, and damping values that were assigned to each foundation model are given in Table 1. Formulas for obtaining these values may be found elsewhere (*19,22,24,25*). The fundamental periods for the bent ranged from 0.53 sec for the fixed-base foundation to 0.68 sec for the most flexible foundation.

Recorded acceleration histories from actual earthquakes formed the basis of the seismic excitation applied to the bent-foundation system. The two earthquake records chosen were the S00E component of the El Centro record of the 1940 Imperial Valley Earthquake (referred to as the "El Centro" record) and the N86E component of the Olympia record of the 1949 Western Washington earthquake (or "Olympia" record). Acceleration history plots are given in Figure 3.

To incorporate variations in record intensity in the study, both records were scaled to an intensity of 0.25 g effective peak acceleration ("lower" intensity) and to an intensity of 0.40 g effective peak acceleration ("higher" intensity). The definition of effective peak acceleration is outlined in the recommendations of the National Earthquake Hazards Reduction Program (*26*).

Results

The performance of the various foundation models was assessed in terms of their effects on the response of the bent structure. Specifically, three aspects of the bent's response were selected to be studied: column displacement, that is, the displacement of the column top relative to the bottom, the moment at the top of the column, and the plastic-hinge rotation at the column top. This information was provided by the program in the form of time histories. The results were then interpreted in terms of their implications for column ductility demand and energy dissipation demands. One should note that the column moment values reported by NEABS include a dynamic component from damping in addition to the usual moment that results from stiffness.

A number of analyses were performed, consisting of five foundation models, three soil stiffness values, and four seismic input records. Four graphs of the data from each NEABS analysis were used, examples of which are shown in Figures 4 and 5. In Figure 4, the time histories of the column displacement and column moment for the higher intensity El Centro earthquake record, soft

TABLE 1 Parameter Values for Spread Footing Foundation Models

		Soft Soil				Intermediate Soil				Stiff Soil			
		D01	D03	D05	D11	D01	D03	D05	D11	D01	D03	D05	D11
Lateral Translation	k1	1.52E+05	1.52E+05	1.52E+05	1.04E+05	8.26E+05	8.26E+05	8.26E+05	5.64E+05	2.85E+06	2.85E+06	2.85E+06	1.94E+06
	k2				2.98E+05				1.62E+06				5.59E+06
	k3				1.00E+05				5.45E+05				1.88E+06
	k4				3.15E+05				1.71E+06				5.91E+06
	c1		2.06E+03	1.80E+03	2.30E+03		4.81E+03	4.20E+03	5.36E+03		8.94E+03	7.81E+03	9.95E+03
	c2			0.00E+00	6.31E+03			0.00E+00	1.47E+04			0.00E+00	2.73E+04
	c3				3.47E+02				8.10E+02				1.50E+03
	c4				4.33E+03				1.01E+04				1.88E+04
	c5				5.32E+03				1.24E+04				2.31E+04
	m1		7.92E+00	0.00E+00	9.23E+00		7.92E+00	0.00E+00	9.23E+00		7.92E+00	0.00E+00	9.23E+00
	m2			0.00E+00	5.21E+01			0.00E+00	5.21E+01			0.00E+00	5.21E+01
Vertical Translation	k1	1.72E+05	1.72E+05	1.72E+05	1.91E+05	9.37E+05	9.37E+05	9.37E+05	1.04E+06	3.23E+06	3.23E+06	3.23E+06	3.59E+06
	k2				2.44E+05				1.33E+06				4.58E+06
	k3				7.88E+04				4.29E+05				1.48E+06
	k4				3.11E+05				1.70E+06				5.85E+06
	c1		3.11E+03	2.45E+03	2.39E+03		7.27E+03	5.72E+03	5.58E+03		1.35E+04	1.06E+04	1.04E+04
	c2			8.23E+02	5.50E+03			1.91E+03	1.28E+04			3.54E+03	2.39E+04
	c3				1.28E+03				2.98E+03				5.54E+03
	c4				4.29E+03				1.00E+04				1.86E+04
	c5				4.90E+03				1.14E+04				2.12E+04
	m1		2.11E+01	0.00E+00	6.88E+01		2.11E+01	0.00E+00	6.88E+01		2.11E+01	0.00E+00	6.88E+01
	m2			6.04E+00	4.44E+01			6.04E+00	4.44E+01			6.04E+00	4.44E+01
Rocking	k1	3.39E+05	3.39E+05	3.39E+05	1.48E+05	1.85E+06	1.85E+06	1.85E+06	8.04E+05	9.87E+09	9.87E+09	9.87E+09	4.30E+09
	k2				5.73E+05				3.12E+06				1.67E+10
	k3				5.14E+05				2.80E+06				1.50E+10
	k4				3.68E+05				2.01E+06				1.07E+10
	c1		1.87E+03	0.00E+00	-1.90E+03		4.36E+03	0.00E+00	-4.43E+03		8.10E+03	0.00E+00	-8.22E+03
	c2			2.42E+03	7.28E+03			5.64E+03	1.70E+07			1.05E+04	3.15E+07
	c3				4.52E+03				1.05E+04				1.96E+04
	c4				3.57E+02				8.34E+02				1.55E+03
	c5				3.82E+03				8.91E+03				1.65E+04
	m1		3.13E+01	0.00E+00	1.39E+02		3.13E+01	0.00E+00	1.39E+02		3.13E+01	0.00E+00	1.39E+02
	m2			2.89E+01	4.43E+01			2.89E+01	4.43E+01			2.89E+01	4.43E+01

Note: unit of force = kN, unit of length = m, unit of rotation = radian, unit of time = sec.

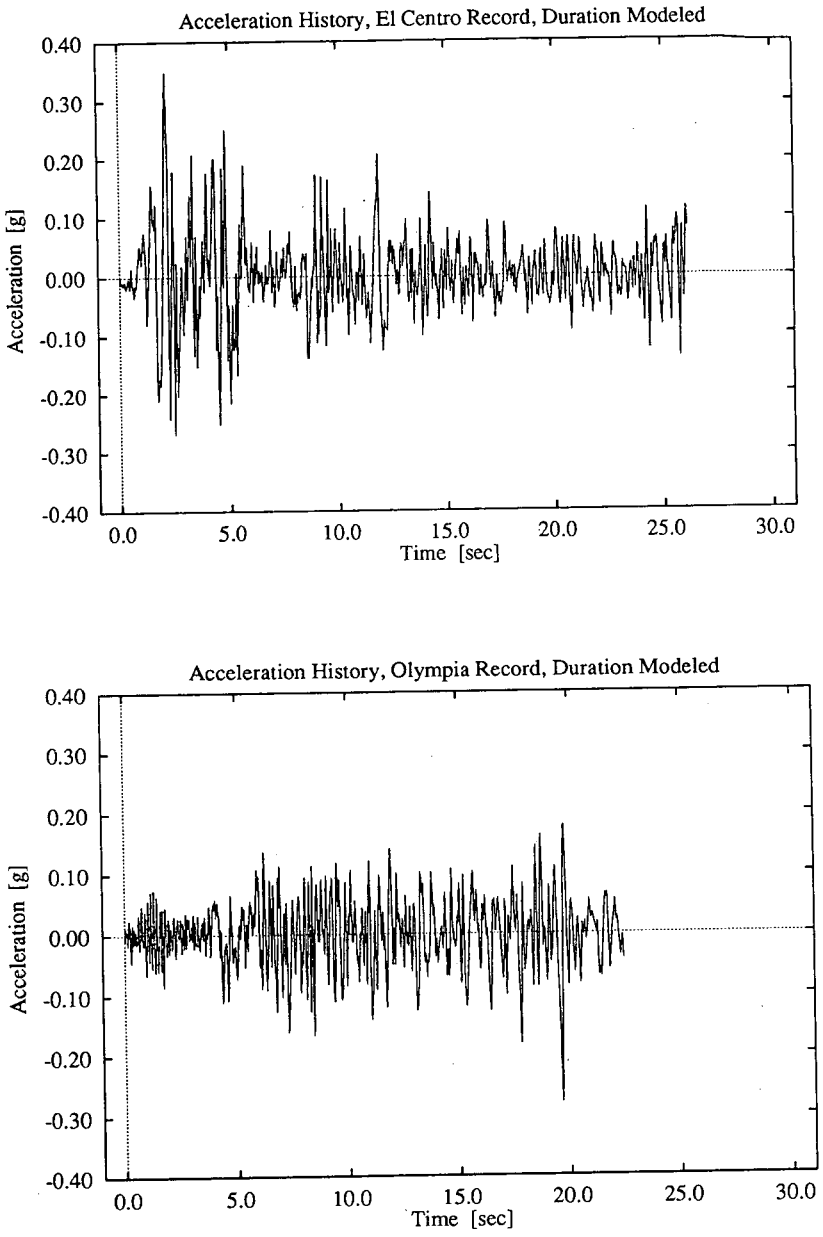

FIGURE 3 Earthquake acceleration history plots.

soil, and 11-parameter foundation model are given. The third graph, shown in Figure 5 for the same analysis, depicts the column moment-displacement hysteresis, which may be used as an indicator of energy dissipation demand. The fourth graph, also shown in Figure 5, is a time history of the plastic-hinge rotation at the top of the column.

Whereas the column remains elastic, the moment in the column does not produce plastic rotation; this condition results in a horizontal line in this graph. A vertical line indicates that a plastic hinge has formed at the column top, and it is being rotated by the moment. The magnitude of these plastic rotations is indicative of instantaneous ductility demand at the top of the column. Also, if the axial force on the columns is assumed to be constant, or nearly so, over the duration of the excitation, then the moment required to yield this column will also be constant. If this is the case, then work done on the plastic hinge over the excitation duration will be the yield moment multiplied by the sum of the absolute values of plastic rotation, represented by the vertical lengths on the graph. As the assumption of nearly constant axial force is reasonable, this graph can also provide an indication of the cumulative energy dissipation demand of the top of the column.

To summarize and compare these results, the maximum plastic rotation (measured from the undeformed state) and the sum of all

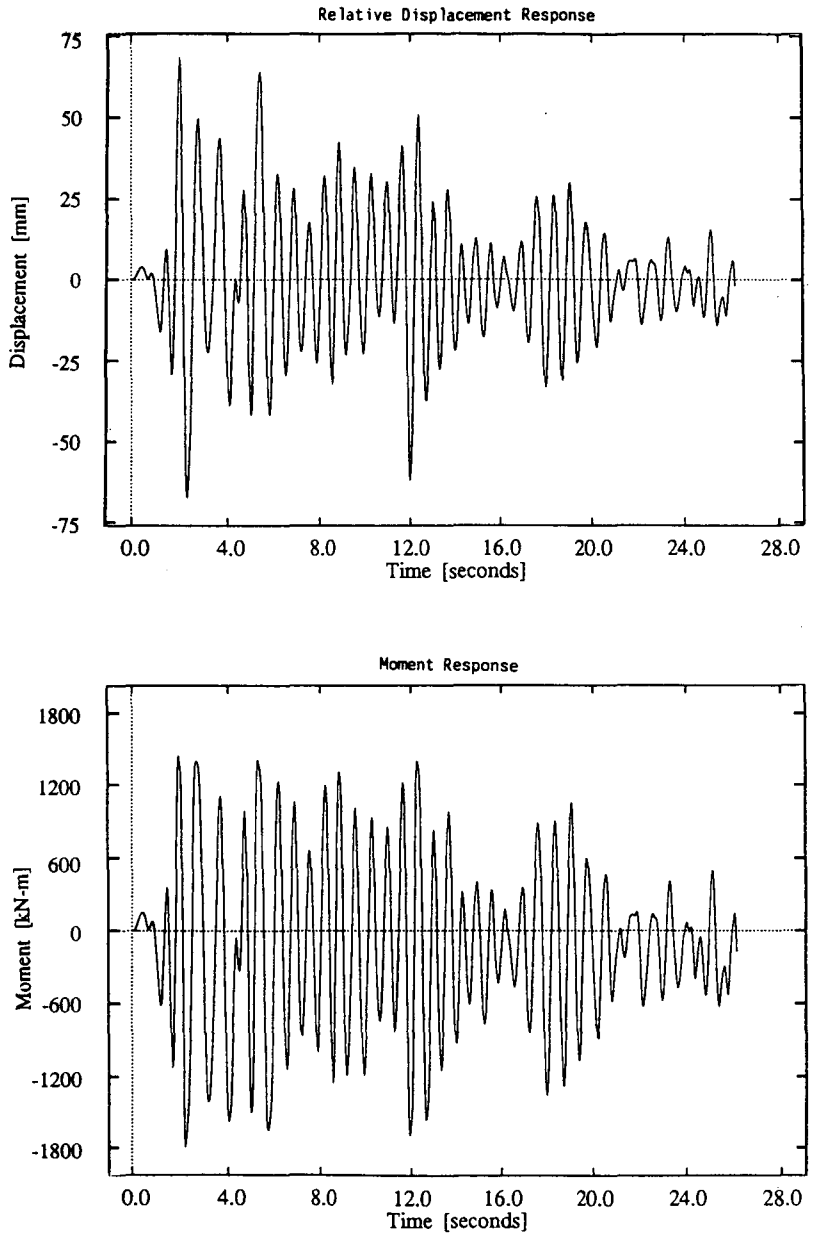

FIGURE 4 Typical time history results.

plastic rotation was calculated for each run. As mentioned, these quantities are related to ductility and energy dissipation demands. These data are given in Figures 6 through 9. Each figure shows a set of bar charts of both the rotation maxima and rotation sums for the given excitation record. Each bar chart shows the results of the four discrete foundation models for each soil stiffness, and allows a comparison with the fixed-support results. In Figure 2, a schematic of each foundation model is shown.

Discussion of Findings

The response of the bridge bent to the two earthquake records is somewhat different, although the intensity of each earthquake resulted in plastic-hinge formation for almost all analyses. For both El Centro records, the stiff and intermediate foundation models led to nearly the same instantaneous and cumulative demands as those of the fixed-base model. The soft foundation model resulted in a significant increase in cumulative demand for both intensities, and it led to increased instantaneous demand for the lower intensity record. The instantaneous demand for the higher intensity El Centro record was approximately the same for all of the foundation models.

The flexible foundation caused an increase rather than a reduction in column demand. By comparing the earthquake record of Figure 3 with the example plastic-hinge rotation history of Figure 5, one may observe that much of the damage results from peak

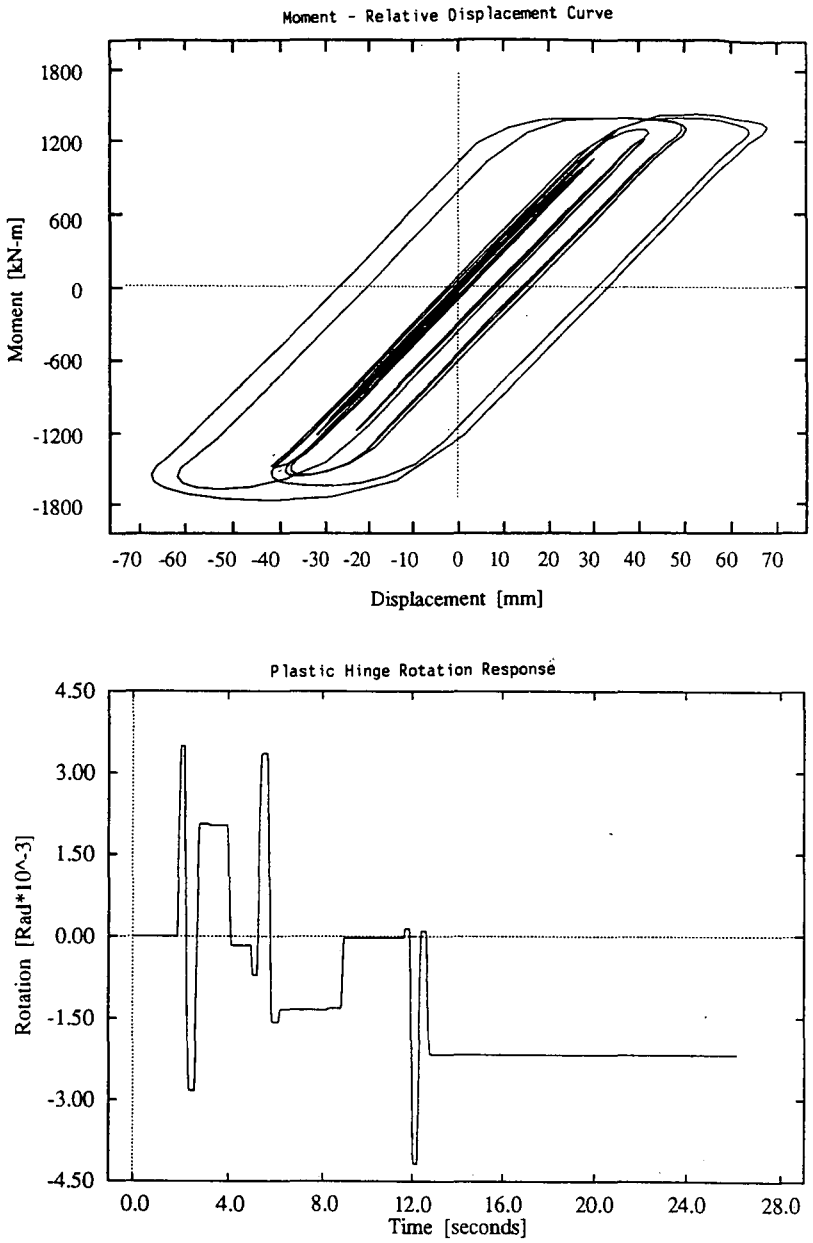

FIGURE 5 Typical hysteresis and plastic hinge rotation results.

accelerations at approximately 2 sec, 5 sec, and 12 sec. The pulse at 12 sec seems to be the major source of the increase in demand over the other foundations because its period of application is close to the fundamental period of the structure with the flexible foundation.

Damping in the discrete foundation model had a negligible effect on the column demands for the intermediate and stiff foundations. However, the damped foundations (the 3-, 5-, and 11-parameter models) caused a reduction in demand in the order of 15 to 20 percent, when compared to the spring foundation alone, for the soft soil. Also, little change was observed between the simple and more complex damped models. This is likely due to the fact that the damping and mass values for the three-parameter model are relatively insensitive to the loading frequency for translational motion, which seemed to dominate the response.

For the Olympia earthquake records, the instantaneous demands on the column were of the same order as those of the El Centro records for the intermediate and stiff foundation models, but much less for the soft foundation model. Indeed, no column yielding was indicated for the lower intensity Olympia record and the soft foundation. This appears to be the result of the frequency content of the earthquake versus the natural frequencies of the structure-foundation system.

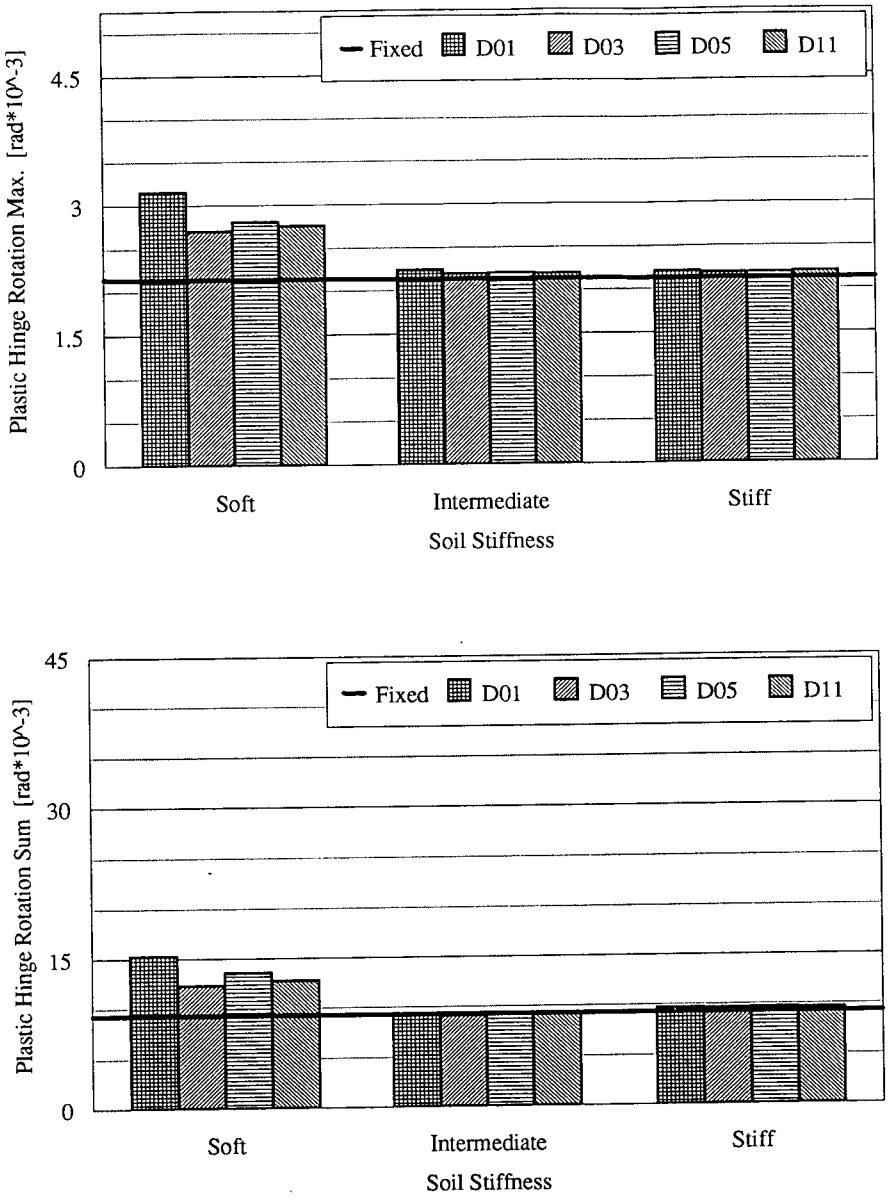

FIGURE 6 Comparison of instantaneous and cumulative column demands, lower intensity El Centro earthquake record, spread footing foundation.

The cumulative demand, however, was significantly less for all foundations when compared to that of the El Centro earthquake. The two earthquake records were scaled to the same effective peak accelerations, but, from Figure 3, it is apparent that the Olympia record is dominated by a single peak at approximately 20 sec. Because the majority of the column damage is caused by this peak, as opposed to several different peaks in the El Centro record, the total amount of plastic-hinge rotation is reduced.

As with the El Centro earthquake, radiation damping was significant only for the column cumulative demand and the soft foundation. The reduction in demand from damping ranged from approximately 25 to 35 percent.

CONCLUSIONS

A new and versatile foundation element has been developed and implemented into the nonlinear, dynamic, bridge analysis program, NEABS. Because of its ability to include concentrated dampers and bilinear springs with strain hardening, stiffness degradation, and a gap algorithm, the new element can be used to model the behavior of various types of bridge supports, including footings, elastomeric bearing pads, base isolation devices, piles, and abutments. Here, a parametric study was performed to investigate the effect of different foundation models and soil types on

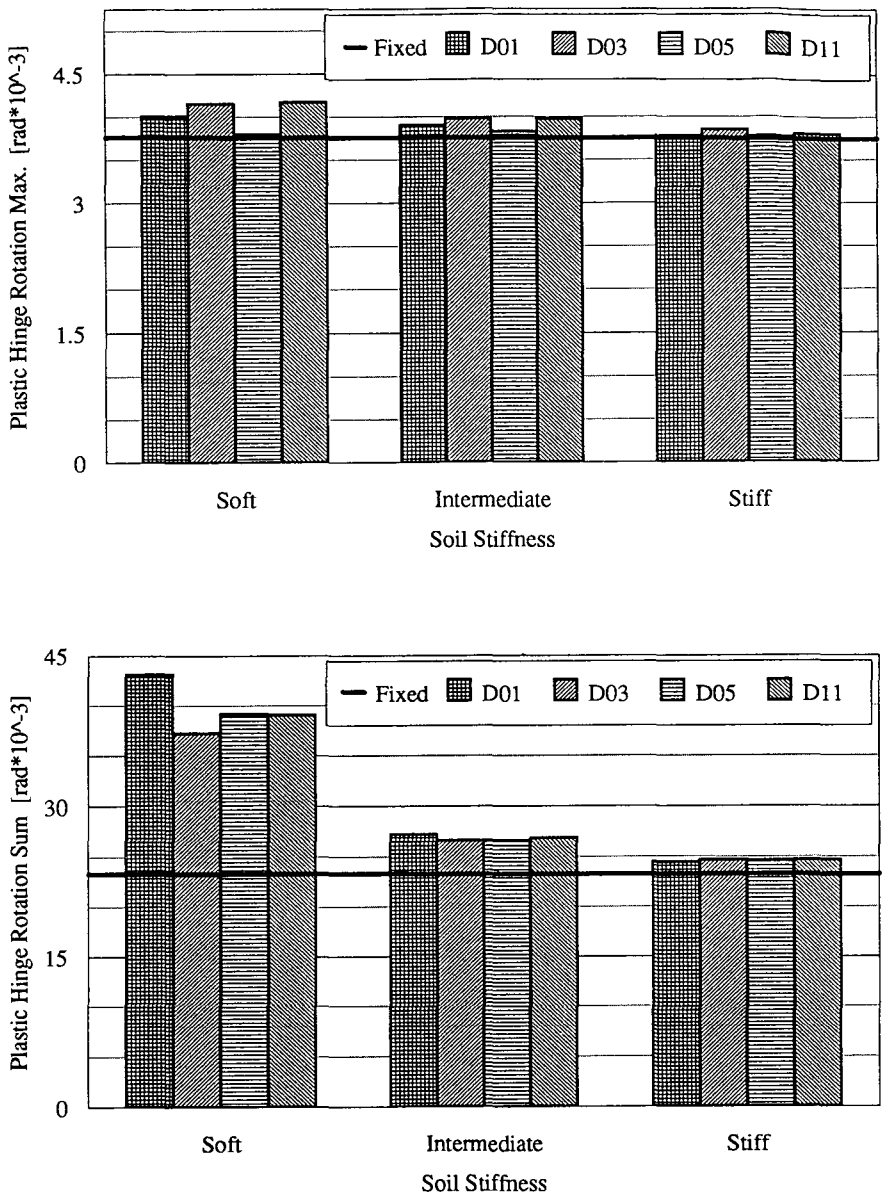

FIGURE 7 Comparison of instantaneous and cumulative column demands, higher intensity El Centro earthquake record, spread footing foundation.

the response to earthquake excitation of a bridge bent on spread footings. From the results, several conclusions may be drawn.

The enhancement of a fixed-base model to include foundation flexibility has a dramatic influence on the column demands during strong earthquakes. This seems to be a result of variations in the natural frequencies of the system, and the actual effect depends on the frequency content of the earthquake. For the El Centro records, increased column demands were noted for the flexible foundation, whereas, for the Olympia records, the intermediate foundation was critical. Thus, no conclusion can be drawn regarding whether one foundation is more critical than another. However, the results indicate that a fixed-base model could easily underpredict column demands for an earthquake analysis. One should note that, in order to evaluate the effect of foundation properties on bridge response in a consistent manner, no attempt was made to alter the earthquake records on the basis of an assumed soil layer. To include such effects, a separate analysis to obtain free field motion at the site must be performed.

The addition of concentrated dampers to model radiation damping had a significant effect only when the foundation was soft. As expected, the energy absorption of the dampers acted to reduce cumulative demand on the columns. Neglecting the radiation damping would probably have little effect on the response of similar structures when founded on soil of high or intermediate stiff-

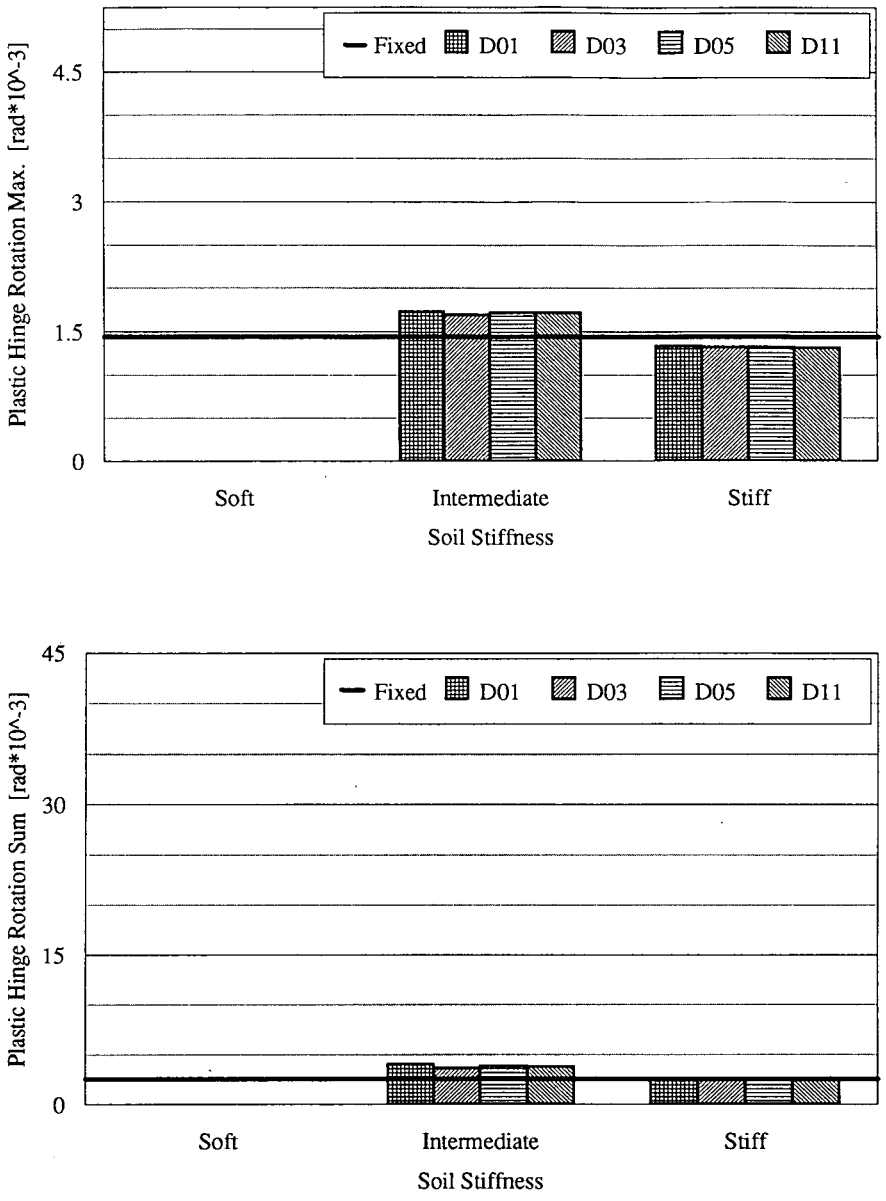

FIGURE 8 Comparison of instantaneous and cumulative column demands, lower intensity Olympia earthquake record, spread footing foundation.

ness. For soil of low stiffness, however, the use of elastic foundations alone could lead to a somewhat conservative prediction of inelastic demand. If damping is added, the simpler, three-parameter model produced results that were in close agreement with those of the more complex models.

The foundation models were based upon the assumptions of elastic half-space theory. Refinements to the theory, including solutions for a layered half-space and a viscoelastic half-space, have been proposed. Hysteretic action around the supports and gap behavior could be modeled by employing a nonlinear near-field element in series with a far-field element based on half-space theory, such as those we have described. Near-field properties must be defined for specific foundation types, however, such as piles and abutments. These are items for further research.

ACKNOWLEDGMENT

The research presented in this paper was funded by the Washington State Transportation Center. The authors acknowledge the valuable assistance of Mark R. Wallace, Richard B. Stoddard, and Edward H. Henley, Jr., of the Washington State Department of Transportation.

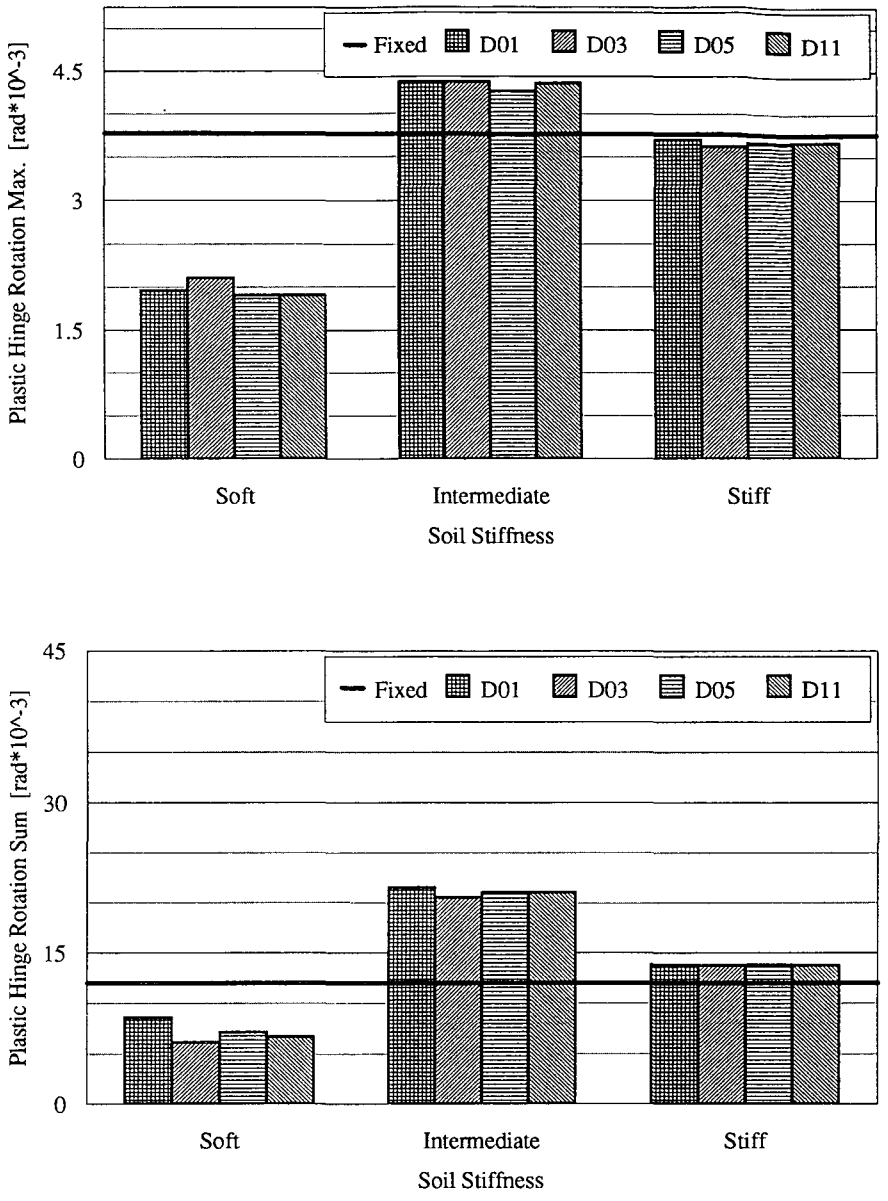

FIGURE 9 Comparison of instantaneous and cumulative column demands, higher intensity Olympia earthquake record, spread footing foundation.

REFERENCES

1. Werner, S. D., J. L. Beck, and M. B. Levine. Seismic Response Evaluation of Meloland Road Overpass Using 1979 Imperial Valley Earthquake Records. *Earthquake Engineering and Structural Dynamics*, Vol. 15, 1987, pp. 249–274.
2. Liu, W. D., F. S. Nobari, and R. A. Imbsen. Dynamic Response Prediction for Earthquake Resistance Design of Bridge Structures. *Proc., ASCE Structures Congress, Seismic Engineering: Research and Practice*, 1989, pp. 1–10.
3. Wilson, J. C., and B. S. Tan. Bridge Abutments: Formulation of a Simple Model for Earthquake Response Analysis. *Journal of Engineering Mechanics*, ASCE, Vol. 116, No. 8, 1990, pp. 1828–1837.
4. Buckle, I. G., R. L. Mayes, and M. R. Button. *Seismic Design and Retrofit Manual for Highway Bridges*. FHWA, 1987.
5. Lam, I., and G. R. Martin. Seismic Design for Highway Bridge Foundations. *Proc., Lifeline Earthquake Engineering: Performance Design and Construction*, ASCE, 1984, pp. 7–21.
6. Penzien, J. Soil-Pile Foundation Interaction. *Earthquake Engineering* (R. L. Wiegel, ed.), Prentice-Hall, Inc., Englewood Cliffs, N.J. 1970, pp. 349–381.
7. Crouse, C. B., B. Hushmand, and G. B. Martin. Dynamic Soil-Structure Interaction of a Single Span Bridge. *Earthquake Engineering and Structural Dynamics*, Vol. 15, 1987, pp. 711–729.
8. Spyrakos, C. C. Assessment of SSI on the Longitudinal Seismic Response of Short Span Bridges. *Engineering Structures*, Vol. 12, No. 1, 1990, pp. 60–66.

9. Mander, J. B. ERBS—Earthquake Resistant Bridge Systems, a Coordinated Research Initiative. *Proc., Second Workshop on Bridge Engineering Research in Progress*, Reno, Nev., 1990, pp. 197–200.
10. Wilson, J. C. Stiffness of Non-Skew Monolithic Bridge Abutments for Seismic Analysis. *Earthquake Engineering and Structural Dynamics*, Vol. 16, 1988, pp. 867–883.
11. Maragakis, E., B. Douglas, and S. Vrontinos. Analysis of the Effects of the Impact Energy Losses Occurring Between the Bridge Deck and Abutments. *Proc., Second Workshop on Bridge Engineering Research in Progress*, Reno, Nev., 1990, pp. 201–204.
12. Barenberg, M. E. and D. A. Foutch. Evaluation of Seismic Design Procedures for Highway Bridges. *Journal of Structural Engineering*, ASCE, Vol. 114, No. 7, 1988, pp. 1588–1605.
13. Norris, G. Lateral and Rotational Stiffness of Pile Foundations. *Proc., Ninth Structures Congress*, ASCE, Indianapolis, Ind., 1991, pp. 749–752.
14. Ghobarah, A. and H. M. Ali. Seismic Performance of Highway Bridges. *Engineering Structures*, Vol. 10, No. 3, 1988, pp. 157–166.
15. Ghobarah, A. Seismic Behavior of Highway Bridges with Base Isolation. *Canadian Journal of Civil Engineering*, Vol. 15, No. 1, 1988, pp. 72–78.
16. Buckle, I. G. and R. L. Mayes. The Application of Seismic Isolation to Bridges. *Proc., ASCE Structures Congress, Seismic Engineering: Research and Practice*, 1989, pp. 633–642.
17. Penzien, J., R. Imbsen, and W. D. Liu. Nonlinear Earthquake Analysis of Bridge Systems. National Information Service for Earthquake Engineering, Earthquake Engineering Research Center, University of California, Berkeley, 1981.
18. Wolf, J. P. *Dynamic Soil-Structure Interaction*. Prentice-Hall, Inc., Englewood Cliffs, N.J., 1985.
19. Wolf, J. P. *Soil-Structure Interaction Analysis in Time Domain*. Prentice-Hall, Inc., Englewood Cliffs, N.J., 1988.
20. Richart, F. E. Jr.; J. R. Hall, Jr.; and R. D. Woods. *Vibrations of Soils and Foundations*. Prentice-Hall Inc., Englewood Cliffs, N.J., 1970.
21. Tseng, W. S. and J. Penzien. Analytical Investigations of the Seismic Response of Long Multiple-Span Highway Bridges. Report No. EERC 73-12. College of Engineering, University of California at Berkeley, Earthquake Engineering Research Center, June 1973.
22. McGuire, J. W., W. F. Cofer, and D. I. McLean. *Analytical Modeling of Foundations for Seismic Analysis of Bridges*. Washington State Department of Transportation, Seattle, Oct. 1993.
23. Eberhard, M. O., M. L. Marsh, T. O'Donovan, and G. Hjartarson. Lateral-Load Tests of Reinforced Concrete Bridge. In *Transportation Research Record 1371*, TRB, National Research Council, Washington, D.C., 1992, pp. 92–100.
24. Veletsos, A. S. and B. Verbic. Vibration of Viscoelastic Foundations. *Earthquake Engineering and Structural Dynamics*, Vol. 2, 1973, pp. 87–102.
25. Jean, W. Y., T. W. Lin, and J. Penzien. System Parameters of Soil Foundation for Time Domain Dynamic Analysis. *Earthquake Engineering and Structural Dynamics*, Vol. 19, 1990, pp. 541–553.
26. National Earthquake Hazards Reduction Program. *Recommended Provisions for the Development of Seismic Regulations for New Buildings*. Earthquake Hazards Reduction Series No. 65, Federal Emergency Management Agency, Washington, D.C., 1991.

Buckling of Friction Piles Supporting Bridge Foundations

MOHAMMED A. GABR AND JIBAI WANG

In practice, evidence suggests that long, slender piles subjected to axial loads can fail under axial stresses below the yield point of the pile material. However, using the minimum potential-energy method, it is possible to quantify a general solution for the critical buckling capacity of long, slender friction piles in clay. The Rayleigh-Ritz method is used to select deflection functions satisfying nine geometric boundary conditions. The equivalent buckling length and the critical axial load of the piles are determined from eigenvalues estimated by the Jacobi Rotation Transformation method. Parameter studies performed to investigate the buckling response of fully and partially embedded piles indicated that the boundary conditions of pile tip have no effect on the critical buckling loads when nondimensional embedment length, h', exceeds a critical value. The critical value depends on the pile-top condition and embedment ratio (defined as embedded length divided by total pile length). Side friction's contribution to buckling stability results in less than a 7-percent variation in critical buckling length. The model's applicability is illustrated using a design example and load-test data reported in the literature.

Pile foundations are used widely, particularly as a foundation type for bridge and harbor structures. Long, slender piles can fail by buckling under axial stresses below the yield point of the pile material (*1*,*2*). Evidence of this has been described for long piles that extend above the ground surface. Experimental data have shown that buckling failure of piles has occurred suddenly, without observable warning (*3*).

There are ways to analyze the buckling of axially loaded piles. Early approaches used Euler stability theory, which verified the analysis using a limited number of buckling tests (*1*,*3*).

A second approach applied a governing differential equation for buckling deflection under axial load to estimate critical loads, assuming constant and linearly increasing subgrade moduli (*4*). In this case, partially embedded piles were treated as freestanding columns with fixed bases, and analyses using this approach were limited to a nondimensional embedded length greater than 4.

A third approach applied the minimum potential energy method to calculate the critical buckling capacities of piles (*5*).

This paper presents a general solution for estimating the equivalent buckling length and critical buckling capacity of long, slender piles in clay using the minimum potential energy method. The Rayleigh-Ritz method is adopted to select deflection functions satisfying the geometric boundary conditions. Subgrade-reaction theory is used to model lateral soil support. Uniform variation of the skin friction as a function of depth is assumed in the analysis. The equivalent buckling lengths and the critical axial loads of the piles are determined from the analysis model. Compared with other methods for determining the buckling capacity, the model presented in this paper encompasses the wide variety of boundary conditions encountered in practice.

Department of Civil and Environmental Engineering, West Virginia University, Morgantown, W. Va. 26506-6101.

A parameter study is performed to investigate the buckling response of fully and partially embedded piles with different embedment ratios (defined as embedded length divided by total pile length) and boundary conditions representative of actual situations. Nine combinations of pile-top and tip-boundary conditions are considered, and comparative results using several combinations of pile-top and pile-tip-boundary conditions presented. Procedures are demonstrated using an example presented by Davisson and Robinson (*4*) and a recommended general analysis procedure. In addition, applicability of the developed model is illustrated through the use of pile load-test data by Klohn and Hughes (*6*).

PILE MODELS AND DEFLECTION FUNCTIONS

Nine boundary-condition cases are selected for modeling the pile buckling analysis, as shown in Figure 1. The cases include modeling the pile's top as fixed with sway, free, and pinned and the pile's tip as fixed, free, and pinned; the cases represent the variety of pile-structure connections now in use. For example, in many bridge structures, the piles continue as a part of the column to support bridge girders. In this case, the pile top may be considered fixed with the entire girder free to translate. Modeling of this condition is achieved by assuming fixity with sway.

Deflection functions for the nine boundary conditions are chosen using Rayleigh-Ritz method, as shown in Table 1. These deflection functions satisfy the geometric boundary condition of the analysis model. There are no limitations on the pile's embeddment ratio.

THEORETICAL BACKGROUND

Assuming elastic conditions, the equilibrium requirement is satisfied if variation in the total potential energy of a given system is zero under small, arbitrary deformation. Assuming elastic conditions for buckling under axial load and a small magnitude of buckling deformation, the change in the total potential energy to satisfy the condition of equilibrium is represented by

$$\delta(U + V) = 0 \tag{1}$$

where U is summation of strain energy of the system due to bending of the pile and elastic deformation of soil and V is potential energy of external loads.

The quantity $\delta\ (U + V)$ represents the incremental change in total potential energy caused by the variation in the displacement.

Using the Rayleigh-Ritz method, a suitable shape for the deformation of the system can be assumed to reduce it from an

infinite-degree-of-freedom system to a finite-degree-of-freedom system. Hence, the governing differential equation (Equation 1) could be obtained.

BUCKLING ANALYSIS OF PILES

Choosing the undeflected state as a convenient datum position, U and V are expressed as

$$U + V = \frac{EI}{2}\int_0^L (y'')^2 dx + \frac{1}{2}\int_0^h q(x)\, y dx - \frac{1}{2}\int_0^L P(x)\,(y')^2 dx \quad (2)$$

where

EI = flexural stiffness of the pile;
L = total pile length;
h = embedded length of pile;
$q(x)$ = soil reaction;
$P(x)$ = axial force of pile, and
y = lateral deflection of pile;
$y' = dy/dx$; and
$y'' = d^2y/dx^2$; the coordinate system is described in Figure 1(a).

The first part of the right-hand side of Equation 2 is the strain energy due to bending of the pile, the second part represents the strain energy from elastic deformation of soil. The third part is the potential energy due to external loads.

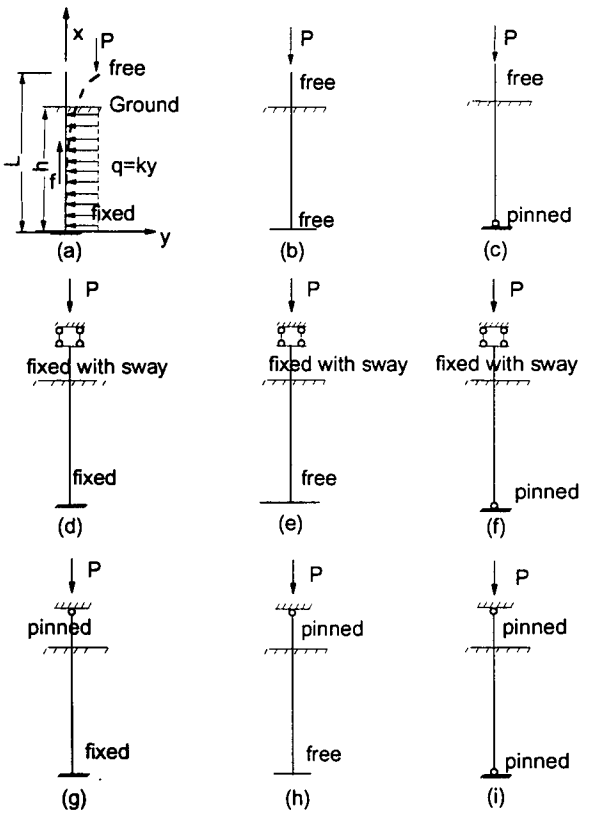

FIGURE 1 Variable boundary condition used in buckling models.

Based on subgrade-reaction theory (*7*), the soil reaction $q(x)$ is expressed as

$$q(x) = ky \quad (3)$$

where k is modulus of subgrade reaction and is assumed to increase linearly with depth. In terms of depth, k is written as

$$k = \eta_h(h - x) \quad (4)$$

where

η_h = constant of horizontal subgrade reaction,
h = embedded pile length, and
x = the distance from the pile tip.

Substituting Equation 4 into Equation 3, the lateral soil reaction is written as

$$q(x) = \eta_h\,(h - x)y \quad (5)$$

Assuming uniform variation of the skin friction as a function of depth, the axial load in the pile is expressed as

$$P(x) = P - uf(h - x) \quad (x \le h)$$
$$P(x) = P \quad (x > h) \quad (6)$$

where

P = axial load,
u = perimeter of pile shaft, and
f = side friction per unit area.

Substituting Equations 5 and 6 into Equation 2, the general equation is established:

$$U + V = \frac{EI}{2}\int_0^L (Y'')^2 dx + \frac{\eta_h}{2}\int_0^h (h - x)y^2 dx - \frac{P}{2}\int_0^L (y')^2 dx + \frac{uf}{2}\int_0^h (h - x)\,(y')^2 dx \quad (7)$$

According to the energy principle, $\delta\,(U + V) = 0$, or

$$\frac{\partial(U + V)}{\partial C_i}\,\delta\,(C_i) = 0 \quad (8)$$

Since the variational displacement δC_i is arbitrary:
where C_i = constants of deflection function,

$$\frac{\partial(U + V)}{\partial C_i} = 0 \quad (9)$$

Substituting Equation 7 in Equation 9, the following equation is obtained:

$$\int_0^L y''\frac{\partial y''}{\partial C_i}dx + \alpha^5\int_0^h (h - x)\,y\frac{\partial y}{\partial C_i}dx - \frac{P}{EI}\int_0^L y'\frac{\partial y'}{\partial C_i}dx + \frac{uf}{EI}\int_0^h (h - x)\frac{\partial y'}{\partial C_i}dx = 0 \quad (10)$$

where

i = 0, 1, 2, ..., n;
n = half-wave number of deflection function; and
α = coefficient of pile-soil compliancy or relative stiffness.

The unit of α is $[\text{LENGTH}]^{-1}$, and α is defined as

$$\alpha = \sqrt[5]{\frac{\eta_h}{EI}} \tag{11}$$

By substituting the deflection functions in Table 1 into Equation 10 and performing the integration, a set of homogeneous linear equations in terms of C can be obtained. This system of homogeneous linear equations possesses nonzero solutions only if the determinant of the linear equations equals zero. For boundary conditions (*a*), (*c*), (*d*), (*f*), (*h*), and (*i*), as shown in Figure 1, the determinant is expressed as follows:

$$\Delta = \begin{vmatrix} b_{s,s}-P' & b_{s,s+1} & b_{s,s+2} & \cdots\cdots & b_{s,n} \\ b_{s+1,s} & b_{s+1,s+1}-P' & b_{s+1,s+2} & \cdots\cdots & b_{s+1,n} \\ \cdots\cdots & \cdots\cdots & \cdots\cdots & \cdots\cdots & \cdots\cdots \\ b_{n,s} & b_{n,s+1} & b_{n,s+2} & \cdots\cdots & b_{n,n}-P' \end{vmatrix} = 0 \tag{12}$$

For boundary condition (*b*) and (*e*), the determinant is

$$\Delta = \begin{vmatrix} \frac{\pi^6 h^2}{2\alpha^5 L^7} & a_s & a_{s+1} & a_{s+2} & \cdots\cdots & a_n \\ a_s & b_{s,s}-P' & b_{s,s+1} & b_{s,s+2} & \cdots\cdots & b_{s,n} \\ a_{s+1} & b_{s+1,s} & b_{s+1,s+1}-P' & b_{s+1,s+2} & \cdots\cdots & b_{s+1,n} \\ \cdots\cdots & \cdots\cdots & \cdots\cdots & \cdots\cdots & \cdots\cdots & \cdots\cdots \\ a_n & b_{n,s} & b_{n,s+1} & b_{n,s+2} & \cdots\cdots & b_{n,n}-P' \end{vmatrix} = 0 \tag{13}$$

TABLE 1 Deflection Functions and Boundary Conditions

Model No.	Boundary conditions		Deflection functions
	Top	Tip	
a	free	fixed	$y=\sum_{n=1}^{\infty} c_n(1-\cos\frac{2n-1}{2L}\pi x)$
b	free	free	$y=c+\frac{x}{L}c_0+\sum_{n=1}^{\infty} c_n\sin\frac{n\pi}{L}x$
c	free	pinned	$y=\frac{c_0}{L}x+\sum_{n=1}^{\infty} c_n\sin\frac{n\pi}{L}x$
d	fixed-sway	fixed	$y=\sum_{n=1}^{\infty} c_n(1-\cos\frac{n\pi}{L}x)$
e	fixed-sway	free	$y=c_0+\sum_{n=1}^{\infty} c_n\sin\frac{2n-1}{2L}\pi x$
f	fixed-sway	pinned	$y=\sum_{n=1}^{\infty} c_n\sin\frac{2n-1}{2L}\pi x$
g	pinned	fixed	$y=\sum_{n=1}^{\infty} c_n(\cos\frac{2n+1}{2L}\pi x-\cos\frac{2n-1}{2L}\pi x)$
h	pinned	free	$y=c_0(1-\frac{x}{L})+\sum_{n=1}^{\infty} c_n\sin\frac{n\pi}{L}x$
i	pinned	pinned	$y=\sum_{n=1}^{\infty} c_n\sin\frac{n\pi}{L}x$

For boundary condition (g), the determinant is

$$\Delta = \begin{vmatrix} b_{1,1}-(2\times1^2+0.5)P' & b_{1,2}+(1+0.5)^2P' & b_{1,3} \\ b_{1,2}+(1+0.5)^2P' & b_{2,2}-(2\times2)^2+0.5)P' & b_{2,3}+(2+0.5)^2P' \\ b_{1,3} & b_{2,3}+(2+0.5)^2P' & b_{3,3}-(2\times3^2+0.5)P' \\ b_{1,4} & b_{2,4} & b_{3,4}+(3+0.5)^2P' \\ \cdots\cdots & \cdots\cdots & \cdots\cdots \\ b_{1,n} & b_{2,n} & b_{3,n} \end{vmatrix}$$

$$\begin{vmatrix} b_{1,4} & \cdots\cdots & b_{1,n} \\ b_{2,4} & \cdots\cdots & b_{2,n} \\ b_{3,4}+(3+0.5)^2P' & \cdots\cdots & b_{3,n} \\ b_{4,4}-(2\times4^2+0.5)P' & \cdots\cdots & b_{4,n} \\ \cdots\cdots & \cdots\cdots & \cdots\cdots \\ b_{4,n} & \cdots\cdots & b_{n,n}-(2n^2+0.5)P' \end{vmatrix} = 0 \quad (14)$$

where

$$P' = \frac{PL^2}{\pi^2 EI} \quad (15)$$

and a_i and $b_{i,j}$ are intermediate parameters for calculation. The ranges of i, j and values of a_i, $b_{i,j}$ and s vary depending on the boundary conditions. For example, with boundary condition (h) (pinned and free)

$$b_{i,i} = i^2 + m_{i,i}A + s_{i,i}B$$

$$b_{i,j} = b_{j,i} = m_{i,j}A + s_{i,j}B \quad (16)$$

where

i = 0, 1, 2, ..., n;
j = i + 1, i + 2, ..., n; and

$$A = 2\left(\frac{\alpha L}{\pi}\right)^5$$

$$B = \frac{2ufL^3}{EI\pi^4} \quad (17)$$

$$m_{0,0} = \frac{\pi^3 h^2}{24L^2}\left(6 - \frac{4h}{L} + \frac{h^2}{L^2}\right)$$

$$m_{0,j} = \frac{1}{\sqrt{2}j^2}\left[\frac{h}{L}\pi - \frac{L-h}{jL}\sin\frac{jh\pi}{L} - \frac{2}{j^2\pi}\left(1 - \cos\frac{jh\pi}{L}\right)\right] \quad (18)$$

$$s_{0,0} = \frac{h^2\pi^2}{4L^2}$$

$$s_{0,j} = \frac{-1}{\sqrt{2}j^2}\left[1 - \cos\frac{jh\pi}{L}\right] \quad (19)$$

where

j = 1, 2, ..., n; and

$$m_{i,j} = \frac{1}{2ij\pi(i-j)^2}\left[1 - \cos\frac{(i-j)h\pi}{L}\right] - \frac{1}{2ij\pi(i+j)^2}\left[1 - \cos\frac{(i+j)h\pi}{L}\right] \quad (20)$$

$$s_{i,j} = \frac{1}{2(i+j)^2}\left[1 - \cos\frac{(i+j)h\pi}{L}\right] + \frac{1}{2(i-j)^2}\left[1 - \cos\frac{(i-j)h\pi}{L}\right] \quad (21)$$

where

i = 1, 2, ..., n; and
$j = i, i + 1, \ldots\ldots, n$.

The determinants of Equations 12, 13, and 14 are symmetric along the diagonal, with P' unknown. The smallest root of Equations 12, 13, and 14 solves P' for all models. The Jacobi method is used to find the eigenvalues of the eigen-matrices for the determinants given in Equations 12 and 14. An iterative approach is used to solve Equation 13 because it cannot be solved using the Jacobi method. Once P′ is obtained, the critical buckling capacity is defined as

$$P_{cr} = \frac{\pi^2 EI}{L^2} P' \quad (22)$$

or expressed in terms of equivalent buckling length, L_e,

$$P_{cr} = \frac{\pi^2 EI}{L_e^2} \quad (23)$$

where

$$L_e = \frac{L}{\sqrt{P'}} \quad (24)$$

Solutions of Equations 12, 13, and 14 are calculated by the Axial Buckling Capacity of Piles computer program. With the program, it is possible to solve for the equivalent length L_e under the different boundary conditions defined in Table 1.

PARAMETER STUDY

To investigate the effects of key analysis parameters on the buckling capacity of piles and to develop simplified methodology for estimation of critical buckling capacities, a parameter study was conducted.

$$L' = \alpha L$$

$$h' = \alpha h$$

$$L_e' = \alpha L_e$$

$$\beta = \frac{uf}{\alpha^3 \pi EI}$$

where

L' = nondimensional length of pile,
h' = nondimensional embedded length of pile,
L_e' = nondimensional equivalent buckling length, and
β = nondimensional influence coefficient of the side friction.

The key soil and pile parameters assumed in this analysis were as follows:

EI = 1.4 × 10^6 kNm^2

η_h = 700 kN/m^3

f = 35 kPa

u = 3.14 m

β = 0.0006

Figures 2–10 show the variations of nondimensional equivalent buckling length L_e' as a function of h'. The nine boundary-condition models are used for this analysis. The values of e are varied from 0.5 to 1, the value of 1 representing a fully embedded pile. In this analysis, the nondimensional embedded length h' is not limited to a value greater than 4. For boundary models (*b*), (*c*), and (*h*), as h' approaches a value less than 1, the value of L_e' tends to be infinite, implying a P_{cr} = 0, as shown in Figures 3, 4, and 9.

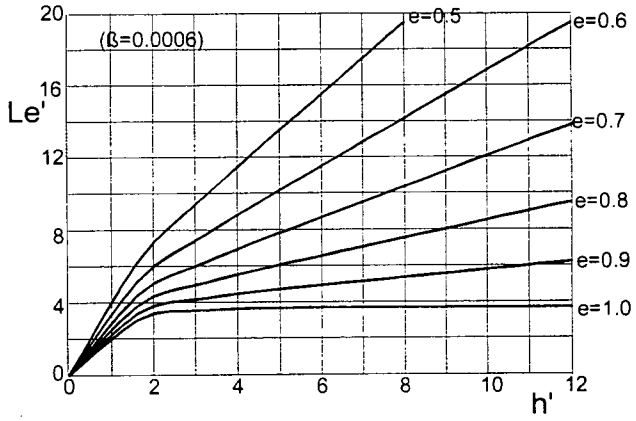

FIGURE 2 Nondimensional equivalent buckling length (L_e)' versus nondimensional embedded length of pile (h') with free top and fixed tip.

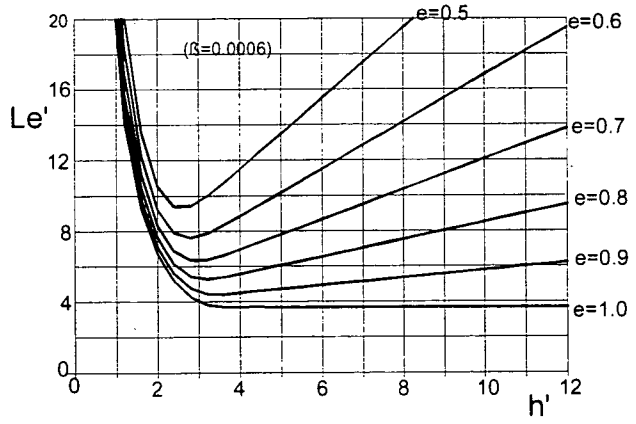

FIGURE 3 Nondimensional equivalent buckling length (L_e') versus nondimensional embedded length of pile (h') with free top and free tip.

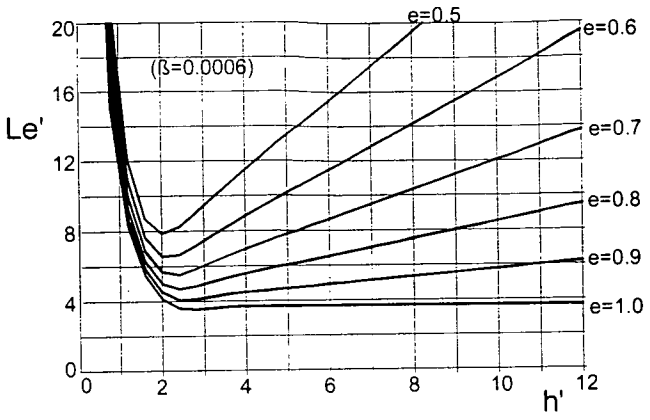

FIGURE 4 Nondimensional equivalent buckling length (L_e') versus nondimensional embedded length of pile (h') with free top and pinned tip.

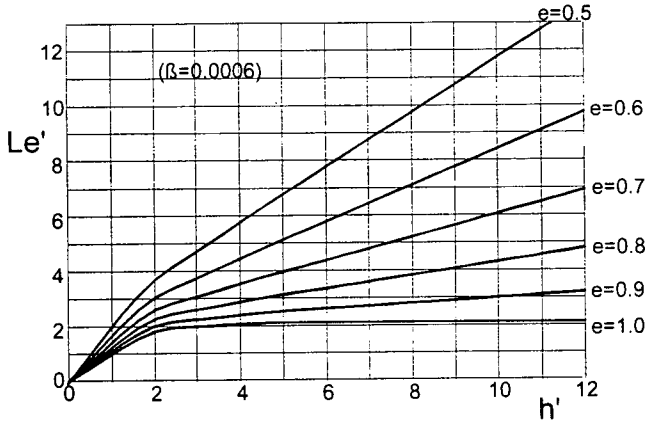

FIGURE 5 Nondimensional equivalent buckling length (L_e') versus nondimensional embedded length of pile (h') with fixed-with-sway top and fixed tip.

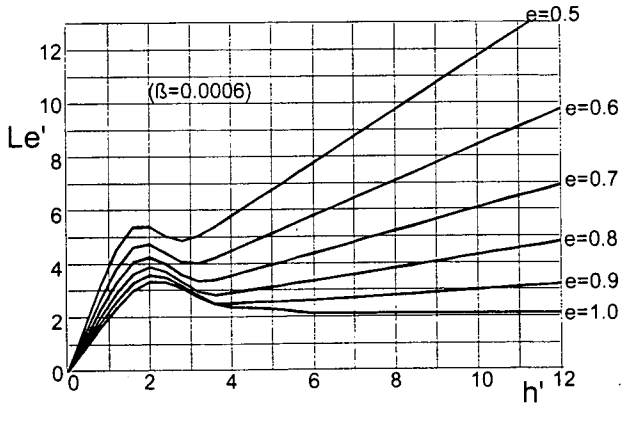

FIGURE 6 Nondimensional equivalent buckling length (L_e') versus nondimensional embedded length of pile (h') with fixed-with-sway top and free tip.

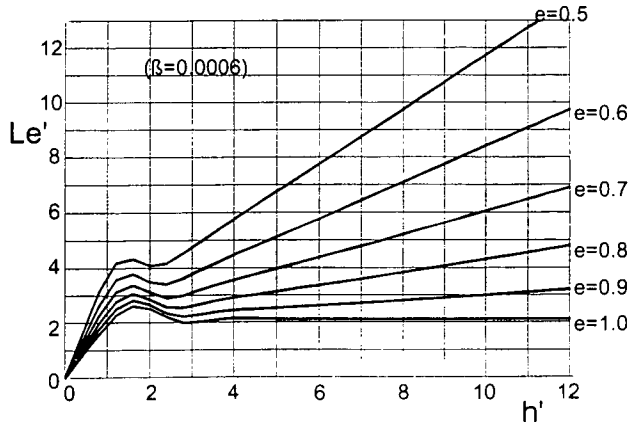

FIGURE 7 Nondimensional equivalent buckling length (L_e') versus nondimensional embedded length of pile (h') with fixed-with-sway top and pinned tip.

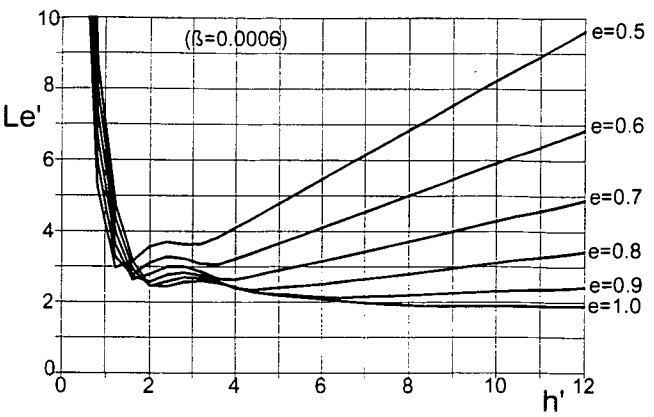

FIGURE 9 Nondimensional equivalent buckling length (L_e') versus nondimensional embedded length of pile (h') with pinned top and free tip.

In all cases, buckling failure occurred more readily in the partially embedded piles, as compared with the fully embedded piles. As the embedment ratio e decreases, the equivalent buckling length increases and the load magnitude that will cause buckling decreases. The effect of embedment length on the buckling load of fully embedded piles is less pronounced than on partially embedded piles. As shown in Figures 2–10, for fully embedded piles, this effect is almost negligible after h' exceeds a value of approximately 3.4 for free-top conditions, 6.0 for fixed-with-sway top conditions, and 8.2 for pinned-top conditions.

Based on the model and parameter study, buckling potential may be evaluated using these steps.

1. Compute the pile stiffness using its material properties.
2. Estimate the constant of subgrade reaction η_h according to the soil conditions around the pile.
3. Compute the coefficient of pile-soil compliancy α.
4. Compute nondimensional embedded pile length $h' = \alpha h$.
5. Compute pile embedment ratio $e = h/L$.
6. Estimate the unit skin friction f according to soil conditions and pile driving method. Compute the influence coefficient β of the side friction.
7. Find nondimensional equivalent buckling length of pile L_e' (from nondimensional curves).
8. Compute the equivalent buckling length I_e and pile-buckling capacity P_{cr} using L_e', α, and EI.
9. Determine allowable buckling load, $(P_{cr})_{all} = P_{cr}/FS$.

EFFECT OF BOUNDARY CONDITIONS

Figures 11(*a*), (*b*), and (*c*) show the variation of L_e' as a function of h' for different tip boundaries with free-top boundary, fixed-with-sway top boundary, and pinned-top boundary, respectively. As shown in Figure 11(*a*), for the case of free-top boundary and fully embedded conditions, and as h' reaches a critical value of 3.3, curves representing different tip conditions but the same top condition tend to conicide. Similar behavior was observed for cases of fixed-with-sway top boundary and pinned-top boundary, their critical values evaluated to be 5.6 and 7.6, respectively.

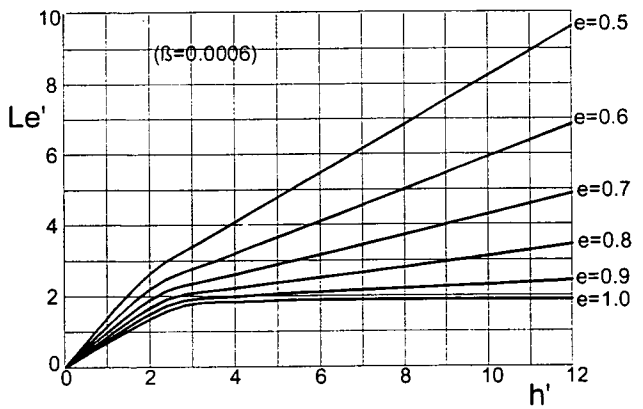

FIGURE 8 Nondimensional equivalent buckling length (L_e') versus nondimensional embedded length of pile (h') with pinned top and fixed tip.

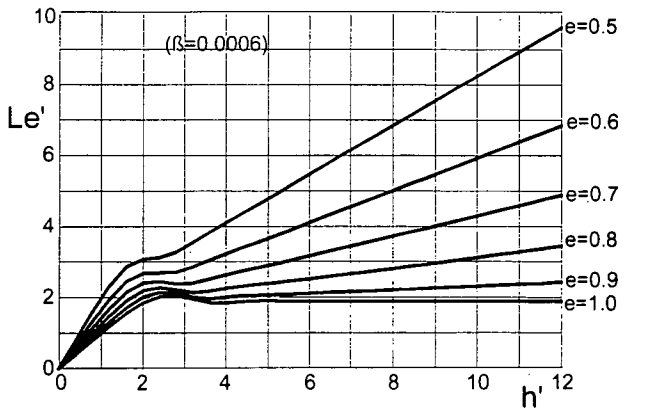

FIGURE 10 Nondimensional equivalent buckling length (L_e') versus nondimensional embedded length of pile (h') with pinned top and pinned tip.

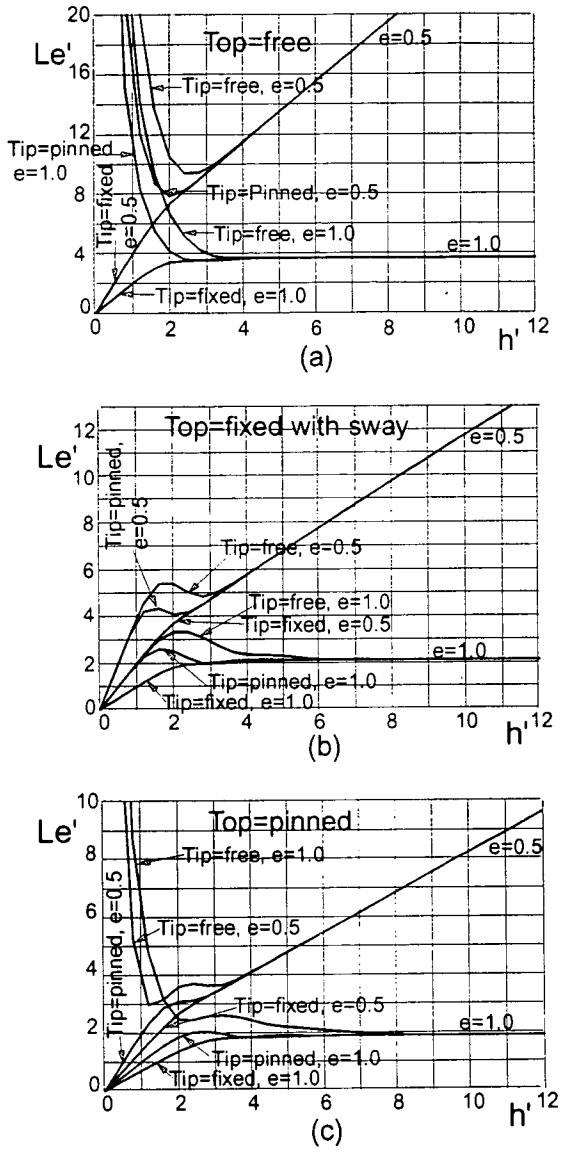

FIGURE 11 Comparison among different tip boundaries; (*a*) free top, (*b*) fixed-with-sway top, and (*c*) pinned top.

The pile-top conditions controlled the buckling behavior when h' reached a critical value. Accordingly, given the analysis parameters, it is postulated that for cases with h' greater than the critical value, the boundary conditions at the pile tip have no effect on the equivalent lengths or buckling capacities. For fully embedded piles, the critical h' values are evaluated to be 3.3 for free-top boundaries, 5.6 for fixed-with-sway top boundaries, and 7.6 for pinned-top boundaries. As shown in Figure 11, this distinct behavior is observed for both cases of partially embedded and fully embedded piles.

Figure 12(*a*) shows the comparison among different pile-top conditions of fully embedded piles with pinned tip. A similar comparison is shown for partially embedded piles in Figure 12(*b*). Results from these figures indicate that piles with free-top boundary are more susceptible to buckling failure than piles with a pinned- or fixed-with-sway–top boundary. The observed behavior is applicable both to fully embedded and partially embedded piles.

EFFECT OF SKIN FRICTION

Figure 13(*a*) shows the effect of skin friction on nondimensional equivalent buckling length of fully embedded piles with three different boundary conditions. In this analysis, $\beta = 0$ indicates that no skin friction is considered. As shown in Figure 13(*a*), the effect of skin friction on equivalent buckling capacity is not significant in this case. Because the buckling load varies linearly with $1/L_e^2$, L_e' was replaced by $L_e'^2$ in Figure 13(*b*) to investigate the effect of the skin friction in the case of partially embedded piles. Assuming $e = 0.5$ and a β range of 0 to 0.01, less than 7 percent variation in the critical buckling length is predicted. Given the model parameters, this analysis indicates that generally the effect of β on the pile's buckling behavior is minor.

APPLICABILITY OF DEVELOPED MODEL

Klohn and Hughes (*6*) published results of full-scale buckling load tests to failure on a 0.33-m diameter timber pile. Results from the tests indicate pile failure from buckling, without advance warning. The test data and the analysis model presented in this paper were used to predict critical buckling capacity. Structure and soil conditions were provided by Klohn and Hughes (*6*). Unsupported pile length was 16.76 m, and embedded length 15.24 m. Effective pile diameter was 0.33 m; Young's modulus of the timber pile was 11.7×10^6 kN/m^2.

The wharfpiles were driven through soft silt into an underlying, dense gravel layer. The modulus of subgrade reaction was considered to vary linearly with depth, assuming a zero value at the mud line. The estimated value of η_h was set between 700 KN/m^3 and 1.5×10^3 kN/m^3 (*6*). Unit skin friction was estimated to range

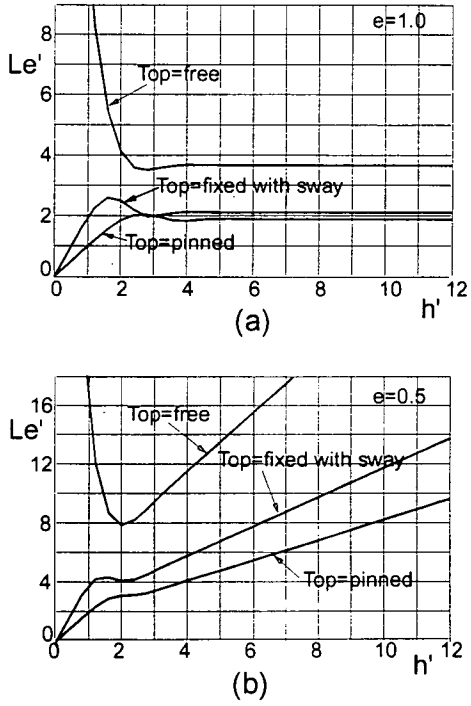

FIGURE 12 Comparison among different top boundaries with pinned tip; (*a*) $e = 1.0$, and (*b*) $e = 0.5$.

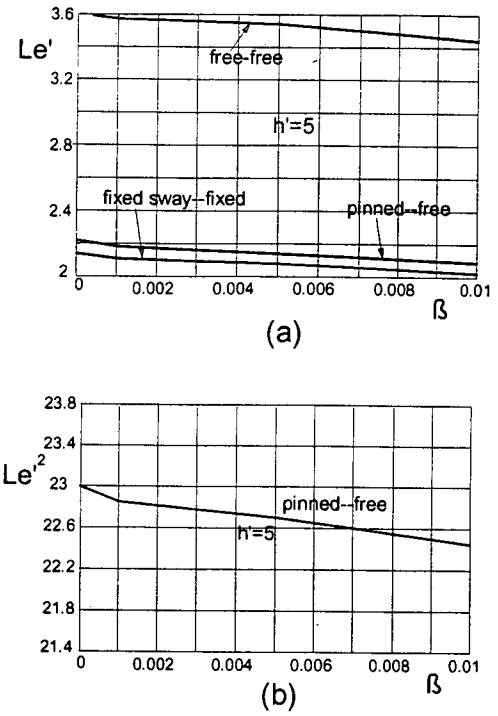

FIGURE 13 Effect of skin friction; (*a*) e = 1.0, and (*b*) e = 0.5.

between 10 kN/m^2 and 60 kN/m^2 (*6*). The average eccentricity of the test piles was 0.127 m, assuming a pinned pile top and fixed pile tip.

Predicted variation of P_{cr} as a function of f for different η_h values is shown in Figure 14; and eccentricity is considered. The P_{cr} value as measured by Klohn and Hughes ranged from 267 kN to 302.5 kN, (Figure 14). A comparison between the predicted and measured capacity favorably verifies the presented model's applicability. As Figure 14 illustrates, the effect of η_h on buckling capacity is considerable. Increasing the η_h value from 200 kN/m^3 to 500 kN/m^3 increases the critical buckling load approximately 20 percent.

DESIGN EXAMPLE

In addition to the case study above, applicability of the developed model also is illustrated using the design example presented by Davisson and Robinson (4). In this example, a 0.324-m outside diameter steel-pipe section is embedded 15.24 m into a soft, organic silt. EI (flexural stiffness) for this pile was 2.4 × 10^4 kNm^2 and the coefficient of lateral subgrade reaction for the silt was 542.9 kN/m^2. The unsupported length of the pile was 6.1 m. The pile top was considered fixed with sway with a fixed pile tip. Using the model presented in this paper, analysis of the pile is conducted as follows:

$$\alpha = \sqrt[5]{\frac{542.87 \text{ kN/m}^3}{2.4 \times 10^4 \text{ kN/m}^2}} = 0.46869 \text{ m}^{-1}$$

$$h' = \alpha h = 7.1428$$

$$e = \frac{50}{50 + 20} = 0.714$$

If no skin friction is considered (as none was presented by Davisson and Robinson), L_e' is estimated to equal 4.70; therefore

$$L_e = \frac{L_e'}{\alpha} = 10.03 \text{ m}$$

$$P_{cr} = \frac{\pi^2 EI}{L_e^2} = 2360 \text{ kN}$$

Davisson and Robinson's solution was L_e = 9.93 m and P_{cr} = 2406.3 kN. If a skin friction of f = 35 kN/m^2 is considered, then

$$\beta = \frac{uf}{\alpha^3 \pi EI} = 0.0045$$

The results are L_e = 9.83 m and P_{cr} = 2454.2 kN.

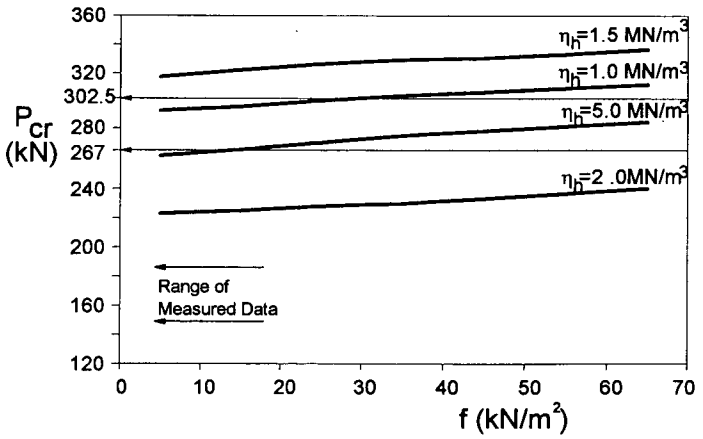

FIGURE 14 Prediction of P_{cr} as a function of unit skin friction for different η_h value.

SUMMARY AND CONCLUSIONS

A theoretical model for estimating the buckling loads of piles with skin friction was developed. The minimum potential-energy method was used to develop the model. The Rayleigh-Ritz method was adopted to select suitable deflection functions for buckling models. Nine pile models with various boundary conditions were analyzed, and it was assumed modulus of subgrade reaction increased linearly with depth. A comprehensive parameter study was conducted to analyze the effect of pile-top and tip conditions as well as skin friction on equivalent buckling length and buckling loads. The models' applicability was evaluated using results from full-scale buckling load tests to failure by Klohn and Hughes (*6*). In addition, a design example presented by Davisson and Robinson was used to demonstrate the general analysis procedure. Based on the analysis and results presented, these conclusions can be advanced:

- The boundary conditions of a pile tip have minimal effect on a pile's critical buckling loads if h' exceeds a critical value (for fully embedded piles, this value is approximately 3.3 for free-top conditions; 5.6 for fixed-with-sway top; and 7.6 for pinned top). Similar behavior is observed for partially embedded piles.
- In all cases analyzed, buckling failure occurred more readily in partially embedded piles, as compared with fully embedded piles. As the embedment ratio e decreased, the equivalent buckling length increased and the load magnitude needed to cause buckling decreased.
- The effect of embedment length on the buckling load of fully embedded piles is less pronounced than on partially embedded piles. For fully embedded piles, this effect is nearly negligible after h' exceeds a value of 3.4 for free-top conditions, 6.0 for fixed-with-sway top conditions, and 8.2 for pinned-top conditions.
- The side-friction contribution to buckling stability is minor. In the case of $e = 0.5$ and a β range of 0 to 0.01, less than 7 percent variation in the critical buckling length is predicted. The analysis assumes uniform distribution of skin friction with depth.
- Comparison between the results from a pile load test and the model presented in this paper verify the model's applicability. The effect of the η_h value on the predicted buckling capacity is considerable. In the case-study analyses, increasing the η_h value from 200 kN/m^3 to 500 kN/m^3 increased the critical buckling load approximately 20 percent.

REFERENCES

1. Golder, H. G. and B. O. Skipp. The Buckling of Piles in Soft Clay. *Proc., 4th International Conference on Soil Mechanics and Foundation Engineering*, London, England, 1957.
2. Bergfelt, A. The Axial and Lateral Load Bearing Capacity, and Failure by Buckling of Piles in Soft Clay. *Proc., 4th International Conference on Soil Mechanics and Foundation Engineering*, London, England, 1957.
3. Brandtzaeg, A. and E. Harboe. Buckling Tests of Slender Steel Piles in Soft, Quick Clay. *Proc., 4th International Conference on Soil Mechanics and Foundation Engineering*, London, England, 1957.
4. Davisson, M. T. and K. E. Robinson. Bending and Buckling of Partially Embedded Piles. *Proc., 6th International Conference on Soil Mechanics and Foundation Engineering*, Canada, 1965.
5. Reddy, A. S. and A. J. Valsangkar. Buckling of Fully and Partially Embedded Piles. *Journal of Soil Mechanics and Foundations*, ASCE, Nov. 1970, pp. 1951–1965.
6. Klohn, E. J. and G. T. Hughes. Buckling of Long Unsupported Timber Piles. *Journal of Soil Mechanics and Foundations*, ASCE, Nov. 1964, pp. 107–123.
7. Terzaghi, K. Evaluation of Coefficients of Subgrade Reaction. *Geotechnique*, Vol. 5, 1955. pp. 297–326.

Use of Deep Blast Densification for Bridge Foundation Improvement on SR-504

DAVID V. JENKINS, ALAN P. KILIAN, AND JOSEPH E. HACHEY

A case history describing the use of blast densification by the Washington State Department of Transportation to densify a 40-m-deep, loose debris flow is presented. Debris flow from the 1980 eruption of Mount St. Helens would pose a high risk for liquefaction and ground settlement should a seismic event occur. A single-span bridge was to be constructed on the debris flow. It was determined that the only practical means of supporting the structure were spread footings founded on the debris flow, once improved by ground densification. Blast densification was chosen over more common means to improve the ground; it was considered the most cost-effective and feasible method of construction through boulder-laden debris flow. First, a test section was constructed to verify the blast design and to confirm its feasibility given the unusual geologic deposit. The goal was to improve the relative density of the deposit, as measured by standard penetration testing (SPT) and Becker penetration testing. Additionally, the site was instrumented to measure ground response. Instrumentation included surface and subsurface settlement devices, inclinometers, piezometers, ground-vibration instruments, and geophysical surveys. Blast densification successfully increased the SPT values of the deposit from an average $N_{1(60)}$ = 8 to $N_{1(60)}$ = 20 above 15 m, to $N_{1(60)}$ = 19 below 15 m.

The case history presented in this paper describes the design, construction, and test results of a deep-soil densification project. The project used explosives at approach-fill areas that were chosen for a new bridge structure. The densification work was performed by the Washington State Department of Transportation (WSDOT) as part of an 11-km SR-504 extension into the Mount St. Helens National Volcanic Monument; it was part the work to be performed in construction of Bridge No. 12 across South Coldwater Creek.

The Mount St. Helens National Volcanic Monument is situated in Cowlitz and Skamania counties in southwestern Washington State. The new 11-km extension begins at the outlet of Coldwater Lake at an elevation of 730 m and traverses eastward, crossing South Coldwater Creek. It then enters the South Coldwater Creek Valley, which was filled with up to 40 m of debris from the 1980 eruption of Mount St. Helens. South Coldwater Creek is bordered by the Coldwater Divide to the north and Johnston Ridge to the south. The new alignment will end near the summit of Johnston Ridge at an elevation of 1,400 m.

A blast densification project was used to mitigate the potential for liquefaction and dynamic settlement of the approach fills and bridge abutment footings at the new South Coldwater Creek bridge. Blast densification uses the shock and vibration resulting from the detonation of an explosive, aided by the weight of overlying soils, to rearrange soil particles into a denser state.

D. Jenkins, Washington State Department of Transportation, Headquarters Materials Laboratory, P.O. Box 47365, Olympia, Wash. 98504–7365; A. Kilian, FHWA, Western Federal Lands Highway Division, 610 East 5th Street, Vancouver, Wash. 98661; J. Hachey, Golder Associates Inc., 4104–148th Ave., N.E., Redmond, Wash. 98052.

SITE DESCRIPTION

The 1980 eruption of Mount St. Helens triggered a rockslide or debris avalanche and related lateral blast that devastated approximately 325 sq km^2 of ground north of Mount St. Helens (*1*). The north fork of the debris avalanche deposits formed blockages at the outlets to Coldwater Creek and South Coldwater Creek damming lakes with avalanche debris.

The new bridge structure that will span South Coldwater Creek will consist of a 60-m-long, single span, steel-plate girder bridge supported on low-capacity spread footings founded in debris avalanche deposits from the 1980 eruption.

When four borings were drilled during a foundation investigation of the bridge structure, WSDOT encountered loose-debris avalanche, consisting of a multicolored, heterogeneous mixture of sand and gravel with varying amounts of silt, cobbles, and boulders to depths in excess of 40 m. Corrected standard penetration test [SPT, $N_{1(60)}$] blowcounts were typically 8 or less. Pre-1980 deposits below the 40 m depth consisted of dense to very dense, nonstratified, fine to coarse sand, some gravel, and some silt.

Groundwater levels corresponded roughly with the level of water in South Coldwater Creek, which at the bridge site ranges from 2 to 5 m below the existing ground surface.

SEISMIC CONSIDERATIONS

Mount St. Helens Seismic Zone (*2*) is an interpreted 100-km-long, near vertical, right-lateral, strike-slip active fault zone. The zone trends north-northwest through the WSDOT project area. The maximum magnitude recorded for an earthquake in the zone is 5.5 on the Richter scale, for the earthquake measured on February 14, 1981. Its epicenter was near Elk Lake, approximately 5.2 km north of South Coldwater Creek.

Crustal earthquakes (3.3 to 16.6-km deep) greater than the 5.5-magnitude event are possible along the Mount St. Helens Seismic Zone (*3*). WSDOT designed the bridge to withstand a seismic event with a magnitude of 6.5, generating a 0.55 g peak bedrock acceleration. Because the soils at the project site are granular, loose, and saturated, liquefaction was potentially a high risk to the stability of the structure.

Liquefaction analyses were performed based on the SPT data and procedures developed by Seed et al. (*4*) and indicate that about two-thirds of the SPT results fall within the range where liquefaction is a moderate to high risk.

A major liquefaction failure in the vicinity of the bridge could significantly affect a large area. Such a failure could include loss of both vertical and lateral foundation ground support for the bridge, ground subsidence, and lateral spreading. Lateral spreading would be particularly damaging because it probably would displace the bridge laterally even if it were supported on deep piles. Localized liquefaction could induce differential settlement and possibly cause lateral movements that could damage the bridge.

Even if liquefaction did not occur, a seismic event would be likely to induce dynamic settlement of the loose debris avalanche deposit. Resulting ground settlement would cause unacceptable movement of the bridge.

Stability analyses indicate that ground improvement must be full depth (40 m) and conducted over the entire plan area of the approach fill in order to lessen significantly the probability of a deep-seated failure, the objective being to essentially create an "island" of stable soil. To protect against the maximum design event, the upper 15 m requires an $N_{1(60)}$ value of about 25, whereas below 15 m an $N_{1(60)}$ value of 20 is required. These $N_{1(60)}$ values correspond to relative density values of approximately 65 percent in the upper 15 m and approximately 55 percent below 15 m.

FOUNDATION OPTIONS AND DENSIFICATION METHODS

Foundation options were evaluated principally on the basis of seismic risk, cost, and constructability. Because of the extensive boring depth and loose nature of the site's soils, several significant design issues had to be addressed, including foundation support, area and foundation settlement, liquefaction potential, seismically induced settlement, and the advantages of ground modification.

Both shallow and deep foundation-support systems were considered. The site soils generally were not suitable for spread-footing support of a bridge. Yet deep foundation systems, such as driven piles or drilled shafts, would have to deal with downdrag forces from static or dynamic settlement of the recent debris avalanche deposit, lateral load and lateral spreading caused by liquefaction of the deposit, and construction problems related to the presence of boulders in the debris flow.

Static settlement of the foundation soils had a potential impact on the foundation system. Because of the young age of the debris avalanche deposit, its loose saturated nature, and the effects of buried organics, the deposit could still be undergoing natural settlement. This could cause downdrag loads on deep foundations and differential settlement between structure elements. Applying foundation loads and approach-fill loads to this nonuniform deposit could result in unacceptable settlement.

Based on the design earthquake, liquefaction potential was determined to be a high risk. Liquefaction would result in loss of foundation support, lateral spreading, and ground subsidence. All these liquefaction effects were unacceptable for the bridge design. Perhaps liquefaction would not occur at full depth, 40 m, at the site. Yet dynamic settlement of the deposit would likely result in large settlement at the site. In the case of a modest event, the settlement might be 0.2 m; if a large event were to occur, it could be a few meters. Seismically induced ground settlements were considered a controlling design constraint.

Considering the unique nature of the deposit and the need to keep costs in line for a moderate-sized bridge's ground modification, techniques to improve density and strength of soil became important considerations. The benefits of the right technique would be to allow the use of cost-effective shallow foundations and to reduce the risk of seismically induced liquefaction and ground settlement.

Numerous methods are available to improve the density and strength of a loose debris avalanche deposit, including deep dynamic compaction, vibro-compaction, stone columns, deep soil mixing, jet grouting, and blast densification. These methods were viable alternatives, but constructability risks associated with the presence of bouldery soil and related costs made blasting the preferred option.

Densification of granular soils requires first that the original soil structure be broken down so that soil particles can be moved to a new packing arrangement. In saturated, cohesionless materials this is accomplished most readily by inducing liquefaction using dynamic and cyclic loading. In the case of blasting or dynamic compaction, the compression wave generated by the sudden large energy release can give an immediate buildup in pore water pressure, which greatly reduces the shear strength. The compression wave is immediately followed by a shear wave that is responsible for failure of the soil mass. Passage of these two waves ultimately results in the soil particles settling into a denser, more stable position.

DENSIFICATION DESIGN

Densification by blasting differs from normal construction practices in that it has had limited usage, even though documented use of blast densification can be traced back 50 years. Reluctance to use blast densification relates to the lack of a theoretical design basis. Blast design is empirical, based on prior experience which is modified by site trials. To date, the Jebba project in Nigeria (*5*) was the only project documented to have used blasting to a similar depth, that is, in excess of 35 m. Theoretically, there does not appear to be any restriction on the depth of densification achievable.

An advantage of blasting at the WSDOT site was that the problem of the bouldery soil at the site was handled easily with the construction installation methods WSDOT used. Holes were advanced using the Becker Hammer, which experienced little difficulty in penetrating this deposit. The truck-mounted HAV-180 Becker Hammer Drill consists of a double-acting diesel hammer driving a double-walled casing into the ground.

The design of charge spacing and size was empirical, based on data from available case histories. This design was significantly influenced by the blast densification program conducted at the Molikpaq caisson-retained island in the Canadian Beaufort Sea (*6,7*). The Molikpaq data indicated that the maximum densification was achieved within about 3 m above and below the center of a given charge. Based on these results WSDOT decided to space charges at a nominal vertical spacing of about 6 m and locate the first charge about 1.5 m below the water table. Consequently, the charges were placed at depths of 5 m, 11 m, 17 m, 23 m, 29 m and 37 m below the ground surface. The spacing between the bottom two charges was increased to 8 m to allow densification to about 40 m.

The lateral spacing of charges was controlled for the most part by three factors:

1. The need to minimize the total number of holes to be drilled;

2. The decision to use a "two-pass" approach, which is the common approach at most other blasting sites; and
3. The desire to stay within the 5- to 15-m guideline for charge spacing that Mitchell presented (*8*).

The two-pass approach charges are laid out in a pair of superimposed grids. Each grid has the charges laid out in equidistant rows, with the charges for the second grid placed in the centers of the squares formed by the rows of the first grid (Figure 1). The spacing between rows was 5.3 m (resulting in a spacing of 10.5 m between rows in a single pass). The first grid is detonated in the first pass, and the second grid is detonated in the second pass.

The proposed area of densification consisted of two areas approximately 45 m by 25 m each. Using the two-pass approach design resulted in three rows in the first pass, followed by two rows in the second pass and an effective spacing between blast holes of 7.5 m.

The charge sizes were designed based on past experience where the powder factor was between 15 and 25 grams of explosive per cubic meter of treated soil. There was also concern about the potential for "cratering" and the potential for triggering slope failures in the adjacent slopes. Beginning from the top deck down, the initial plan called for 6 decks with 2.3 kg at 5 m, 4.5 kg at 11 m, 6.8 kg at 17 m, 9 kg at 23 m, 11 kg at 29 m, and 13.6 kg at 37 m. This resulted in a powder factor of approximately 15 g/m^3. The term "powder factor" means the mass of explosive used divided by the total volume of soil improved by blasting in one blast sequence or "pass."

The intent of blast densification is to produce settlement by inducing liquefaction. During earthquakes, liquefaction results from cyclic loading of the soil, and for a given soil density, the occurrence of liquefaction depends upon the magnitude of the cyclic load and the number of cycles experienced by the soil. There were two timing-design options available for testing whether the blast design would accomplish liquefaction. The first option was to detonate all of the charges at once, to increase the magnitude of the load at the expense of the number of cycles. The second option was to detonate a smaller number of charges at any one time and induce a greater number of cycles at the expense of reducing the magnitude of the loads. It was decided to use delays to create a larger number of cyclic loads. No case histories were found in the literature wherein the primary focus of the study was to evaluate the effects of blast densification by varying the delays between charges. WSDOT decided to use delays between charges, as charges were fired one row and one deck at a time, from the bottom deck up, with a 75-msec delay between rows and a 0.4 sec delay between decks.

Soil densification by inducing liquefaction requires the concurrent removal of water. To aid water removal, vertical drains were installed equidistant from the blast holes. The drains consisted of 76-mm diameter, Schedule 40 polyvinylecloride, with 3.0-mm-sized slots.

BLAST DENSIFICATION CONTRACTING

The technical objectives were to densify the soil at full depth and an area large enough to create a "stable island" that would withstand strong ground-shaking. Improvement in densification was measured by means of the SPT as an indicator. The goal was to increase the average SPT value [$N_{1(60)}$] from about 8 to 25 in the upper 15 m of ground and increase it to 20 below a depth of 15 m.

Using relatively new technology creates a lot of uncertainty when contracting. Consequently, one objective was to share the risk of the project by not including the explicit SPT blow counts in the contract. Also, an advisory specification was included in the contract describing the interpreted geologic conditions and expected difficulty in drilling the bouldery deposit.

An additional project constraint was the requirement to minimize damage to the surrounding terrain. The project is within the Mount St. Helens National Monument, and the existing topogra-

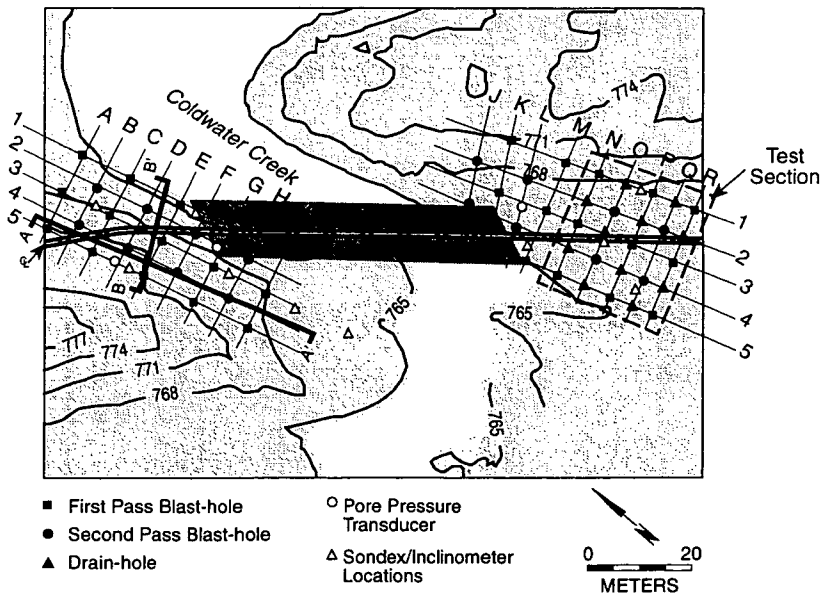

FIGURE 1 Blast-hole and instrumentation location plan.

phy is valued highly. The mandate was to do an absolute minimum amount of damage to the topography outside of the planned roadway.

The first step was to speed up the ground densification portion of the major highway project. This would allow time to evaluate the success of densification and not to risk using a new construction technique on the major project before making any needed change to the blasting plan.

A workable contracting method would include a prequalification requirement for contractors. The contract would specify a base program in terms of number of holes and spacing, construction sequencing, energy and blast depth. The contractor would bid on the base program with unit-price add/deducts for the actual program implemented. The base program would also include an initial "test section" phase that would involve varying selected procedures during the initial phase of work. In the unlikely event that the method was found to be unsuitable, the contract would provide for equitable, early termination of the work. Finally, the contract would specify the types of construction instrumentation required to control and monitor the densification effort.

The program did not specify drilling method or explosive type, but left selected details to the contractor. The actual production blasting program used was chosen by WSDOT based on the results of the "test section" phase. The bid items were intended to be flexible enough to provide for the actual program being implemented including any changes.

The blast densification contract consisted of three phases. Phase 1 consisted of drilling and blasting in a test section that amounted to approximately one-fourth of the total blast area proposed. Phase 2 was a 1-week evaluation during which WSDOT would study the results of the blasting in the test section. This phase also allowed WSDOT the option to cancel the contract or to proceed with the remainder of the densification program with possible modifications to the blast plan. Phase 3, the production phase, would be implemented to blast densify the remaining 75 percent of the proposed blast area.

Test Section Phase

Drilling for the test section took place between October 30, 1992, and November 8, 1992, and was conducted by Foundex Inc. of Bellingham, Washington. Instrumentation consisted of surface settlement hubs, two sondex casings installed to a depth of 38 m. Sondex rings were placed every meter at full depth, and borros anchors at 20 and 28 m below the ground surface.

During installation of the 40-m-deep vertical drains, it was observed that significant siltation was occurring within the drain pipes several days after installation. As much as 10 to 25 m of silt and fine sand was deposited in each of the drain holes. There was some discussion as to whether the slot size of the drains should be reduced to decrease siltation. It was thought that if the slot size was reduced significantly to prevent siltation, the drain slot would then be too small to move water effectively. Also, the silt in the drains probably was sufficiently loose that it would be dislodged by the fluid pressure generated during blasting.

The first pass of blasting in the test section consisted of detonating a total of nine blast holes in a 3-by-3 array. A 0.4-sec delay was used between the 6 decks and a 0.75-msec delay between rows. Nitropel, which is a pelletized form of TNT, was used as the explosive charge.

Surface settlement from the first blast averaged about 0.28 m within the blast zone. It was anticipated that there would be 1 to 1.5 m of settlement from the two passes of blasting. There did not appear to be any signs of cratering from the blast, nor were there any signs of large slope movements in the adjacent slopes. Minor slope movement had occurred as evidenced by the development of several tension cracks. On the basis of these results, it was decided that larger charges were warranted, but that the top charge would remain at 11 kg. The new charge profile consisted of 2.3 kg, 9 kg, 11.4 kg, 15.9 kg, 15.9 kg, and 27.3 kg at the 5-m, 11-m, 17-m, 23-m, 29-m and 37-m levels. This increase in charge resulted in a powder factor of $25 g/m^3$.

The new blast profile was used for the second pass at the test section. A total of four blast holes on a 2-by-2 array were detonated. Settlements from the second pass averaged about 0.21 m for a total settlement in the blast zone of 0.49 m. Again, there was little evidence of cratering, and there were no large slope movements. The fact that almost the same amount of settlement was achieved on the second pass, despite the fact that fewer blast holes were used and the ground was already somewhat denser from settlement after the first pass, confirmed the larger charge sizes were warranted.

Evaluation Phase

The contract allowed for a 1-week evaluation period during which a decision would be made about whether to proceed with the remainder of the densification program and potential modifications to the contract blast plan could be examined. The contract had been bid on a unit-price basis that gave WSDOT flexibility to alter quantities and procedures. On the basis of the results of the test section, WSDOT elected to proceed with the contract, but developed modifications to the blast plan that would be incorporated into the blast plan in Phase 3, the production blasting.

The following modifications to the blast plan were made:

- The charge profile used in the second pass of the test section was used for the production blasting. This resulted in a powder factor of $25 g/m^3$.
- The vertical drains were deleted. Visual observations indicated that the blast-holes drained more water than the vertical drains and that sand boils developed in areas where there were no drains or blast-holes.
- The 75-msec delay between rows was deleted and the 0.4-sec delay between decks was reduced to 0.3 sec. It was postulated that damping at the site could have reduced vibration levels more than anticipated and that this could also have reduced settlement.

Production Phase

Drilling at the site resumed on November 23, 1992, and blasting was completed on December 15, 1992. The blast densification resulted in vertical settlements of up to 1.5 m and significant increases in liquefaction resistance, as measured by SPT and BPT results.

TESTING AND INSTRUMENTATION

Instrumentation and testing were conducted as part of the blast densification project. Instrumentation locations are shown in Fig-

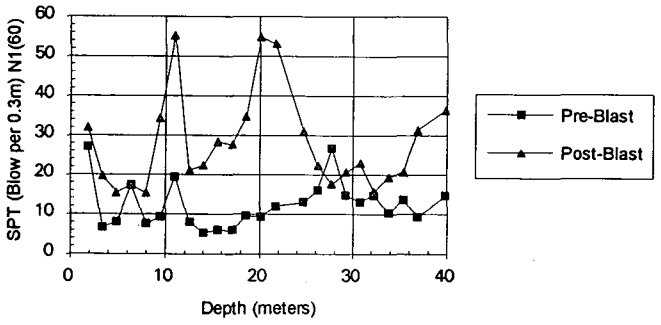

FIGURE 2 SPT pre- and post-blast penetration data (location D2).

ure 1. Penetration test location descriptions (e.g., D2) refer to the intersection of grid lines as shown in Figure 1. A location designation of L3/M4 indicates a location that is approximately midway between grid points L3 and M4.

Penetration Testing

Two types of penetration tests were performed on this project: SPT and Foundex mudded Becker penetration tests (FBPT). Results of SPT and FBPT testing at Pier 1 (D2) are summarized in Figures 2–4.

Standard penetration testing was conducted in accordance with ASTM D-1586, Penetration Test and Split-Barrel Sampling of Soils. Energy transfer was found to average about 43 percent of theoretical during testing, resulting in a 28 percent reduction of SPT N-values during normalization.

The preblast SPT data from the four boreholes drilled in 1991 during the foundation investigation of the bridge were used to compare with the postblast SPT testing conducted in January 1993. The SPT results for Pier 1 (site D2) are shown in Figure 2. There is significant scatter in the SPT results however, and many of the higher blow counts may have been affected by gravel. The presence of gravel reduces confidence in the SPT tests; however, the difference between 1991 and 1993 results clearly indicate a significant increase in density.

The BPT is similar in concept to SPT, and correlations between the tests have been published by various authors (*9*). The major differences between the tests are the tip diameter and the fact that skin friction increases with depth in the BPT, as the casing extends the full depth of the hole. BPT casing used in this test was 168 mm in diameter, driven closed end. The scale of the BPT has a significant benefit in coarse soil deposits, as the BPT results are less influenced by the presence of gravel particles; however, the

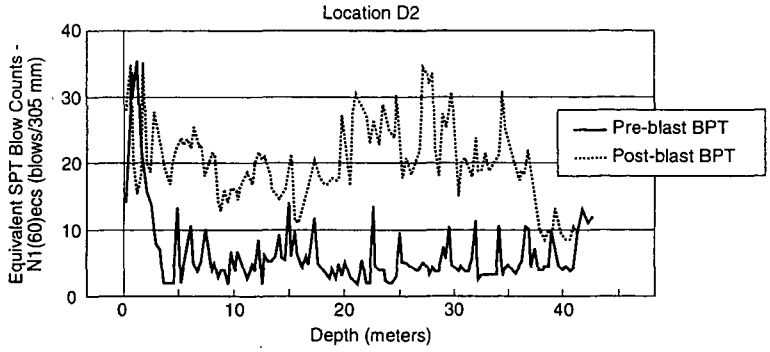

FIGURE 3 Pre- and post-blast penetration data.

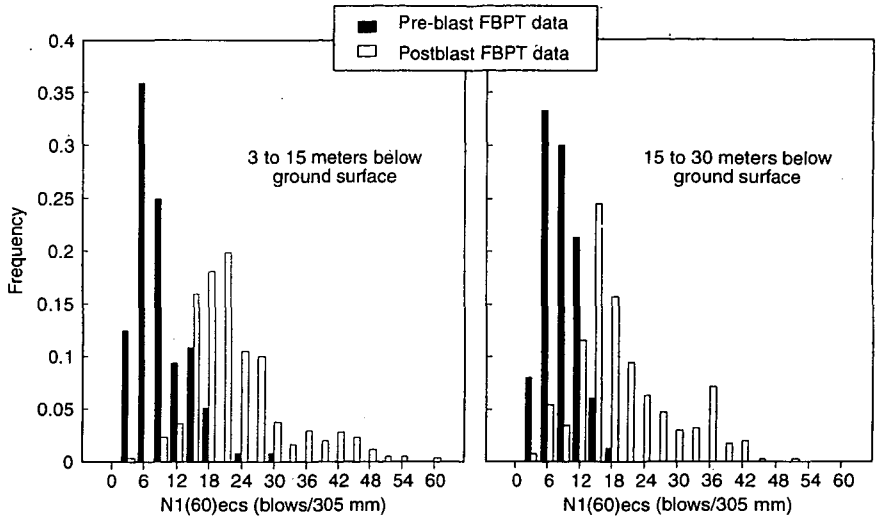

FIGURE 4 Distribution of $N_{1(60)ecs}$ values.

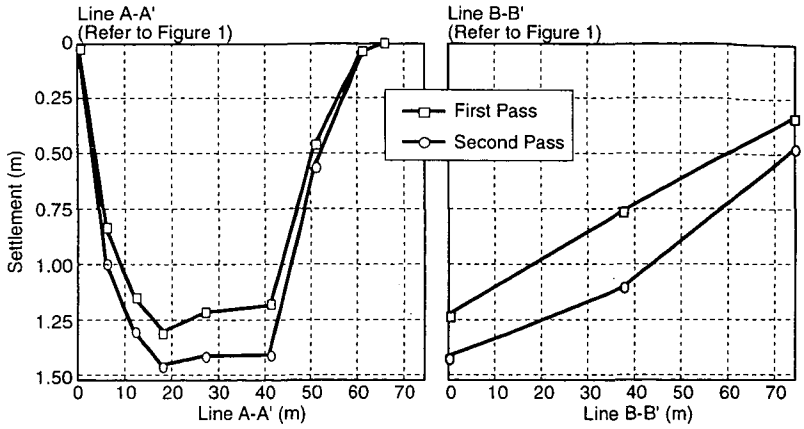

FIGURE 5 Ground settlement, west abutment.

increase in skin friction with depth makes SPT/BPT correlations less reliable below about 13 m in depth. The FBPT was developed by Foundex Inc. to reduce the problems associated with skin friction in developing SPT/BPT correlations.

A study by Foundex (*10*) for the Canadian government showed that the FBPT showed better correlations to the SPT than did the standard BPT, and the correlation was not significantly affected by depth below the ground surface.

The contract required three series of tests composed of four FBPTs in each series. The first series of FBPTs was conducted before blasting to develop a preblast baseline data base. The second series of FBPTs was done approximately 3 weeks after production blasting was complete. The last series of FBPTs was completed approximately 4 months after blasting to study the affects of blast aging.

Figure 3 shows a typical pair of replicated BPTs from the west abutment (site D2), conducted before and after blasting. The blow counts are presented as $N_{1(60)cs}$ values. The Liao and Whitman (*11*) method was used to correct for overburden stress, and a silt-content correction of 2 blows/0.3 m was used. It is obvious that there has been a significant increase in penetration resistance over the entire depth of the deposit. Figure 4 presents all of the FBPT data in the form of histograms showing penetration resistance. The histograms reveal that loose zones still exist within the debris flow, but the average blow count has increased by about 12 blows/0.3 m.

FBPT testing was conducted over a 4-month period to evaluate the effects of aging and it did not indicate a significant increase in penetration resistance. It was concluded, therefore, that the full affects of aging occurred within 3 weeks after blasting.

Settlement Measurements

Surface settlement measurements were conducted using wood survey hubs and settlement plates. The steel plates consisted of 0.09-m^2 plates buried 0.3 m below the ground surface, and a steel post extending above the ground surface to serve as a survey stake. Settlement cross sections at the west abutment are shown in Figure 5. The settlement data indicate vertical strains of about 4 percent.

Subsurface settlement monitoring was considered to be important for this project because of the depth of the zone of loose materials. An important issue was whether liquefaction could occur below 15 m and, if not, whether densification was required below this depth. Deep settlement devices were installed to determine where settlement was occurring and whether it was occurring uniformly. This monitoring was of particular importance during the test phase of the project, during which final decisions on the blast plan were to be developed.

The Sondex tube is a corrugated plastic pipe capable of compressing or extending in length during ground movement. Steel rings are placed in the groves of the pipe at 1-m intervals. The steel rings can be detected by a probe lowered down the center of the pipe, to determine their elevations. Sondex casing was the preferred deep-settlement instrument because it provides a number of measurement points in a single bore hole and can be used to obtain a settlement profile with depth.

Sondex data (Figure 6) indicated that the vertical strain was fairly uniform with depth, as indicated by a fairly linear data plot on the graph. The settlement remained uniform, even when surface settlements of 1.5 m were achieved.

Slope Inclinometers

Slope inclinometers were installed with the Sondex casing at selected locations within and outside the perimeter of the blast zone.

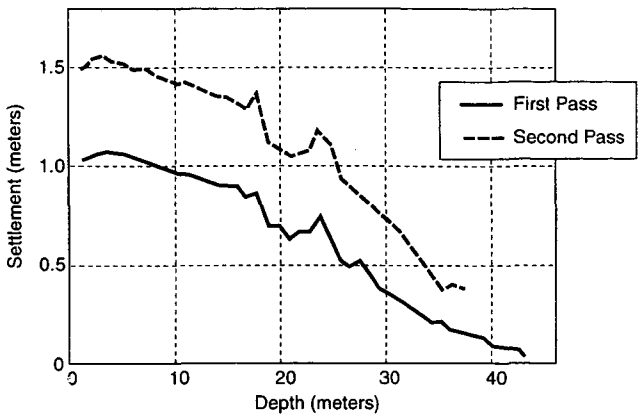

FIGURE 6 Settlement results—Sondex D/E5, west abutment.

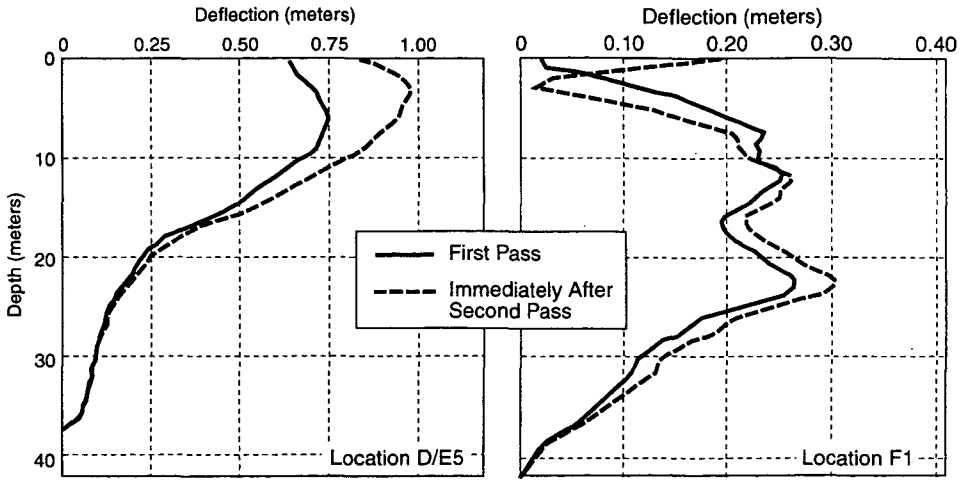

FIGURE 7 Slope indicator results, west abutment.

The most interesting data from the slope inclinometers came from the west abutment. The inclinometer located in the vicinity of D/E5 showed up to 1 m of lateral movement inward toward the blast zone (Figure 7). The slope inclinometer in the vicinity of F1, which is approximately 180 degrees from the inclinometer at D/E5, showed about 0.25 m of movement toward the center of the blast zone. These inclinometers are roughly 15 m apart. Thus the average lateral compressive strain was about 4 percent. When added to the vertical strain, this resulted in a total volumetric compressive strain of about 8 percent.

Pore Pressure Measurements

Series of four pore-pressure transducers located at various depths were installed at three locations in the blast area. The transducers were located at depths of 14 m, 20 m, 26 m, and 35 m. Figure 8 shows pore-pressure measurements from a piezometer group on the west abutment. Complete liquefaction appears to have occurred at all depths, as indicated by normalized pore pressure, *Ru*, values of unity shown in Figure 9. Pore-pressure dissipation to near static conditions was complete 24 hr after blasting.

Physical manifestation of the pore pressure was evidenced by sand boils and a high volume of water migrating to the surface approximately 30 min after detonation. Water continued to flow to the surface several hours after blasting.

Shear-Wave Velocity Survey

Down-hole shear-wave velocity, *Vs*, tests were conducted by Palmer before and after blasting was complete (*12*). Results from the survey indicate the *Vs* in the upper 6 m did not change after blasting from its nominal value of 150 m/s. *Vs* between 6 and 12 m increased from 161 m/s to a post-blast value of 247 m/s. *Vs* between 12 and 24 meters increased from 213 m/s to a post-blast value of 253 m/s. Below 24 m, no significant increase in shear-wave velocity was measured.

SUMMARY

The WSDOT project showed ground densification using blasting could improve soil density sufficiently to mitigate the high liquefaction potential at the test site and the probability of extreme ground settlement if there were a seismic event. The site of the Mount St. Helens National Monument was improved enough to support a bridge structure on spread footings.

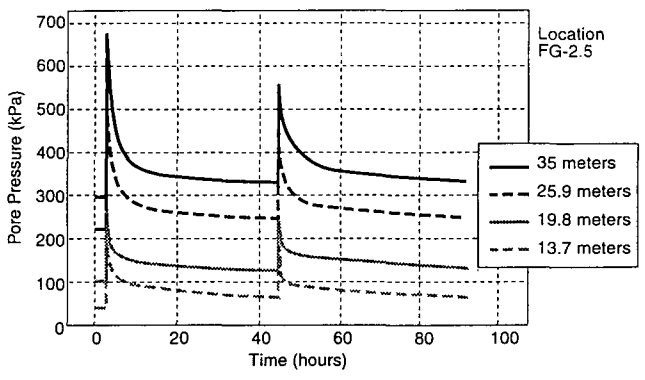

FIGURE 8 Pore water pressure, west abutment.

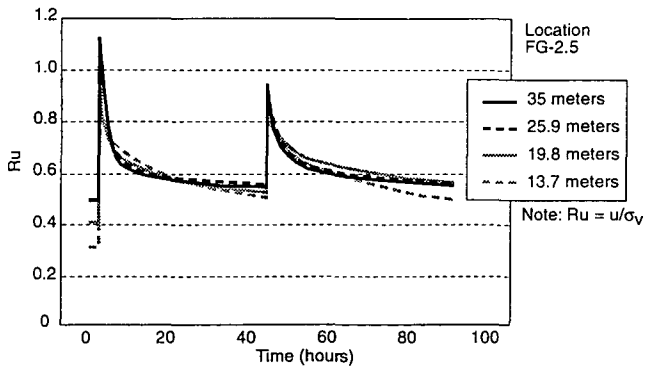

FIGURE 9 Normalized pore water pressure, west abutment.

REFERENCES

1. Voight, B., H. Glicken, R. J. Janda, and P. M. Douglass. Catastrophic Rockslide Avalanche of May 18. In The 1980 Eruptions of Mount St. Helens, Washington, (P. W. Lipman and D. R. Mullineaux, eds.), U.S. Geological Survey Professional Paper 1250, Reston, Va., 1981.
2. Weaver, C. S. and S. W. Smith. Regional Tectonic and Earthquake Hazard Implication of the Crustal Fault Zone in Southwestern Washington. *Journal of Geophysical Research*, 1983.
3. Meyer, W., M. A. Sabol, H. X. Glicken, and B. Voight. The Effects of Groundwater, Slope Stability, and Seismic Hazard on the Stability of the South Fork Castle Creek Blockage in the Mount St. Helens Area, Washington. U.S. Geological Survey Professional Paper 1345, Reston, Va., 1985.
4. Seed, H. B., I. M. Idriss, and I. Arango. Evaluation of Liquefaction Performance Using Field Performance Data. *Journal of Geotechnical Engineering*, ASCE, Vol. 109, No. 3, March 1983.
5. Solymar, Z. V. Compaction of Alluvial Sands by Deep Blasting. *Canadian Geotechnical Journal*, Vol. 21, 1984.
6. Rogers, B. T., C. A. Graham, and M. C. Jefferies. Compaction of Hydraulic Sand in Molikpaq Core. *Proc., 43rd Canadian Geotechnical Conference*, Quebec City, Quebec, Canada, Oct. 10–12, 1990.
7. Stewart, H. R. and W. E. Hodge. Molikpaq Core Densification with Explosives at Amauligak F-24. *Proc., 20th Offshore Technology Conference*, Houston, Tex., May 2–5, 1988.
8. Mitchell, J. K. Soil Improvement, State-of-the-Art Report. *Proc., 10th International Conference on Soil Mechanics and Foundation Engineering*. Stockholm, Sweden, 1981, pp. 509–565.
9. Harder, L. F. and H. B. Seed. Determination of Penetration Resistance for Coarse-Grained Soils Using the Becker Hammer Drill. Earthquake Engineering Research Center Report No. UCB/EERC-86-06, Berkeley, Calif. 1986.
10. *A Testing Technique for Earthquake Liquefaction Prediction in Gravelly Soils, Improvements to the Becker Penetration Test for Estimation of SPT Resistance*. Report to the National Research Council of Canada, Industrial Research Assistance Program, Report No. IRAP-M 40401W. Foundex, Vancouver, British Columbia, Canada, 1992.
11. Liao, S. C. and R. V. Whitman. Overburden Corrections for SPT in Sand. *Journal of Geotechnical Engineering*, ASCE, Vol. 112, No. 3, March 1984.
12. Palmer, S. P. *Final Report SR 504 Blast Densification Project Surface-to-Downhole Shear Wave Velocity Surveying*. Report to the Washington State Department of Transportation, Seattle, July 6, 1993.

Determining Lengths of Installed Timber Piles by Dispersive Wave Propagation

J. DARRIN HOLT, SHUNYI CHEN, AND ROBERT A. DOUGLAS

Timber piles are used as a primary means of support for many structures, such as bridges, throughout the continental United States and must periodically be inspected. Sometimes a pile's overall length is not known because pile records are incomplete or nonexistent; so, calculating the effects of scour on its embedment length can present a problem. A new nondestructive testing method is described that employs dispersive stress-wave propagation and special signal-processing techniques to find the lengths of installed timber piles. The method was studied and developed in the laboratory and then applied to installed piles in the field for which there were records. Some piles were pulled to verify the method directly. The computed pile lengths, compared with records or measurements after pulling, were within error bounds of approximately ±10 percent. The test method holds promise for calculating the depth and physical condition of deeply embedded piles as well as those embedded in shallow concrete footings, and it has been shown to be predictive for piles of varying physical conditions and ages.

Timber pilings are still used widely as a primary means of support for many structures. For example, of an estimated 13,900 state-maintained bridges in North Carolina, 6,500 or more are supported, at least in part, by timber piles. If this number were extrapolated to the continental United States using a more conservative estimate (5,000 bridges per state), as many as 240,000 bridges nationwide may be supported by timber. Further, if each bridge were supported by 4 to 6 piles, (the number of piles often exceeds 100 per bridge), then the total number of piles exceeds 1 million, and it may easily be twice that number. The estimates do not include the number of timber piles used in structures such as marine fender systems, pier structures, fishing piers, or mountain chalets and beach cottages.

With so many timber piles in use today across the country, it is important for any agency charged with inspecting them to be able to determine, in-place, whether a pile is still able to support a structure safely. The question is How can a pile's overall length and embedded length as well as physical condition be evaluated after years of service? Adequate testing and computational methods need to be available to inspectors and engineers so they can have the capabilities of nondestructively evaluating the current capacities of installed timber piles.

A research project was conducted to investigate a proposed testing procedure that employs dispersive stress-wave propagation to determine the lengths of installed timber piles (*1*). The test involves striking a pile on its side to create bending waves (transverse waves). The bending waves generated by the strike are dispersive; they are detected as they pass accelerometers (gages) mounted on the pile's side and are recorded on a digital oscilloscope. Once the wave speeds (phase velocities) of a selected group of frequencies and the times required for them to travel to the pile's buried toe (tip) and back are determined, the total distance traveled can be computed. With these measurements, a pile's overall and embedded length can be calculated from the locations of the gages and the pile's exposed length. The authors wanted to determine the feasibility of using such a method in the field. When piles of known lengths were tested in the field, the method was shown to be effective for predicting a wide range of physical conditions, installment ages, and pile treatments.

J. D. Holt, Civil Engineering Department, North Carolina State University, 839-A Barringer Drive, Raleigh, N.C. 27606. S. Chen, Civil Engineering Department, North Carolina State University, APT M-102 E. S. King Village, Raleigh, N.C. 27607. R. A. Douglas, Civil Engineering Department, North Carolina State University, Mann Hall, Room 208, Raleigh, N.C. 27695-7908.

MOTIVES FOR RESEARCH

To date there have been few investigations into nondestructively evaluating pile lengths (*2–4*). Years of scour have taken place since most of the timber piles still in use today were installed; although their overall length may be the same, their embedment (penetration) is not. If a pile's overall length and penetration are not known, it is difficult to determine how much embedment is left. A pile's bearing capacity actually may have diminished to the point that the structure it supports is unsafe to use.

The effects of scour on a pile's embedment can be measured directly, if a pile's overall length were recorded. However, timber piles in use today often were installed so long ago that there is no existing record of their installment. Even if records do exist, they may be incomplete or wrong. Finally, even accurate pile records won't indicate whether an internal deterioration or fracture has occurred that now prohibits adequate embedment.

USING DISPERSIVE WAVES TO FIND IN-PLACE PILE LENGTHS

Dispersion occurs when individual frequencies in a signal travel at their own velocity. Conventional signal-analysis techniques for dispersive behavior are based upon the Fourier transform. Such methods find relative phase angles for individual frequencies between two gage locations. The relative phase is used to determine the time required for the frequencies to travel a known distance, thus allowing phase velocity to be computed. However, it is not possible to tell whether the computed phase is the actual value or whether the actual value is the computed value plus some integer multiple of the frequency's period. For this reason, Fourier transform methods are inherently difficult to use when calculating the wave speeds and travel times of frequency components in a dispersive signal.

In recent years, researchers at North Carolina State University (NCSU) have been able to perform dispersive-wave computations successfully using a mathematical technique known as the Short Kernel Method (SKM). The SKM technique made it possible to design the testing procedure the authors describe. The wave speeds and travel times of the harmonic components of dispersive, bending waves can be monitored and used to calculate a pile's overall length using the SKM method.

Use of Bending Waves

Several types of stress waves are generated whenever a solid with a bounded geometry is struck. The waves include longitudinal, shear, surface, and bending waves. Within a bounded geometry, all these waves, including the longitudinal wave, will be dispersive in nature. Bending waves are the easiest to create in the context of an installed piling, however, and they contain a high percentage of the total energy of wave motion. Therefore, they were chosen as the agent for determining in-place pile lengths.

Striking a pile transversely to its longitudinal axis creates two separate sets of bending waves. One set travels upward toward the pile's head (butt or top) where it is reflected and sent downward along the pile. The second wave set travels toward the pile's buried toe where it is reflected and sent back upward. These two wave sets traverse the length of a pile, one behind the other, reflection after reflection, until they eventually die out. During their travels, dispersion causes the waves' forms to change continuously, and tracking the waves individually becomes increasingly difficult. If bending waves were not dispersive, it would be possible to simply measure the distance between two characteristic features of a wave directly with an accelerometer. As a wave passed the gage's locations, wave speeds and travel times would be recorded, and from these records the wave's travel distance could be calculated. In contrast, to find wave speeds and travel times for a dispersive wave, one must first find these quantities for a chosen range of the wave's harmonic components.

Separating a dispersive wave into its harmonic components to determine the phase velocities of its individual frequencies, and the time they take to travel a pile's length, can be accomplished by either of two signal-processing techniques: the Fourier phase method or SKM. Both of these methods have been used in dispersive signal analysis, although the Fourier phase method has been predominant. The SKM is a dispersive signal-analysis procedure that was developed by R. A. Douglas for finding the wave speeds of dispersive signals recorded from inversely layered media (*5–7*).

Mathematical Basis for Determining Pile Length

SKM is a frequency-dependent scanning operation based on the cross-correlation procedure described by Bendat and Piersol (*8*). Mathematically, a single value of the SKM at some particular frequency can be stated as follows:

$$\mathrm{SKM}(j, k) = \sum_{i=1}^{N_2-N_1} f(\tau_i) \cdot g[(\tau_i + j \cdot \Delta t), k] \cdot \Delta t \qquad (1)$$

where

SKM (j, k) = j^{th} term of the cross-correlation currently being performed at the k^{th} frequency,
f = the time record from one accelerometer,
g = the fragment of kernel used to perform the cross-correlation,
$N2$ = the number of data points in f, and
$N1$ = the number of data points in g.

SKM uses a user-determined frequency, the kernel seed, and aligns it with the signal so that the first points are adjacent. The cross products are then formed and summed, keeping all algebraic signs. This summation represents the first point on an SKM plot of the signal. Next, the kernal is shifted by a preselected number of data points and the cross products formed again to obtain another point on the SKM graph. The process is repeated either to $N2$ points or to some lesser limit. After a time record is scanned, the resulting SKM plot will have positive and negative peaks. The amplitudes of these represent the degree of correlation between the kernel and its frequency counterpart in the original time record.

Figures 1 and 2 offer a descriptive explanation. Figure 1 represents a typical test setup, and Figure 2 presents accelerometer records stored from a test using such a setup. In Figure 2, with abscissa labeled as time and ordinate as amplitude, the top trace is the time record stored from the accelerometer closest to the

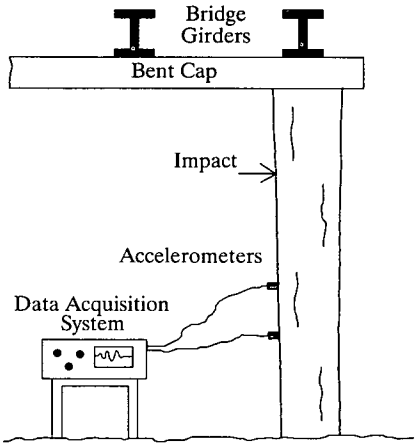

FIGURE 1 Typical field-test setup.

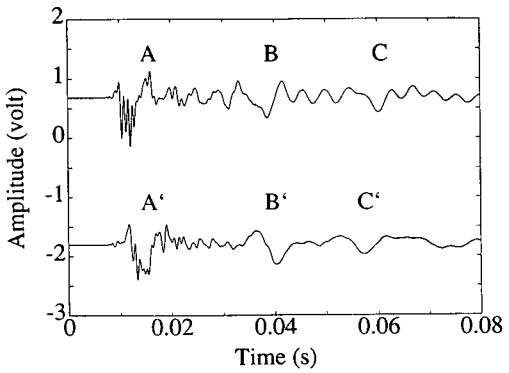

FIGURE 2 Time records from two accelerometers.

pile's head in Figure 1, and the bottom trace is recorded from the gage nearest the ground. The two regions in Figure 2 labeled A and A′ are the first wave recorded as it passed the gage's locations traveling downward from the impact; regions B and B′ are the second wave that first traveled from the impact toward the pile head, reflected, and then passed through the gages on its way down; and regions C and C′ are the wave, first appearing in regions A and A′, after reflecting from the pile's buried toe, and having traveled back under the accelerometers.

Figure 3 shows the superimposed SKM plots of the two time records in Figure 2, assuming a 1-cycle 500-Hertz (Hz) kernel. The solid line is the SKM of the uppermost time record in Figure 2, whereas the dotted line is the SKM plot of the bottom record. Again, the abscissa is labeled as time and the ordinate as amplitude. As seen in Figure 3, the SKM has acted as a "sieve," in that it extracted the 500-Hz component from the signals and displayed its approximate location inside both time records. One can use the first significant positive peaks in the SKM plots, labeled as D and E, to compute a phase velocity. To do this, simply find the number of data points between these two peaks and use Equation 2.

$$C_p = \frac{G_L}{Npts \cdot \Delta t} \tag{2}$$

where

C_p = the phase velocity,
G_L = the gage length (distance) separating the accelerometers,
$Npts$ = the number of data points between peaks D and E, and
Δt = the time step at which the time records were stored originally.

The peaks labeled F and G in Figure 3 can be identified as the return of the 500-Hz frequency from the pile toe. This return signal can be identified easily because the SKM trace from the second gage, the dotted line, appears to lead the one from the first gage, the solid line, as it should. By finding the difference in time between peaks D and G, or E and F, along with the phase velocity from Equation 2, a length can be calculated. The computed length actually will be twice the distance from either accelerometer used for the computation to the pile's toe. The pile's overall length can be determined by adding to this computed value the distance from the pile's head to the accelerometer, Equation 3.

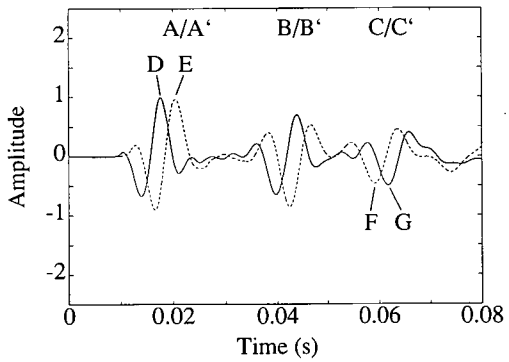

FIGURE 3 SKM Plot using a 1-cycle 500-Hz kernel.

$$OL = T_b + \frac{C_p \cdot Npts \cdot \Delta t}{2} \tag{3}$$

where

OL = the pile's overall length,
T_b = the distance from the head to the particular gage being used for the computation,
C_p = the phase velocity from Equation 2,
$Npts$ = the number of data points between peaks D and G or E and F, and
Δt = the time step at which the accelerometer records were stored.

In choosing the negative peaks F and G in Figure 3, the assumption was made that the 500-Hz component reverses its algebraic sign once it is reflected from the pile toe. This may not always be the case; sign reversal is possibly dependent upon the degree of confinement of the embedded portion of the pile. Both assumptions were made during the analysis and a range of lengths were reported. Note that no knowledge of soil conditions surrounding a pile was available when performing the computations.

RESEARCH METHODOLOGY

This research involved the analysis of data gathered from both the laboratory and field. The initial phase involved writing software for the data analysis and developing a hands-on approach and laboratory models that included a 9-m timber pile. Following the laboratory work, test piles were made available by the North Carolina Department of Transportation (NCDOT), including four freestanding, installed timber piles that ranged in length from 7 m to 12 m. The four piles were driven to selected depths of embedment at the NCDOT Bridge Maintenance Yard in Raleigh, North Carolina, and were an invaluable means of testing concepts developed in the laboratory.

The field work focused on piles chosen from a list of bridges supplied by the NCDOT for which there were existing records. Bridge piles were selected so as to obtain a mix of both interior-bent and end-bent piles, ranging from new to badly deteriorated. Their in-place ages ranged from 1 to 42 years. Two of the piles tested were part of a marine fender line at the North Carolina State Ports Authority in Wilmington, North Carolina. As was agreed, NCDOT did not make any records from the bridges available to the research team until after testing and computations were completed.

TEST EQUIPMENT

Equipment used for data generation and acquisition was easily transported to the field each time and quickly set up. Equipment included a digital oscilloscope, accelerometers (waterproof and non-waterproof), signal conditioners, power supplies, tools for creating the signals, and a laptop computer for storing data. Accelerometers were mounted with their axes oriented transversely to the pile's longitudinal axis, as shown in Figure 1. Wood mallets and metal hammers of various sizes were used to create analyzable signals; no standardized device was needed because the signals

did not need to be identical. All data recorded were stored on the laptop for later analysis on a laboratory PC.

TEST RESULTS

A total of 40 piles were tested, including the 4 test piles installed at the NCDOT Bridge Maintenance Yard. Of the 40 piles, 26 permitted comparison between the calculated values and overall length values, either from pile records or from measurements taken after pulling. Sixteen of the 26 piles were friction piles (supported by shear forces), and the other 10 were supported by concrete footings. The remaining 14 could not be analyzed either because of bad signals, because no return wave was found in their time records, or the pile's records were not clear enough for identification.

Figure 4 is a graph displaying results for the 26 valid piles, and Figure 5 is an enlarged view of the lower portion of Figure 4. Diagonal lines extending from the origin in both of these figures are the lines of zero difference between computed and recorded or measured values. The lines to either side of the zero-difference line represent a ±10 percent difference. The term "percent difference" is used here rather than "percent error" because the "actual" lengths were taken from pile records. Such records are subject to error because they may not account for partial or complete fracture(s), brooming of the pile toe, or wearing away of the toe that could have occurred during driving. When such events occur, they effectively decrease a pile's overall length, although the pile's overall length before driving may be all that is recorded.

The 16 piles supported by shear forces (skin friction) were the ones of principal interest in this research. The 16 piles are represented in the figures by horizontal bars whose lengths are a measure of the range of lengths computed for a particular piling, with vertical terminator bars at each end. The range of values for any one pile reflects the dispersion phenomenon, in that different frequencies were found to have different wave speeds and return times by the SKM computations. The computed results showed correlation with the pile records to the extent that percent differences ranged from −11.8 percent to +8.5 percent. The negative percentage implies the computed lengths were too short and the positive value indicates that computed lengths were too long.

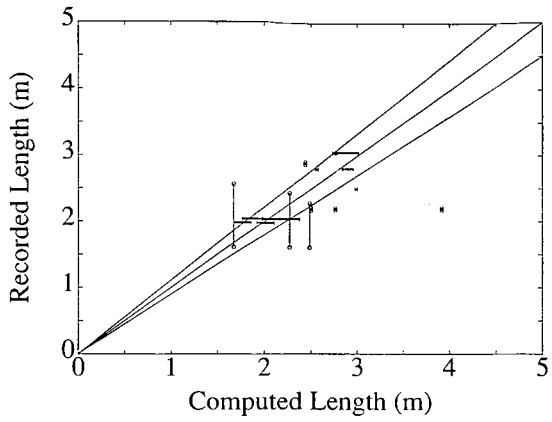

FIGURE 5 Computed overall-length values compared with pile records or measurements after pulling (lower portion).

In Figure 5, the symbols representing piles resting on rock and set in concrete are indicated by vertical lines. The single computed value shown for any vertical line is the average of all the length calculations for that pile. It is compared with the distance from the pile head to the top of the concrete, the lower value on a vertical line, and the distance from the head to rock, the upper value on the line. The only exception to this notation is that of the three piles represented by horizontal bars located between the computed values of 2.56 m and 2.98 m and the recorded values of 2.50 m to 2.80 m. These three piles were also found to be embedded in concrete, but no distance from the pile head to the top of the rock was available. Therefore, a range of computed answers is given for them, which is compared only with the head-to-concrete distance.

Of the 26 piles shown in Figures 4 and 5, 7 were pulled up by NCDOT; they are displayed independently in Figure 6. These are the only piles that permitted direct comparison of the test method results against true measured lengths. The results showed correlation with the measured values to the extent that percentage errors ranged from −10.8 percent to +6.7 percent.

One pile was pulled that did not permit an overall-length computation because no return signal was found during the test. The

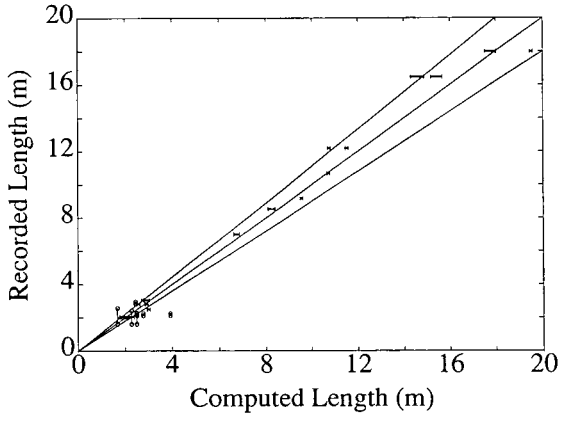

FIGURE 4 Computed overall-length values compared with pile records or measurements after pulling (all piles).

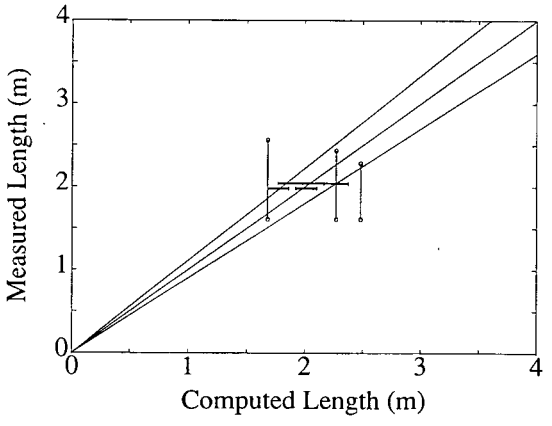

FIGURE 6 Computed overall-length values compared with measurements of piles pulled after testing.

pile was found to have been broken sometime during its service life and disfigured to the point that it was no longer straight. Analysis of this pile may indicate that if a pile's time records are unusually "noisy" or cannot be deciphered, there may be grounds to question a pile's condition. At this stage in the development of the method, however, more evidence is needed.

Piles with Shallow Embedments in Concrete Footings

The 10 piles resting on rock and embedded in concrete were shorter and had more shallow embedments as compared with the other piles. Whether the testing method can determine the actual length of a pile in a concrete footing has not been proven. In all cases, computations gave varying answers that were either (a) too short and above the footing, or (b) a value within the footing, or (c) sometimes below and past the footing.

Factors Affecting Overall-Length Calculations

At the outset of the research, it was recognized that several factors could affect the calculations of overall length, including structural constraints, soil confinement, pile condition, and the effects of a pile's taper on wave speeds. For example, preliminary test results indicate that bending-wave speeds diminish as a wave moves to lesser diameters, as they would in a tapered pile, and speed up again after they reflect off the pile toe. No further information or mathematical correction for the taper effect were available at the time the data were analyzed; however, a more comprehensive investigation was being conducted by Douglas and Holt (*1*).

As regards the effects of structural constraints, such as cross-bracing, no formal, experimental investigation was conducted. An attempt was made to minimize such effects, however, by creating signals whose lateral oscillation was perpendicular to the plane of the bracing. The effects of pile confinement by the surrounding soil was not addressed due to time constraints. The effect of pile condition was being investigated at the time of the research, but results were not available. No corrections were made to the overall-length calculations previously presented for any of these possible effects. One or more of these factors may have been at play for piles that did not yield computational results when tested.

OTHER TESTS

A number of other tests were performed on each pile during the field work. It was realized early in the research program that it would be potentially valuable to start creating a data base to relate measurable parameters to a pile's mechanical and observable condition. Wave propagation tests for condition and wave speeds were conducted, sounding tests were performed, and visual inspections and descriptions were recorded in detail. One of the wave-propagation tests involved using a pitch-catch-type velocity meter to measure the time for a mechanical pulse to travel a known distance. Such time measurements were made routinely along a pile's diameter (radially) and in the direction of its longitudinal axis. These measurements then were used to compute both longitudinal and radial wave speeds for comparison with the wave speeds found from the SKM computations.

Figure 7 shows a graph of SKM wave speed versus radial wave speed. A relationship of this type may prove useful for evaluating piles with such a short, exposed length that it would be difficult to mount two accelerometers. In such cases, if one gage can be mounted and a return signal identified, then radial-velocity measurements may provide an indication as to an approximate SKM wave speed to use in making the length calculations. The degree of error that will be present in such wave-speed approximations has not yet been determined.

Another wave-propagation test was conducted each time to indicate a pile's physical condition. This test involved wave-speed determinations and frequency-amplitude loses between two accelerometers moved along a pile's exposed length. Time records were processed according to the Fourier transform in order to examine frequency and magnitude data. SKM wave speed calculations also were done for frequencies higher than those used in the length computations. Results from these tests were preliminary at the time of this paper.

CONCLUSIONS

For timber piles that depend on embedment and shear forces to carry load, the proposed wave-propagation method for determining overall lengths, using bending waves and digital signal-processing of dispersive signals by SKM, has been demonstrated to hold promise. The percent difference between computed lengths and pile records varied from −11.8 percent to +8.5 percent. The percent error between computed lengths for piles measured after being pulled varied from −10.8 percent to 6.7 percent. The method also holds promise for identifying piles with short embedment. The objectives of our research were met: The dispersive-wave method was shown to be feasible for determining in-place pile lengths, and a field-testing method was developed.

ACKNOWLEDGMENTS

This paper presents results of a research project conducted in the NCSU Civil Engineering Department. Principal funding was provided by NCDOT and FHWA. The condition studies related to this work, as well as useful contributions to the overall length

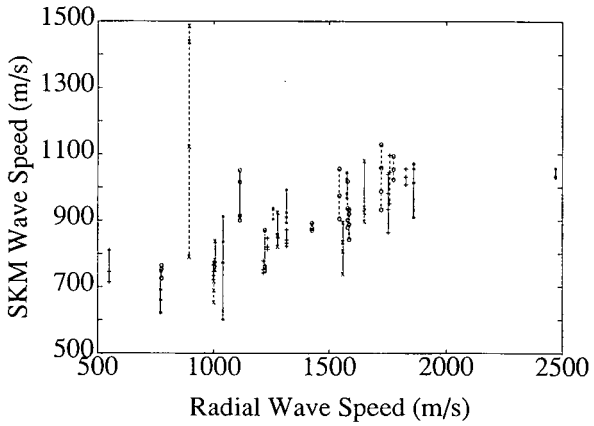

FIGURE 7 SKM wave speed versus radial wave speed.

studies, were made possible by a grant from the Sea Grant program of the National Oceanic and Atmospheric Administration.

REFERENCES

1. Douglas, R. A. and J. D. Holt. *Determining Length of Installed Timber Pilings by Dispersive Wave Propagation Methods*. Final Report, Research Project Number 23241-92-2. North Carolina Department of Transportation; FHWA, June 1993.
2. *Determining In-Situ Timber Pile Length Using Stress Waves*. Report to Timber Bridge Initiative Special Projects Program of USDA Forest Service, Engineering Data Management, Inc., Fort Collins, Colo., Oct. 1992.
3. Ryan, Edmond P. *Measurement of Embedded Lengths of Existing Piles*. Final Report, Project Number 99100-7736-04. Tennessee Department of Transportation, Nashville, Aug. 1988.
4. Alexander, A. M. *Development of Procedures for Nondestructive Testing of Concretes Structures, Report 2, Feasibility of Sonic Pulse Echo Technique*. Miscellaneous Paper C-77-11. U.S. Army Corps of Engineer Waterways Experiment Station, Vicksburg, Miss., April 1980.
5. Douglas, R. A. and G. L. Eller. Nondestructive Pavement Testing by Wave Propagation: Advanced Methods of Analysis and Parameter Management. In *Transportation Research Record 1070*, TRB, National Research Council, Washington, D.C., 1986, pp. 53–62.
6. Eddy, J. L. *A Laboratory Model of a Multi-Layer System For Nondestructive Testing*. M.S. thesis. North Carolina State University, Raleigh, 1988.
7. Douglas, R. A., J. L. Eddy, and H. E. Wahls. On Transforms and the Dispersion Computations Used for Evaluating Layer Properties. *Nondestructive Testing of Pavements and Back Calculation of Moduli*. (A. J. Bush III and G. Y. Baladi, eds.), ASTM STP 1062, 1989, ASTM, Philadelphia, Pa., pp. 612–627.
8. Bendat, J. S. and A. G. Piersol. *Engineering Applications of Correlation and Spectral Analysis*. John Wiley and Sons, Inc., New York, N.Y., 1980.

Bitumen Coating for Downdrag Mitigation in Cohesionless Soils

KAMAL S. TAWFIQ AND JOSEPH A. CALIENDO

Effectiveness of bitumen coating in mitigating downdrag in cohesionless soils was investigated using direct shear apparatus and a rod shear test. Tests on soft and stiff bitumen sheared with sand and crushed limestone showed that changes in temperature, shear-strain rate, and normal stress significantly affected the shearing characteristics of bitumen coating. Increasing the normal stresses caused an increase in the soil-particle penetration layer into the bitumen and altered the viscous behavior of the material. High friction resistance was recorded when crushed limestone was used to shear the bitumen layers. Stiff bitumen coating provided better protection against soil penetration than soft bitumen. However, at high temperatures, both bitumens lost their protective capabilities, resulting in a significant soil penetration into the bitumen coating. Bitumen-coated samples tested with sand exhibited the lowest friction. The effectiveness of bitumen coating in this case was 98 percent; it dropped to 54 percent when crushed limestone was used.

Proprietary mechanically stabilized earth (MSE) walls are commonly constructed at bridge abutments in Florida and many other states. Before wall construction, end-bent concrete piles are driven behind the proposed wall. Subsequently, as the wall is constructed, backfill is placed adjacent to the piles and compacted to the desired density. If compressible soil deposits are encountered at the site, relative settlement of the soil surrounding the piles might take place. Accordingly, part of the weight of the soil transfers to the piles, thereby, exerting downdrag forces against the pile shafts. This downdrag effect is commonly termed "negative skin friction," since downward shear stresses are mobilized along the shaft. Observations have indicated that a relative downward movement of about 1 percent of the pile diameter of the soil with respect to the pile is sufficient to fully mobilize the negative skin friction (*1*).

Various methods have been suggested to predict downdrag forces on piles. These methods are based on different assumptions of the behavior of soils adjacent to the pile shaft, and on the distribution of the negative skin friction in the settling zone.

In most cases, the predicted or measured settlement of the soil surrounding a pile shaft is clear indication of a potential downdrag problem within pile foundations. Unless some action is taken to mitigate its effect, the downdrag force could detrimentally affect the economy of the project, and it should be included in the design as an additional axial load.

Small downdrag forces on piles are often neglected in the design. For higher values, the downdrag can be resisted either by

- Providing additional piles;
- Using a preloading method;
- Using bentonite slurry; or
- Using bitumen coating to ease the effect of relative settlement.

According to Machan and Squier (*2*), benefit/cost studies of each of these alternatives have suggested that bitumen coating is the most cost-effective approach for reducing downdrag in piles.

Several investigators have studied the effectiveness of bitumen coating in mitigating downdrag in piles (*3–6*). Baligh et al. (*7*) suggested a simplified method for determining downdrag loads on bitumen coated piles. For fine-grained soils, the skin friction can be estimated by the following expression:

$$\tau_s = m\left(\frac{\dot{\gamma}}{\dot{\gamma}_o}\right)^n \tag{1}$$

$$\dot{\gamma} = \frac{\dot{\rho}_{av}}{a} \tag{2}$$

where

$\dot{\gamma}$ = average shear strain rate in the bitumen,
$\dot{\rho}_{av}$ = average settlement rate in the soil layer,
a = in situ bitumen coating thickness,
$\dot{\gamma}_o$ = reference shear rate chosen arbitrarily to be 10^{-5} sec^{-1}, and
m, n = temperature-dependent bitumen parameters.

For coarse-grained soils, the maximum value of τ_s can be estimated using the beta (β) method and a reduction parameter ranging from 0.5 to 1.

Fellenius (*8*), on the other hand, stated that one can either rely on actual field tests, if reliance is justified by time and economical considerations, or use the conservative assumption that a properly applied bitumen coat can reduce the negative skin friction to a value of about 200 lb/ft^2. According to Fellenius, this value will adequately predict the downdrag load.

Based on pile-uplift test results, Machan and Squier (*2*), measured 90 percent reduction in downdrag forces on bitumen-coated piles. When downdrag was predicted using bitumen viscosity, the forces were lower than the field measurements. For a precise estimate of downdrag forces of bitumen-coated piles, Machan and Squier emphasized the need for refinement of existing prediction techniques.

STUDY OBJECTIVES

The purpose of the study was to evaluate the effect of temperature, particle size, shearing rate, and normal stresses on the shearing

K. S. Tawfiq, Department of Civil Engineering, Florida Agricultural Mechanical University/Florida State University College of Engineering, Tallahassee, Fla. 32316-2175; J. A. Caliendo, Department of Civil Engineering, Utah State University, Logan, Utah 84322.

characteristics of bitumen coating and to conduct a thorough investigation in order to refine existing approaches for estimating the negative skin friction, τ_s, on bitumen-coated piles—taking into account the shearing properties of the bitumen-soil matrix. To meet these objectives, concrete blocks coated with two types of bitumens were tested in the laboratory using two different cohesionless soils and a direct shear apparatus. Additional tests were performed in the laboratory using concrete rods coated with bitumen and sheared in a steel mold under loading and ambient conditions similar to those applied in the direct-shear test.

TESTING PROGRAM

In this study, two different particle sizes of cohesionless soils were tested. The first soil was reddish-brown sand with some fines. The second soil was coarse-grained, crushed, Florida limestone. These two types of soils were selected to suit the size of the direct-shear box and the steel mold of the rod-shear test and to fit within the backfill range of MSE walls proposed by the Florida Department of Transportation. Grain-size analysis showed that the first soil was a well-graded sand with 2 percent fines, and the second one was a well-graded gravel with less than 1.3 percent fines. In the study soil, 8 percent of the particles were larger than the thickness of the bitumen coating used in the investigation, whereas 70 percent of the soil particles in the crushed limestone were larger than that thickness.

For bitumen coating, AC-5 and AC-30 bitumens were selected. AC-5 has a minimum penetration grade of 212 at 25°C, whereas AC-30 has a minimum penetration grade of 70 at 25°C. The flash points for the first and the second bitumen were 268°C (515°F) and 257°C (495°F), respectively.

SAMPLE PREPARATION AND PROCEDURE

Direct-Shear Test

To simulate the shearing mechanism between the pile shaft and the coating material during downward movement of the soil, concrete blocks were prepared to model the pile surface. These blocks were also used to replace the lower half of the shear box in the direct-shear apparatus. The blocks were 12.7 cm × 12.7 cm × 1.25 cm and were reinforced with wire mesh to avoid any cracking during load application and to expedite the distribution of temperature during testing. A large number of these blocks was prepared and cured before coating them with bitumens. The following two sets of samples were prepared for direct-shear testing: (*a*) concrete-bitumen-soil samples and (*b*) concrete-soil samples without bitumen coating.

A typical coated concrete sample was prepared for direct-shear test by heating the bitumen to 150°C and then pouring the emulsion in a 6-cm × 6-cm steel mold to adepth of 0.32 cm. This depth was in accordance with the Florida Department of Transportation's requirements for the thickness of bitumen coating (*9*). Before pouring the bitumen, the steel mold was lubricated using high-vacuum grease, to facilitate the detachment of the mold upon bitumen solidification. The bitumen layer was positioned on the concrete block so that it coincided with the soil sample in the upper half of the shear box. To avoid any distortion during the storage period, the cured bitumen remained in the steel mold until minutes before it was transferred to the direct shear apparatus. After setting the coated block in the direct shear container, the upper half of the shear box was then lubricated and carefully lowered on the bitumen layer to a distance of about 1 mm from the concrete surface. A preweighed soil specimen was then placed in the shear box and carefully tamped to the desired density.

Figure 1 shows a schematic of the shear box used in testing. In this investigation, the normal stresses varied from 18.85 kPa to 40.64 kPa. Shearing stresses on the samples were applied at a constant rate of deformation. In this study, three rates of deformation were used. These rates varied from 0.0025 mm/min to 1 mm/min. Accordingly, the rates of shear strain, $\dot{\gamma}$, ranged from 1.3×10^{-5} sec^{-1} to 5.25×10^{-3} sec^{-1}. The shear strain rate, $\dot{\gamma}$, in the bitumen coating equals the deformation rate of the upper half of the shear box divided by the coating thickness.

The concrete-bitumen-soil samples were tested at 25°C (77°F), 56°C (133°F), and 5°C (41°F). During testing, measurements of vertical deformation, horizontal deformation, and shear load were recorded for further analysis. After testing, the samples were visually examined to assess the amount of disturbances in the bitumen layers and to evaluate the effect of the shear stresses, temperature, and normal stresses on the soil-particle penetration into the bitumen coating.

Rod Shear Test

A rod shear test was devised in the laboratory to simulate the negative skin friction induced by the relative movement between the pile and the soil (Figure 2). A similar testing approach was used by Bush et al. (*10*) except that the coated rod was sheared against the steel mold.

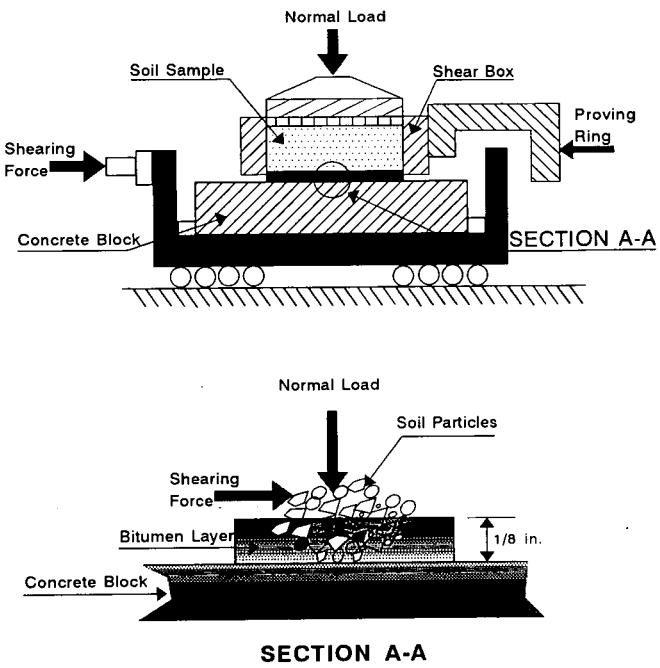

FIGURE 1 Schematic of direct shear test.

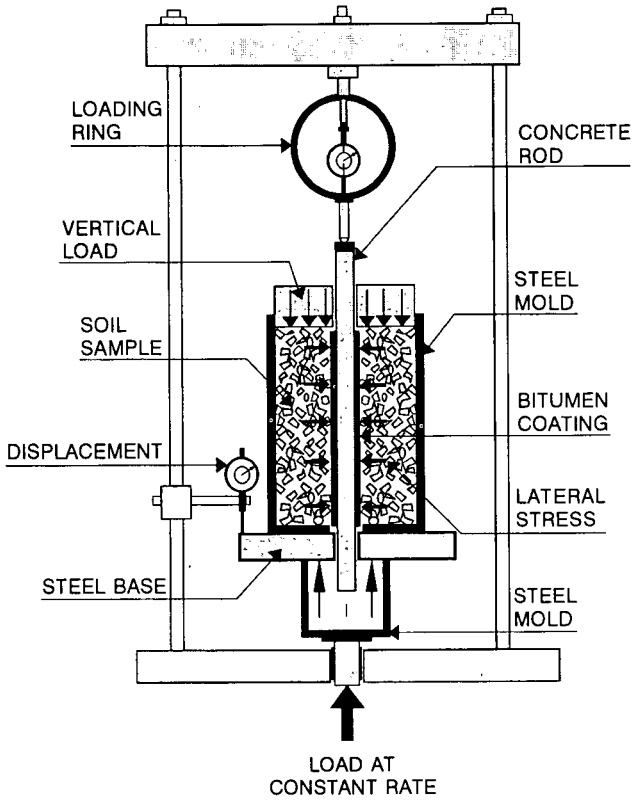

FIGURE 2 Schematic of rod shear test.

In the rod shear test, a concrete rod, 30 cm in length and 3 cm in diameter, was coated with a 3.2-mm bitumen layer. The rod was placed vertically in a steel mold 15.2 cm in diameter and 17.8 cm high. A hole with a 3.7-cm diameter was drilled in the base of the mold so that the rod could advance through it during testing. After centering the rod in the mold, a soil sample was placed adjacent to the coated portion of the rod. The entire length of the coated part (16 cm) was in contact with the soil. The soil samples used were the same as for the direct shear tests. The setup was placed on a loading frame, and a predetermined vertical load was then placed on the soil surface to produce lateral effective stresses, $\overline{\sigma_h}$, which ranged from 2 kPa to 5 kPa. These stresses were obtained as follows:

$$\overline{\sigma_h} = \overline{\sigma_v} \cdot k_o \tag{3}$$

where $\overline{\sigma_v}$ is vertical effective stress and k_o is $1 - \sin \phi$. It was not possible to obtain higher lateral stresses because of the limited number of dead loads that could be added to the setup. Vertical loading was applied on the concrete rod under controlled rate of displacement.

Testing a typical rod was initiated by driving the steel mold upward using a stepping motor while the bitumen-coated rod was kept in place by the loading ring. The shear resistance induced by the relative displacement was recorded from the loading ring, and the rate of deformation was measured from the dial gage attached to the mold base. Shear-strain rates used in the rod shear testing ranged from 1.3×10^{-5} sec^{-1} to 5.25×10^{-3} sec^{-1}. At the end of each test the coated rod was removed from the mold and visually inspected to evaluate the severity of the soil-particle penetration into the bitumen.

DISCUSSION OF RESULTS

Test results from 96 samples showed that the ambient temperature and the shear-strain rate have a significant effect on the shearing behavior of bitumen-coated blocks. The normal stress σ_h and the grain size affected the penetration of the soil particles into the bitumen layers. The unavoidable penetration caused a significant increase in the friction resistance of the bitumen-soil matrix. Figures 3 to 5 depict the shearing behavior of the samples at different shearing rates, temperatures, and normal stresses. These relationships are plotted in terms of shear-stress ($\log\tau_s$) versus shear-strain rate ($\log \dot{\gamma}$). Similar representations for the shearing behavior of different bitumens were followed by Baligh et al. (*7*). The shear strain rate $\dot{\gamma}$ equals the horizontal displacement rate of the upper shear box divided by the bitumen coating thickness, *d*. These plots constituted liner relationships in which the slopes and the points of intersection of the lines represent the values of *m* and *n* parameters in Equation 1.

For the AC-5-bitumen-coated samples sheared with sand (less than 5 percent of the particles were larger than the coating thickness), the shear resistance τ_s was the highest at 5°C. As the temperture increased, the shear resistance decreased until it reached the lowest value at 56°C. This increase in the ambient temperature decreased the viscosity of the bitumen to a level at which the bitumen functioned as a lubricant material to the sand particles. The shear resistance, τ_s, at 56°C was significantly lower than the resistance at 5°C. The effect of the soil-particle penetration on the shearing of the bitumen-coated samples was apparent at all the temperatures used in testing. Increasing the normal stresses caused an increase in the shear resistance. However, the shearing behavior of the bitumen (without soil penetration) should be independent of normal stresses.

The same behavior was observed in the AC-30-bitumen-coated samples sheared with both types of soils. As the ambient temperature increased, the shear resistance of the bitumen coating decreased. At 56°C, the shear resistance, τ_s, of the crushed limestone samples (70 percent of the particles were larger than the bitumen-coating thickness) increased abruptly once the normal stress was increased to 40.64 kPa, and it exceeded the shear resistance obtained at 25°C. This mobilization of the shear stresses was a clear indication that full-particle penetration was attained at this normal stress. At 25°C and 5°C, a gradual increase in the values of the shearing resistance, τ_s, with the increase of the normal stresses was recorded.

This increase was also caused by the built-up friction between the soil particles and the concrete surface. At this stage, the bitumen functioned as a visco-frictional material. Measurements of the vertical deformation proved that full soil penetration had taken place during direct shear testing. These measurements showed that the amount of vertical deformation exceeded the thickness of the bitumen coating. In addition, a visual inspection after testing ascertained that a substantial penetration by the large particles occurred in the bitumen coating.

Results from the rod shear testing corresponded with those obtained from the direct shear tests. The shear-stress versus strain-rate relationships of the rod shear tests (Figures 3 to 5) exhibited the same slopes, *n*, as they had for the direct shear lines. However,

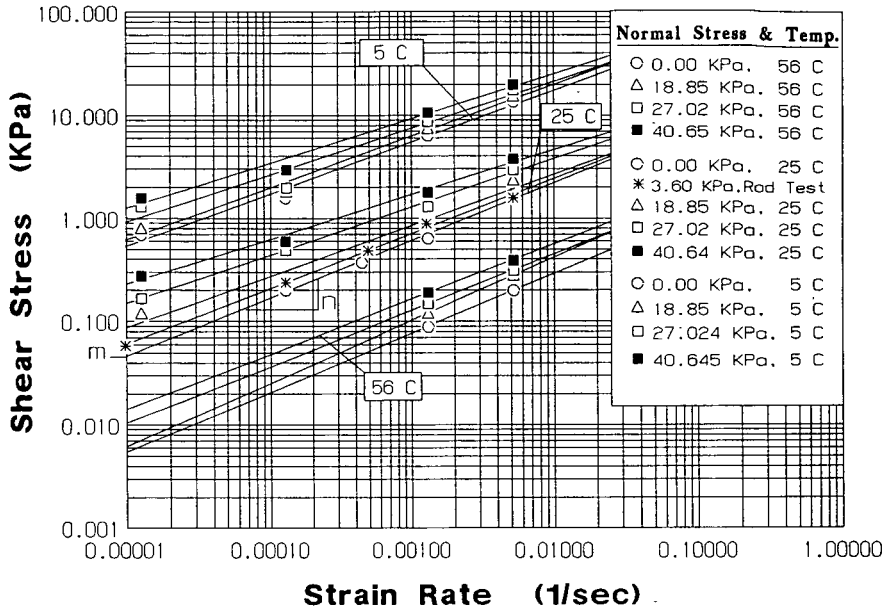

FIGURE 3 Shear stress versus shear strain rate of concrete-bitumen-soil samples, AC-5 bitumen and sand.

the effect of the sand-particle penetration on the shear resistance of bitumen coating in the rod shear test was less insignificant. This is because the magnitudes of the normal stresses that could be attained in this method were too small to induce considerable soil penetration. However, the induced lateral stresses were sufficient to produce full penetration of the limestone particles into the bitumen layer.

Characterization of Shear Resistance in Bitumen Coating

The magnitude of the downdrag forces in bitumen-coated piles is governed by the viscoelastic behavior of the bitumen material, which, in turn, is dictated by the ambient temperature and the rate of shear strain, $\dot{\gamma}$, in the bitumen coating. The strain rate in the

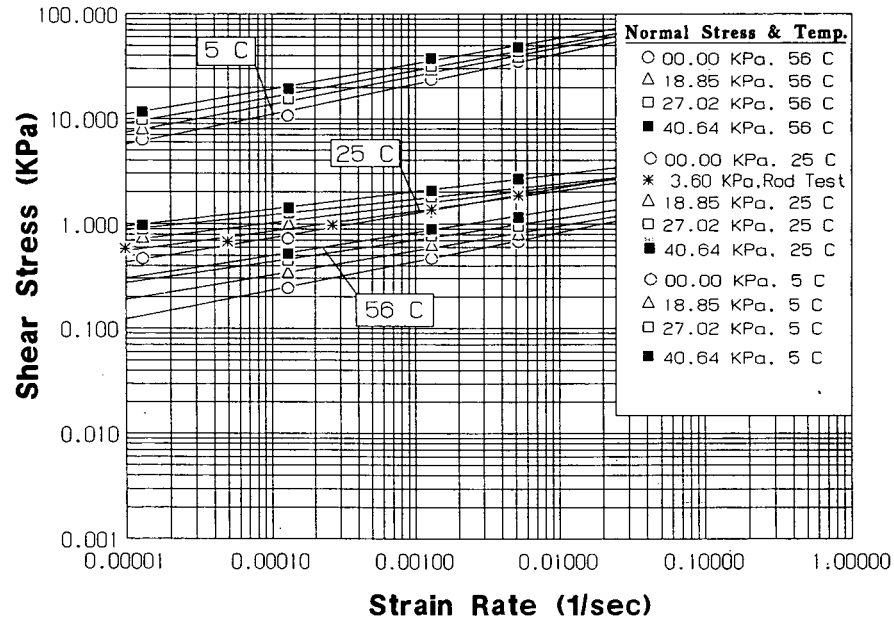

FIGURE 4 Shear stress versus shear strain rate of concrete-bitumen-soil samples; AC-30 bitumen and sand.

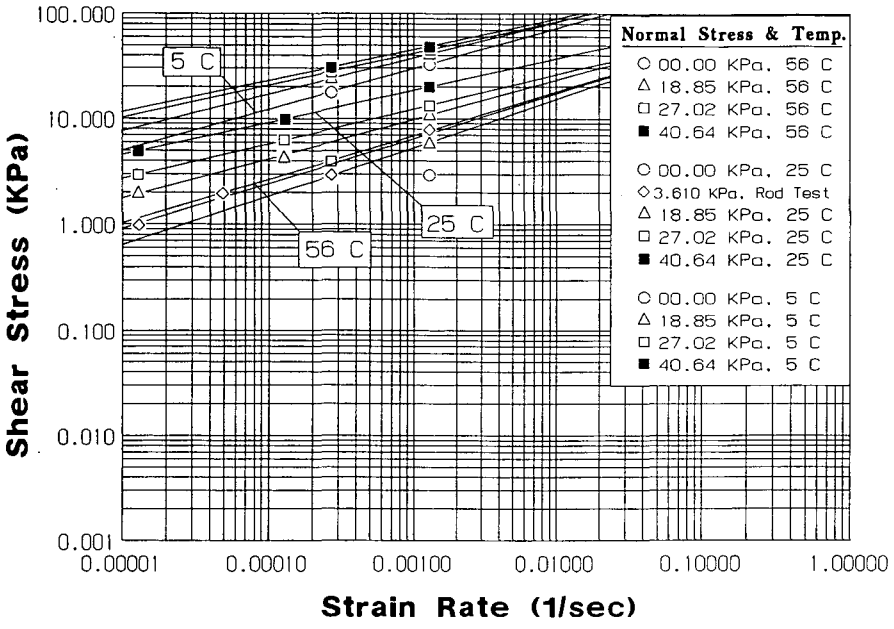

FIGURE 5 Shear stress versus shear strain rate of concrete-bitumen-soil samples; AC-30 bitumen and crushed limestone.

bitumen is proportional to the rate of settlement of the soil layers surrounding the pile shaft. The downdrag on a bitumen coated pile can be determined from

$$F_s = \tau_s (P \cdot L) \tag{4}$$

where

F_s = downdrag force,
τ_s = shear stress in the bitumen coating,
L = length of the embedded portion of the coated pile, and
P = perimeter of the pile.

The shear stress in bitumen coating is proportional to the shear strain rate $\dot{\gamma}$, and it can be expressed as follows:

$$\log\tau_s = \log m + n \cdot \log\left(\frac{\dot{\gamma}}{\dot{\gamma}_o}\right) \tag{5}$$

where

$\dot{\gamma}_o$ = a reference strain rate equal to 10^{-5} sec^{-1},
m = shear stress at the reference strain rate,
n = slope of the logτ versus log$\dot{\gamma}$ relationship.

The magnitude of m and n parameters can also be obtained from the following relationships:

$$m = m_o\, 10^{-\alpha_m T} \tag{6}$$

$$n = n_o + \alpha_n T \tag{7}$$

where

m_o and n_o = values of m and n at T = 0°C;
α_m = slope of the relationship of m parameter versus temperature; and
α_n = slope of the relationship of n parameter versus temperature (Figures 6 to 9).

In the present study, these parameters were found to be dependent on the effective normal stress and on the type of soil used to shear against the bitumen coating.

Considering the effect of soil-particle penetration on the shearing behavior of bitumen coating, Equations 5–7 alone may not be sufficient to characterize the shear resistance in the bitumen-soil matrix. The results of this investigation showed that the viscous behavior of the bitumen must be modified to accommodate the friction resistance associated with the presence of the soil particles in the bitumen layer. On the basis of the parameters used in this study, Equations 6 and 7 were modified to model the effect of soil-particle penetration on the shear resistance between the bitumen-soil matrix and the pile surface. The following expressions can be used to describe the effect of temperature and normal stress on the soil-particle penetration and, thus, on the shear stresses of bitumen-coated piles:

$$m = m_o\, 10^{\Delta\sigma_n(\tan\phi_o + T\tan\xi) - \alpha_m T} \tag{8}$$

$$n = (n_o + \alpha_n T) - \Delta\sigma_n (\tan\psi + T\tan\theta) \tag{9}$$

where

$\Delta\sigma_n$ = effective normal stress increment,
ϕ_o = angle of friction of the bitumen-soil matrix at T = 0°C and $\dot{\gamma}_o = 1 \times 10^{-5}$ sec^{-1},
ξ = variation in α_m with respect to $\Delta\sigma_n$,
$\psi = \tan^{-1}(n_o - n_T)/\Delta\sigma_o$, and
θ = variation in α_n with respect to $\Delta\sigma_n$.

These parameters depend on the soil and bitumen type. For materials used in this study, the values of these parameters can be obtained from Table 1 along with the values of m_o, n_o, α_m, and α_n. Parameters for samples coated with AC-30 bitumen and tested with crushed limestone were almost similar to those obtained from

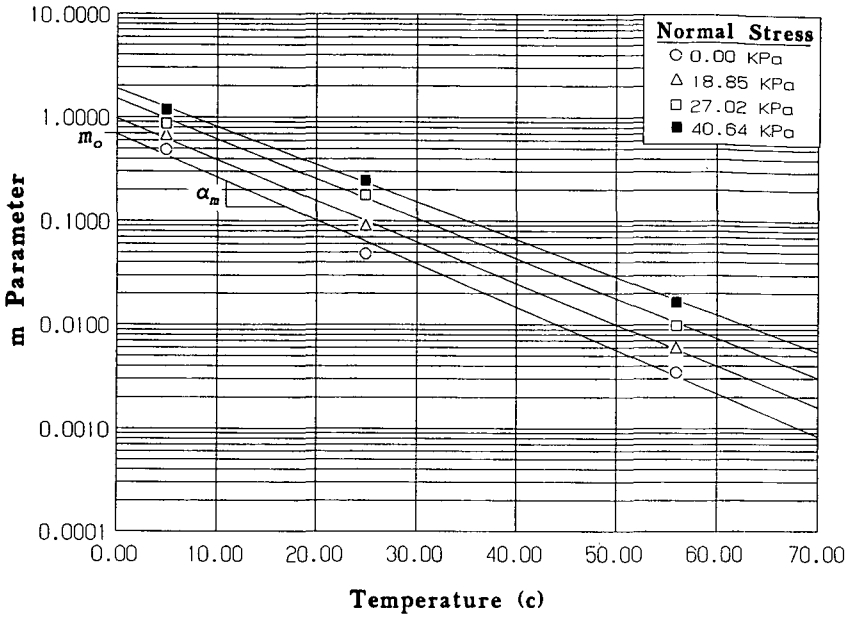

FIGURE 6 Shear parameter *m* of AC-5 bitumen and sand.

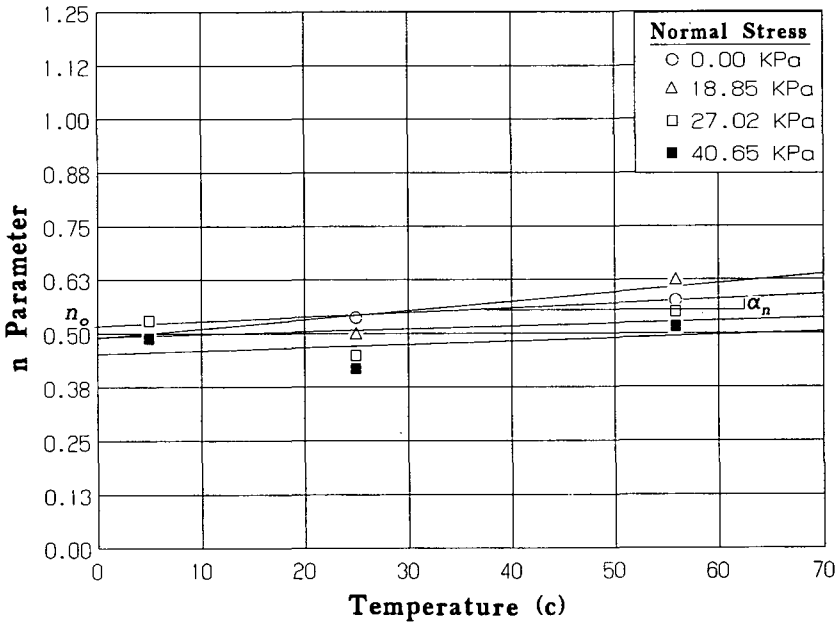

FIGURE 7 Shear parameter *n* of AC-5 bitumen and sand.

samples coated with the same bitumen and tested with sand at 5°C and 25°C. However, the considerable penetration of the crushed limestone particles into the bitumen layer at 56°C and 40.6 kPa caused the friction resistance to exceed the values of the shear resistance obtained at 25°C. This sudden increase in the friction complicated the prediction of the shearing behavior of the these samples at 56°C. Therefore, the shear parameters presented in Table 1 for the crushed limestone samples should be used for predicting shear stresses only at temperature levels lower than 56°C.

Other ranges of values can also be obtained for different bitumens and soils. The variation in these values might not be very significant, especially for ϕ_o and ξ, which influence the *m* parameter. However, ϕ_o and ξ were found to have more impact on the shear resistance, τ_s, than ψ and θ parameters.

Illustrative Example

Consider a typical 0.61-m (24-in.) square bitumen-coated pile in a 6-m (18.3-ft) cohesionless backfill behind a proprietary MSE

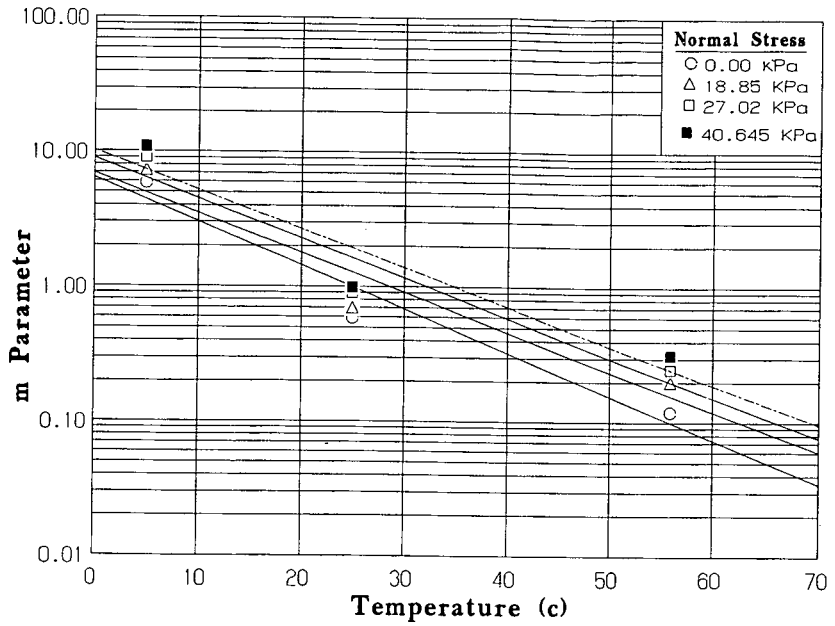

FIGURE 8 Shear parameter *m* of AC-30 bitumen and sand.

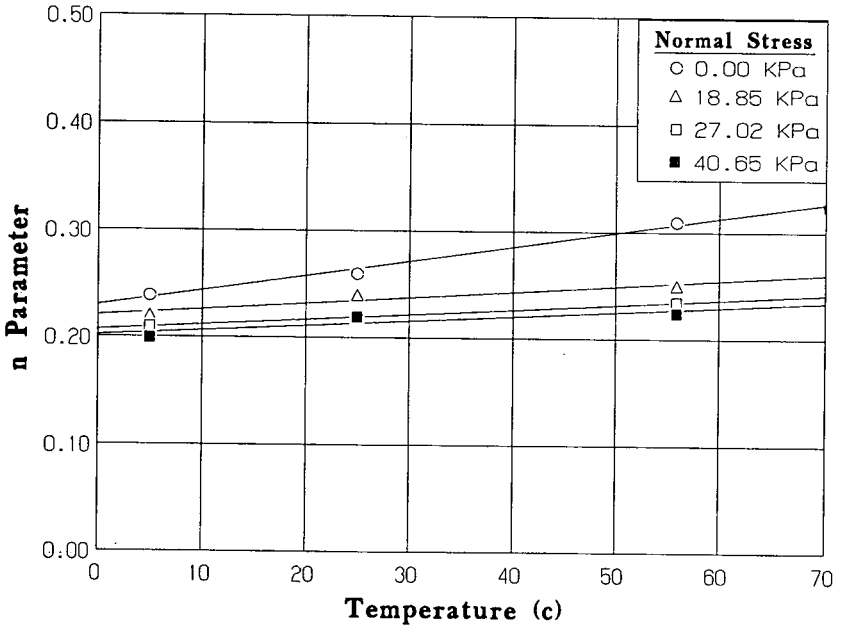

FIGURE 9 Shear parameter *n* of AC-30 bitumen and sand.

wall. The temperature at the site varies during the year from 38°C (100°F) to 0°C (32°F). The ground settlement rate, $\dot{\rho}$, is 12.7 mm/day (½ in. per day). This rate corresponds to the maximum settlement reported by Machan and Squier (*2*) for the Mocks Bottom bridge. Two bitumens, AC-5 and AC-30, are to be used to coat the pile with a 3.2-mm (⅛-in.) layer. Based on the rate of settlement, the value of the strain rate, $\dot{\gamma}$, in the bitumen coating is 4.6×10^{-5} sec^{-1}.

From Table 1, substitute the shear parameters of AC-5 and AC-30 bitumens into Equations 7 and 8 to obtain *m* and *n*, and consider that the subsurface temperature is about 5°C lower than the air temperature at the site. Using Equation 1 for shear-strain rate of 4.6×10^{-5}, the magnitude of the unit friction, τ_s, and the downdrag forces of both bitumens are presented in Table 2. The downdrag force, F_s, on pile without coating is about 138.5 kN (14 tons).

If crushed limestone is to be used as a backfill and AC-30 bitumen for coating, the downdrag load, F_s, on the pile will be equal to 65.88 kN (6.6 tons). This signifies a 54 percent reduction in downdrag. It is clear from Table 2 that the most effective con-

TABLE 1 Shear Parameters of the Concrete-Bitumen-Soil Samples

BITUMEN TYPE	ϕ_o	ξ	ψ	θ	α_m	α_n	n_o	m_b
AC-5-SAND	0.642	0.007	0.102	0.0015	0.042	0.0016	0.526	0.70
AC-30-SAND	0.623	0.005	0.05	0.001	0.0324	0.0014	0.233	6.5
AC-30-LIMESTONE	0.624	0.006	0.062	0.001	0.0324	0.0015	0.35	6.5

TABLE 2 Downdrag on Bitumen-Coated Pile in Cohesionless Soil

BITUMEN TYPE	T = 35° C	T = 25° C	T = 0.0° C
AC-5	m = 0.065	m = 0.17	m = 0.9
	n = 0.54	n = 0.52	n = 0.51
	τ_s = 0.149 kPa	τ_s = 0.373 kPa	τ_s = 1.93 kPa
	F_s = 1.1 kN	F_s = 2.73 kN	F_s = 14.13 kN
	Effectiveness= 98%	Effectiveness= 97%	Effectiveness= 89%
AC-30	m = 0.80	m = 1.8	m = 6.2
	n = 0.26	n = 0.22	n = 0
	τ_s = 1.127 kPa	τ_s = 2.52 kPa	τ_s = 8.47 kPa
	F_s = 8.25 kN	F_s = 18.43 kN	F_s = 62 kN
	Effectiveness= 94%	Effectiveness= 86%	Effectiveness= 54%

dition for mitigating downdrag forces on piles is for piles to be adjacent to sand backfill (particle sizes less than the coating thickness) and coated with AC-5 bitumen (or any bitumen with high-penetration grade).

CONCLUSION

This study evaluated experimentally the effect of temperature, particle size, shearing rate, and normal stresses on the shear resistance of bitumen coating. The study indicated that at certain temperatures the effectiveness of bitumen in mitigating downdrag in cohesionless soils is governed by the bitumen's characteristics and the particle size of the soil. The larger the soil particles, the higher the soil penetration into the bitumen coating. The presence of the soil particles in the bitumen could adversely affect its efficiency in mitigating negative skin friction. For the same bitumen, changing the temperature, the strain rate, and the normal stress influences the amount of skin friction on piles. Stiff bitumens such as AC-30 provide better penetration resistance. However, the viscosity of this bitumen is rather high; consequently, the downdrag forces are also high.

To account for the presence of the soil particles in the bitumen coating and for the build up in friction from the increase in the normal stresses, equations were introduced to modify the shear parameters of the bitumen, m and n. The new shear parameters ϕ_o, ξ, ψ, and θ were suggested to model the visco-frictional behavior of the bitumen-soil matrix. Use of these equations in a parametric analysis showed that as these parameters increase, the downdrag force decreases.

On the basis of the analysis, it was found that the reduction in downdrag could attain 98 percent with soft bitumen coating and sand backfill. The larger the soil particles, the lower the bitumen coating's effectiveness. Finally, it should be noted that the effectiveness of any friction reducer in mitigating downdrag forces should not be ruled out based on the shearing characteristics of the friction reducer acting alone. Rather, the effectiveness of the total matrix (concrete-reducer-soil) should be evaluated under different temperatures and loading conditions.

ACKNOWLEDGMENTS

Research of this paper was supported by the Florida Department of Transportation. The authors are grateful for the support provided. Appreciation is extended to Jean Louis Briaud of Texas A&M University for his suggestions on this project.

REFERENCES

1. Vesic, A. S. *NCHRP Synthesis of Highway Practice 42: Design of Pile Foundations*. National Research Council, Washington, D.C., 1972, 68 pp.

2. Machan, G., and L. R. Squier. Bitumen Coating on Piles to Reduce Downdrag, *Highway Focus*, U.S. Department of Transportation, 1981.
3. Brons, K. F., A. W. Amesz, and J. Rink. The Negative Skin Friction Along the Shaft of a Foundation Pile. *Proc., Seventh International Conference on Soil Mechanics and Foundation Engineering*, Specialty Session, Mexico City, Mexico, 1969.
4. Bjerrum, L., I. J. Johnessen, and O. Eide. Reduction of Negative Skin Friction on Steel Piles to Rock. *Proc., Seventh International Conference on Soil Mechanics and Foundation Engineering*, Mexico City, Mexico, Vol. 2, pp. 27–34.
5. Claessen, A. I. M. and E. Horvat. Reducing Negative Friction with Bitumen Slip Layers. *Journal of the Goetechnical Engineering Division*, ASCE, Vol. 100, No. GT8, Aug. 1974, pp. 925–944.
6. Koerner, R. M. and C. Mukhopadhyay. Behavior of Negative Skin Friction on Model Piles in Medium Plasticity Silt. In *Highway Research Record 405*, HRB, National Research Council, Washington, D.C., 1972, pp. 34–44.
7. Baligh, M. M., H. Figi, V. Vivatrat, and A. S. Azzouz. Design of Bitumen Coating to Reduce Downdrag on Piles. Research Report R80-42. Department of Civil Engineering, Massachusetts Institute of Technology, Cambridge, Mass., 1981.
8. Fellenius, B. H. Downdrag on Piles in Clay Due to Negative Skin Friction. *Canadian Geotechnical Journal*, Vol. 9, Nov. 1972.
9. Standard Specifications for Road and Bridges Construction, Florida Department of Transportation, Tallahassee, 1991, Appendix C-6, pp. 631, 632.
10. Bush, R. K., R. Viswanathan, S. Jeong, and J. L. Briaud. Downdrag on Bitumen-Coated Piles. Preliminary Interim Report for the National Cooperative Highway Research Program, TRB, National Research Council, Washington, D.C., 1991.